



**UNIVERSITA' DEGLI STUDI DI MESSINA**

**Dipartimento CHIBIOFARAM**

---

**TESI DI DOTTORATO DI RICERCA IN SCIENZE CHIMICHE**

Curriculum: progettazione, sintesi, analisi e proprietà di sistemi  
molecolari funzionali

**XXXI CICLO**

Synthesis, photophysical and biological properties of photoactive  
molecules possessing natural residues.

**Tania M. G. Salerno**

Coordinator

Prof. Sebastiano Campagna

Supervisor

Prof.ssa Paola Bonaccorsi

---

**2015-2018**

*“Noi (chimici) montiamo e smontiamo delle costruzioni molto piccole. Ci dividiamo in due rami principali, quelli che montano e quelli che smontano, e gli uni e gli altri siamo come dei ciechi con le dita sensibili [...] perché le cose che manipoliamo sono troppo piccole per essere viste, anche coi microscopi più potenti; e allora abbiamo inventato diversi trucchi intelligenti per riconoscerle senza vederle”*

*Primo Levi*

## Abstract

One of the greatest opportunities for chemists is the possibility to interface during their work with biologists, physicists engineers and put their work at the service of knowledge of life. For instance, small photoactive molecules, with tailored chemical and optical properties, contributed deeply to the advancements in cell biology, “enlightening” studies of cellular components, elucidation of cellular functions and monitoring of relevant biological pathways. Fulfilling the growing need for luminescent molecules requires an understanding of the chemistry that underlies their design and synthesis. My PhD research activity, carried out under the supervision of Professor Paola Bonaccorsi, at the Department CHIBIOFARAM of the University of Messina, gave me the possibility to interact with other groups of research, enriching my work and myself.

In the first chapter of this thesis, after a brief introduction on bichromophoric systems, carbohydrates and BODIPY dyes, I describe the synthesis of new bichromophoric systems hosting carbohydrate residues, their photophysical characterization and studies on their biological properties.

After that, my interest toward luminescent antenna systems moved from carbohydrates toward Curcumin, the most abundant component of *Curcuma Longa*, known also as Turmeric. Curcumin was extensively studied for its numerous pharmacological activities but also because is a dye, exhibiting good optical and electrical properties, owing to a symmetric structure and a highly  $\pi$ -electron delocalized system. In chapter two of this thesis, the synthesis of Curcumin-based bichromophoric systems is described, together with the study of their photophysical properties and some biological results I’ve obtained on these systems. Furthermore, during my PhD, I spent four months at the Newcastle University joining the research group of Dott. Fabio Cucinotta. I

worked on the design, synthesis and characterization of a series of silica nanoparticles appropriately doped with the Curcumin-based luminescent dyes I've already prepared in the laboratory of Messina.

Finally, the third chapter is concerned with the use of the sulfenic acid chemistry, which was already experienced by the research group of Messina, for conceiving Curcumin-derived sulfenic acids to be possibly employed in the detection of biothiols. This final chapter describes the generation of the Curcumin-based sulfenic moiety and its trapping of cysteine or GSH by the formation of a disulphide bond. The system Curc-SOH precursor/Curc-GSH seems to have photophysical characteristics that make it a promising candidate for the conception of a turn-off sensor of biothiols.

In "Final remarks" the results of my three years research work, in terms of publications, oral and poster participations and organization of congresses, are reported.



# Index

<b>Abstract .....</b>	<b>i-ii</b>
-----------------------	-------------

## **Chapter one: Carbohydrates-based bichromophoric species .....pag. 1**

<b>1.1</b> Bichromophoric species.....	2
<b>1.2</b> Carbohydrates.....	9
<b>1.3</b> BODIPY .....	15
<b>1.4</b> Synthesis of a disaccharide-based bichromophoric species.....	20
<b>1.5</b> Photophysical properties of a disaccharide-based bichromophoric species .....	27
<b>1.6</b> Synthesis of a BODIPY-based galactosyl bichromophoric species .....	33
<b>1.7</b> Photophysical properties of a BODIPY-based galactosyl bichromophoric species.....	39
<b>1.8</b> Biological properties of a BODIPY-based galactosyl bichromophoric species .....	45
<b>1.9</b> Conclusions .....	48
<b>1.10</b> Experimentals.....	50
<b>1.11</b> References .....	66

## **Chapter Two: Curcumin-based bichromophoric species.....pag. 70**

<b>2.1</b> Curcumin generals .....	71
<b>2.2</b> Chemical and photophysical properties of Curcumin .....	77
<b>2.3</b> Synthesis of the Curcumin-based bichromophoric species .....	83
<b>2.4</b> Photophysical properties of the Curcumin-based bichromophoric species .....	90
<b>2.5</b> Biological studies on the bichromophoric antenna systems .....	98
<b>2.6</b> Luminescent species in mesoporous silica.....	103

<b>2.7</b> Synthesis of silica nanoparticles with the bichromophoric species and their photophysical characterization .....	110
<b>2.8</b> Conclusions .....	124
<b>2.9</b> Experimentals.....	126
<b>2.10</b> References .....	141

### **Chapter Three: Curcumin-based sulfenic acids and their use in the detection of biothiols..... pag. 146**

<b>3.1</b> Detection of biothiols.....	147
<b>3.2</b> Sulfenic acid generals .....	153
<b>3.3</b> Synthesis and generation of a Curcumin-based sulfenic acid .....	159
<b>3.4</b> Photophysical studies on the detection of biothiols by the Curcumin-based sulfenic acid .....	166
<b>3.5</b> Conclusions .....	169
<b>3.6</b> Experimentals .....	171
<b>3.7</b> References .....	180

Final remarks .....	iii-vi
---------------------	--------

## List of abbreviations

Ac <sub>2</sub> O	Acetic anhydride
APT	Attached proton test
APTES	3-amino-propyl-triethoxysilane
BODIPY	4-4'-difluoro-4-bora-3a-4a-diaza-s-indacene
BSA	Bovine serum albumin
Cys	Cysteine
COSY	Correlation spectroscopy
m-CPBA	<i>m</i> -chloroperbenzoic acid
DCC	N,N'-dicyclohexyl carbodiimide
1,2 DCE	1,2 Dichloroethane
DCM	Dichloromethane
DIEA	ethyl-diisopropylamine
DMAP	4-dimethylaminopyridine
DMF	Dimethylformamide
DMSO	Dimethylsulfoxide
ER	Endoplasmatic Reticulum
ET	Energy Transfer
EtOAc	Ethyl acetate
EtOH	Ethanol
FDA	Food and Drug Administration
FRET	Förster Resonance Energy Transfer
GRAS	Generally recognized as safe
GLUTs	Glucose Transporters
GSH	Glutathione
GSSG	Homocysteine
HCy	Highest Occupied Molecular Orbital
HOMO	Glutathione disulphide

HSQC	Heteronuclear Single Quantum Coherence
IMPS	Invalid metabolic panaceas
LDH	Lactate dehydrogenase
LUMO	Lowest Unoccupied Molecular Orbital
MeCN	Acetonitrile
MeOH	Methanol
mmol	Millimol
mM	Millimolar
$\mu$ M	Micromolar
MSNs	Mesoporous silica nanoparticles
NIR	Near Infrared
NMR	Nuclear Magnetic Resonance
NIS	N-iodosuccinimide
NOESY	Nuclear Overhauser Effect Spectroscopy
NPSH	Non protein thiol
OPEs	Oligo(Phenylene -Ethynylene)s
PAINS	Pan-assay interference compound
PAH	Polycyclic Aromatic Hydrocarbon
PBMCs	Peripheral Blood Mononuclear Cells
PBS	Phosphate Buffered Saline
PEG	Polyethylenglicole
PDI	Perylenediimide
PDT	Photodynamic therapy
PSH	Protein thiol
P123	Pluronic Triblock copolymers
<i>p</i> -TSOH	<i>para</i> -toluenesulfonic acid
ROS	Reactive Oxygen Species
SDAs	Structure directing agents
SNAr	Nucleophilic aromatic substitution

TAS	Transient Absorption Spectroscopy
TBDPS	Tetrabutylammoniumbromide
TBAB	Tert-butildiphenylsilyl
TBET	Trough Bond Energy Transfer
<i>t</i> -BOOH	Tert-butyl-hydroperoxide
TCSPC	Time correlated single photon counting
TEM	Transmission Electron Microscopy
TEOS	Tetraethylorthosilicate
TFA	Trifluoroaceticacid
THF	Tetrahydrofurane
TLC	Thin Layer Chromatography
TMSOTf	Trimethylsilyltrifluoromethanesulfonate
triflic acid	Trifluoromethanesulfonic acid
Triton B	Benzyltrimethylammoniumhydroxide
UV	Ultraviolet
Vis	Visible

# **Chapter One**

---

## **Carbohydrate-based bichromophoric species**

## 1.1 Bichromophoric species

Nowadays, there is considerable interest in long-wavelength, red or near-infrared (NIR) fluorescent dyes for biomedical application, such as *in vivo* fluorescence imaging/sensing, photodynamic therapy, and image-guided surgery.<sup>1</sup> The excitation light coming from these dyes, compared to that of fluorophores requiring blue or green excitation, is able to penetrate deeper into tissue because, in this spectral region, also called “biological window” (650-900nm), both biological chromophores (e.g. haemoglobin) and water absorb and emit minimally<sup>2</sup> (Figure 1.1), thus reducing background interferences and making easier the use of NIR probes for molecular imaging and for sensing applications.

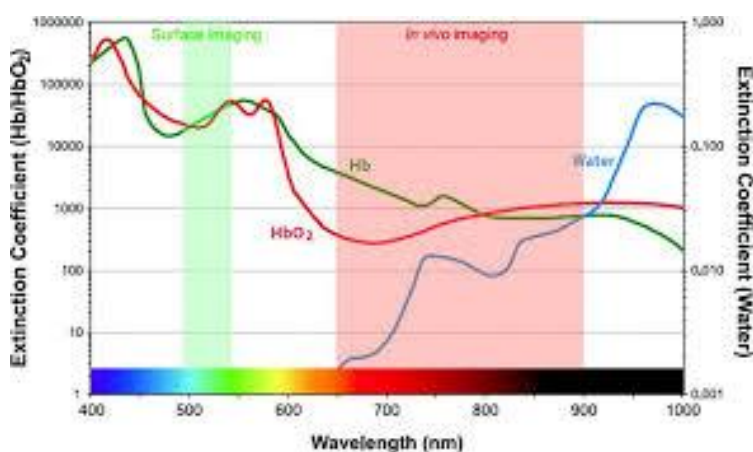


**Figure 1.1:** Definition of the optical window for *in vivo* imaging.

Small Organic fluorophores like fluorescein and rhodamine derivatives, boron-dipyrromethene (BODIPY) and cyanine derivative dyes, are especially important, and they are currently employed as fluorescent labels and probes used for bio-imaging.<sup>3</sup>

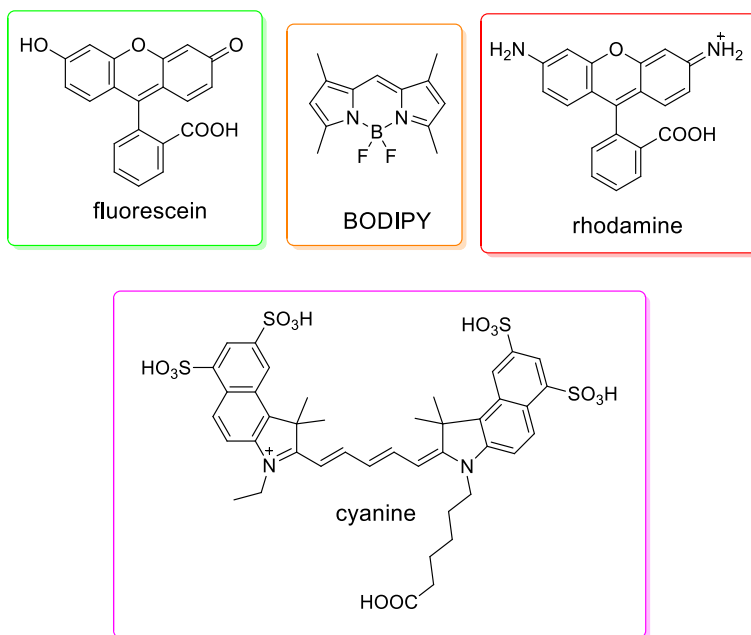


**Figure 1.2:** Classes of fluorophores used in bio-imaging.

Each of the basic structures, shown in figure 1.2, has been modified with functional groups in order to adjust emission wavelength, enhance photostability, and change hydrophobic/hydrophilic balance or to enable conjugation with targeting moieties. In the near-infrared domain (600–900 nm), mainly cyanine, BODIPY and phthalocyanine structures are explored. Nevertheless, these fluorophores still have some disadvantages, e.g. low brightness and poor photostability, low absorption capability and photobleaching, which limit their performance.

To overcome these limitations and to enhance Stokes shift (difference, in wavelength or frequency units, between positions of the band maxima of the absorption and emission spectra) of probes, artificial antenna systems have been developed.<sup>4</sup> In these systems, light is harvested and transported, *via* successive energy transfer hops, and it is converted into emission light of desired energy. In this way the emission can be monitored far away from the excitation wavelength.



In particular, molecular antennae, where two or more fluorescent entities covalently linked *via* an adequate spacer join the same molecule, are called bichromophoric or multichromophoric systems or cassettes. In general, in a bichromophoric system, one of the chromophores, called donor, first absorbs the radiation at the excitation wavelength and then transfers - non radiatively- this energy to a second fluorescent moiety that emits the energy at a longer wavelength; this second moiety is called acceptor (Figure 1.3).

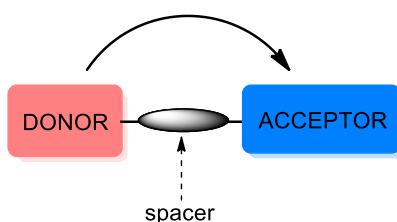


**Figure 1.3:** Schematic bichromophoric system.

If the energy transfer occurs through space, the process is called Forster resonance energy transfer (FRET), if the energy transfer occurs through bond, then the process is called through bond energy transfer (TBET) or Dexter mechanism.<sup>5</sup>

To better comprehend the mechanism, it is easy to refer to the energy diagram reported in figure 1.4; the first step involves absorption of energy by the donor molecule, causing an excitation from the ground state,  $S_0$ , to the excited singlet state,  $S_1$ . Several fates are possible for the excited donor, including spontaneous emission and non-radiative processes. If nearby there is a suitable acceptor fluorophore, then it is possible a non-radiative energy transfer between the donor and acceptor. The result of an ET is the emission of light at a wavelength belonging to the emission spectrum of the acceptor.

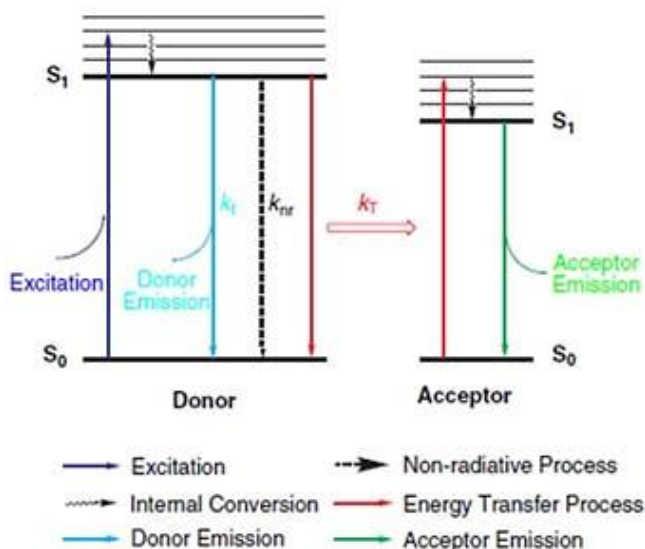


**Figure 1.4:** Mechanism of Energy Transfer.

In particular, FRET is a distance-dependent physical process, which efficiency depends on several factors:

- Spectral overlap of the donor emission spectrum with the acceptor absorbance spectrum, to enable the dipole-dipole coupling;
- Appropriate distance between the donor and the acceptor. The two chromophores should be at a distance below the foster radius;
- Orientation factors;
- Efficiency of alternative de-excitation modes: spontaneous emission of the donor and non-radiative de-excitation process.

Forster energy transfer is the primary mechanism by which energy transfer occurs. However, if the donor and acceptor are linked by a conjugated system of multiple bonds, then through-bond energy transfer can occur. This mode of energy transfer does not follow the same rules of FRET. Good spectral overlap is not required and the main factors affecting through-bond energy transfer are steric interaction, characteristics of the HOMO (highest occupied

molecular orbital) and LUMO (lowest unoccupied molecular orbital), the site of attachment and type of linker between the donor and acceptor.

It becomes clear that the molecular design and careful selection of the components forming the light-harvesting systems is crucial to establish the energy transfer mechanism and the efficiency of the process, which will determine the final emission properties of the photoactive molecules. Appropriate donor and acceptor probes are selected based on their absorption and emission spectral characteristics and should be linked at adequate positions via suitable bridges.

A variety of scaffold or bridge have been used in the construction of artificial antenna systems including, dendrimers, porphyrins and proteins.<sup>6</sup>

An example of artificial antenna system is the one reported in figure 1.5 (a) by Akkaia *et al.*<sup>7</sup> In this system, four BODIPY were linked *via* Click chemistry to a perylenediimide (PDI) core. In this light-harvesting dendrimer, excitation energy is efficiently channelled from the BODIPY to the PDI core. Akkaya *et al.*<sup>8</sup> also proved in 2010 that increasing the number of the BODIPY from 4 to 8 enhances the efficiency of the process (Figure 1.5, b).

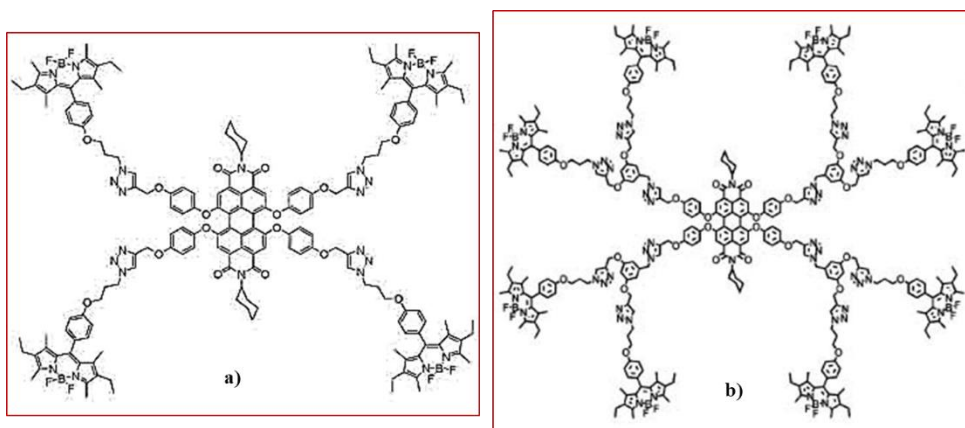


**Figure 1.5:** Tetra BODIPY-PDI artificial antenna system (a); octa BODIPY-PDI artificial antenna system (b).

As it concerns TBET system, first studies of systems involving BODIPY as donor unit and porphyrin as acceptor, were made by Lindsey<sup>9</sup> (Figure 1.6, a). Due to the energy transfer occurring along the conjugate system, this TBET arrays have been described as molecular wires. Despite the distance between the donor and acceptor, an efficient energy transfer still occurs with almost 70 % efficiency.

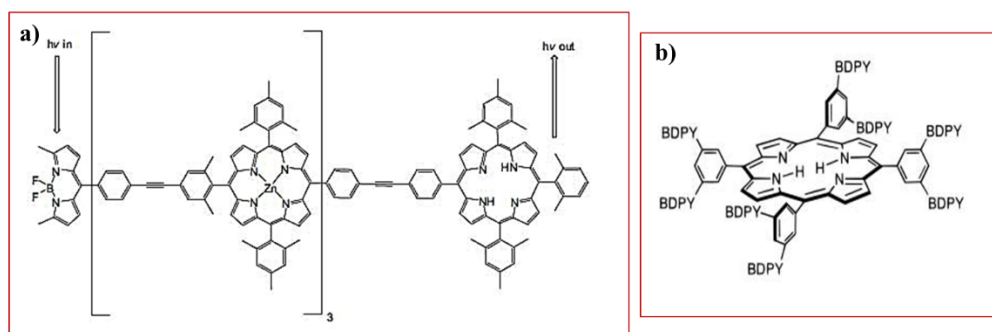


**Figure 1.6:** Molecular wire (a); multi-BODIPY-porphyrin-array (b).

Since then, a series of through-bond energy-transfer cassettes with multi-BODIPY-porphyrin-arrays has been synthesised, in order to increase the antenna effect of the BODIPY units.<sup>10</sup> One, two four and eight multi-BODIPY have been attached, (Figure 1.6, b). As seen for the multi-BODIPY and PDI arrays,<sup>7,8</sup> increasing the number of BODIPY units has little effect on the energy-transfer efficiency.

In 2012 the research group in which I have performed my PhD exploited for the first time the use of carbohydrates as suitable scaffolds to assemble luminophores on a biologically-relevant platform.<sup>11</sup> Bi- and multichromophoric systems, based on two different BODIPY linked to an enantiopure  $\alpha$ -D-glucopyranoside platform, were synthesized and spectroscopic features were studied.

In these multi BODIPY systems, ultrafast energy transfer takes place from the high-energy BODIPY colored in red to the lower-energy one, the green

BODIPY. Particularly after excitation, all the energy is channelled to the emitting chromophor, with 100% yield of the transfer process, resulting in an emission around 770 nm, thus making this multi-chromophoric system particularly interesting from a biological point of view (Figure 1.7).

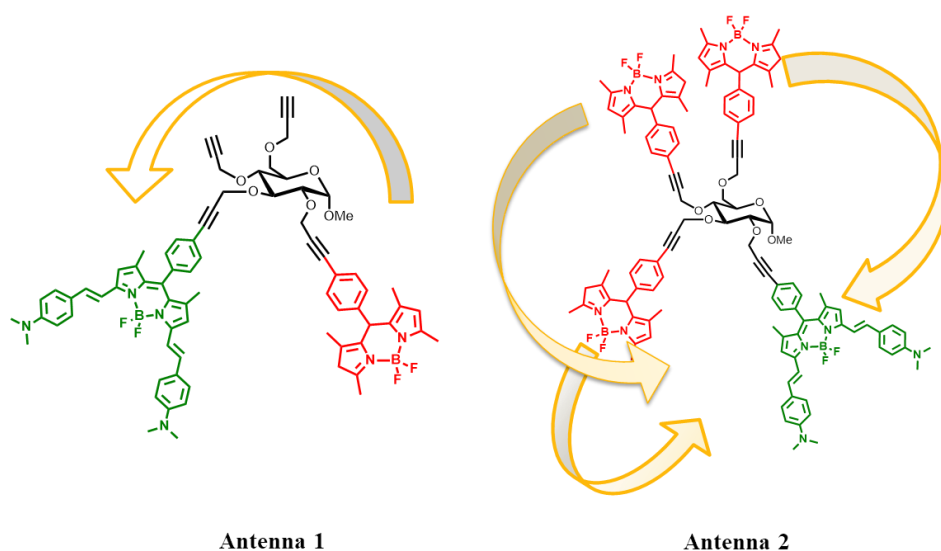


**Figure 1.7:** Carbohydrate based BODIPY and multi-BODIPY artificial antenna systems.

## 1.2 Carbohydrates

Carbohydrates, the most abundant naturally occurring molecules, are present in all kind of organisms and beside their structural and metabolic task, they are involved in wide range of physiological and pathological processes, including viral and bacterial infections, immune response, autoimmune disorders and chronic inflammations.<sup>12</sup> The effects of carbohydrates on these processes depend on the carbohydrate binding activity of proteins, and thus carbohydrate-binding sites represent attractive targets for drug design.<sup>13</sup> Figure 1.8 reports a short number of biological active carbohydrates.<sup>14</sup>

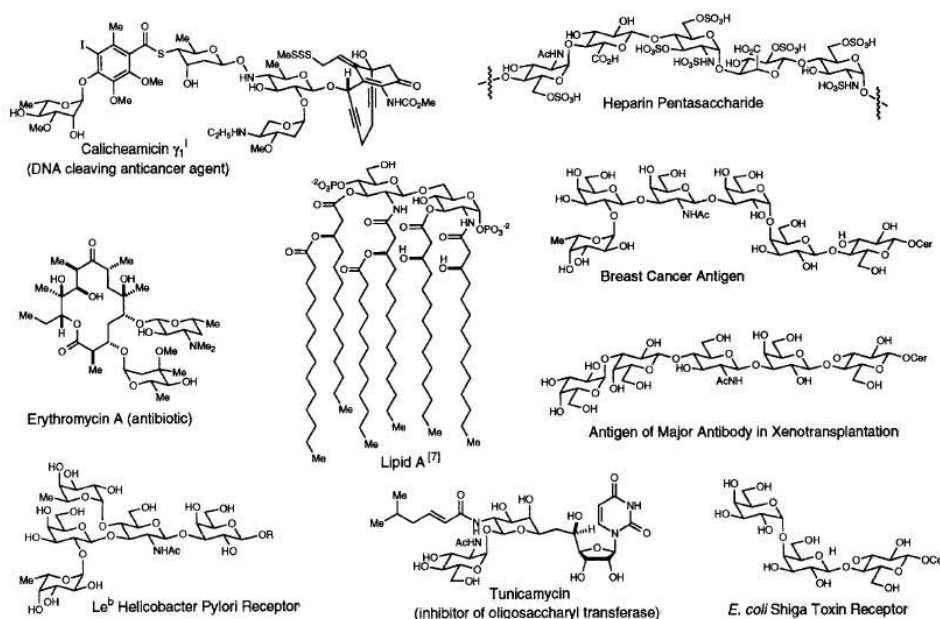


**Figure 1.8:** Examples of biological active carbohydrates.

Carbohydrates are also extremely important for processes involved in cell transformation and tumour genesis. Almost a century ago, the scientist Otto Warburg discovered that cancerous tissues consume large amounts of glucose compared to non-transformed tissue and have high rates of aerobic glycolysis.<sup>15</sup> Glucose transporters (GLUTs), which are located on

membranes of endothelial cells and facilitate the entry and the diffusion of glucose and other carbohydrates into cells, are widely overexpressed in human cancers. One promising strategy for drug design is glycoconjugation: the linking of a drug to glucose or other mono- and disaccharides. The synthesis and evaluation of sugar-conjugated anticancer drugs was first reported in the literature in 1995, with conjugate glufosfamide, explicitly designed and evaluated as a cancer-targeting cytotoxic compound. Glufosfamide (Figure 1.9) was developed to decrease the toxicity and increase the cancer selectivity of its aglycone, the DNA alkylating agent ifosfamide mustard.<sup>16</sup>

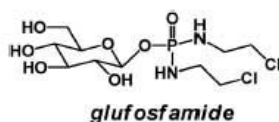


**Figure 1.9:** Molecular structure of glucofosfamide.

Since then, this field has grown exponentially and other sugars such as galactose, mannose, fucose, etc., have been used as powerful scaffolds, installed on drug molecules, for targeting specific tissues including brain and liver cancers.<sup>17</sup>

From a synthetic point of view, carbohydrates present a rigid structure made up of one or more furanose and/or pyranose cycles with various hydroxyl groups having different orientation depending on the type of saccharide. Each hydroxyl group can be linked to suitable molecules or can be opportunely transformed into a different functional group, generating multiplicity of different compounds (Figure 1.10).

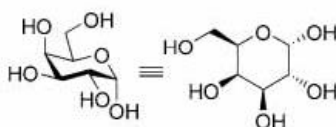


**Figure 1.10:** Structure and spatial orientation of a pyranose-like carbohydrate.

From a biological point of view, the position of the hydroxyl groups in a given monosaccharide creates a distinct binding pattern with its regulatory protein, so any substitution could impact on their biological function. Hergenrother *et al.*<sup>18</sup> reported in their review, for example, a simple scheme that summarizes the effect that glucose substitution could have on the activity on GLUT transporters (Figure 1.11).

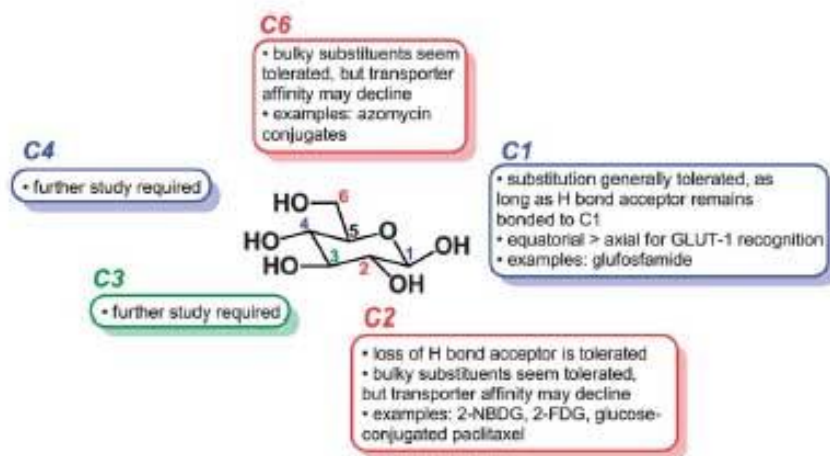


**Figure 1.11:** Structure-activity relationship of D-glucopyranose as a substrate for the GLUT-1 transporters.

With the aim of targeting carbohydrate metabolism in the discovery process of new therapeutic anticancer agents, Bonaccorsi *et al.*<sup>19</sup> reported in 2009 and 2012 the obtainment of bis- $\beta$ -D-glucopyranosides containing thioalkane or thioarene spacers of different lengths and flexibility and the results of biological tests conducted on some of them. The general prototype of a glycoconjugate comprises a core molecule that serves as an oligovalent scaffold, sugar moieties, and suitable spacers that link the sugar moieties to the central core. The presence of sulfur atoms in the skeleton of glucoconjugates, such as those reported in figure 1.12, offers the opportunity to vary the oxidation state of sulfur atoms and to study the effect that this



variation can play on the biological profile of the corresponding thioglucoconjugates.

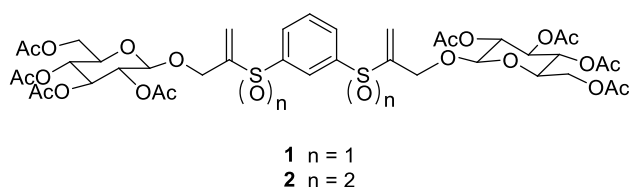


**Figure 1.12:** Thioglucoconjugated sulfoxide and sulfone.

Two compounds of this family showed specific cytotoxic potential attributable to induction of cell death by apoptosis. Moreover, the obtained data on the biological activity of this new class of compounds indicate that their effects vary according to their molecular structure. Control of molecular architecture and saccharide spacing could play a significant role on the enhancement of the apoptotic activity and for these reason authors introduced into the molecular skeleton of compounds, similar to the ones shown before (Figure 1.12), the disulphide bond which is present in many biological systems and is hydrolysis-resistant. A series of glyconjugated disulphide were synthesized (Figure 1.13), bearing two or three disulphide arms connecting to glucose or galactose moiety, and biological evaluation on various cell lines were performed.

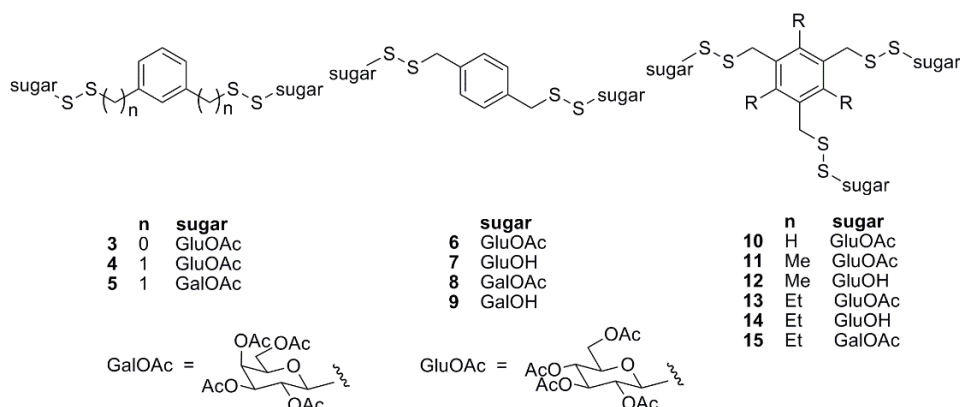


**Figure 1.13:** Glyconjugated disulphide.

The biological studies on the synthesized molecules showed that some of the galactoconjugates bis(disulfides) depicted in figure 1.13, specifically cause cell death ascribed to apoptosis on cancer cells like U937 histiocytic lymphoma cells. In particular, the significant and comparable effect of apoptotic death on U937 cells caused by compounds 5 and 8 of the figure was further characterized by investigating the expression impact of the anti-apoptotic Bcl-2 protein on apoptosis induced by bis-disulfide 8. These experiments indicated that apoptosis induced in U937 cells by this new class of compounds corresponds to the classical, Bcl-2-sensitive, mitochondrial-dependent, intrinsic form of apoptotic cell death. Incidentally, the effect of inducing apoptotic the cell death of compounds 5 and 8 was extended to a panel of human cancer cell lines, some of which are considered as very aggressive and resistant to chemotherapeutic agents. Finally, the apoptotic effect of bis-disulfide 5 on U937 cells was compared with that exerted on non-malignant cells, using peripheral blood mononuclear cells (PBMCs) from healthy donors. Levels of apoptosis detected on PBMCs were appreciable only after 48 h incubation at the high concentrations and even in this case they were significantly lower than those observed in U937 cells.

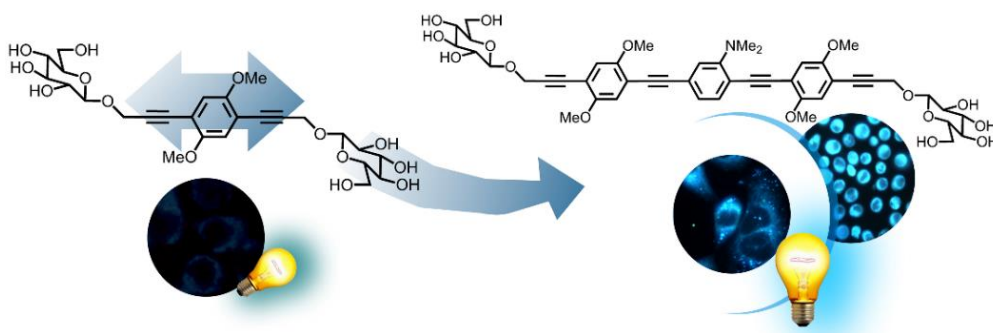


**Figure 1.14:** GlycoOPEs used as photosensitizers in PDT.

More recently, in 2014, Barattucci *et al.*<sup>20</sup> designed and synthesized a number of end-glucose functionalized OPEs [oligo(phenylene ethynylene)s] structures, a class of luminescent dyes with stable,  $\pi$ -conjugated, rigid rod like skeletons, and reported their ability to permeate the cellular cancer membrane and to localize in cytoplasmic organelles. Biological evaluation tests demonstrated that some of these OPEs derivatives were non-cytotoxic, and can be used as biocompatible photosensitizers targets in PDT, against HeLa and HEp-2 tumour cell lines. The presence of hydrophobic (aryl conjugated fragments) and hydrophilic (glucose) moieties in these structures facilitate cellular membrane permeation (Figure 1.14).

### 1.3 BODIPY

The term BODIPY usually refers to a well-known class of compounds derived from 4-4'-difluoro-4-bora-3a-4a-diaza-s-indacene, first discovered in 1968 by Treibs and Kreuzer.<sup>21</sup> These compounds are dyes that strongly absorb in the UV region with high molar extinction coefficients and emit with sharp fluorescence peaks and high fluorescence quantum yields. They are stable to pH, possess good thermal and photochemical stability, and small modification of the skeleton enable the tuning of their spectroscopic characteristics.<sup>22</sup> Application fields of BODIPY are numerous, from biology for labelling proteins, to optoelectronics to construct electroluminescent devices.<sup>23</sup>

The simplest member of the family has the structure reported in figure 1.15, and it is commonly described as a boradiazaindecene for the analogy with the tricyclic structure of s-indacene. The numbering of the substituents follows the rules set up for the carbon poly-cycles, while the 8 position is called *meso* for the analogy with the porphyrinic system,  $\alpha$  and  $\beta$  position are the same used for the dipyrromethane.

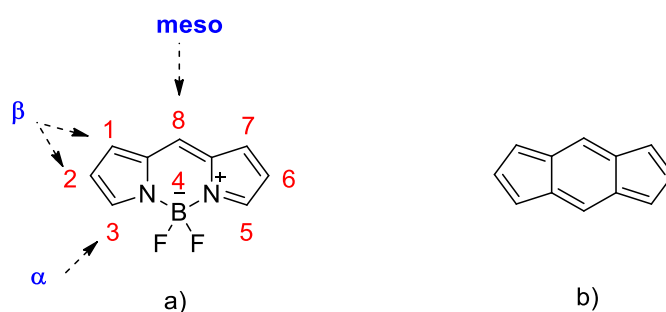
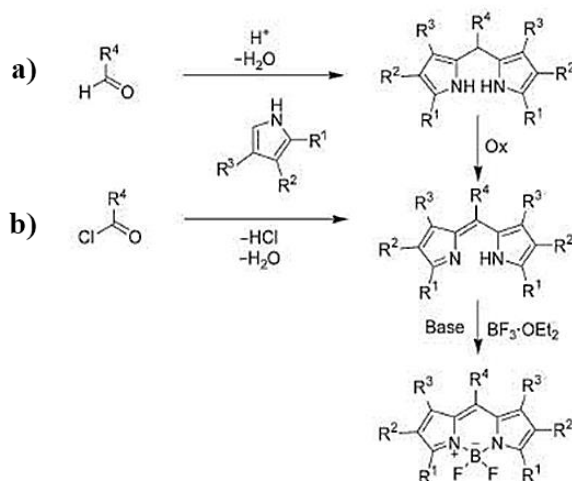


**Figure 1.15:** BODIPY “core” (a); structure of s-indacene (b).

Starting from commercially available pyrrole-based materials, it is relatively easy to obtain a multitude of boron-dipyrromethene modified dyes. The general synthetic path is showed in scheme 1.1.



Scheme 1.1

The first reaction is a pyrrole condensation with an electrophilic carbonyl compound. If the carbonylic compound is an aldehyde (Scheme 1.1, a) the dipyrromethane intermediate is obtained and subsequently oxidised to dipyrromethene. Otherwise, if the carboxylic compound is an acyl chloride (Scheme 1.1, b), the dipyrromethene intermediate is directly obtained. Last reaction, the complexation using  $BF_3OEt_2$ , leads to the desired BODIPY.<sup>24</sup>

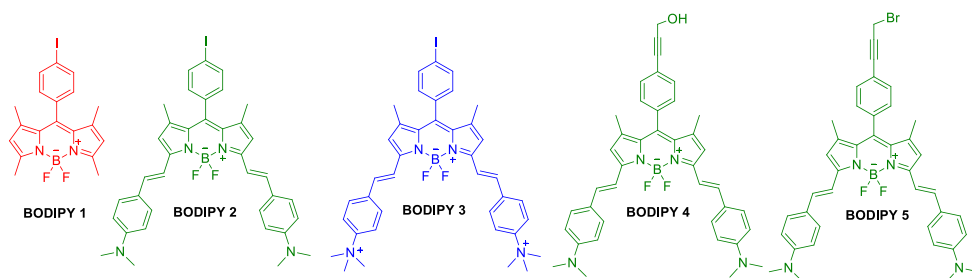
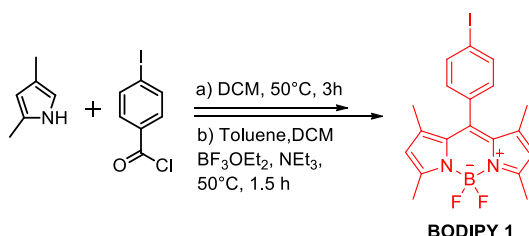


**Figure 1.16:** The chemical structures of the used BODIPY dyes.<sup>1</sup>

<sup>1</sup> The colour of the figure is representative of the colour of the compounds at the solid state, so we usually refer to these products as red, green and blue BODIPY.

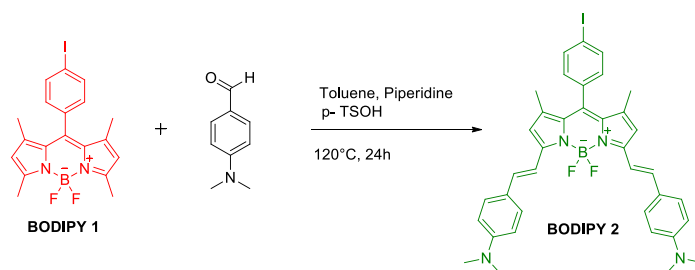
In this thesis I've used the BODIPY derivatives reported in figure 1.16 and their synthesis is described as follows.

**BODIPY 1** was obtained in 60% yield, modifying a one-pot procedure already reported in literature (Scheme 1.2).<sup>25</sup>



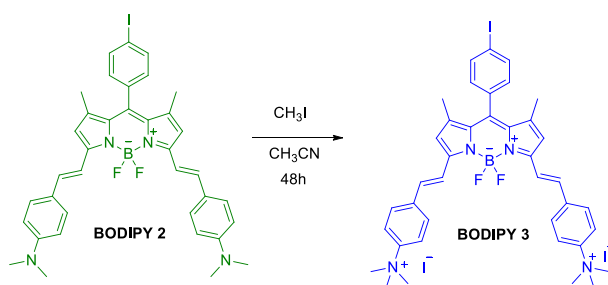
**Scheme 1.2**

**BODIPY 2** can be obtained from **BODIPY 1** by condensation with 4,4'-dimethylaminobenzaldehyde (Scheme 1.3).<sup>26</sup> The reported yield for this reaction is around 60%, however I obtained almost quantitative yield by leaving the reaction for 48h with a Dean-Stark apparatus.



**Scheme 1.3**

**BODIPY 3** was obtained in quantitative yield by methylation of **BODIPY 2** with iodomethane (Scheme 1.4).<sup>26</sup>



**Scheme 1.4**

**BODIPY 4** and **5** are not yet reported in literature, their synthesis will be discussed in chapter 2 of this thesis.

As said before, biological application requires dyes that emit over 600 nm and water-soluble derivatives, for these reasons, since their first discovery, efforts have been made for the synthesis of new BODIPY derivatives with improved stability, low cytotoxicity and enhanced photophysical properties. In 2013 Vincente et al.<sup>27</sup> reported the synthesis of a series of new Near-IR BODIPY-PEG and carbohydrate conjugates. These compounds, reported in figure 1.17, emit in the range of 642-732 nm and due to the presence of the sugar, showed enhanced cellular targeting and permeability. The result shows that BODIPY conjugates accumulated within the cells about 5 times more than the corresponding BODIPY. Furthermore, *in vitro* cellular investigations using human carcinoma HEP2 cells indicate that all BODIPY conjugates are cell permeable, localize preferentially in the cell endoplasmatic reticulum (ER), and are non-cytotoxic, up to 100  $\mu$ M concentrations investigated.

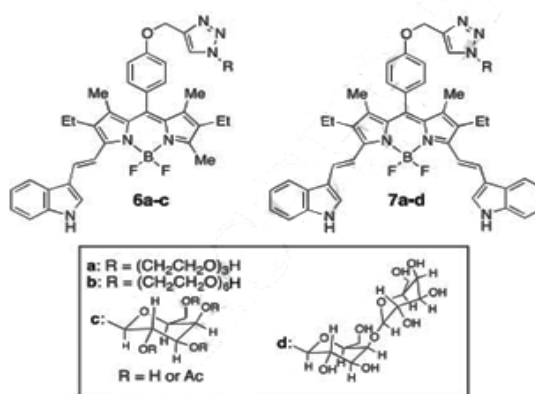


**Figure 1.17:** Structure of Near-IR emitting BODIPY-PEG and carbohydrate conjugates.

Bonaccorsi *et al.*<sup>28</sup> in 2014, reported the cell internalization of a BODIPY-based fluorescent dyes bearing carbohydrate residues. A red-absorbing, distyryl derived BODIPY dye (**BODIPY 3**) free or linked to a sugar platform,

was internalized in VERO cells (African green monkey kidney) and THP-1 (human monocytic) cells. The result of this study showed that the presence of the sugar does not affect the good photochemical properties of the dye and positively influences cell biocompatibility, facilitating the cell internalization. The compounds were not cytotoxic at the very low concentration (1nM) needed. Furthermore, studies of the endocytosis pathway demonstrated that the mechanism of endocytosis for the BODIPY derivatives linked to sugar moiety (Figure 1.18, A and B), is clathrin-dependent and hence inhibited by the presence of sucrose, whereas for the blue **BODIPY 3**, the mechanism of endocytosis is not specific, thus confirming that the presence of the sugar affects the endocytosis pathway.

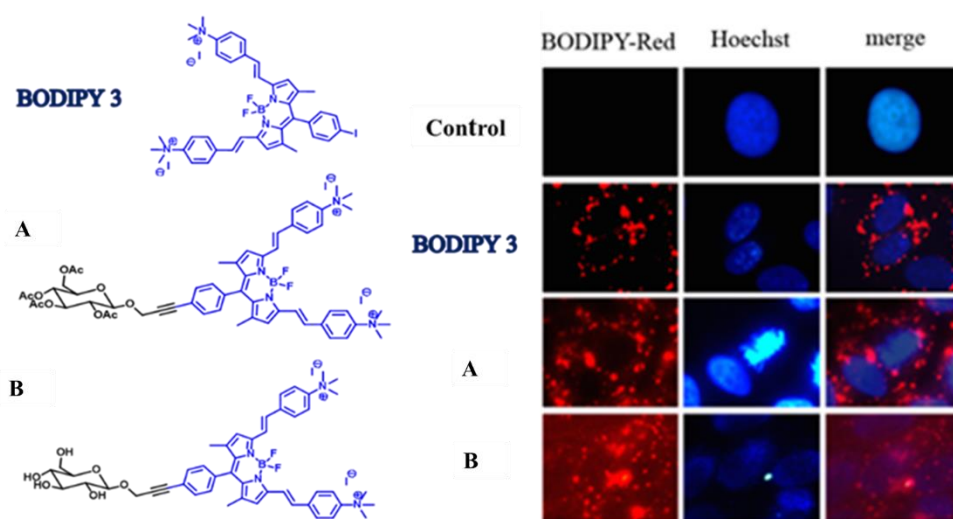


**Figure 1.18:** Internalization imaging of distyryl derived BODIPY dyes (**BODIPY 3**) with protected sugar (A) or deprotected sugar (B) into VERO cells line.



## 1.4 Synthesis of a disaccharide-based bichromophoric species

During the first year of my PhD, to continue the study on carbohydrate-based luminescent probes, I decided to synthesize a new bichromophoric system, constituted of a disaccharide scaffold and two BODIPY derivatives.

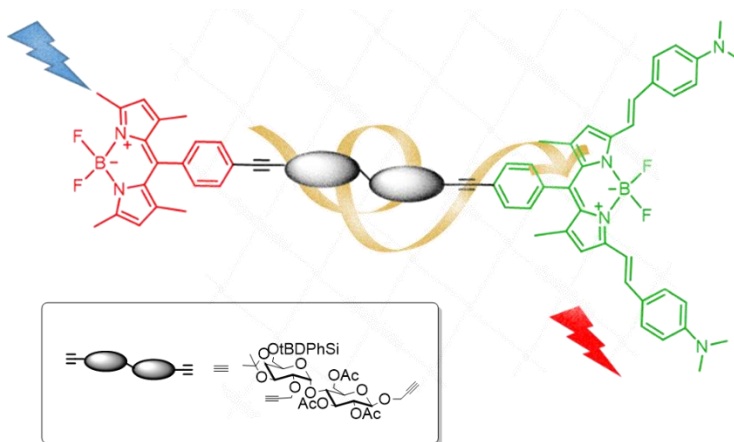


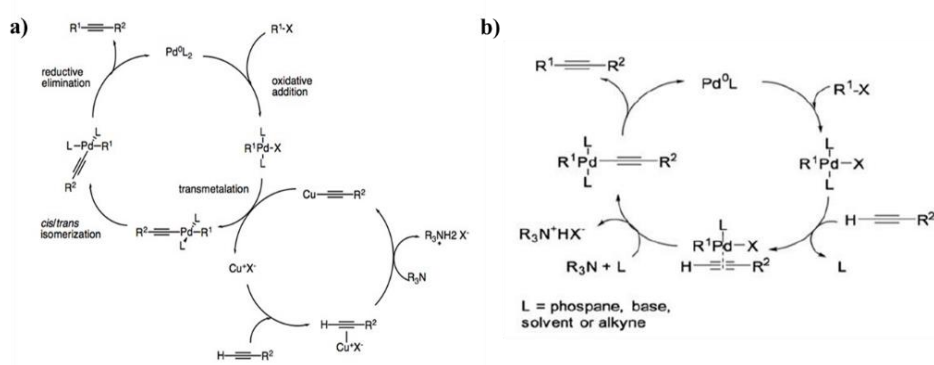
**Figure 1.19:** Schematic representation of a disaccharide BODIPY antenna systems.

In particular, the spacer is a disaccharide made up of D-galactose and D-glucose derivatives. This sugar scaffold has a dual function; it acts as an interface toward biological networks and represents a suitable spacer between donor and acceptor chromophores. In this way, the two chromophores, with different absorption/emission properties, are separated enough to minimize self-quenching, without sacrificing the efficiency of the inter-chromophoric energy transfer and let the molecule function as an efficient artificial antenna system.

The synthesis of this multicomponent system can be rationalized by describing apart the preparation of each of the components. The synthesis of **BODIPY 1** and **BODIPY 2** chromophores is described in paragraph 1.3 (pg. 16-18), while the synthesis of the disaccharide scaffold will be discussed in

this chapter. The final antenna system is built up with sequential copper-free Sonogashira cross couplings.<sup>29</sup>

Briefly, a Sonogashira reaction is an extremely useful reaction in organic chemistry for the formation of new C-C bonds and represents one of the most important method to prepare aryl-alkynes. It is a palladium-catalysed  $sp^2$ - $sp$  coupling reaction between aryl or alkenyl halides and terminal alkynes, and can be conducted with or without the presence of a copper(I) cocatalyst.



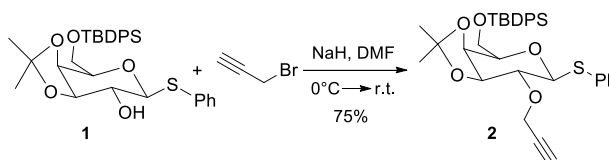
**Scheme 1.5**

The copper-cocatalyzed Sonogashira reaction occurs through two catalytic cycles as shown in scheme 1.5, path a. In the first catalytic cycle, there is an oxidative addition of  $R^1-X$  (aryl or vinyl halide) to the Pd catalyst, thus generating the initial palladium complex ( $R^1-Pd^{II}-L_2-X$ ). The next step in the Pd-cycle connects with the cycle of the copper cocatalyst (the Cu-cycle). Here, a transmetalation from the copper acetylide, formed in the Cu-cycle, generates a  $R^1-Pd^{II}-L_2$ -alkyne species with the elimination of Cu-X. Finally, the desired coupled alkyne is obtained, after reductive elimination, together with the regeneration of the catalyst. The mechanism of the copper-free Sonogashira reaction (scheme 1.5, path b) is not well-known. The first step is the oxidative addition of  $R^1-X$  to the  $Pd(0)$  catalyst. However, the second step is still not clear, the amines generally employed are usually not able to

deprotonate the alkyne; therefore, complexation of the alkyne to the Pd complex is supposed to proceed first with displacement of one ligand. As a consequence, the ligated alkyne would be more easily deprotonated by the amine, forming the new complex  $R^1\text{-Pd}^{\text{II}}\text{-L2-alkyne}$  that undergoes reductive elimination, to provide the coupled alkyne.

In previous experience with these reactions<sup>11</sup> researchers of my group noticed that, if sugars are involved as substrates, yields of the Sonogashira reaction are higher when the use of copper iodide is avoided. For this reason all the Sonogashira reaction reported in these chapter of the thesis will be copper-free.

For the synthesis of the disaccharide scaffold, the preparations of the two monosaccharides are reported separately. For the D-galactose moiety, I started from the galactopyranoside **1**, that I obtained following literature procedure.<sup>30</sup>

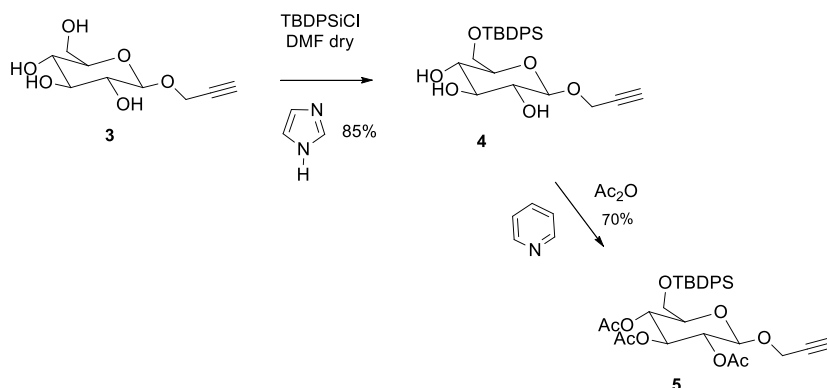


**Scheme 1.6**

Functionalization at C-2 of compound **1** with the alkyne moiety was conducted with 3-bromo-1-propyne in the presence of NaH, in dry DMF. (Scheme 1.6). Purification of the crude by column chromatography with silica gel afforded the functionalized galactopyranoside **2** in good yield.

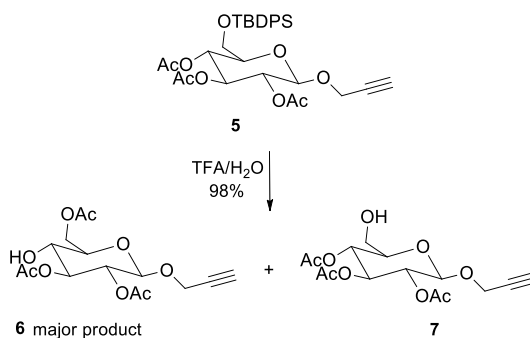
For the D-glucose moiety, I started from the glucopyranoside **3**, that I obtained following a procedure already applied by the research group.<sup>11</sup> To protect the primary alcoholic function of the sugar, glucopyranoside **3** was reacted with *t*-butyldiphenylsilyl (TBDPS) chloride, in presence of imidazole, to obtain the protected sugar **4** that was used without any further

purification. After a protection of the remaining secondary OH groups with acetic anhydride in presence of an excess of pyridine, I obtained glucopyranoside **5** (Scheme 1.7).



Scheme 1.7

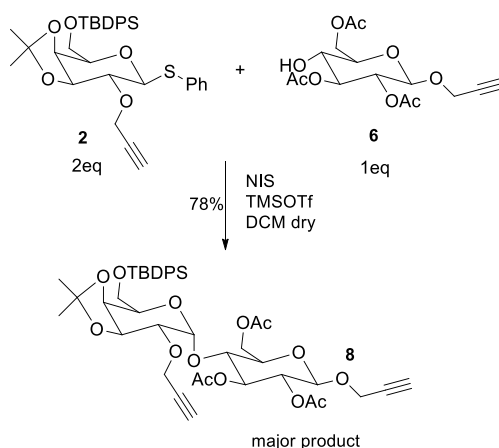
Deprotection of the primary hydroxyl group of sugar **5**, by aqueous trifluoroacetic acid,<sup>31</sup> led to the formation of monosaccharides **6** and **7**, with glucopyranoside **6** as major product (**6:7** 8.5:1), due to the easily migration of acetyl group from C-4 to the primary hydroxyl function at C-6 (Scheme 1.8).<sup>32</sup>



Scheme 1.8

The glucopyranoside mixture **6+7** was purified by column chromatography and anomer **6** was involved in the glycosylation reaction with galactopyranoside **2**. The methodology I've chosen for the glycosylation is

comprise of the mixture of both the donor **2** and the acceptor **6**, addition of the activating agent, N-iodosuccinimide (NIS) and a catalytic amount of trimethylsilyl trifluoromethanesulfonate (TMSOTf), followed by a sonication of the reaction mixture,<sup>33</sup> under argon (Scheme 1.9).



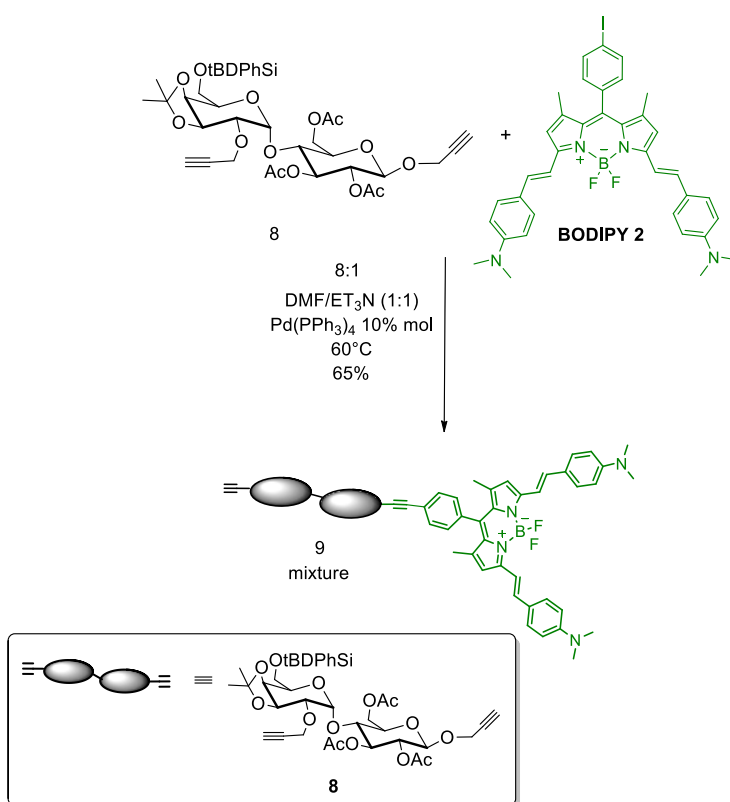
**Scheme 1.9**

The reaction was repeated several times changing solvents and donor/acceptor ratio; the best conditions are reported in scheme 1.9. With these glycosylation procedure I obtained the disaccharide **8** in good yield and with a high  $\alpha$ -selectivity ( $\alpha$ : $\beta$  9:1). The stereoselectivity found was expected on the basis of previous observations on the glycosylation reactions of galactopyranoside donors with various acceptors and various activating systems.<sup>34</sup> In particular, it is well known that NIS/TMSOTf enhances  $\alpha$  selectivity for mannose substrates,<sup>35</sup> but no case were described for its use with glucose substrate.

The carbohydrate based bichromophoric system **10** was obtained with two consecutive copper-free Sonogashira reactions involving disaccharide **8** and the two BODIPY derivatives **BODIPY 1**<sup>25</sup> and **BODIPY 2**<sup>26</sup> (see paragraph 1.3). I've chosen to prepare compound **10** first reacting disaccharide **8** with

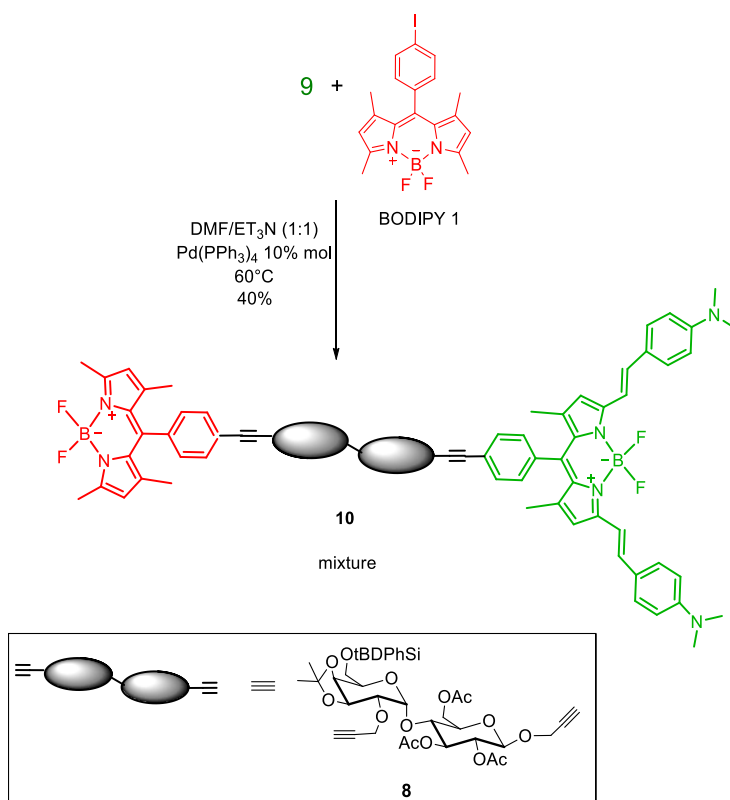
**BODIPY 2** and then with **BODIPY 1**, basing on previous experiences with the building of analogous bichromophoric systems.<sup>11</sup>

The first cross-coupling was conducted using a large excess of compound **8** with respect to **BODIPY 2** (Scheme 1.10), to obtain the glucoconjugate **9**. This compound is a 1:2 mixture of the two possible isomers, the one with the luminescent moiety **BODIPY 2** linked to the triple bond positioned on the anomeric carbon of the glucopyranoside portion, and the other with **BODIPY 2** connected to the triple bond of C-2 in the galactopyranoside moiety.



**Scheme 1.10**

The second copper-free Sonogashira reaction was performed directly on the mixture of disaccharide **9** with an equal amount of **BODIPY 1**, giving the bichromophoric species **10** (1:2 mixture) in 40% yield (Scheme 1.11).



Scheme 1.11

I reasoned about the opportunity to separate the 1:2 mixture of compound **10**, but, taking into account a work founded in literature,<sup>36</sup> I considered that the sugar spacer is small if compared to the BODIPY units and the two luminescent moieties in both isomers are separated by the same distance in the space. Therefore, structural diversity of the two isomers of compound **10** can be considered nullified and the mixture can be regarded as a unique object, as confirmed by the photophysical studies conducted on **10** (see next paragraph).

## 1.5 Photophysical properties of the disaccharide-based bichromophoric species

To determine if the system **10** could work as antenna and to study the properties of this new bichromophoric species, a series of photophysical experiments including absorption, emission and transient absorption spectroscopy, were performed in collaboration with the photochemistry group of Prof. Campagna and Prof. Puntoriero from the Department of Scienze Chimiche Biologiche Farmaceutiche ed Ambientali of the University of Messina.

The spectroscopic behaviour of compound **10** and precursors, **BODIPY 1** and **BODIPY 2**, was studied in solution of acetonitrile (MeCN), and the results are reported in this chapter.

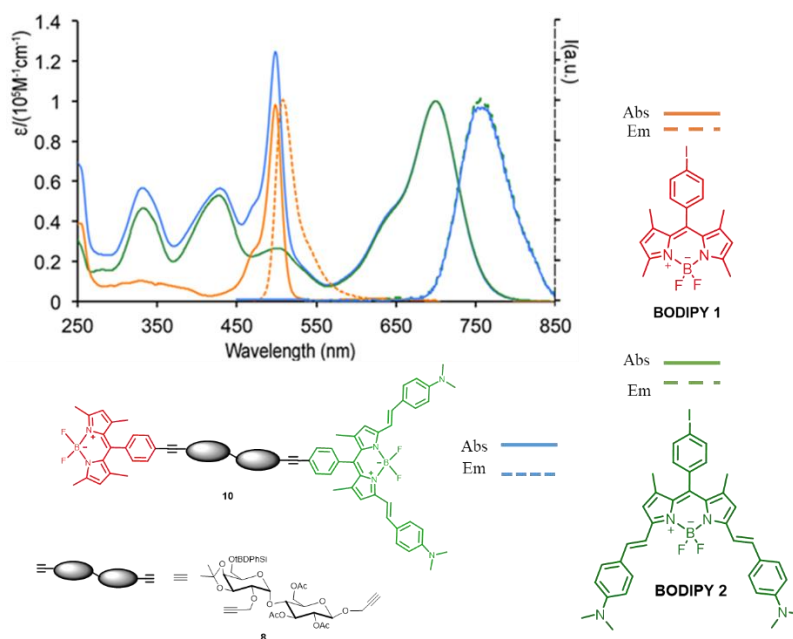


**Figure 1.20:** Absorption spectra in MeCN of **BODIPY 1** (full orange line), **BODIPY 2** (full green line) and compound **10** (full blue line), and their emission spectra (dashed lines).



The absorption spectrum of **10** in acetonitrile solution at room temperature exhibits features that, on the basis of literature data,<sup>11</sup> can be assigned to  $\pi$ - $\pi^*$  spin-allowed transitions involving the two BODIPY frameworks. In particular, the band with absorption maximum at around 500 nm is assigned to the red **BODIPY 1** moiety, whereas the lowest-energy absorption band around 700 nm is centred on the green **BODIPY 2** subunit.<sup>11</sup> By comparison with the absorption spectra of the two precursors, **BODIPY 2** and **BODIPY 1** (Figure 1.20), the absorption contribution of the two BODIPY fragments are essentially additive in **10**: this indicates that each chromophoric subunit retains its spectroscopic properties in the multicomponent system, and that inter-chromophoric interaction is weak, so confirming the supramolecular nature of **10**. The luminescence spectrum of **10** in MeCN is characterized by an intense fluorescence band with maximum at about 770 nm that is almost identical to the one exhibited by **BODIPY 2** (Figure 1.20), independently of the excitation wavelength used. For this reason, this emission is attributed to the deactivation of the excited state localized on the lowest-energy **BODIPY 2** component.

The quantum yield for this emission has been calculated to be equal to 0.2 with an excited state life-time of 2.5 ns.

The corrected excitation spectrum, recorded at 770 nm overlaps with the absorption spectrum of **10**. This and the emission spectrum demonstrate that a very efficient energy transfer takes place in **10** from the highest-energy lying **BODIPY 1** (red-coloured) to the lowest-energy emissive **BODIPY 2** subunit (green-coloured), as shown in figure 1.21.

To study in more detail this photoinduced process, ultrafast transient absorption spectroscopy experiments were performed.

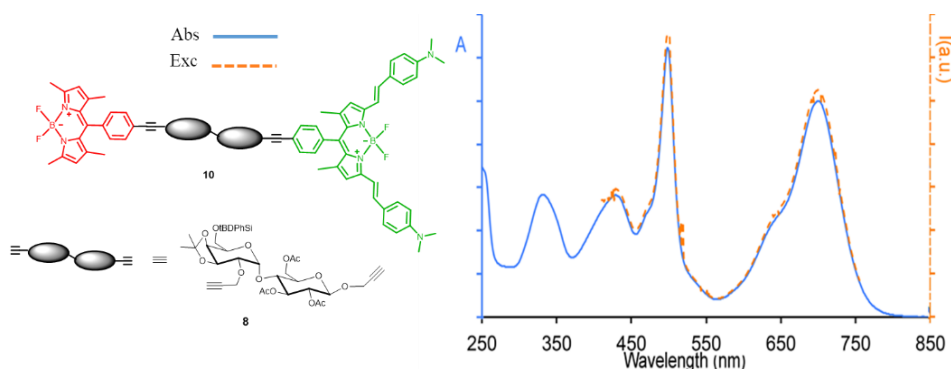


**Figure 1.21:** Absorption (full blue line) and excitation spectra (registered at 770 nm, orange dashed line) of **10** in MeCN.

The initial transient absorption spectrum (TAS), registered after the pump pulse, is characterized by a relatively intense transient absorption band in the range 450-650 nm and a bleaching centred at 700 nm (Figure 1.22). As already demonstrated, these features are the spectral signatures for the presence of the excited state of the green **BODIPY 2** dye.<sup>11</sup>

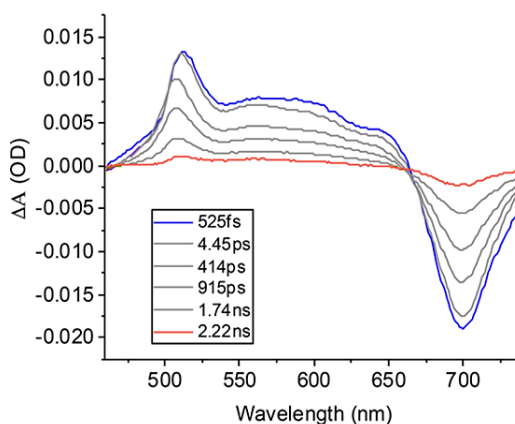


**Figure 1.22:** TAS of **10** in MeCN (100 fs @ 400 nm).

These experiments were performed by using laser pulse of 100 fs at 400 nm as pump. In these conditions, the selective excitation of the high-energy **BODIPY 1** dye (the red coloured) is not possible because of its relative small contribution in absorption at this wavelength, but at times comparable with

the excitation amplitude (15-100 fs) it is still possible to observe a bleaching band at around 500 nm (Figure 1.23).

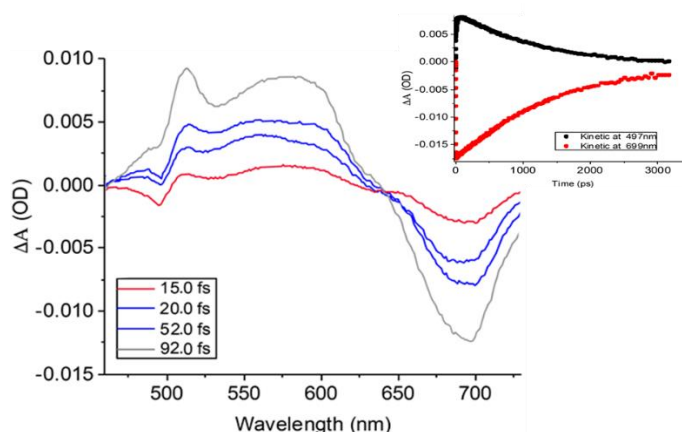


**Figure 1.23:** TAS of **10** in MeCN (100 fs @ 400 nm). Inset kinetics.

This small contribution, representative of the excited state localized on the red **BODIPY 1**, overlays with the absorption band of the excited state of the green **BODIPY 2**. The kinetic (Figure 1.23, inset), registered at 500 nm, shows a fast recover of this apparent bleaching in the tens of ps timescale. This recovery at 500 nm should be concomitant with an increase of the bleaching at 700 nm. Unfortunately, the spectral changes, in this spectral region, in the early times after the excitation, are quite complicated, since the intrinsic excited state decay of the green **BODIPY 2** moiety undergoes a complex kinetic behaviour that includes changes also at 700 nm and overlaps in time with the energy transfer process in compound **10**.

To analyse this behaviour deeply, a global analysis was performed across the whole spectra/time matrix. A clear spectral contribution, located on the red **BODIPY 1** fragment (with 500 nm bleaching) and disappearing in about 28 ps, was observed (Figure 1.24). This consents to attribute the spectral evolution at 500 nm (Figure 1.23) to the inter-BODIPY energy transfer with a rate constant of  $3.57 \times 10^{10} \text{ s}^{-1}$ .

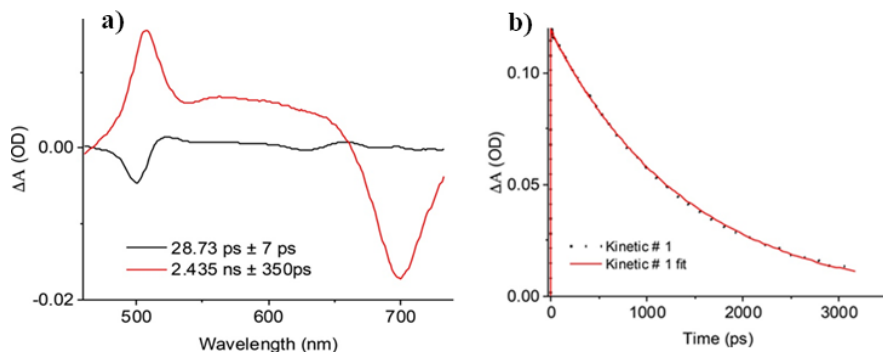


**Figure 1.24:** Global decays analysis (a) and kinetic fitting (b) of compound **10**.

Considering the nature of the chromophores, the spectral overlap between the emission spectrum of the red **BODIPY 1** and the absorption spectrum of the green **BODIPY 2** subunit and the fast rate constants measured, the Förster mechanism is assumed to drive the energy transfer process by about 0.70 eV. By using the simplified Förster equation (eq. 1.1) it is possible to calculate the rate for this energy transfer process.

$$k_{en}^F = 8.8 \times 10^{-25} \frac{K^2 \Phi}{n^4 r_{AB}^6 \tau} J_F \quad \text{eq. 1.1}$$

In equation 1.1,  $k_{en}^F$  is the rate constant of the energy transfer process,  $K$  is an orientation factor which accounts for the directional nature of the dipole-dipole interaction,  $\Phi$  and  $\tau$  are the luminescence quantum yield and lifetime of the donor, respectively,  $n$  is the solvent refractive index,  $r_{AB}$  is the distance (in Å) between donor and acceptor.

Since each BODIPY subunit is freely rotating along the linear axis, the random value for the orientation factor (0.667) is assumed.  $J$  is the overlap integral for Förster interaction, calculated according to equation 1.2:

$$J_F = \frac{\int F(\bar{\nu})\varepsilon(\bar{\nu})/\bar{\nu}^4 d\bar{\nu}}{\int F(\bar{\nu})d\bar{\nu}} \quad \text{eq. 1.2}$$

In particular, using the calculated J value ( $1.70 \times 10^{-13} \text{ cm}^6$ ) and assuming 23.5 Å as the average donor acceptor distance in **10** (distance obtained from optimized CPK modelling), an energy transfer rate constant of 31 ps ( $k_{\text{ET}} = 3.22 \times 10^{10} \text{ s}^{-1}$ ) is calculated for this species, in agreement with the experimental results from the decay global analysis.

## 1.6 Synthesis of a BODIPY-based galactosyl bichromophoric species

To continue the research exploring the use of sugar units in the construction of artificial antenna systems, a D-galactose unit was used as a bridging between two BODIPY units (Figure 1.25). D-galactose was chosen for an easier use of protecting groups with this substrate. No significant change was expected in galactose-mediated inter-chromophoric interactions, in particular as far as energy transfer (ET) is concerned, respect to the D-glucose.<sup>11</sup> The system was designed to contain two BODIPY subunits with largely different absorption and emission spectra, the red coloured **BODIPY 1** and the blue coloured **BODIPY 3** (see chapter 1.3).

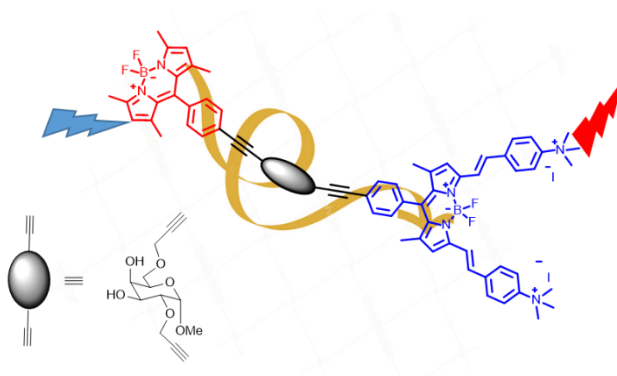


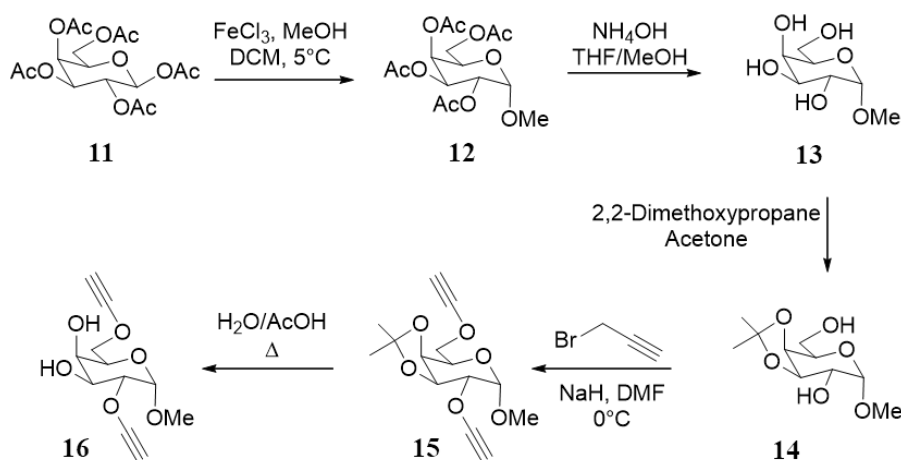
**Figure 1.25:** Schematic representation of the galactosyl BODIPY antenna system.

As previously reported, ET by Förster mechanism could occur in the designed compound from the high-energy dye **BODIPY 1** (the donor) to the lower-energy **BODIPY 3** (the acceptor). Moreover, the **BODIPY 3** subunit is water-soluble and is positively charged, so absorption and emission properties are expected to depend on the environment, as a consequence of its charge and the charge-transfer nature of its excited state(s). This could be

considered a useful tool to obtain environmental-dependent luminescence properties.

The synthesis of the bichromophoric system can be accomplished in the same way described in the previous chapter for the disaccharide-based bichromophoric species. First, I synthesized the carbohydrate platform and then assembled the luminophores systems, using the Sonogashira cross coupling reaction.

The D-galactose platform **16** was obtained following the synthetic pathway reported in scheme 1.12.

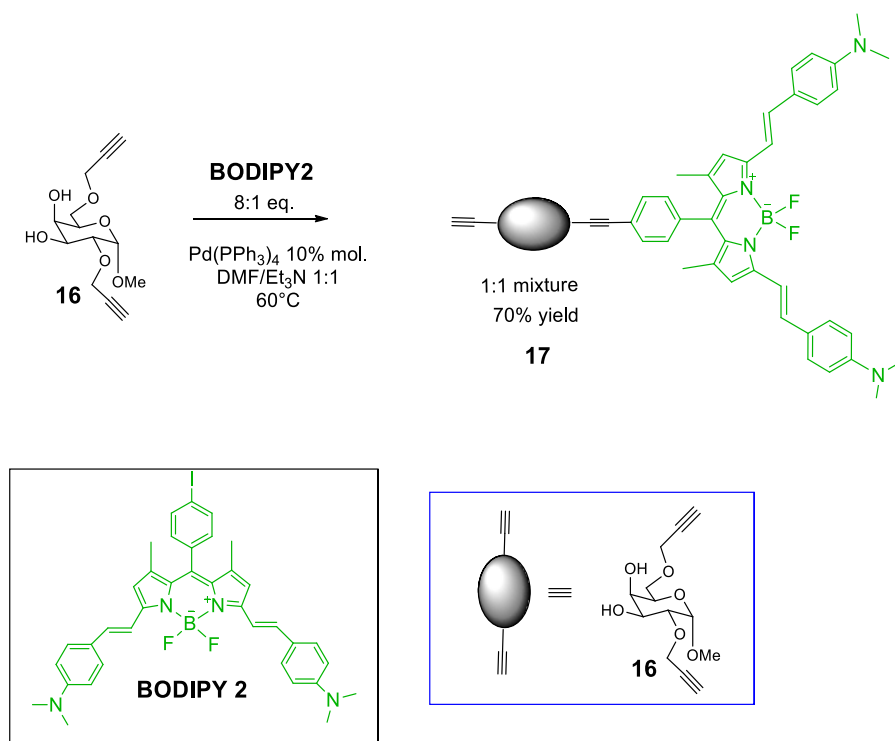


**Scheme 1.12**

Although methyl- $\alpha$ -D-galactopyranoside **13** is commercially available, it was easily obtained from  $\beta$ -D-galactopyranoside pentacetate **11** in two steps.<sup>37,38</sup> First, a selective  $\alpha$  glycosidation, using  $\text{FeCl}_3$  as catalyst, led to **12** in 90% yield, followed by a deacetylation with ammonium hydroxide to obtain **13** in quantitative yield. To get the alkyne functionality in C-2 and C-6, a selective protection on the C-3 and C-4 function of the galactose derivative was done by means of the formation of acetals, so C-4 and C-3 of the pyranose ring of **13** were protected using 2,2-dimethoxypropane in acetone to afford **14**.<sup>39</sup> The alkyne terminal chains at the C-6 and C-2 position

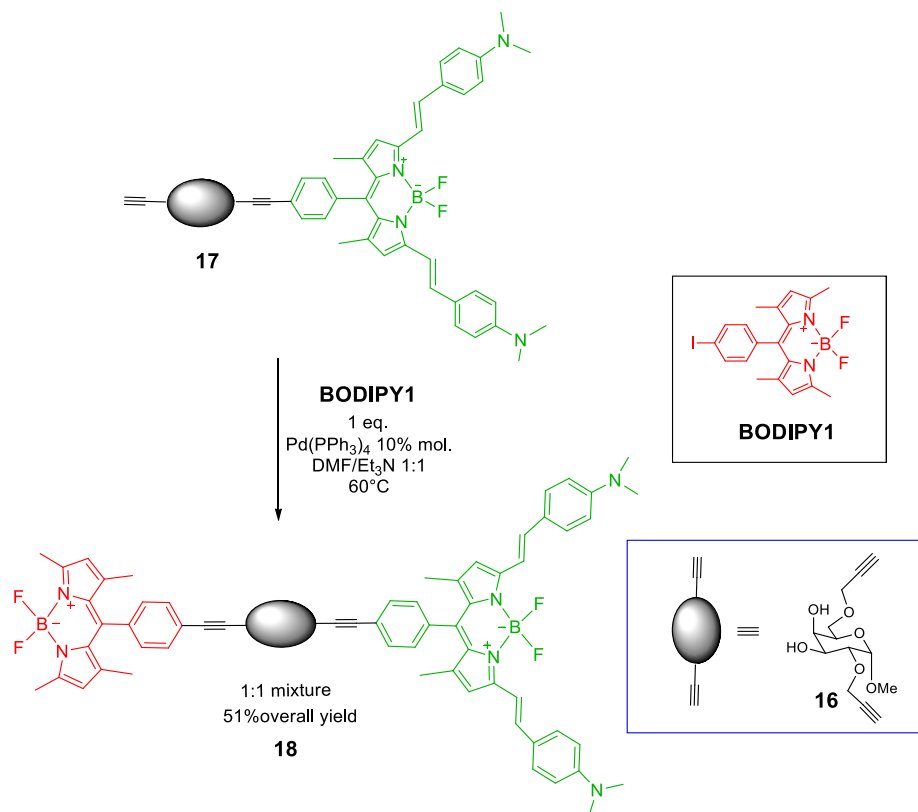
to the D-galactoderivative **14** were added using first sodium hydride to dehydrogenate the hydroxyl function and then propargyl bromide in DMF.<sup>40</sup> Purification of the crude with chromatographic column afforded the desired compound in 75% yield. Finally, hydrolysis in acidic conditions of D-galactopyranoside **15** to remove the protecting group gave us the desired D-galactose platform **16**.<sup>41</sup>

To assemble the bichromophoric platform I performed two consecutive copper-free Sonogashira cross couplings. The first was conducted with an excess of sugar **16** with respect to **BODIPY 2** (8:1 ratio) to obtain the mixture **17** (Scheme 1.13), that, was involved without separation in a second copper-free Sonogashira reaction with an equivalent amount of **BODIPY 1** to give **18** (1:1 mixture) in a 51% two-steps overall yield (Scheme 1.14).



Scheme 1.13



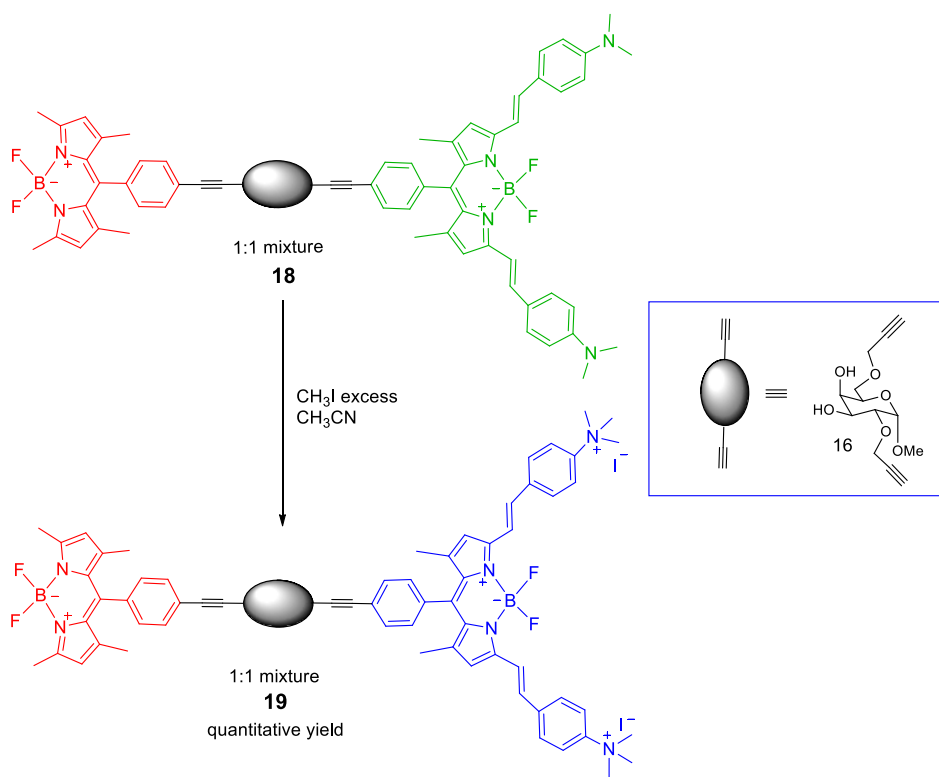


Scheme 1.14

As previously discussed in chapter 1.4, compound **18** is a mixture of the two possible isomers, the one with the luminescent moiety **BODIPY 2** linked to the triple bond positioned on the C-6 carbon of the galactopyranoside portion, and the other with **BODIPY 2** connected to the triple bond of C-2. For the same reasons explained before (paragraph 1.4, pag. 27) I decided not to separate the mixture.

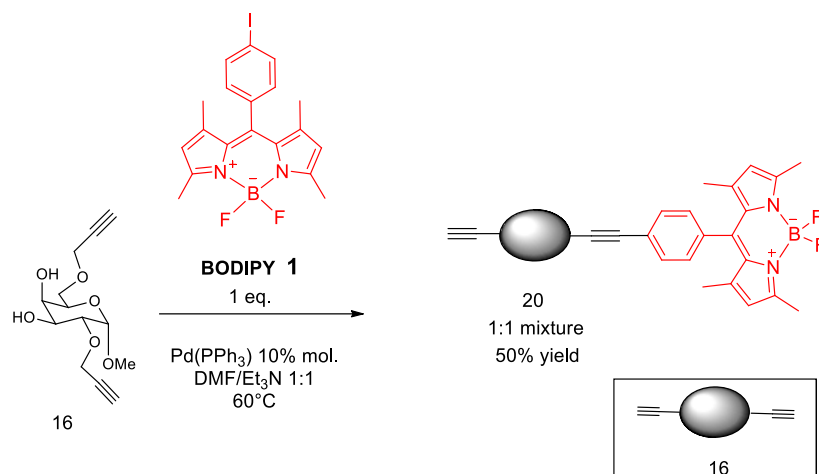
An excess of methyl iodide in acetonitrile was used for the quaternization of the dimethylamino substituents of **18**.<sup>26</sup> This reaction provided **19** in quantitative yields, as 1:1 mixture (Scheme 1.15). The bichromophoric system **19** is water soluble and, therefore, suitable for cellular studies.

To study the photophysical and biological properties of the antenna system **19** it was necessary to compare the spectroscopic behaviour and the cellular up-take of **19** with those of the single subunits.



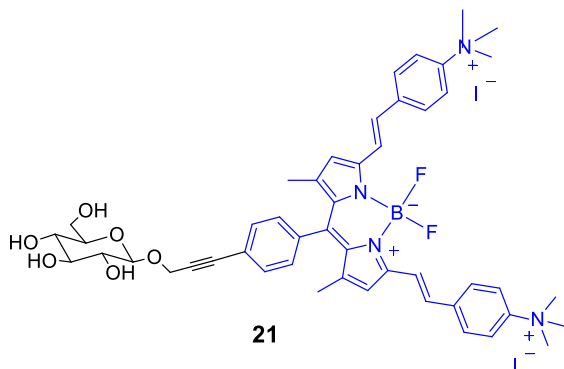
Scheme 1.15

For these reasons we synthesize **20**, the donor red **BODIPY 1** linked to the galactose platform, using again a copper-free Sonogashira cross coupling (Scheme 1.16). Compound **20** was obtained as a 1:1 mixture by reacting **BODIPY 1** with the sugar moiety **17** in 50% yield.



Scheme 1.16

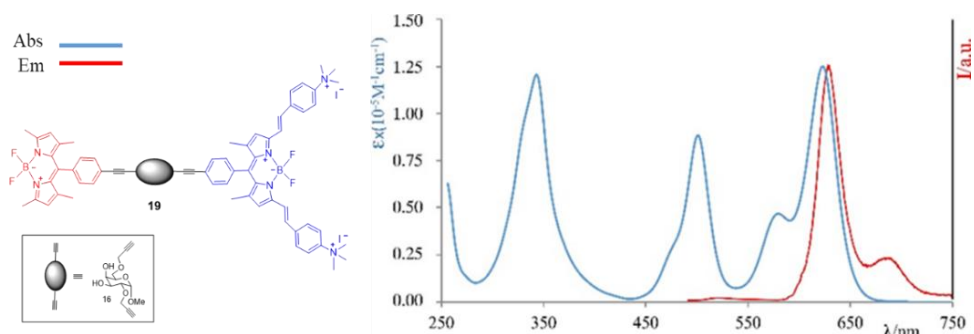
Whereas glucose derivative model **21** in figure 1.26, with the acceptor blue **BODIPY 3** linked to D-glucose derivative, was previously synthesized and its photophysical properties and cellular compatibility studied (paragraph 1.3).<sup>28</sup>

Figure 1.26: Glucose derivative linked to **BODIPY 3**.

## 1.7 Photophysical properties of the BODIPY-based galactosyl bichromophoric species

To study the photophysical properties of this new bichromophoric system and to determine if the system could work as antenna, absorption and emission transient absorption spectroscopy experiments and lifetime measurement were done in cooperation with the photochemistry group of my Department. Spectroscopic study were performed both in organic solvent such as acetonitrile to compare with previous results and in water/ PBS buffer phosphate or oil to mimic the biological (aqueous and lipidic) environments.

The absorption spectrum of **19**, recorded in acetonitrile, can be considered as the sum of to the absorption spectra of the two chromophoric subunits, (Figure 1.27) the donor and the acceptor of the bichromophoric system.



**Figure 1.27:** Absorption (blue) and emission spectra (red) of **19**.

In particular, by comparison with the spectra of the two subunits (Figure 1.28 panel a for the donor and b for the acceptor) the band with absorption maximum at about 500 nm is assigned to the red **BODIPY 1** dye of **20**, whereas the band with maximum at about 620 nm is attributed to the blue, **BODIPY 3** dye of **21**.<sup>11, 26, 28</sup>

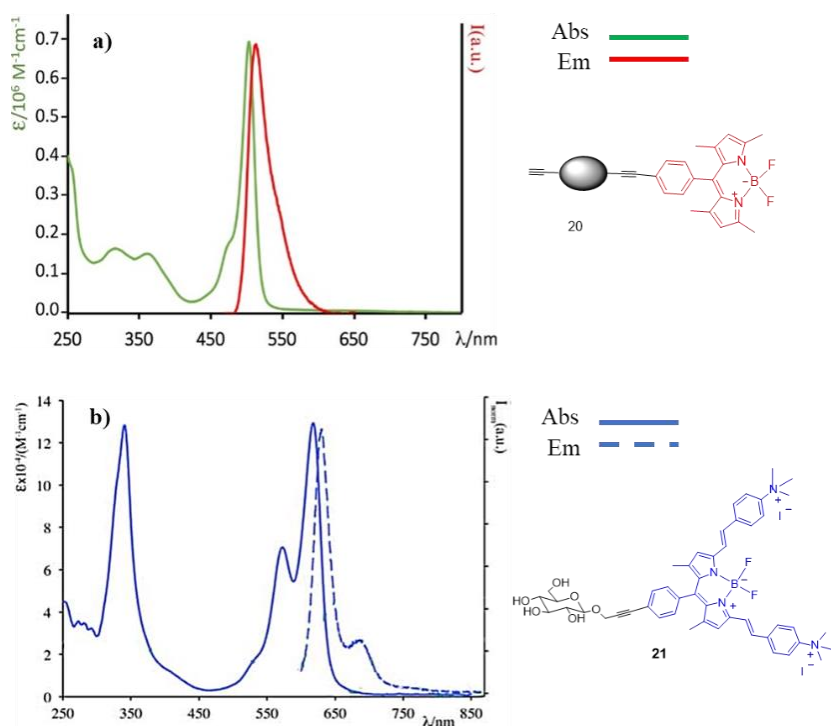


**Figure 1.28:** Absorption and emission spectra of **20** (a); absorption and emission spectra of **21** (b). Spectra recorded in MeCN.

Compound **19** exhibits a relatively intense ( $\Phi = 0.7$ ) emission in acetonitrile solution, with a lifetime of 5.4 ns, almost identical to that of **21**, (Table 1.1) independent of the excitation wavelength. This indicates that fast ET takes place from the (higher-energy) lowest singlet state involving the red **BODIPY 1** dye to the (lower-energy) lowest singlet state centred in the blue **BODIPY 3** dye.

**Table 1.1:** Spectroscopic values characteristic of the compound **19** and subunits **20** and **21**.

Compound	absorption	emission		
	$\lambda_{\text{max}}$ , nm ( $\epsilon$ , $\text{M}^{-1} \text{cm}^{-1}$ )	$\lambda_{\text{max}}$ , nm	$\tau$ , ns	$\Phi$
<b>19</b>	620 (129,100)	630	5.4	0.7
<b>21</b>	618 (129,100)	629	5.3	0.7
<b>20</b>	500(69,200)	510	3.1	0.4

To further study the ET process, Pump-probe transient absorption spectroscopy (TAS) was used. The initial transient absorption spectrum (TAS), registered in MeCN after the pump pulse, is characterized by a transient absorption band in the range 450-650 nm and a bleaching centred at 620 nm. (Figure 1.29).

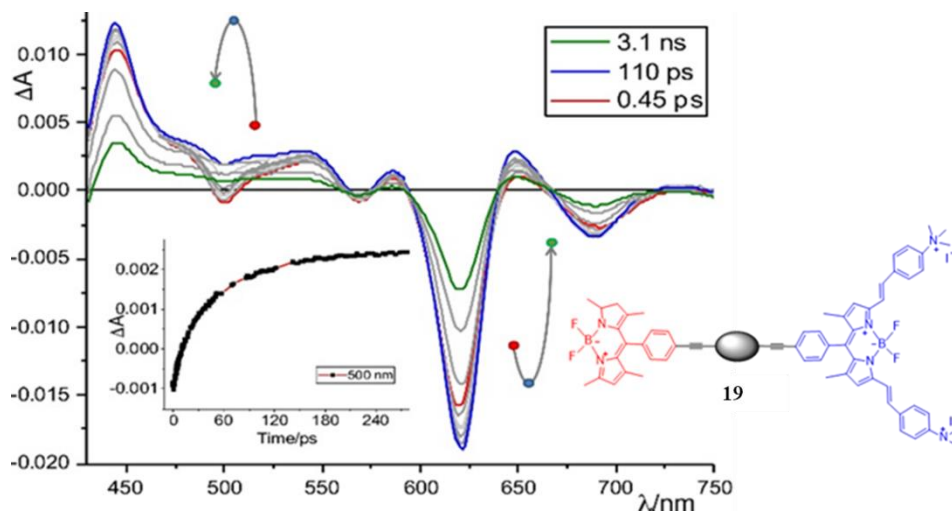


**Figure 1.29:** Transient absorption spectra of **19** in acetonitrile. In the inset, kinetic registered at 500 nm (pulse: 400 nm; 100 fs).

As already demonstrated,<sup>11,28</sup> these bands are the spectral signatures for the presence of the excited state of the blue **BODIPY 3** dye whereas the presence of bleaching band at around 500 nm is typical of the red **BODIPY 1** dye. These were proved also recording the TAS of compound **20** and **21** in which it is possible to observe the typical signature of the two BODIPY dyes (Figure 1.30). The ET process interval can be considered 79 ps. In this small time frame the signature at 500 nm (red **BODIPY 1** dye) disappears and the signature at 620 nm (blue **BODIPY 3** dye) increases. Therefore, the energy is fast and is efficiently transferred (100% efficiency) from the donor red **BODIPY 1** subunit to the acceptor blue **BODIPY 3**.

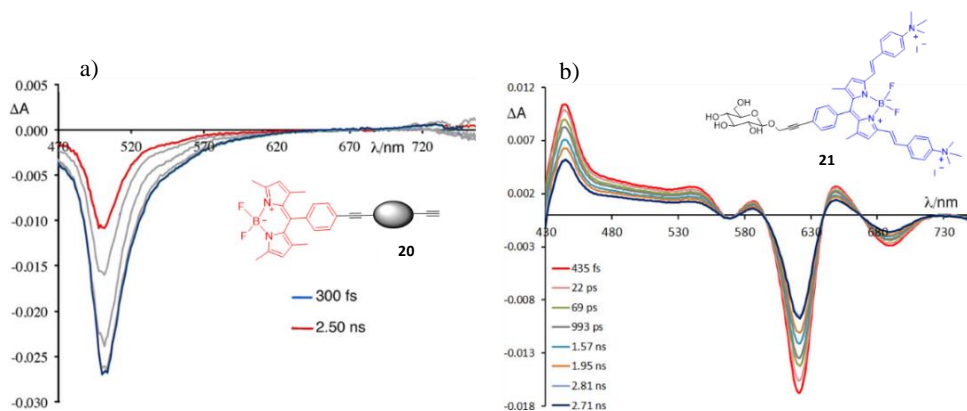


**Figure 1.30:** TAS at different delays of **20** (a); TAS of **21** (b). Solvent MeCN.

The rate constant of ET,  $k_{\text{en}}^{\text{F}}$ , and the spectral overlap integral were calculated using equation 1.1 and equation 1.2 reported in paragraph 1.5 and their values of  $1.3 \times 10^{10} \text{ s}^{-1}$  and  $2.67 \times 10^{-13} \text{ cm}^6$  are in agreement with the Förster mechanism.

To investigate the spectroscopic behaviour of the compound in biological environments, we performed photophysical experiments using water. The recorded absorption and emission spectra in aqueous solution at pH 7 (PBS buffer, Figure 1.31, a), shows a significantly changed situation.

While the absorption spectra remain unchanged, the emission of **19** results to be almost totally quenched, thus confirming the dependence of the excited-state properties of the acceptor blue **BODIPY 3** subunit on the environment. Most likely, water molecule vibrations are strongly coupled with excited-state decay of the polar blue **BODIPY 3** subunit, so promoting fast radiationless decay. This result is quite useful for several reasons: for example, if **19** localizes within hydrophobic environments, its luminescence could be restored (Figure 1.31, a, dotted red line)

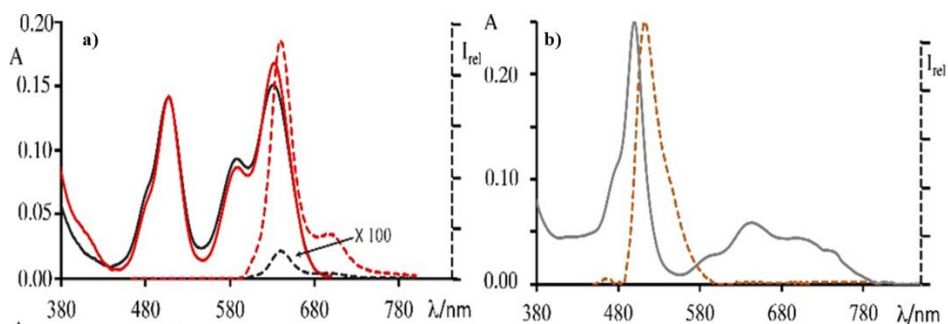


**Figure 1.31:** Absorption (black full line) and emission (100 folded, black dashed line) spectra of **19** in PBS buffer solution; absorption (red full line) and emission spectra (dashed red line) registered after addition of 10 mg/mL of BSA to 2 mL PBS buffer solution of **19** ( $[\mathbf{19}] = 5 \times 10^{-6}$  M) (a); absorption (grey line) and emission (orange line) spectra of **19** in oil ( $[\mathbf{19}] = 5 \times 10^{-6}$  M) (b). Emission spectra were obtained upon excitation at 450 nm.

To mimic the behavior of **19** in biologically relevant environment such as proteins and lipidic sites, we performed spectroscopic and photophysical experiments in oil (for mimicking the lipidic environment) and in serum albumin (BSA, for the proteic environments). Figure 1.31 shows the results: in a proteic environment, the emission of **19** is restored in comparison to the quenched emission in aqueous solution, indicating that the protein protects the emissive state of **19** from the deactivating effect of the aqueous environment. In this condition, the emission properties of **19** ( $\Phi = 0.75$ ,  $\tau = 6$  ns) are similar to those recorded in acetonitrile. The absorption spectrum of **19** in BSA is also close to that in acetonitrile, further confirming the absence of strong interactions of the subunits of **19** with the environment (Figure 1.31, a, dashed red line). A different situation is found in oil: in this condition, the emission spectrum of **19** (Figure 1.31, b) is dominated by the emission of the red **BODIPY 1** dye, so indicating that ET from the red **BODIPY 1** dye to the blue **BODIPY 3** one is less effective. The ET inefficiency is due to a change in the absorption spectrum of **19**, in particular the lowest energy absorption band of the blue **BODIPY 3** dye (approximately 620 nm) becomes broader and less intense with respect to that in acetonitrile or in BSA (Figure 1.27 and



Figure 1.31). The broadness of the absorption spectrum of the acceptor dye reduces the overlapping factor  $JF$  ( $1.21 \times 10^{-13} \text{ cm}^6$ ), and therefore the rate constant of the Förster ET ( $2.4 \times 10^9 \text{ s}^{-1}$ ) that now is almost one order of magnitude slower than in acetonitrile.

The process is reversible, by addition of DCM to the oil solution of **19** absorption and emission spectra that are very close to those recorded in acetonitrile are obtained. In figure 1.32 is now again clearly visible the sharp absorption peak of the blue **BODIPY 3** subunit (Figure 1.28, b). This indicates the reversibility of the process and the restoring of ET process.

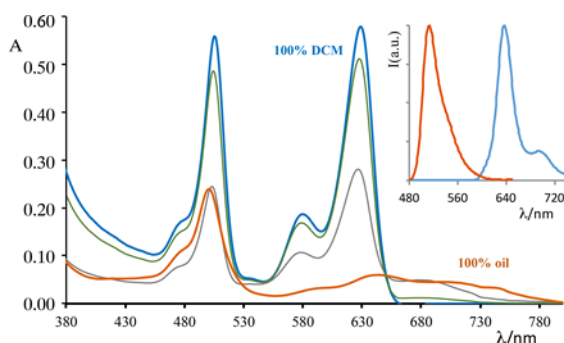


**Figure 1.32:** Absorption (orange line) spectra of **19** in oil ( $[11]=5 \times 10^{-6} \text{ M}$ ), in oil/DCM (4/1 v/v, grey line), in oil/DCM (1/1 v/v, green line) and in DCM (blue line). In the inset: emission spectra in oil (orange) and in DCM solution (blue line).

The combination of all the results of the photophysical experiments recorded in buffered aqueous solution, in lipidic and proteic environments suggests that **19** could exhibit different emission spectra when located in different compartments of biological systems, independently of concentration, an unprecedented feature for a single multicomponent molecule.

## 1.8 Biological properties of the BODIPY-based galactosyl bichromophoric species

Once studied the photophysical properties, the cellular destiny of **19** was investigate, thus a series of biological experiments were performed by Doctors Maurizio Viale and Patrizio Castagnola from the Azienda Ospedaliera Universitaria San Martino, Istituto Nazionale per la Ricerca sul Cancro (IRCCS-IST) of Genova.

Cell labeling and epifluorescence analysis were performed on A2780, human cell lines (ovary, adenocarcinoma). Cells were incubated with **19** for 1h. The results are illustrated in figure 1.33. In green (A, C) is clearly visible that the signal is mainly localized in lipid droplets (arrows) and at a lesser extent in the nuclear envelop and in the ER. In red (B, C) the staining is mainly localized in the nuclear envelop and in the ER

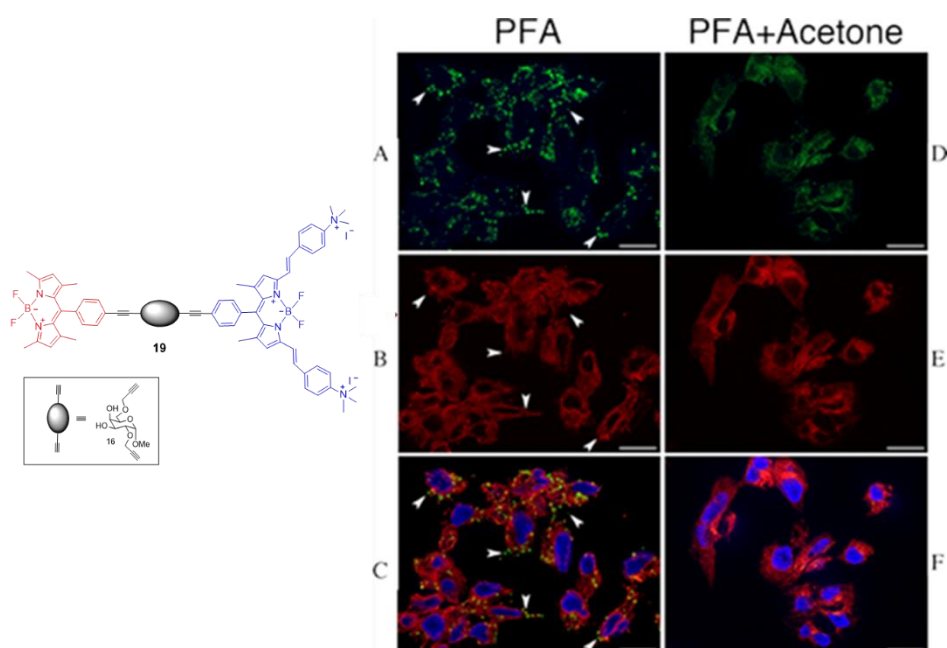


**Figure 1.33:** Cell labeling with **19**. Epifluorescence confocal image of A2780 cells incubated with **19** for 1h and fixation (A-C) or fixation plus acetone treatment (D-F). Nuclei were labeled with Hoechst (Blue signal) (C). Bar = 20  $\mu$ m.

Such a figure shows that **19** illuminates simultaneously two different cell compartments with different emission colors. In particular, **19** illuminates with a green emission, typical of its donor subunit, the red **BODIPY 1**, mainly cytoplasmic lipid droplets and at a lesser extent the nuclear envelope and the ER (Figure 1.33; A, C). Whereas it labels with a red emission, typical of its acceptor component, the **BODIPY 3**, mainly the nuclear envelope and the ER (Figure 1.33; B, C). Acetone treatment, performed after the fixation procedure, dramatically reduces the presence of green-labeled lipid droplets (Figure 1.33; D-F), thus indicating the extraction of the lipid component. Presence of lipid droplets in untreated A2780 cells was confirmed by Oil Red O staining (Figure 1.34). Red Oil O is a diazo-derived dye extremely soluble in lipids and it is used to demonstrate the presence of fat or lipids in fresh, frozen tissue sections by colouring on red the lipidic zone of the cells.<sup>42</sup>

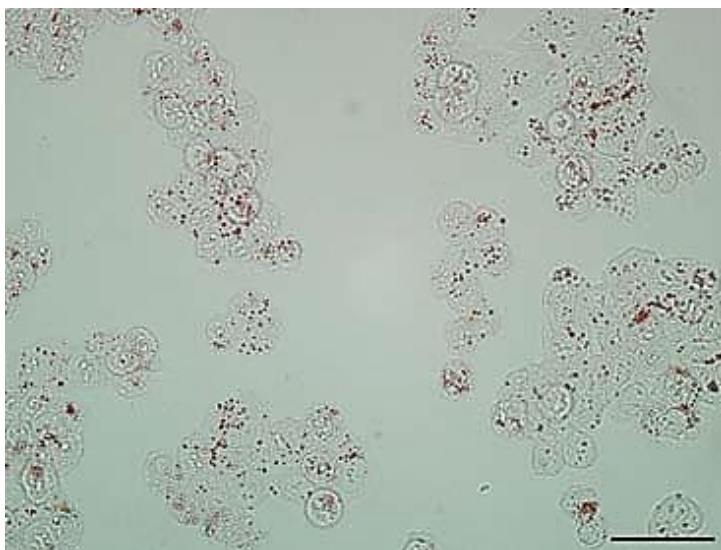


**Figure 1.34:** Red Oil O test performed on A2780 cells.

For completion purposes, and for a further check of our results, the behavior of **20** was investigated on SW480 cells (human colorectal carcinoma): this compound showed a green emission localized in the nuclear envelope and in

the ER as demonstrated by experiment with calreticulin, a resident ER protein, which also mediates nuclear export (Figure 1.35).<sup>43</sup>

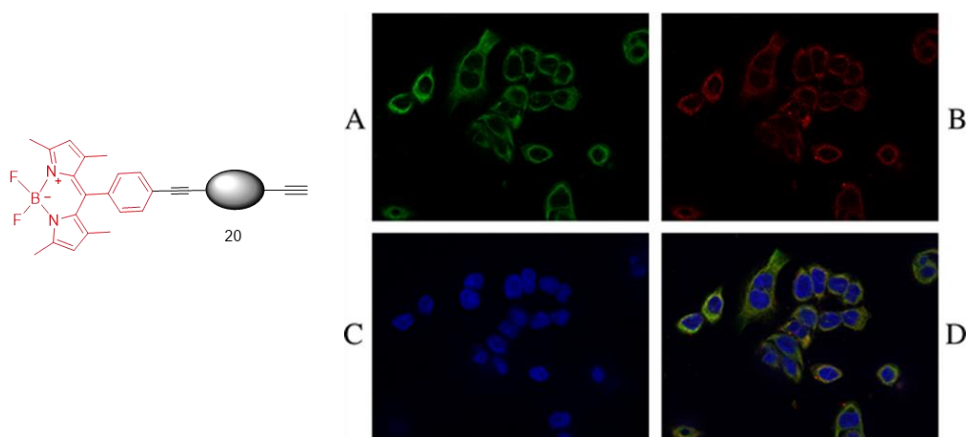


**Figure 1.35:** Cell labeling with **20**. Epifluorescence confocal image of SW480 cells incubated with **20** for 1 h fixed, permeabilized and stained with an anti-reticulin antibody. The green signals are from **20** (A, D) while the red signal reveals calreticulin (B, D). Nuclei were labeled with Hoechst (Blue signal) (C, D).

Bichromophoric species **19** and **20** were then tested to evaluate their antiproliferative activity against five cell lines of different histological origin (Table 1.2). In most cases, both compounds did not show a pharmacologically relevant antiproliferative activity, here defined by  $IC_{50}$ <sup>s</sup> lower than 30  $\mu$ M. This indicates that they could be safely used for imaging purposes.

**Table 1.2:**  $IC_{50}$  values (in  $\mu$ M) for **19** and **20** with different cancer cell lines.

Cell lines	A2780	A549	MDA-MB-231	SKMel28	SHSY5Y
<b>19</b>	18.1 $\pm$ 1.0 (4)	>30 (7)	>30 (4)	26.5 $\pm$ 6.3 (6)	>30 (6)
<b>20</b>	>30 (4)	>30 (3)	>30 (4)	>30 (4)	>30 (4)

## 1.9 Conclusions

---

In conclusion, I have described synthetic approaches to obtain bichromophoric supramolecular systems, with a saccharide core as spacer between two BODIPY units that can act as an energy donor-acceptor dyad.

In compound **10** (Figure 1.19, paragraph 1.4), the spacer is a disaccharide, constituted of D-galactose and D-glucose derivatives linked by a 1,4- $\alpha$ -glycosidic bond, that has been obtained with very good results in terms of stereoselectivity by developing the NIS/TMSOTf/Sonication methodology for the glycosylation, that was extensively studied just for mannose and galactose substrates.

The photophysical results demonstrate that the spatial distance between the two BODIPY units in compound **10** does not preclude their ability to interact in energy transport. A very efficient photo-induced energy transfer takes place in 28 ps from the donor red **BODIPY 1** to the acceptor green **BODIPY 2**, independently from the used excitation wavelength. Noteworthy, **10** emits in the so-called "biological window" 600-900 nm allowing for possible biological applications as dyes of such a family of glycoconjugates since their luminescent characteristics are compatible with *in vivo* studies.

In the bichromophoric species **19** (Figure 1.25, paragraph 1.6) the spacer is a D-galactose unit, obtained in good yield with a few step synthesis. Two different BODIPY subunits were appropriately chosen for the synthesis of **19** in order to enhance its photophysical and biological properties. The donor red **BODIPY 1** subunit, is lipophilic and green emitter, whereas the acceptor blue **BODIPY 3** is water soluble and red emitter. Moreover, **BODIPY 3** is positively charged and its emission properties are related to its charge and to the charge transfer nature of its excited states, resulting in an environmental-depending intercomponent ET. The photophysical measurement performed

in organic solvent, water and oil confirmed this dependence; the ET, highly efficient in aqueous and organic medium, is ineffective in oil.

When internalized in A2780 cancer cell lines, **19** showed an unprecedented property, due to the unusual environmental controlled intercomponent ET. This artificial antenna system can simultaneously and differentially illuminate different cell compartments, staining in red the ER and in green the lipidic droplets. Moreover, these different emission outputs are a function of its cell compartment localizations and are independent on the concentration. This demonstrates that the bichromophoric species **19** can give useful information on cell composition, without requiring the simultaneous use of several different compounds, so paving the way to the use of environment-controlled intercomponent energy transfer for cell information based on luminescence imaging.

## 1.10 Experimentals

---

**General Synthetic Methods.** Solvents were purified according to standard procedures. All of the reactions were monitored by TLC on commercially available precoated plates (silica gel 60 F254) or Alugram® (Alox N/UV 254), eluted with Hexane/EtOAc, DCM/MeOH and MeCN/H<sub>2</sub>O and the products were visualized with vanillin [1 g dissolved in MeOH (60 mL) and conc. H<sub>2</sub>SO<sub>4</sub> (0.6 mL)] and UV lamp. Silica gel 60 and Aluminium oxide neutral Fluka were used for column chromatography. <sup>1</sup>H and <sup>13</sup>C NMR spectra were recorded in acetone-*d*<sub>6</sub> with a Varian 500 spectrometer (at 500 MHz for <sup>1</sup>H; and 125 MHz for <sup>13</sup>C). Chemical shifts are given in parts per million (ppm) ( $\delta$  relative to residual solvent peak for <sup>1</sup>H and <sup>13</sup>C), coupling constants (J) are given in hertz, and the attributions are supported by Heteronuclear Single Quantum Coherence (HSQC) experiments, Correlation spectroscopy (COSY), Nuclear Overhauser Effect Spectroscopy (NOESY), Attached Proton Test (APT). Elemental analysis were determined by a FISON EA1108; in %. Melting points were determined on a Kofler hot-stage apparatus and are uncorrected.

**General Photophysical Methods.** UV/Vis absorption spectra in solution were recorded with a Jasco V-560 spectrophotometer. For steady-state luminescence measurements, a Jobin Yvon-Spex Fluoromax P spectrofluorimeter equipped with a Hamamatsu R3896 photomultiplier was used. For correcting the emission spectra for the photomultiplier response, a program purchased with the fluorimeter was used. For the luminescence lifetimes, an Edinburgh OB 900 time-correlated single-photon-counting spectrometer was used. As excitation sources, a Hamamatsu PLP 2 laser diode (59 ps pulse width at 408 nm) and/or the nitrogen discharge (pulse width 2 ns at 337 nm) were

employed. Emission quantum yields for deaerated solutions were determined using the optically diluted method.<sup>44</sup> As luminescence quantum yield standards, I used a dimethylammonium-phenylstyryl BODIPY species ( $\Phi=0.2$  in MeCN) for compound **10** and trimethylammonium-phenylstyryl BODIPY species ( $\Phi=0.69$  in MeCN) for **19**.<sup>28</sup>

Time-resolved transient absorption experiments were performed using a pump–probe setup based on the Spectra-Physics MAI-TAI Ti:sapphire system as the laser source and the Ultrafast Systems Helios spectrometer as the detector. The pump pulse was generated using a Spectra-Physics 800 FP OPA instrument. The probe pulse was obtained by continuum generation on a sapphire plate (spectral range 450-800 nm). The effective time resolution was around 200 fs, and the temporal chirp over the white-light 450-750 nm range around 150 fs; the temporal window of the optical delay stage was 0-3200 ps. In order to cancel out orientation effects on the dynamics, the polarization direction of the linearly polarized probe pulse was set at a magic angle of  $54.7^\circ$  with respect to that of the pump pulse. All the transient spectra shown are chirp corrected. The chirp correction was done by using the pump induced absorption signals themselves in the same conditions used for each single experiment. All the time-resolved data were analyzed with the Ultrafast Systems Surface Explorer Pro software.

## General Biological Methods

### • *Evaluation of antiproliferative activity*

Human cell lines A2780 (ovary, adenocarcinoma), MDA-MB-231 (breast carcinoma), A549 (lung carcinoma), SHMel28 (melanoma), and SHSY5Y (neuroblastoma) were plated at the desired concentrations (range: 1600-3000/well) into flat-bottomed microtiter plates. After 6-8h



cells were treated with 20  $\mu$ l containing 10X concentrations of 1:10 fold serial dilutions of compounds **11** (starting concentration, 30  $\mu$ M) and **19** (starting concentration, 100  $\mu$ M). After 72 hours cells were stained with MTT (Sigma, St. Louis, MO, USA) as described elsewhere.<sup>45</sup>

IC<sub>50</sub>s were calculated on the basis of the analysis of single concentration–response curves, each final value being the mean of 4-7 independent experiments.

- *Reagents for cell experiments*

The stock solutions of our complexes were prepared in DMSO (30 and 100 mM, 3  $\mu$ l) and then frozen at -20 °C. Before use 3  $\mu$ l DMSO and 294  $\mu$ l distilled water were added in order to achieve the final concentration of 300 and 1000  $\mu$ M. The final concentration of DMSO in the cell culture medium did not exceed 0.2%.

- *Epifluorescence analysis*

Cells were seeded and grown on glass coverslip in growth medium for 16h in 24 multiwells plates for cell culture. Thereafter, the growth medium was discarded and fresh medium, supplemented with the indicated compound at 50 $\mu$ M final concentration, was added in each well. After 1h of incubation in a humidified incubator at 37°C and in a 5% O<sub>2</sub> atmosphere, the medium was discarded and cells were fixed with 3.7% paraformaldehyde in phosphate buffered saline (PBS) containing 2% sucrose (fixing solution) for 5 min at room temperature. After a single wash with PBS, coverslip were either mounted on glass slides with Permafluor Aqueous Mounting Medium (Lab Vision, ThermoScientific, Waltham, MA USA) or subjected to incubation with acetone at -20°C for 5' and a further PBS wash before mounting or processed for immunofluorescence analysis.

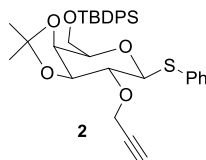
Immunofluorescence staining was performed after fixation with fixing solution. Cells were permeabilized with 20 mM HEPES pH 7.4, 300 mM sucrose, 50 mM NaCl, 3 mM MgCl<sub>2</sub>, and 0.5% Triton X- 100 for 5 min at

0°C. Non-specific binding was prevented by incubation with pure Goat serum for 30 min at 0°C. Coverslips were incubated with the anti calreticulin antibody PA3-900 (Thermoscientific) for 2h at 0°C. An alexa-594 conjugated anti-rabbit antibody (Thermoscientific) was used to reveal the anti-calreticulin antibody. Nuclei were stained with Hoechst 33258 in PBS for 5 min at 0°C. Coverslips were mounted on glass slides as described above. Images were captured using a Zeiss Axio Imager M1 microscope (Carl Zeiss, Jena, Germany) equipped with the fluorescent filter sets: Zeiss 49, Zeiss 10 and Omega XF102-2 (Omega Optical, Brattleboro, VT, USA). Where indicated, optical sections along the z axis were acquired by structured epi-fluorescent illumination, using a Zeiss Apotome module and processed with Axiovision software (Carl Zeiss).

### Synthesis of Compounds 2-8 and 14-16

**Phenyl 3,4-*O*-(1-methylethylidene)-6-*O*-[(1,1dimethylethyl)diphenyl silyl]-2-*O*-2-propyn-1-yl-1-thio-β-D galactopyranoside (2).** To a solution of methyl 2,6-bis-*O*-(tert-butyldiphenylsilyl)-β-D-galactopyranoside **1** (1.5 g, 2.7 mmol) in dry DMF (14 mL) NaH (60% w/w in mineral oil, 0.16 g, 4.1 mmol) was added at 0°C. Propargyl bromide (0.8 mL, 6.8 mmol) was then added slowly and the mixture was stirred at 0°C for 20' and maintained at rt for 3h. TLC (Hexane/EtOAc 80:20) indicated the disappearance of the starting material. The reaction mixture was cooled to 0°C and MeOH (14 mL) was added. The solvents were removed under reduced pressure. The residue was suspended in water and extracted with ethyl acetate. The combined organic layers were washed with saturated aqueous NaCl, dried over anhydrous Na<sub>2</sub>SO<sub>4</sub>, filtered and concentrated under reduced pressure, to give a brown oil which was purified by column chromatography (eluant:

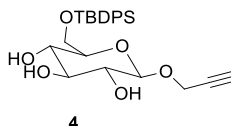
Hexane/EtOAc 50:50) on silica gel. Compound **2** is a pale oil obtained from the reaction crude with 75% yield. *R*<sub>f</sub>: 0.48 (Hexane/EtOAc 80:20).



<sup>1</sup>H NMR: δ 7.8-7.2 (m, 15H, ArH), 4.78 (d, <sup>3</sup>*J*<sub>1,2</sub>=9.8, 1H, H-1), 4.43 and 4.40 (split AB system, <sup>2</sup>*J*<sub>gem</sub>=15.6, <sup>4</sup>*J*= 2.5, 2H, 2-OCH<sub>2</sub>C≡), 4.40 (dd, <sup>3</sup>*J*<sub>3,4</sub>=6.2, <sup>3</sup>*J*<sub>4,5</sub>=2.0, 1H, H-4), 4.28 (t, <sup>3</sup>*J*<sub>2,3</sub> 6.2, <sup>3</sup>*J*<sub>3,4</sub> 6.2, 1H, H-3), 4.20 (ddd, <sup>3</sup>*J*<sub>4,5</sub> 2.0, <sup>3</sup>*J*<sub>5,6A</sub> =5.6, <sup>3</sup>*J*<sub>5,6B</sub> =6.9, 1H, H-5), 3.94 and 3.91 (split AB system, <sup>3</sup>*J*<sub>5,6A</sub> =5.6, <sup>3</sup>*J*<sub>5,6B</sub> =6.9, <sup>2</sup>*J*<sub>6A,6B</sub> =10.4, 2H, H<sub>2</sub>-6), 3.63 (dd, <sup>3</sup>*J*<sub>1,2</sub> =9.8, <sup>3</sup>*J*<sub>2,3</sub> =6.2, 1H, H-2), 2.94 (t, <sup>4</sup>*J* = 2.5, 1H, ≡CH), 1.44 and 1.30 [two s, 6H, OC(CH<sub>3</sub>)<sub>2</sub>], 1.05 [s, 9H, SiC(CH<sub>3</sub>)<sub>3</sub>]. <sup>13</sup>C NMR: δ 135.4, 134.6, 133.1, 133.0, 129.7, 129.6, 129.1, 128.7, 127.6, 127.3, and 126.6 (ArC), 109.4 [C(CH<sub>3</sub>)<sub>2</sub>], 85.0 (C-1), 79.5 (C≡CH), 79.2 (C-3), 77.0 (C-2), 76.5 (C-5), 75.2 (≡CH), 73.7 (C-4), 63.3 (C-6), 57.6 (2-OCH<sub>2</sub>C≡), 27.2 and 25.5 [OC(CH<sub>3</sub>)<sub>2</sub>], 26.1 [SiC(CH<sub>3</sub>)<sub>3</sub>], 18.7 [SiC(CH<sub>3</sub>)<sub>3</sub>]. Anal. Calcd for C<sub>30</sub>H<sub>40</sub>O<sub>5</sub>SSi: C, 69.35; H, 6.85. Found: C, 69.46; H, 6.86.

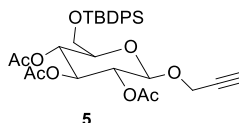
**2-Propyn-1-yl 6-O-[(1,1-dimethylethyl)diphenylsilyl]-β-D-glucopyranoside (4).** Propargyl β-D-glucopyranoside **3** (1.8 g, 8.25 mmol) was dissolved in dry DMF (6 mL) and imidazole (1.23 g, 18.15 mmol, 2.2 eq) was added. *Tert*-butyldiphenylsilyl chloride (2.48 mL, 9.1 mmol, 1.1 eq) was then added dropwise and the reaction was stirred for 5h at room temperature, before being concentrated in vacuo. The residue was dissolved in Et<sub>2</sub>O (40 mL), washed with NH<sub>4</sub>Cl sat., NaHCO<sub>3</sub> and water (20 mL). The aqueous layers were extracted with DCM (2 x 30 mL) and the combined organic layers were dried over MgSO<sub>4</sub>, filtered and concentrated under reduced pressure.

Compound **4** is an oil obtained in quantitative yield *R*<sub>f</sub>: 0.59. (CHCl<sub>3</sub>/MeOH 90:10).



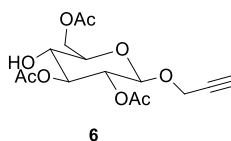
<sup>1</sup>H NMR: δ 7.8-7.4 (m, 10H, ArH), 4.49 (d, <sup>3</sup>*J*<sub>1,2</sub> = 7.8, 1H, H-1), 4.45 and 4.37 (split AB system, <sup>2</sup>*J*<sub>gem</sub> = 15.7, <sup>4</sup>*J* = 2.4, 2H, 2-OCH<sub>2</sub>C≡), 4.27, 4.21 and 4.17 (d, *J* 3.9, 3xOH), 4.06 and 3.94 (split AB system <sup>3</sup>*J*<sub>5,6A</sub> = 1.9, <sup>3</sup>*J*<sub>5,6B</sub> = 5.4, <sup>2</sup>*J*<sub>6A,6B</sub> = 10.8, 2H, H<sub>2</sub>-6), 3.51-3.40 (m, 3H, H-3-5), 3.24 (ddd, *J*<sub>2,OH</sub> = 3.9 <sup>3</sup>*J*<sub>2,1</sub> = 7.8, <sup>3</sup>*J*<sub>2,3</sub> = 11.7, 1H, H-2), 2.98 (t, <sup>4</sup>*J* = 2.5, 1H, ≡CH), 1.05 [s, 9H, SiC(CH<sub>3</sub>)<sub>3</sub>]. <sup>13</sup>C NMR: δ 137.3, 136.7, 136.2, 135.6, 134.6, 134.5, 134.3, 130.5, 130.0, 128.6 and 128.3 (ArC), 101.8 (C-1), 80.2 (C≡CH), 77.8, 76.0, 71.0, and 70.9 (C-2-5), 74.7 (≡CH), 64.4 (C-6), 55.7 (1-OCH<sub>2</sub>C≡), 27.1 [SiC(CH<sub>3</sub>)<sub>3</sub>], 19.8 [SiC(CH<sub>3</sub>)<sub>3</sub>].

**2-Propyn-1-yl 6-O- [(1,1-dimethylethyl) diphenylsilyl]-β-D-glucopyranoside 2,3,4-triacetate (5).** 2-Propyn-1-yl β-D-glucopyranoside **4** (1.6 g, 3.5 mmol) was added to an excess of Pyridine (3.5 mL) and the mixture was stirred at 0°C for 15', then, an excess of Ac<sub>2</sub>O was added (3.5 mL) and the mixture was stirred for 12h at room temperature. The crude was dissolved in EtOAc (40 mL) and washed three times with an aqueous solution of HCl 2N (20 mL). The organic layer was then washed with saturated NaCl solution (20 mL, twice), dried over MgSO<sub>4</sub>, filtered and concentrated under reduced pressure to give a brown oil that was purified by column chromatography (eluants: Hexane/EtOAc 80:20) on silica gel. Compound **5** is an oil obtained in 70% yield. *R*<sub>f</sub>: 0.50 (Hexane/EtOAc 80:20).



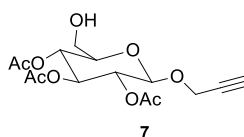
$^1\text{H}$  NMR:  $\delta$  7.8-7.4 (m, 10H, ArH), 5.3-5.2 (m, 2H, H-1, H-6<sub>A</sub>), 5.0-4.9 (m, 2H, H-3, H-6<sub>B</sub>), 4.44 and 4.37 (split AB system,  $^2J_{\text{gem}} = 15.8$ ,  $^4J = 1.8$ , 2H, 1-OCH<sub>2</sub>C $\equiv$ ), 3.9-3.8 (m, 3H, H-2, H-4, H-5), 3.04 (t,  $^4J = 1.8$ , 1H,  $\equiv\text{CH}$ ), 1.99 and 1.94 (two s, 9H, 3 x COCH<sub>3</sub>), 1.05 [s, 9H, SiC(CH<sub>3</sub>)<sub>3</sub>].  $^{13}\text{C}$  NMR:  $\delta$  169.3 and 168.6 (CO), 135.2, 133.1, 132.8, 129.6, 127.6, and 127.5 (ArC), 98.1 (C-1), 78.5 ( $\text{C}\equiv\text{CH}$ ), 75.7 ( $\equiv\text{CH}$ ), 74.0, 72.9, 71.0, 68.0 (C-2-5), and 62.0 (C-6), 55.2 (1-OCH<sub>2</sub>C $\equiv$ ), 26.0 [SiC(CH<sub>3</sub>)<sub>3</sub>], 19.5 (COCH<sub>3</sub>), 18.7 [SiC(CH<sub>3</sub>)<sub>3</sub>].

**2-Propyn-1-yl  $\beta$ -D-glucopyranoside 2,3,6-triacetate (6).** Propargyl  $\beta$ -D-glucopyranoside **5** (1.94 g, 3.9 mmol) was dissolved in aqueous TFA (95%, 14.08 mL). The mixture was stirred for 1h at room temperature. TLC (Hexane/EtOAc 40:60) indicated the disappearance of the starting material. Toluene (47.26 mL) was added to the reaction crude. The organic layer was dried over MgSO<sub>4</sub>, filtered and concentrated under reduced pressure to give a solid that was purified by chromatography (eluants: Hexane/EtOAc 60:40) on silica gel. Compound **6** is a white solid obtained in 85% yield. M.p. 130-140°C. *R*<sub>f</sub>: 0.48 (Hexane/EtOAc 40:60).



$^1\text{H}$  NMR:  $\delta$  5.11 (t,  $^3J_{2,3} = ^3J_{3,4} = 9.0$ , 1H, H-3), 4.82 (d,  $^3J_{1,2} = 7.8$ , 1H, H-1), 4.79 (dd,  $^3J_{1,2} = 7.8$ ,  $^3J_{2,3} = 9.0$ , 1H, H-2), 4.38 and 4.26 (split AB system,  $^3J_{5,6A} = 2.2$ ,  $^3J_{5,6B} = 5.3$ ,  $^2J_{6A,6B} = 12.1$ , 2H, H<sub>2</sub>-6), 4.37 and 4.33 (split AB system,  $^2J_{\text{gem}} = 15.6$ ,  $^4J = 2.4$ , 2H, 1-OCH<sub>2</sub>C $\equiv$ ), 3.72 (m, 1H, H-5), 3.66 (br t,

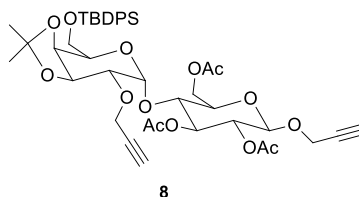
$^3J_{3,4} = ^3J_{4,5} = 9.0$ , 1H, H-4), 3.00 (t,  $^4J = 2.4$ , 1H,  $\equiv\text{CH}$ ), 2.03, 1.98, and 1.97 (three s, 9H, 3 x  $\text{COCH}_3$ ).  $^{13}\text{C}$  NMR:  $\delta$  171.6, 171.1, and 170.4 (CO), 99.9 (C-1), 80.3 ( $\text{C}\equiv\text{CH}$ ), 76.7 ( $\equiv\text{CH}$ ), 77.1, 75.4, 72.9, 69.9 (C-2-5) and 64.2 (C-6), 57.0 ( $1\text{-OCH}_2\text{C}\equiv$ ), 21.4 and 21.3( $\text{COCH}_3$ ). Anal. Calcd for  $\text{C}_{15}\text{H}_{20}\text{O}_9$ : C, 52.32; H, 5.85. Found: C, 52.30; H, 5.84. From the same chromatography column **2-Propyn-1-yl  $\beta$ -D-glucopyranoside 2,3,4-triacetate (7)** was recovered as an oil in 10% yield.



$^1\text{H}$  NMR:  $\delta$  5.30 (t,  $^3J_{2,3} = ^3J_{3,4} = 9.0$ , 1H, H-3), 5.09-4.95 (m, 2H, H-2 and H-4), 4.81 (d,  $^3J_{1,2} = 7.8$ , 1H, H-1), 4.43-4.35 (m, 2H, and  $1\text{-OCH}_2\text{C}\equiv$ ), 3.80-3.52 (m, 3H, H-2-6, H-5), 2.48 (t,  $^4J = 2.4$ , 1H,  $\equiv\text{CH}$ ), 2.07 and 2.02 (three s, 9H, 3 x  $\text{COCH}_3$ ).  $^{13}\text{C}$  NMR ( $\text{CDCl}_3$ ):  $\delta$  170.2, 170.1, and 169.4 (CO), 98.4 (C-1), 78.2 ( $\text{C}\equiv\text{CH}$ ), 76.6 ( $\equiv\text{CH}$ ), 74.1, 72.6, 71.1, 68.6, and 61.2 (C-2-6), 56.1 ( $1\text{-OCH}_2\text{C}\equiv$ ), 20.7 and 20.6( $\text{COCH}_3$ ).

**2-Propyn-1-yl 4-O-[3,4-O-(1-methylethylidene)-6-O-[(1,1-dimethylethyl)diphenylsilyl]-2-O-(2-propyn-1-yl)- $\alpha$ -D-galactopyranosyl]- $\beta$ -D-glucopyranoside 2,3,6-triacetate (8).** The donor, phenyl 1-thio- $\beta$ -D-galactopyranoside **2** (0.58 g, 0.98 mmol) and the acceptor, 2-Propargyl  $\beta$ -D-glucopyranoside **6** (0.15 g, 0.49 mmol) were dissolved in anhydrous DCM (9.8 mL), under nitrogen. NIS (0.36 g, 1.57 mmol) and TMSOTf (0.04 g, 0.196 mmol) were added and the mixture, which took on a dark red coloration, was sonicated for 20'. After completion of the reaction examined by TLC (Hexane/EtOAc 60:40), the reaction was stopped with two drops of triethylamine (TEA), the solvent was removed under reduced pressure and

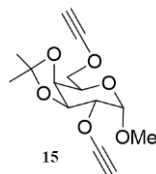
the crude was purified by column chromatography (eluants: Hexane/EtOAc 90:10 up to 50:50) on silica gel. Compound **8** was recovered as a transparent oil in 70% yield. *R<sub>f</sub>*: 0.54 (Hexane/EtOAc 60:40).



$^1\text{H}$  NMR:  $\delta$  7.8-7.4 (m, 10H, ArH), 5.24 (t,  $^3J_{2,3} = ^3J_{3,4} = 9.3$ , 1H, Glu H-3), 5.06 (d,  $^3J_{1,2} = 2.9$ , 1H, Gal H-1), 4.86 (d,  $^3J_{1,2} = 7.8$ , 1H, Glu H-1), 4.82 (dd,  $^3J_{1,2} = 7.8$ ,  $^3J_{2,3} = 9.3$ , 1H, Glu H-2), 4.5-4.2 (m, 9H, Gal H-3, Gal and Glu H<sub>2</sub>-6, 2 x OCH<sub>2</sub>C $\equiv$ ), 3.9-3.8 (m, 4H, Gal and Glu H-4, H-5), 3.71 (dd,  $^3J_{1,2} = 2.9$ ,  $^3J_{2,3} = 7.1$ , 1H, Gal H-2), 3.03 and 3.00 (two t,  $^4J = 2.5$ , 2H, 2 x  $\equiv\text{CH}$ ), 2.03, 1.98, and 1.97 (three s, 9H, 3 x COCH<sub>3</sub>), 1.47 and 1.33 [two s, 6H, OC(CH<sub>3</sub>)<sub>2</sub>], 1.06 [s, 9H, SiC(CH<sub>3</sub>)<sub>3</sub>].  $^{13}\text{C}$  NMR:  $\delta$  171.2, 170.9, and 170.4 (CO), 137.1, 137.0, 134.8, 134.7, 131.3, 129.3, and 129.2 (ArC), 110.3 [OC(CH<sub>3</sub>)<sub>2</sub>], 100.4 (Gal C-1), 99.6 (Glu C-1), 81.5 and 80.2 ( $\text{C}\equiv\text{CH}$ ), 78.2, 77.3, 77.1, 76.4, 75.3, 74.4, 74.3, 72.9, and 70.8 (Gal and Glu C-2-5,  $\equiv\text{CH}$ ), 64.3 and 64.1 (Gal and Glu C-6), 59.4 and 56.9 (Gal and Glu OCH<sub>2</sub>C $\equiv$ ), 28.8 and 26.9 [OC(CH<sub>3</sub>)<sub>2</sub>], 27.8 [SiC(CH<sub>3</sub>)<sub>3</sub>], 21.8 and 21.3 (COCH<sub>3</sub>), 20.4 [SiC(CH<sub>3</sub>)<sub>3</sub>]. Anal. Calcd for C<sub>43</sub>H<sub>54</sub>O<sub>14</sub>Si: C, 62.76; H, 6.61. Found: C, 62.65; H, 6.60.

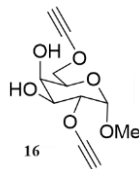
**$\alpha$ -D-Galactopyranoside derivatives 12-14** are already reported in literature.<sup>37,38,39</sup>

**Methyl 3,4-Di-O-isopropiliden-2,6-di-O-propargyl- $\alpha$ -D-galactopyranoside (15)**. It was synthesized following literature procedure.<sup>40</sup>



$^1\text{H}$  NMR:  $\delta$  4.79 (d, 1H,  $J = 3.4$  Hz, H-1), 4.35 (d, 2H,  $J = 2.4$  Hz,  $\text{CH}_2\text{-C}\equiv\text{CH}$ ), 4.26 (dd, 1H,  $J = 8.8$  Hz, H-4), 4.23 (d, 2H,  $J = 2.4$  Hz,  $\text{CH}_2\text{-C}\equiv\text{CH}$ ), 4.18 (t, 1H,  $J = 5.4$  Hz, H-3), 4.11 (m, 1H, H-5), 3.79-3.67 (dd, 2H,  $J = 10.8$  and  $1.5$  Hz, 2xH-6), dd, 1H,  $J = 9.8$  and  $3.4$  Hz, H-2), 3.35 (s, 3H,  $\text{OCH}_3$ ), 2.96 (m, 2H, 2 x  $\text{-C}\equiv\text{CH}$ ), 1.48, 1.29 ( $\text{C}(\text{CH}_3)_2$ );  $^{13}\text{C}$  NMR  $\delta$ : 110.2, 99.5, 81.6, 81.5, 77.7, 77.2, 76.6, 76.5, 75.4, 70.7, 68.0, 59.5, 58.6, 56.0, 29.1, 27.3.

**Methyl 2,6-di-O-propargyl- $\alpha$ -D-galacto pyranoside (16).** It was synthesized following literature procedure.<sup>41</sup>



$^1\text{H}$  NMR:  $\delta$  4.85 (d, 1H,  $J = 3.4$  Hz, H-1), 4.35 (d, 2H,  $J = 2.4$  Hz,  $\text{CH}_2\text{-C}\equiv\text{CH}$ ), 4.20 (d, 2H,  $J = 2.4$  Hz,  $\text{CH}_2\text{-C}\equiv\text{CH}$ ), 4.03 (broad s, 1H, OH), 3.89-3.68 (m, 7H, OH, H-2, H-3, H-4, H-5 and 2xH-6), 3.33 (s, 3H,  $\text{OCH}_3$ ), 2.93 (t, 2H,  $\text{C}\equiv\text{CH}$ );  $^{13}\text{C}$  NMR:  $\delta$  99.8, 82.2, 81.5, 77.7, 76.4, 76.2, 71.4, 70.9, 70.7, 70.5, 59.5, 59.0, 55.7.

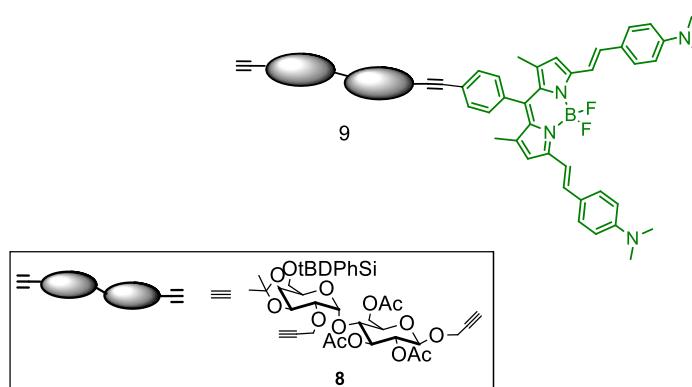
### General procedure for the copper-free Sonogashira reactions

$[\text{Pd}(\text{PPh}_3)_4]$  (10% mmol) was added to a degassed solution of **BODIPY 2** or **BODIPY 1** and the saccharide species (8 or 1 eq.) in DMF/TEA (1:1). The mixture was then heated at  $75^\circ\text{C}$  for **BODIPY 2** or  $60^\circ\text{C}$  for **BODIPY 1**,



under argon, for 3-4h, until the disappearance of starting compounds was observed by TLC. The solvents were removed under vacuum.

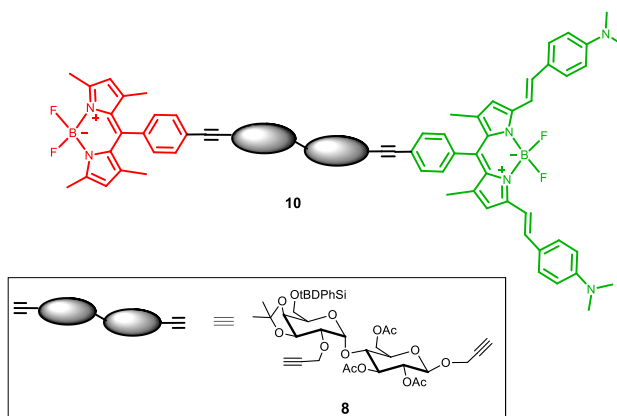
**Compound 9.** Disaccharide **8** was reacted with **BODIPY 2** (ratio 8:1) following the general procedure. The reaction crude was purified by silica gel column chromatography (eluants: Hexane/EtOAc 80:20 up to 40:60) for obtaining compound **9** as a deep green solid (1:2 isomeric mixture) in 65 % yield. M.p. 100-105°C. *R*<sub>f</sub>: 0.28 (Hexane/EtOAc 50:50).



$^1\text{H}$  NMR:  $\delta$  7.8-7.4 (m, 12H, 8 x benzeneH and 2 x CH=CH of both isomers), 6.82 (d,  $^3J_{\text{ortho}} = 8.8$ , 4H, 4 x benzeneH of both isomers), 6.80 (s, 2H, 2 x pyrroleH of both isomers), 5.289 and 5.287 (two t,  $^3J_{2,3} = ^3J_{3,4} = 9.2$ , 1H, Glu H-3 of both isomers), 5.16 (d,  $^3J_{1,2} = 2.9$ , 0.3H, Gal H-1 of one isomer), 5.08 (d,  $^3J_{1,2} = 3.0$ , 0.7H, Gal H-1 of the other isomer), 5.04 (d,  $^3J_{1,2} = 7.8$ , 0.7H, Glu H-1 of one isomer), 4.9-4.8 (m, 1H, Glu H-2 of both isomers), 4.87 (d,  $^3J_{1,2} = 7.8$ , 0.3H, Glu H-1 of the other isomer), 4.73-4.23 (m, 9H, Gal H-3, Gal and Glu H<sub>2</sub>-6, 2 x OCH<sub>2</sub>C $\equiv$  of both isomers), 3.94-3.83 (m, 4H, Gal and Glu H-4,5 of both isomers), 3.81 and 3.72 (dd,  $^3J_{1,2} = 3.4$ ,  $^3J_{2,3} = 7.3$ , 1H, Gal H-2 of both isomers), 3.06 [s, 12H, 2 x N(CH<sub>3</sub>)<sub>2</sub> of both isomers], 3.04 (m, 1H,  $\equiv\text{CH}$  of both isomers), 1.99 and 1.98 (two s, 9H, 3 x COCH<sub>3</sub> of both isomers), 1.50, 1.48, 1.47, 1.35, and 1.33 [four s, 12H,

OC(CH<sub>3</sub>)<sub>2</sub> and pyrroleCH<sub>3</sub> of both isomers], 1.06 [s, 9H, SiC(CH<sub>3</sub>)<sub>3</sub> of both isomers]. <sup>13</sup>C NMR (the resonances of both isomers are reported without differentiation): δ 171.2, 170.4, and 169.8 (CO), 154.4, 152.6, 142.5, 138.5, 137.2, 135.3, 133.5, 132.0, 131.5, 131.3, 130.7, 129.1, 126.2, 124.7, 119.0, 116.0, and 114.6 (ArC and CH=CH), 110.2 [OC(CH<sub>3</sub>)<sub>2</sub>], 100.3 (Gal C-1), 99.5 (Glu C-1), 88.6 and 86.4 (C≡CH), 78.2, 77.4, 77.1, 76.6, 75.2, 74.2, 73.4, and 71.3 (C-2-5, ≡CH), 64.3 and 64.1 (C-6), 60.1, 59.5, 57.5, and 56.9 (OCH<sub>2</sub>C≡), 40.8 [N(CH<sub>3</sub>)<sub>2</sub>], 28.8 and 27.0 [OC(CH<sub>3</sub>)<sub>2</sub>], 27.8 [SiC(CH<sub>3</sub>)<sub>3</sub>], 21.8, and 21.4 (COCH<sub>3</sub>), 20.2 [SiC(CH<sub>3</sub>)<sub>3</sub>], 15.6 (pyrroleCH<sub>3</sub>). Anal. Calcd for C<sub>80</sub>H<sub>89</sub>BF<sub>2</sub>N<sub>4</sub>O<sub>14</sub>Si: C, 68.27; H, 6.37. Found: C, 68.21; H, 6.38.

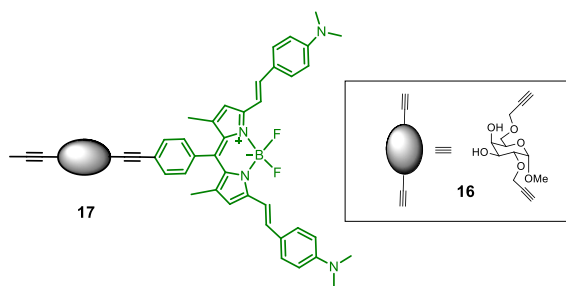
**Compound 10.** Compound **9** was reacted with **BODIPY 1** (ratio 1:1) following the general procedure. The reaction crude was purified by silica gel column chromatography (eluants: Hexane/EtOAc (80:20 up to 60:40) for obtaining compound **10** as a deep green solid (1:2 isomeric mixture) in 40 % yield. M.p. 120-140°C. *R*<sub>f</sub>: 0.31 (Hexane /EtOAc 50:50).



<sup>1</sup>H NMR (the resonances of both isomers are almost coincident): δ 7.8-7.4 (m, 16H, 12 x benzeneH and 2 x CH=CH), 6.82 (d, <sup>3</sup>J<sub>ortho</sub> = 8.8, 4H, 4 x benzeneH), 6.81 (s, 2H, 2 x **BODIPY 2**-pyrroleH), 6.11 (s, 2H, 2 x **BODIPY 1**-pyrroleH), 5.328 (t, <sup>3</sup>J<sub>2,3</sub> = <sup>3</sup>J<sub>3,4</sub> = 9.5, 1H, Glu H-3 of one isomer), 5.326 (t,

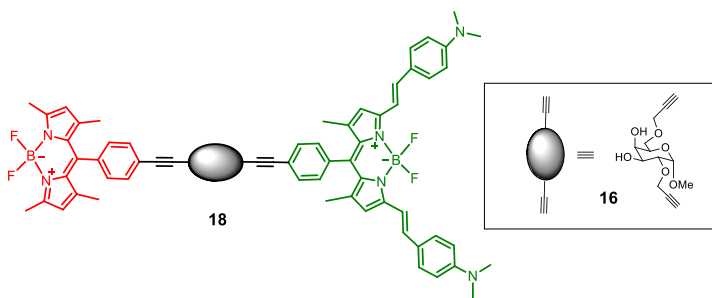
$^3J_{2,3} = ^3J_{3,4} = 9.5$ , 1H, Glu H-3 of the other isomer) 5.19 (d,  $^3J_{1,2} = 3.0$ , 0.3H, Gal H-1 of one isomer), 5.18 (d,  $^3J_{1,2} = 3.4$ , 0.7H, Gal H-1 of the other isomer), 5.06 (d,  $^3J_{1,2} = 7.8$ , 0.7H, Glu H-1 of one isomer), 5.03 (d,  $^3J_{1,2} = 7.8$ , 0.3H, Glu H-1 of the other isomer), 4.88 (dd,  $^3J_{1,2} = 7.8$ ,  $^3J_{2,3} = 9.5$ , 1H, Glu H-2), 4.7-4.2 (m, 9H, Gal H-3, Gal and Glu H<sub>2</sub>-6, 2 x OCH<sub>2</sub>C≡), 4.0-3.8 (m, 4H, Gal and Glu H-4,5), 3.80 (dd,  $^3J_{1,2} = 3.4$ ,  $^3J_{2,3} = 7.3$ , 1H, Gal H-2), 3.06 [s, 12H, 2 x N(CH<sub>3</sub>)<sub>2</sub>], 2.50 (s, 6H, 2 x **BODIPY 1**-pyrrole 2-CH<sub>3</sub>), 1.99, 1.98 and 1.96 (three s, 9H, 3 x COCH<sub>3</sub>), 1.50, 1.48, 1.47, 1.43, 1.41, 1.35, and 1.29 [seven s, 18H, OC(CH<sub>3</sub>)<sub>2</sub>, 2 x **BODIPY 1**-pyrrole 4-CH<sub>3</sub>, and 2 x **BODIPY 2**-pyrrole CH<sub>3</sub>], 1.06 [s, 9H, SiC(CH<sub>3</sub>)<sub>3</sub>]. <sup>13</sup>C NMR (the resonances of both isomers are reported without differentiation): δ 171.2, 170.5, and 169.9 (CO), 156.0, 154.5, 152.9, 146.2, 144.3, 143.1, 142.5, 138.4, 137.1, 137.0, 134.8, 134.0, 133.8, 131.5, 131.3, 130.9, 130.1, 129.3, 129.2, 126.2, 122.8, 118.9, 115.8, and 113.7 (ArC and CH=CH), 110.3 [OC(CH<sub>3</sub>)<sub>2</sub>], 100.4 (Gal C-1), 99.7 (Glu C-1), 88.6, 87.4, and 86.4 (C≡C), 78.5, 76.4, 75.4, 74.5, 74.3, 73.1, 70.8 (C-2-5), 64.4, and 64.3 (C-6), 60.0, and 57.6 (OCH<sub>2</sub>C≡), 40.9 [N(CH<sub>3</sub>)<sub>2</sub>], 29.0, and 27.0 [OC(CH<sub>3</sub>)<sub>2</sub>], 27.9 [SiC(CH<sub>3</sub>)<sub>3</sub>], 21.9, and 21.4 (COCH<sub>3</sub>), 20.4 [SiC(CH<sub>3</sub>)<sub>3</sub>], 15.6, 15.3, 15.2 (pyrrole CH<sub>3</sub>). Anal. Calcd for C<sub>99</sub>H<sub>106</sub>B<sub>2</sub>F<sub>4</sub>N<sub>6</sub>O<sub>14</sub>Si: C, 68.75; H, 6.18. Found: C, 68.80; H, 6.19.

**Compound 17.** Galactopyranoside **16** was reacted with **BODIPY 2** (ratio 8:1) following the general procedure. Compound **17** was obtained as a 1:1 mix of isomers and purified by chromatography column using Hexane/EtOAc 50:50 up to 20:80. Purification led to a deep green solid with a 70% yield. TLC: *R<sub>f</sub>* 0.55 (EtOAc 100%). Mp 175-185°C.



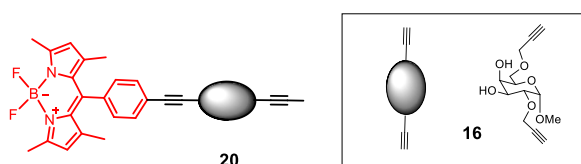
$^1\text{H}$  NMR:  $\delta$  7.71-7.39 (m, 24H), 6.87 (d,  $J$  = 7.8 Hz, 8H), 6.81 (s, 4H), 4.97 e 4.87 (d, 2H,  $J$  = 2.9 Hz,  $2\times\text{H}_1$ ), 4.61 and 4.49 (s, 4H,  $2\times\text{CH}_2\text{-C}\equiv\text{C}$ ), 4.33 and 4.21 (d, 4H,  $J$  = 2.0 Hz,  $2\times\text{CH}_2\text{-C}\equiv\text{CH}$ ), 4.15 and 4.06-3.71 (m, 16H, 4 OH,  $2\times\text{H}_2$ ,  $2\times\text{H}_3$ ,  $2\times\text{H}_4$ ,  $2\times\text{H}_5$  and  $2\times\text{H}_6$ ), 3.36 (s, 6H,  $2\times\text{OCH}_3$ ), 3.06 (s, 24H,  $4\times\text{N}(\text{CH}_3)_2$ ), 2.94 (m, 2H,  $2\times\text{-C}\equiv\text{CH}$ ), 1.49 (s, 12H);  $^{13}\text{C}$  NMR:  $\delta$  154.5, 152.9, 142.2, 138.3, 137.2, 133.3, 132.5, 130.9, 130.3, 126.2, 125.0, 119.0, 116.0, 114.1, 99.9, 92.4, 88.5, 86.7, 81.7, 78.0, 77.7, 77.3, 76.4, 76.2, 71.1, 70.9, 68.1, 60.2, 59.5, 58.6, 55.8, 41.1, 15.6. Anal. Calcd for  $\text{C}_{50}\text{H}_{53}\text{BF}_2\text{N}_4\text{O}_6$  (854,79): C 70.26, H 6.25, N 6.55. Found: C 70.40, H 6.26, N 6.53.

**Compound 18:** Compound **17** was reacted with **BODIPY 1** (ratio 1:1) following the general procedure. Compound **18** was purified by flash chromatography as a 1:1 mixture of isomers using as eluants Hexane/EtOAc 30:70 gradient to EtOAc 100% and obtained as deep green solid with a yield of 77%. TLC (Hexane/EtOAc 1:1)  $R_f$ : 0.27. Mp 175-185°C.



$^1\text{H}$  NMR:  $\delta$  7.70-7.39 (m, 32H), 6.82 (d,  $J$  = 8.8 Hz, 8H), 6.79 (s, 4H), 6.11 (s, 4H), 4.99 (m, 2H, 2xH<sub>1</sub>), 4.61 and 4.50 (s, 8H, 4xCH<sub>2</sub>-C $\equiv$ C), 4.13 (m, 2H, 2xOH), 3.97-3.82 (m, 14H, 2xOH, 2xH<sub>2</sub>, 2xH<sub>3</sub>, 2xH<sub>4</sub>, 2xH<sub>5</sub> and 2x2H<sub>6</sub>), 3.39 (s, 6H, 2xOCH<sub>3</sub>), 3.05 (s, 24H, 4xN(CH<sub>3</sub>)<sub>2</sub>), 2.49 (s, 12H), 1.48 and 1.43(s, 24H);  $^{13}\text{C}$  NMR  $\delta$  157.0, 154.5, 152.9, 144.5, 142.8, 142.2, 138.4, 137.2, 136.6, 134.0, 133.9, 133.7, 132.5, 130.9, 130.3, 130.0, 126.2, 125.3, 125.0, 122.8, 118.9, 115.7, 113.7, 99.9, 89.3, 88.7, 86.7, 86.5, 78.0, 71.6, 71.2, 70.8, 70.6, 60.2, 59.8, 55.9, 40.9, 15.6, 15.3, 15.2. Anal. Calcd for C<sub>69</sub>H<sub>70</sub>B<sub>2</sub>F<sub>4</sub>N<sub>6</sub>O<sub>6</sub> (1176,95): C 70.41, H 5.99, N 7.14. Found: C 70.62, H 6.00, N 7.16.

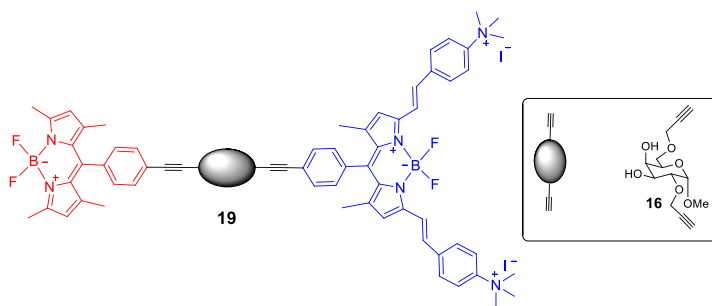
**Compound 20.** Galactopyranoside **16** was reacted with **BODIPY 1** (ratio1:1) following the general procedure. Purification by column chromatography of the crude (eluants: Toluene/MeCN 60:40) gave compound **20** as an orange solid (1:1 mix of isomers) with a 50% yield. TLC:  $R_f$  0.50 (Toluene/MeCN 40:60). Mp 90-95°C.



$^1\text{H}$  NMR:  $\delta$  7.69 (d,  $J$  = 7.9 Hz, 4H), 7.45 (d, 4H), 6.13 (s, 4H), 4.95 and 4.87 (d, 2H,  $J$  = 2.9 Hz, 2xH<sub>1</sub>), 4.60 and 4.49 (s, 4H, 2xCH<sub>2</sub>-C $\equiv$ C), 4.32 and 4.20 (d, 4H,  $J$  = 1.5 Hz 2xCH<sub>2</sub>-C $\equiv$ CH), 4.15-3.68 (m, 16H, 4 OH, 2xH<sub>2</sub>, 2xH<sub>3</sub>, 2xH<sub>4</sub>, 2xH<sub>5</sub> and 2x2H<sub>6</sub>), 3.35 (s, 6H, 2xOCH<sub>3</sub>), 2.94 (m, 2H, 2 x -C $\equiv$ CH), 2.50 (s, 12H), 1.49 (s, 12H);  $^{13}\text{C}$  NMR:  $\delta$  157.0, 144.5, 142.9, 136.6, 137.2, 133.9, 132.5, 130.1, 130.0, 129.7, 125.3, 122.9, 122.7, 99.9, 99.8, 89.3, 88.7, 86.5, 86.2, 82.2, 77.7, 76.4, 76.2, 71.4, 71.1, 70.6, 60.2, 59.8, 59.5, 59.1,

55.9, 15.3. Anal. Calcd for  $C_{32}H_{35}BF_2N_2O_6$  (592,44): C 64.87, H 5.95, N 4.73. Found: C 64.83, H 5.96, N 4.72.

**Compound 19.** A large excess of  $CH_3I$  (500 eq.) was added to a solution of compound **18** (1 eq.) in acetonitrile (0.01M). The resulting mixture was stirred at RT for three days. The course of the reaction was followed by TLC on neutral aluminium oxide using a mixture of MeCN/ $H_2O$  (80:20). After disappearance of the starting material, the deep-blue solution was evaporated to dryness. The reaction crude was purified by flash column chromatography on aluminium oxide (eluants: MeCN/ $H_2O$  90:10). Compound **19** was obtained as a deep blue solid (1:1 mixture of isomers) in quantitative yield. TLC (MeCN/ $H_2O$  9:1) *R<sub>f</sub>*: 0.35. Mp 170-175°C.



$^1H$  NMR:  $\delta$  8.32 (d, 8H,  $J = 9.3$  Hz), 7.93 (d, 8H,  $J = 9.3$  Hz), 7.83-7.44 (m, 24H), 6.96 (s, 4H), 6.11 (s, 4H), 4.92 (d, 2H,  $J = 3.4$  Hz,  $H_I$ ), 4.65, 4.64, 4.53 and 4.52 (s, 8H,  $4 \times CH_2-C \equiv CH$ ), 4.00 (s, 36H,  $4 \times N(CH_3)_3$ ), 3.99-3.82 (m, 12H,  $2 \times H_2$ ,  $2 \times H_3$ ,  $2 \times H_4$ ,  $2 \times H_5$  and  $2 \times H_6$ ), 3.40 (s, 6H, OCH<sub>3</sub>), 2.48 (s, 12H), 1.55 and 1.44 (s, 24H);  $^{13}C$  NMR (150 MHz,  $CD_3COCD_3$ ):  $\delta$  157.0, 153.7, 148.8, 144.5, 140.2, 138.1, 136.6, 135.6, 134.0, 130.3, 130.1, 125.2, 123.0, 120.3, 113.6, 99.5, 88.8, 86.6, 73.2, 72.8, 72.0, 71.7, 70.9, 68.1, 60.2, 59.1, 58.6, 56.2, 15.7, 15.6, 15.3. Anal. Calcd for  $C_{71}H_{76}B_2F_4I_2N_6O_6$  (1458,81): C 58.38, H 5.24, N 5.75. Found: C 58.26, H 5.25, N 5.73.

## 1.10 References

---

1. A. Haque, S. H. Faizi, J. A. Rather, M. S. Khan, *Bio. Med. Chem.*, **2017**, 25, 2017-2034; Q. T. Nguyen, R. Y. Tsien, *Nature Rev. Cancer.*, **2013**, 13, 653-662.
2. H. Kobayashi, M. Ogawa, R. Alfrod, P.L. Choyke, Y. Urano, *Chem. Rev.*, **2010**, 110, 2620-2640.
3. L. D. Lavis, R. T. Raines, *Chem. Biol.*, **2014**, 9, 855–866; E. Oliveira, E. Bértolo, C. Nuñez, V. Pilla, H. M. Santos, J. Fernàndez-Lodeiro, A. Fernàndez-Lodeiro, J. Djafari, J. L. Capelo, C. Lodeiro, *ChemistryOpen*, **2018**, 7, 9-52.
4. K. E. Sapsford, L. Berti, I. L. Medintz, *Angew. Chem. Int. Ed.*, **2006**, 45, 4562-4588.
5. V. Balzani, P. Ceroni, A. Juris. Photochemistry and Photophysics. Concepts, Research, Applications, Wiley-VCH, **2014**; K. Kikuchi, H. Takakusa, T. Nagano, *Trends Anal. Chem.*, **2004**, 23, 407-415.
6. F. Gao, T. Gao, K. Zhou, W. Zeng, *Molecules*, **2016**, 21, 1163-1175.
7. M. D. Yilmaz, O. A. Bozdemir, E. U. Akkaya, *Org. Lett.*, **2006**, 8, 2871-2873.
8. O. A. Bozdemir, M. D. Yilmaz, O. Buyukcakil, A. Siemiarczuk, M. Tutasd, E. U. Akkaya, *New J. Chem.*, **2010**, 34, 151-155.
9. R. W. Wagner, J. S. Lindsey, *J. Am. Chem. Soc.*, **1994**, 116, 9759-9760.
10. R. W. Wagner, J. S. Lindsey, J. Seth, V. Palaniappan, D. F. Bocian, *J. Am. Chem. Soc.*, **1996**, 118, 3996-3997; F. Li, S. I. Yang, Y. Ciringh, J. Seth, C. H. Martin, D. L. Singh, D. Kim, R. R. Birge, D. F. Bocian, D. Holten, J. S. Lindsey, *J. Am. Chem. Soc.*, **1998**, 120, 10001-10017.
11. P. Bonaccorsi, M.C. Aversa, A. Barattucci, T. Papalia, F. Puntoriero, S. Campagna, *Chem. Commun.*, **2012**, 48, 10550-10552.
12. A. Varki, *Glycobiology*, **1993**, 3, 97-130; W. Meutermans, G. T. Le, B. Becker, *ChemMedChem.*, **2006**, 1, 1164-1194.

13. Y. C. Lee, R. T. Lee, *Acc. Chem. Res.*, **1995**, 28, 321-327.
14. J. McGarvey, C.-H. Wong, *Liebigs Ann. Recueil*, **1997**, 1059-1074.
15. O. Warburg, F. Wind, E. Negelein, *J. Gen. Physiol.*, **1927**, 8, 519-530; O. Warburg, *Science*, **1956**, 123, 309-314.
16. J. Pohl, B. Bertram, P. Hilgard, M. R. Nowrousian, J. Stubenand M. Wiessler, *Cancer Chemother. Pharmacol.*, **1995**, 35, 364-370.
17. S. S. Yuan, M. L. Li, J. S. Chen, L. Zhou, W. Zhou, *ChemMedChem.*, **2018**, 13, 764-778
- 18 E. C. Calvaresia, P. J. Hergenrother, *Chem. Sci.*, **2013**, 4, 2319-2333
19. M. C. Aversa, A. Barattucci, P. Bonaccorsi, *Eur. J. Org. Chem.* **2009**, 6355-6359; M. C. Aversa, A. Barattucci, P. Bonaccorsi, F. Marino-Merlo, A. Mastino, M. T. Sciortino, *Bioorg. Med. Chem.*, **2009**, 17, 1456-1463; P. Bonaccorsi, F. Marino-Merlo, A. Barattucci, G. Battaglia, E. Papaiani, T. Papalia, M. C. Aversa, A. Mastino, P. Bonaccorsi, *Bioorg. Med. Chem.*, **2012**, 20, 3186-3195.
20. A. Barattucci, E. Deni, P. Bonaccorsi, M. G. Ceraolo, T. Papalia, A. Santoro, M. T. Sciortino, F. Puntoriero, *J. Org. Chem.*, **2014**, 79, 5113-5120; E. Deni, Alicia Zamarron, P. Bonaccorsi, M. C. Carreno, A. Juaranz, F. Puntoriero, M. T. Sciortino, M. Ribagorda, A. Barattucci, *Eur. J. Med. Chem.*, **2016**, 111, 58-71.
21. A. Treibs, F.- H. Kreuzer, *Liebigs Ann. Chem.*, **1968**, 718, 208-223.
22. N. Boens, V. Leen, W. Dehaen, *Chem. Soc. Rev.*, **2012**, 41, 1130-1172.
23. T. Kowada, H. Maeda, K. Kikuchi, *Chem. Soc. Rev.*, **2015**, 44, 4953-4972; D. Gong, J. Rub, T. Cao, J. Qiana, W. Liua, A. Iqbala, W. Liua, W. Qina, H. Guob, *Sensors and Actuators B*, **2018**, 258, 72-79; M. Benstead, G. H. Mehl, R. W. Boyle, *Tetrahedron*, **2011**, 67, 3573-3601. S. Kolenen, E. U. Akkaya, *Coord. Chem. Rev.*, **2018**, 354, 121-134.
24. G. Ulrich, R. Ziessel, A. Harriman, *Angew. Chem. Int. Ed.*, **2008**, 47, 1184-1201.
25. García-Moreno, A. Costela, L. Campo, R. Sastre, F. Amat-Guerri, M. Liras, F. López Arbeloa, J. Bañuelos Prieto, I. López Arbeloa, *J. Phys. Chem.*, **2004**, 108, 3315-3323.



26. R. Ziessel, G. Ulrich, A. Harriman, M. A. H. Alamiry, B. Stewart, P. Retailleau, *Chem. Eur. J.*, **2009**, 15, 1359-1369; A. C. Benniston, G. Copley, *Phys. Chem. Chem. Phys.* **2009**, 11, 4124-4131.
27. Timsy Uppal, N. V. S. Dinesh K. Bhupathiraju and M. Graça H. Vincente, *Tetrahedron*, **2013**, 69, 4687-4693.
28. T. Papalia, G. Siracusano, I. Colao, A. Barattucci, M. C. Aversa, S. Serroni, G. Zappalà, S. Campagna, M. T. Sciortino, F. Puntoriero, P. Bonaccorsi, *Dyes Pig.*, **2014**, 110, 67-71.
29. R. Roy, S. K. Das, F. Santoyo-Gonzalez, F. Hernandez-Mateo, T. K. Dam, C. F. Brewer, *Chem. Eur. J.*, **2000**, 6, 1757-1762; R. Chinchilla, C. Nàjera, *Chem. Rev.*, **2007**, 107, 874-922.
30. J. N. Demas, G. A. Crosby, *J. Phys. Chem.*, **1971**, 75, 991-1024.
31. X. F. Zhu, J. Williams, A. I. Scott, *Tetrahedron Lett.*, **2000**, 41, 9541-9545.
32. S. Yan, N. Ding, W. Zhang, P. Wanga, Y. Li, M. Li, *Carbohydr. Res.*, **2012**, 354, 6-20.
33. S. Deng, U. Gandadharmath, C. W. T. Chang, *J. Org. Chem.*, **2006**, 71, 5179-5185.
34. Z. Zang, J. R. Ollmann, X. S. Ye, R. Wischnat, T. Baasov, C. H. Wong, *J. Am. Chem. Soc.*, **1999**, 121, 734-753.
35. C. T. Tanifum, C. -W. T. Chang, *J. Org. Chem.*, **2009**, 74, 634-644.
36. Z. Wang, D. Zang, D. Zhu, *J. Org. Chem.*, **2005**, 70, 5729-5732.
37. S. K. Chatterjee, P. Nuhn, *Chem. Commun.*, **1998**, 1729-1780.
38. G. B. Giovenzana, L. Lay, D. Monti, G. Palmisano, L. Panza, *Tetrahedron*, **1999**, 46, 14123-14136.
39. G. Catelani, F. Colonna, A. Marra, *Carbohydr. Res.*, **1988**, 182 297-300.
40. Y. Gao, A. Educhi, K. Kakemi, Y. C. Lee, *Bioorg. Med. Chem.* **2005**, 13, 6151-6157.

41. M. Ortega-Muñoz, F. Perez-Balderas, J. Morales-Sanfrutos, F. Hernandez-Mateo, J. Isac-García, F. Santoyo-Gonzalez, *Eur. J. Org. Chem.*, **2009**, 2454-2473.
42. R. D. Lillie, L. L. Ashburn, *Arch. Pathol.*, **1943**, 36, 432-440.
43. J. M. Holaska, B. E. Black, D. C. Love, J. A. Hanover, J. Leszyk, B. M. Pascal, *J. Cell. Biol.*, **2001**, 152, 127-140.
44. J. N. Demas, G. R. Crosby, *J. Phys. Chem.*, **1971**, 75, 991-1024.
45. S. Cafaggi, E. Russo, R. Stefani, R. Leardi, G. Caviglioli, B. Parodi, G. Bignardi, D. de Toter, C. Aiello, M. Viale, *J. Control. Release*, **2007**, 121, 110-123.

## **Chapter Two**

---

### **Curcumin-based bichromophoric species**

## 2.1 Curcumin generals

Curcumin is a natural compound first recognized in 1815 when Vogel and Pelletier reported the separation of a ‘yellow colouring-matter’ from the rhizomes of *Curcuma Longa* (Turmeric).<sup>1</sup> However, due to the presence of several analogous compounds in the mixture, Curcumin was identified for the first time in 1910, when Milobedzka and Lampe reported the chemical structure of (1E, 6E)-1,7-bis(4-hydroxy-3-methoxy phenyl)-1,6-heptadiene-3,5-dione and acknowledged this as Curcumin (Figure 2.1).<sup>2</sup>

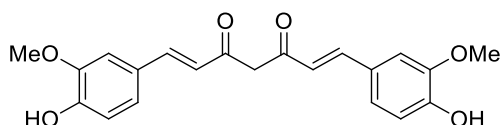


**Figure 2.1:** Chemical structure of Curcumin.

In 1935, Srinivas discovered that there were actually three yellow components in Turmeric, which for their structure similarities, were called curcuminoids.<sup>3</sup> Curcumin represents the major part of curcuminoids in Turmeric extract, approximately 60-70%, whereas the other two components are demethoxycurcumin and bis-demethoxycurcumin that represent respectively the 20-25% and 10-15% of the extract.

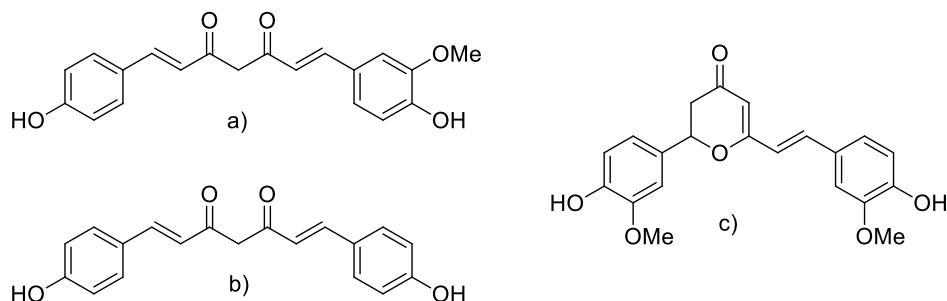


**Figure 2.2:** Demethoxycurcumin a), bis-demethoxycurcumin b) and cyclocurcumin.

A newly discovered component of Turmeric is cyclocurcumin, a <5% component of Turmeric (Figure 2.2).<sup>4</sup> Turmeric is extensively used in food industry, as spice in curries and mustards and as flavouring and natural yellow colouring (E100) in aliments. Turmeric preparations were used since ancient time in both traditional Chinese and Indian medicine, as anti-inflammatory applied to fresh wounds and bruises and as counterirritants for insect bites.<sup>5</sup> They were used for urologic and hepatobiliary diseases and have also been described as a cancer remedy.<sup>6</sup> Therefore, since the identification of Curcumin as the main constituent of Turmeric, many studies were published about Curcumin and its analogues, about their biological activity and their multiple pharmacological activities that include: antimicrobial, antidiabetic, anti-inflammatory, anticancer, and antioxidant properties.<sup>5,6,7</sup> It is not surprising that numerous clinical trials have been done. Figure 2.3 shows the increasing number of papers containing Curcumin as subject, published in the last ten years, whereas figure 2.4 reports a variety of human disorders against which Curcumin's potential has been tested.<sup>8</sup>

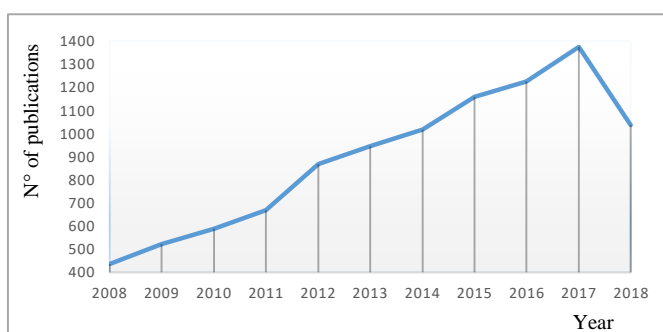


**Figure 2.3:** Publications about Curcumin ([http:// www.ncbi.nlm.nih.gov](http://www.ncbi.nlm.nih.gov)).

Clinical trials in humans indicates that using 1 to 2.5 g of Curcumin per day appears to be safe, thus explaining why Curcumin is “generally recognized as safe” (GRAS) by the U.S. Food and Drug Administration (FDA) as a food

additive, and why Curcumin is available for purchase in several forms including capsules, tablets and energy drinks.

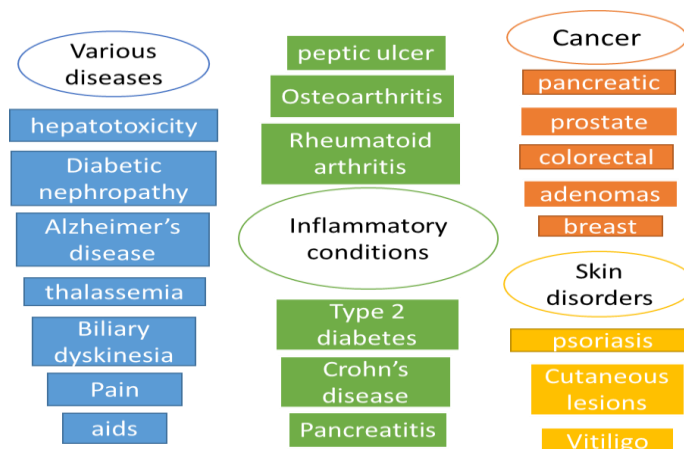
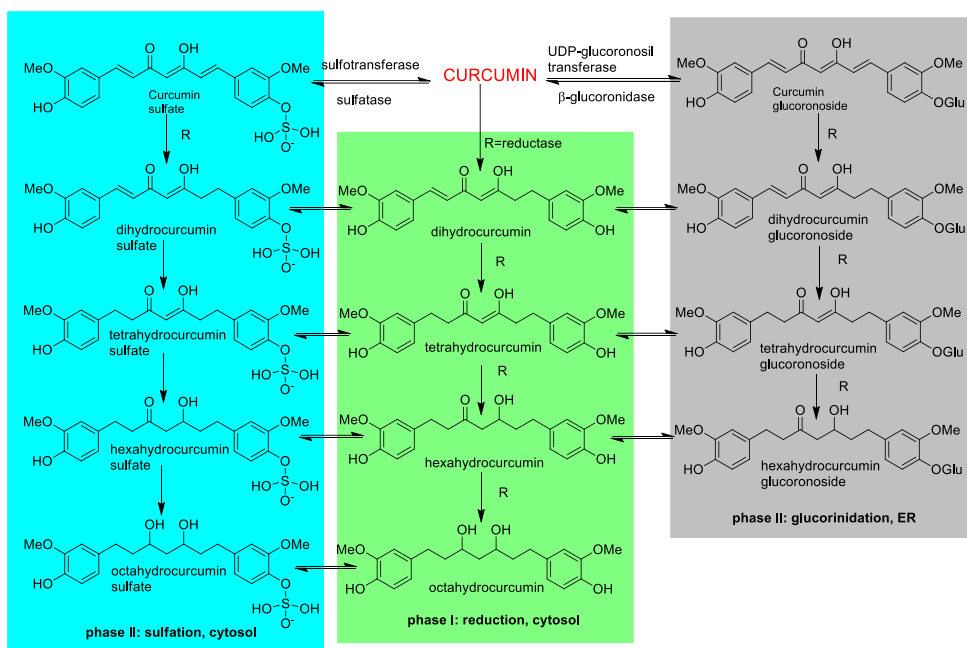


**Figure 2.4:** Variety of human disorders treated with Curcumin.

Phase I and II clinical trials involving several types of disease, revealed the major limitations of Curcumin: high doses are required for significant pharmacological effects. This is owed to its poor bio-availability, caused by low serum levels, restricted tissue distribution, due to slow intestinal absorption and to the rapid metabolism in the liver followed by elimination through faeces. Furthermore, poor solubility in water and conjugation to hydrophobic molecules reduce the bio-availability. Scheme 2.1 reports the multiple ways in which Curcumin is metabolized by phase I and phase II enzymes inside the rodents and humans.<sup>9</sup>

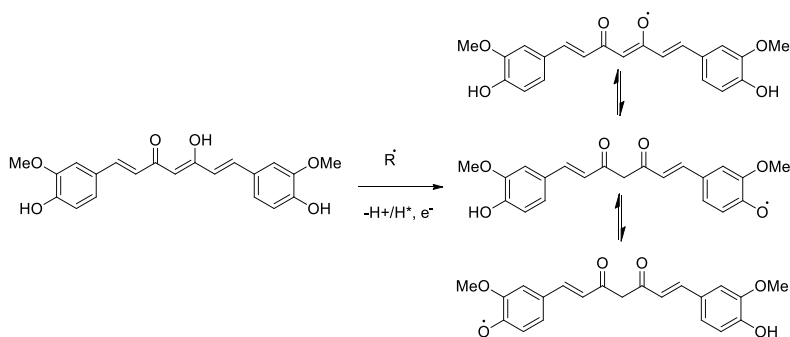
Curcumin is a chemically unstable molecule and sensitive to alkaline medium, pH, oxygen and irradiation. In view of the very low bioavailability of Curcumin and the possible degradation pathway, which includes the obtainment of side-products that may have a better pharmacologic activity than Curcumin itself, the scientist should be conscious when evaluating the activity of Curcumin in various diseases. For these undesirable characteristics and due to a series of false positive in screening, recently Curcumin has been

classified as deceptive molecule and as both a pan-assay interference compound (PAINS) and invalid metabolic panaceas (IMPS) candidate.<sup>10</sup>



**Scheme 2.1**

Many research groups have pursued to overcome these disadvantages and improve the bio-availability and the stability of Curcumin using a number of different strategies. The introduction of various groups instead of phenolic hydroxyl-groups, could avoid the abstraction of protons that leads to the formations of radical species (Scheme 2.2).



**Scheme 2.2**

Moreover, the presence of phenolic hydroxyl groups seems to be connected with the degradation of Curcumin under basic conditions, so a considerable number of compounds with a modified structure were synthesized and the resulting changes in biological stability and activity were evaluated.<sup>11</sup> The aromatic ring glycosylation of Curcumin provides more water-soluble compounds with a greater stability that is a fundamental feature for drug bioavailability (Figure 2.5).<sup>12</sup>

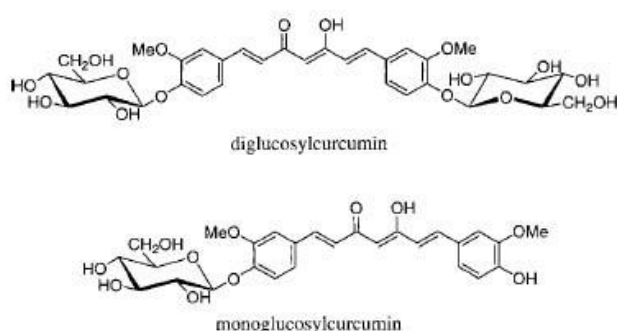


**Figure 2.5:** Glycoside-derived Curcumins.

Complexation with metal ions that involves the diketo-moiety could avoid the degradation pathway. The first complexes of Curcumin with medically valuable transition metals, such as Pd, Pt, Rh, and In, were published in 1997,<sup>13</sup> but there are several other papers reporting complexes of Curcumin with transition, non-transition metal ions and rare earth metals.<sup>14</sup> The structure and physical properties of these complexes depend on the nature of the metal ion that influences their stability and reactivity. In most cases, the resulting complexes exhibited favourable biological activity for a number of molecular targets. Recently, Chakravarty *et al.*<sup>15</sup> reported a ternary copper(II) complexes of BODIPY derivatives and Curcumin (Figure 2.6) that showed a significant photodynamic therapy (PDT) effect in visible light, specifically targeting the mitochondria of the cervical HeLa cancer cells.



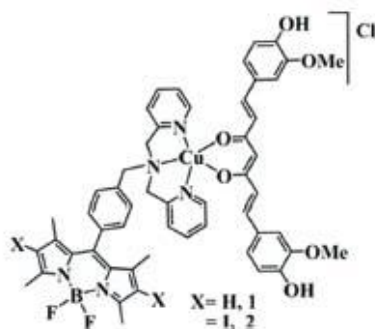


**Figure 2.6:** Copper complexes of BODIPY derivatives and Curcumin.

To overcome the problem of water insolubility, several other strategies have been tested, such as the use of liposomes, nanoparticles and chitosan as drug delivery systems or complexation with phospholipids.<sup>16</sup> For instance, supramolecular assemblies of Curcumin with dextran have been reported. In these systems Curcumin is solubilised by getting entrapped in hydrophobic pockets, mainly through hydrophobic interactions, thus enhancing the biocompatibility and making these systems usable for investigation of anti-cancer activity in cancer cells, and *in vivo* systems (Figure 2.7).<sup>17</sup>

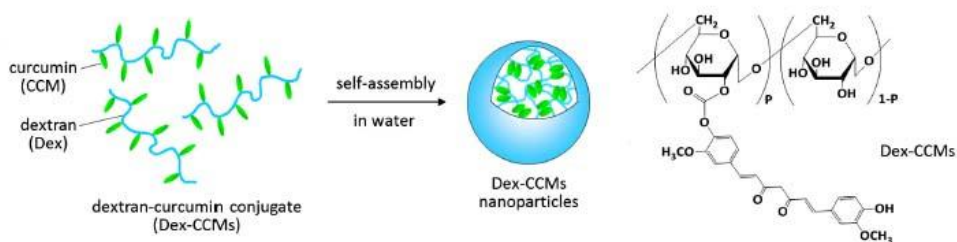
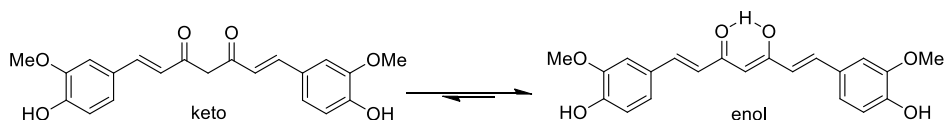


**Figure 2.7:** Schematic representation of the formation of Curcumin-dextran nanoparticles.

The use of inorganic material, like silica, to obtain nanoparticles and the synthesis and the properties of new Curcumin doped mesoporous silica nanoparticles will be discussed further in this chapter.

## 2.2 Chemical and photophysical properties of Curcumin

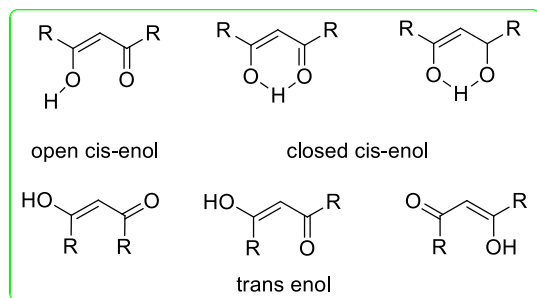
Chemically, Curcumin is constituted by two aromatic ring systems containing *o*-methoxy phenolic groups, connected by a seven carbon linker consisting of an  $\alpha,\beta$ -unsaturated  $\beta$ -diketone moiety. The structure is also described as two ferulic acid units linked together. Curcumin is involved in a keto-enol tautomerism (Scheme 2.3).



Scheme 2.3

Actually, for comparison with analogous  $\beta$ -diketo systems for Curcumin there should be considered more than one diketo and enol form (Figure 2.8). However, it is believed that the enol form is more stable than keto form due to larger dipole moment of the enolic structure that leads to the formation of strong intramolecular hydrogen bond.<sup>18</sup>

(a) different enol forms



(b) different keto forms

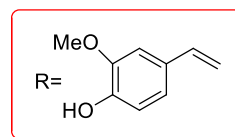
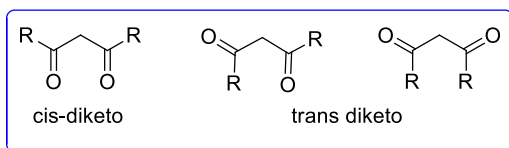
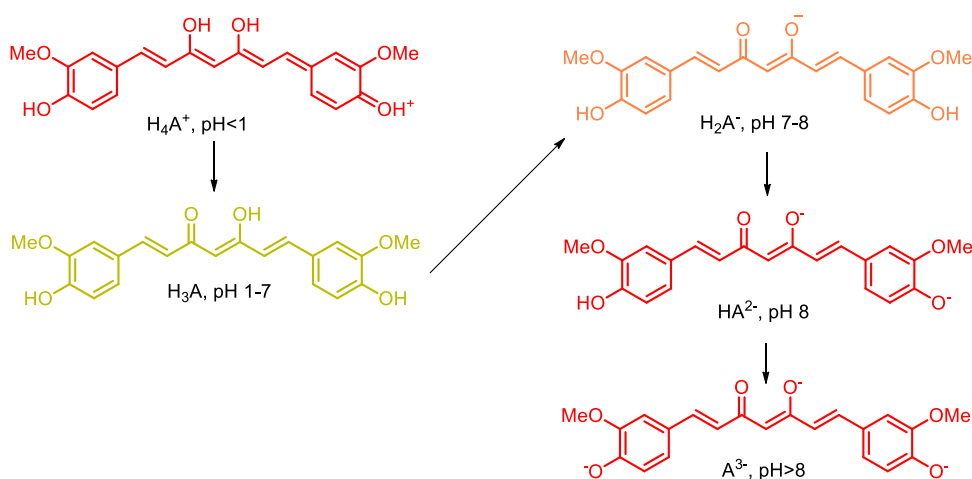


Figure 2.8: Cis–trans and keto–enol forms of Curcumin.

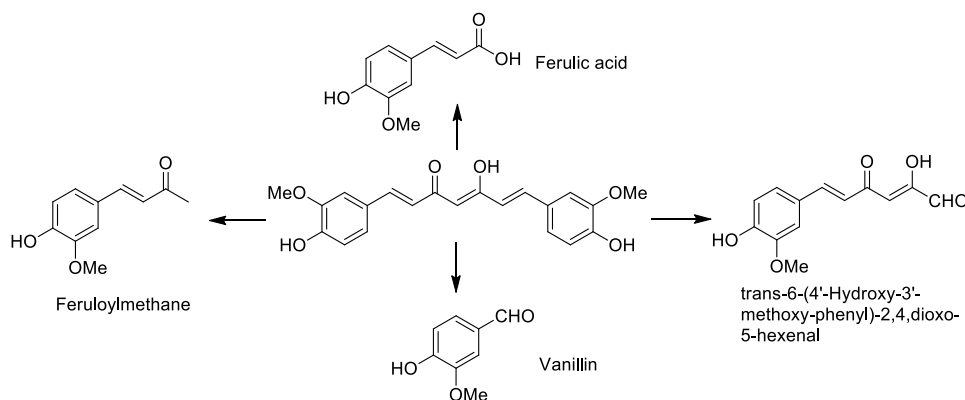
Furthermore, NMR studies using a variety of solvents at pH 3-9 have confirmed that the cis-enol tautomer is the only form of the molecule present in solution; the cis-keto form could be detected only under some special conditions, like low pH and protic solvents.<sup>19</sup> X-ray diffraction studies in solid state, indicates that the cis-enolic form gives extra stabilization to the molecule and allows conjugation between the  $\pi$ -electron systems of the two feruloyl moieties.<sup>20</sup> The keto-enol tautomerism allows donating as well as accepting hydrogen bonds and influences the binding to nucleophiles, the hydrophobicity and polarity of the molecule.

Curcumin possess three acidic protons, one from enol moiety and two from the phenolic groups and shows a strictly dependence to the pH value. At pH<1 Curcumin is in the protonated state and exhibits a red colour, while at pH 1-7 it is bright yellow and exists in the neutral state. At pH>7, deprotonated curcumin exhibits an orange colour, that turns again to red at pH 8 or above, thus indicating that turmeric extract has the properties of an acid–base indicator (Scheme 2.4).



Scheme 2.4

Curcumin undergoes chemical degradation in aqueous-medium that shows strong pH dependence. The degradation increases with the rise in pH. Wang *et al.*<sup>21</sup> demonstrated that in pH range 1.2-6 the degradation is around 10% whereas in phosphate buffer at pH 7.2 more than 90% of Curcumin degrades in 30'. The mayor stability, at acidic pH, is due to the conjugated diene structure. Several important products have been identified as a result of Curcumin degradation. Unlike most phenols that degrade in solution over time forming polymers, the degradation of Curcumin does not occur through the phenolic groups but through the hydrolysis of the  $\alpha,\beta$ -unsaturated  $\beta$ -diketo moiety (Scheme 2.5).<sup>22</sup>



**Scheme 2.5**

Besides its biological properties, Curcumin is also a dye. This yellow-orange pigment exhibits good optical and electrical properties, owing to a symmetric structure and a highly  $\pi$ -electron delocalized system. It is highly soluble in polar organic solvents like methanol, ethanol, DMF, DMSO, chloroform, acetonitrile, toluene, whereas it is poorly soluble in aliphatic or alicyclic organic solvents like hexane and cyclohexane, it is insoluble in water at pH 7, while it is partially soluble in alkaline water.

Curcumin exhibits strong absorption in the UV/Vis region, with an absorption maximum in the range from 400 to 440 nm, concerning a  $S^0$ - $S^1$  electronic transition, depending on the solvent (Figure 2.9).<sup>23</sup>

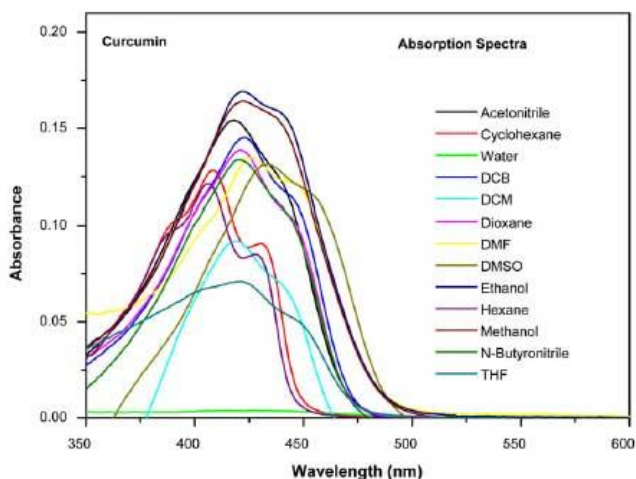


**Figure 2.9:** Absorption spectrum of Curcumin in different solvents.

The spectra in hexane and cyclohexane are structured, while a loss of the vibrational fine structure is observed moving to more polar solvents (e.g. DCM, MeOH). The presence of more than one shoulder probably indicates the presence of more than one isomeric form.<sup>24</sup>

The differences in the absorption spectra in different solvents are still not clear, but it seems they are correlated with the keto-enol equilibrium, while the relative contribution of the keto and enolic tautomers or their cis or trans form seems to be dependent on the solvent. The keto form is less polar than the cis-enol form and may be stabilized in non-polar solvents, thus resulting in a blue shifted absorption spectrum. As the polarity of the solvent is increased, the keto-enol equilibrium is shifted towards the enol conformer, thus consisting in a red shift of the band maximum and in the loss of the spectral structure. Furthermore, at room temperature, the enolic tautomer is in general the predominant form present in solution,<sup>18</sup> confirming that the

major photophysical properties of Curcumin are dictated by the enol tautomer.

As seen for absorption, also emission properties of Curcumin are sensitive to the nature of the solvent. The emission maximum varies depending on the solvent, ranging from 440 to 560 nm (Figure 2.10).<sup>24</sup>

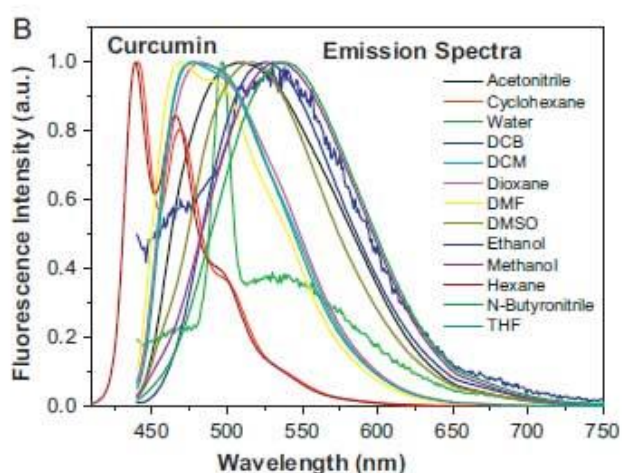


**Figure 2.10:** Emission spectra of Curcumin in different solvents.

Curcumin presents a blue shifted-structured emission in non-polar solvents, like hexane and cyclohexane, whereas increasing the polarity of the solvent the emission is red shifted and results in a broad and structure-less band.

The fluorescence quantum yield, generally around 0.2 for polar solvent, is lower in cyclohexane and hexane and significantly reduced in presence of water.<sup>24</sup> The fluorescence lifetime of the singlet state is very short (300-500 ps) and displays multi-exponential decay profile. Phosphorescence spectra of Curcumin were recorded at 77K in toluene and in ethanol in the wavelength region from 600 to 800 nm with a broad maximum around 725 nm.<sup>25</sup> The spectroscopic data for Curcumin recorded in different solvents are conveniently summarized in table 2.1 reported by Priyadarsini in her review.<sup>24</sup>

**Table 2.1** Absorption and fluorescence maxima, quantum yield, and fluorescence lifetime of Curcumin in different medium.

Medium [reference]	$\lambda_{abs}$ , nm	$\lambda_{fl}$ , nm	Fluorescence quantum yield ( $\phi$ )	Average. fluorescence lifetime ( $\tau_{avg}$ )
CHCl <sub>3</sub>	416, 419	504, 503	0.154, 0.094	372, 596, 130
CDCl <sub>3</sub>	414	494	0.136	332
Toluene	420	460, 488	0.067	
Benzene	418	464	0.052	201, 240
Cyclohexan	408, 429	446, 443, 471, 502	0.014, 0.006	64, 89
n-Hexane	409	444, 469, 500		
Ethanol	430, 427, 430	549, 553	0.063, 0.033	260
Ethanol + KOH	535.2			
Acetone	418, 420	513, 510	0.159, 0.174	388, 708
Acetonitrile	422, 418, 419	524, 538, 521	0.104, 0.075, 0.156	376, 484, 552, 695
DMF	430, 430, 431	540, 542, 536	0.027, 0.022, 0.041	194, 199, 251
Methanol	420, 423, 428	560, 546, 566	0.017, 0.028, 0.022	148, 162
DMSO	429, 434	549, 535, 550	0.024, 0.050, 0.026	196, 166, 238, 155
DMSO- <i>d</i> <sub>6</sub>	431	536	0.045	237
Isopropanol	431	545	0.114	476
Ethyl acetate	419	494	0.105	467
Ethylene glycol	433	566	0.022	232
Glacial acetic acid	422			
0.5 M NaOH	463, 462.6			

Curcumin undergoes faster degradation in solutions exposed to sunlight. The products identified during photodegradation are vanillin, ferullic acid, and other small phenols, indicating a similar product distribution as in chemical degradation in solution (Scheme 2.5). This photodegradation involves formation of the excited states. Curcumin generates singlet oxygen and other ROS upon photoexcitation and this is actually responsible for the photobiological and photodynamic activity of Curcumin. In such case, the degradation of Curcumin after photoexcitation must proceed through the triplet excited state.<sup>26</sup>

## 2.3 Synthesis of the Curcumin-based bichromophoric species

After spending the first year of my PhD working with carbohydrates-based bichromophoric species, I moved my interest toward other natural compounds. In particular, the idea of this new project was to substitute the photophysically inactive sugar linkers, used in the construction of the previously described bichromophoric systems (Chapter 1, paragraphs 1.4-1.8), with a molecule that is still natural, to enhance the biocompatibility, but also a chromophore. Therefore, during the second year of PhD, I synthesized and studied the spectroscopic properties of Curcumin-based bichromophoric systems, in which Curcumin was linked to different chromophores, like the Anthracene-Curcumin compound **1** in figure 2.11, or like the Curcumin-BODIPY compounds **2**, **3** and **4** of figure 2.12.

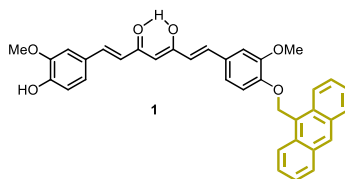


**Figure 2.11:** Anthracene-Curcumin bichromophoric system.

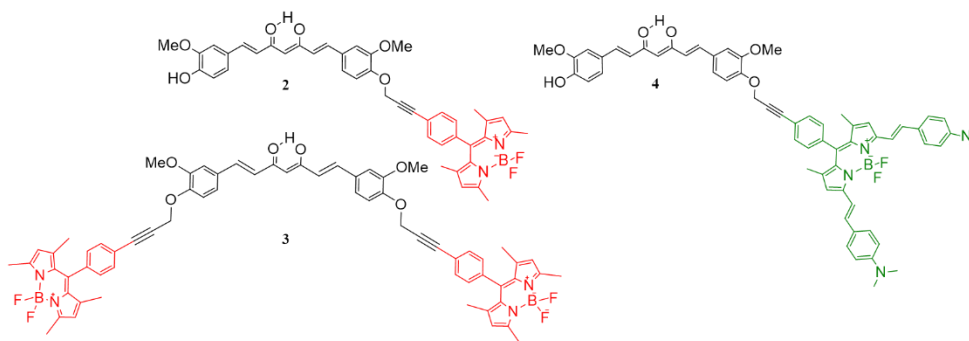
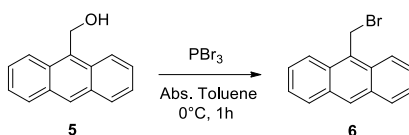


**Figure 2.12:** Curcumin-BODIPY bichromophoric systems.



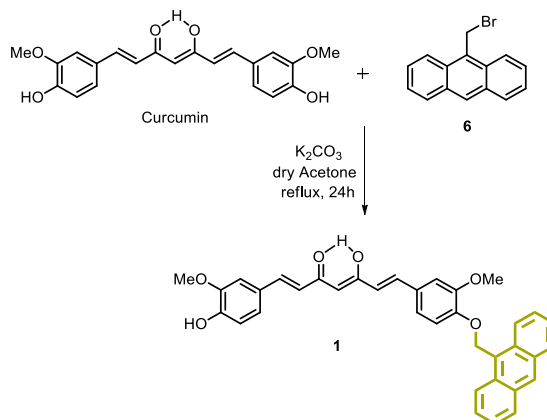
These new bichromophoric systems were built up starting with the synthesis of the chromophores. BODIPY moieties were synthesised as already described in chapter one.

9-Bromo-methyl-anthracene **6** was obtained from anthracene-9-ylmethanol **5**, using a procedure reported in literature (Scheme 2.6) and was used without further purification.<sup>27</sup>



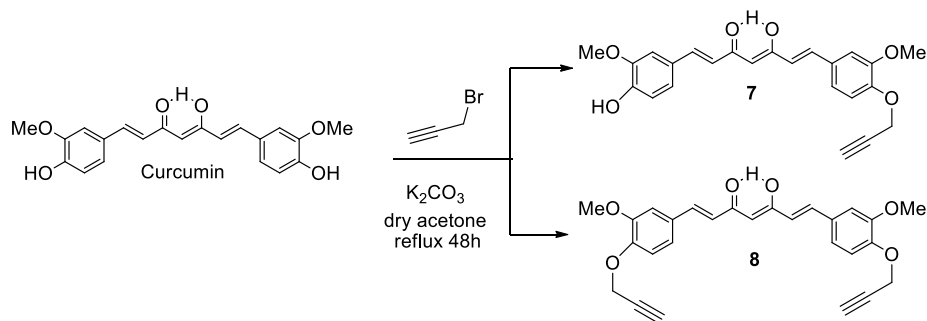
**Scheme 2.6**

The Curcumin that I bought from Aldrich (C1386, purity >65%) is a mixture of Curcumin, demethoxycurcumin and bis-demethoxycurcumin (Figure 2.2). After the initial attempts to use the mixture as it is and the very difficult separation of the obtained compounds, I decided to prior purify Curcumin. The purification was made by column chromatography on silica gel using  $\text{CHCl}_3$ /Hexane 90:10 as eluents. The amount of Curcumin obtained after purification was around 70%. Reaction of purified Curcumin with compound **6**, in ratio 1:0.5, using  $\text{K}_2\text{CO}_3$  as base, followed by purification with column chromatography, afforded the bichromophoric system **1** in 42% yield (Scheme 2.7).



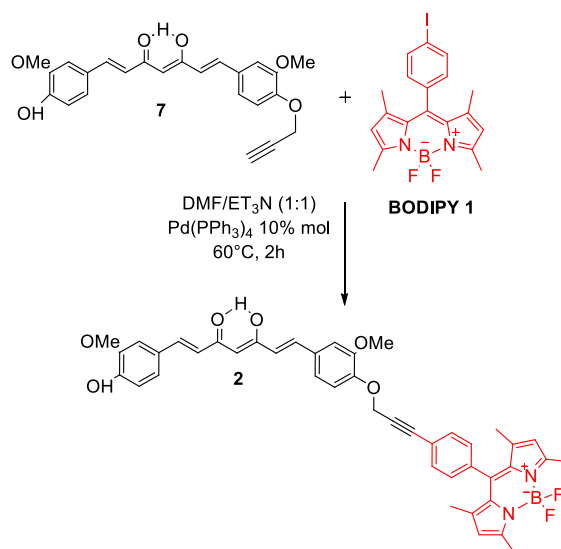
**Scheme 2.7**

During my first year of PhD I have experienced the copper-free Sonogashira reaction for connecting a triple bond to the BODIPY moiety. To obtain the bichromophoric species **2-4** depicted in figure 2.11, I decided to use the synthetic approach already applied for carbohydrate-based bichromophoric species (chapter 1, paragraphs 1.4, 1.6), starting with the addition of the necessary alkyne terminal functionalities to the Curcumin skeleton. The reaction of functionalization was performed by modifying a literature procedure.<sup>28</sup> After a number of attempts to improve yields of the reaction and lower the quantity of side products, Curcumin was reacted with a defect of propargyl bromide and  $K_2CO_3$  (ratio 1:0.5) for 24h after which, an equivalent amount of the reactant was added and the reaction was monitored for other 24h. Purification of the crude afforded the monoalkyne-Curcumin derivative **7** in 47% yield and the dialkyne-Curcumin derivative **8** in 34% yield (Scheme 2.8).



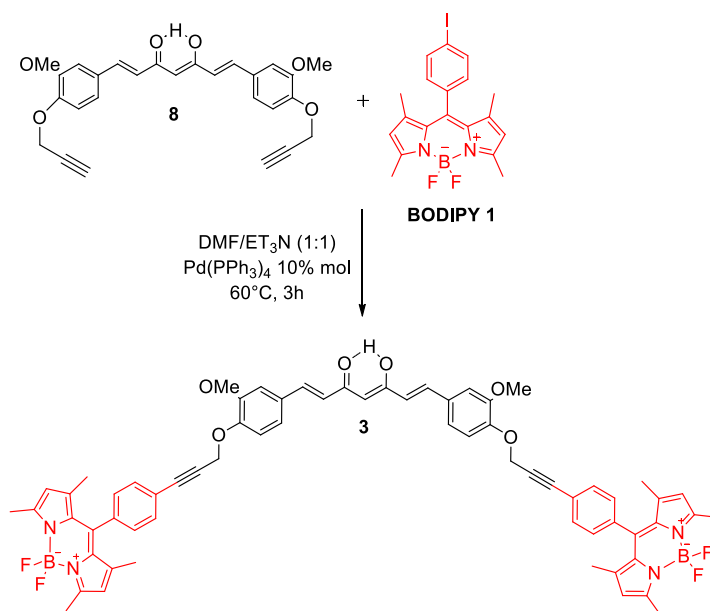
Scheme 2.8

Compound **7** was then reacted with the **BODIPY 1** chromophor, in a copper-free Sonogashira cross-coupling, using 10% of  $Pd(PPh_3)_4$  as catalyst, to obtain compound **2** in 65% yield (Scheme 2.9).



Scheme 2.9

The reaction of Curcumin derivative **8** with the red **BODIPY 1**, afforded compound **3** in 35% yield (Scheme 2.10), together with a mono substituted homologue that was identified by NMR in the crude but not purified.



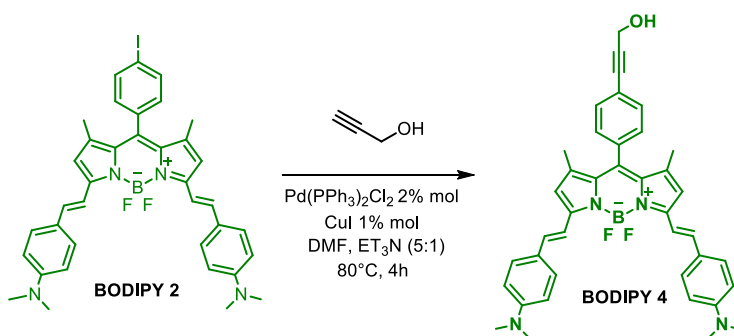
Scheme 2.10

The same conditions were applied to obtain the bichromophoric species **4** (Figure 2.11, page14), but there was no evidence of formation of the desired compound. The copper-free Sonogashira reaction was performed several times on substrate **7** with **BODIPY 2** varying the experimental conditions, such as temperature, time and catalyst percentage but, none of these attempts provided compound **4**. Furthermore, classic Sonogashira reaction, using  $\text{Pd}(\text{PPh}_3)_2\text{Cl}_2$  as catalyst and  $\text{CuI}$  as co-catalyst, was also tried.<sup>29</sup> Experimental conditions are summarized in table 2.2. The results were always negative.

**Table 2.2:** Experimental conditions for the synthesis of compound **4**.

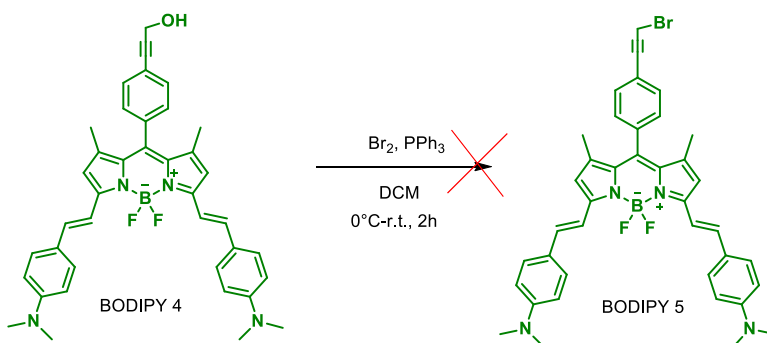
Catalyst	co-catalyst	% of catalyst	time	temperature (°C)	yield
$\text{Pd}(\text{PPh}_3)_4$	-	10%	2h	80	0%
$\text{Pd}(\text{PPh}_3)_4$	-	20%	2h	60	0%
$\text{Pd}(\text{PPh}_3)_4$	-	20%	4h	80	0%
$\text{Pd}(\text{PPh}_3)_2\text{Cl}_2$	$\text{CuI}$	2% /1%	2h	60	0%
$\text{Pd}(\text{PPh}_3)_2\text{Cl}_2$	$\text{CuI}$	2% /1%	2h	80	0%

An alternative synthetic strategy was necessary to obtain compound **4**. Therefore, I decide to convert **BODIPY 2** into **BODIPY 5** (Figure 1.16, chapter 1, pag. 16). **BODIPY 2** was first reacted with a slightly excess of propargyl-alcohol (1:1.2) in a classic Sonogashira reaction, using 2% of  $\text{Pd}(\text{PPh}_3)_2\text{Cl}_2$  as catalyst and 1% of  $\text{CuI}$  as co-catalyst. **BODIPY 4** was obtained in 90% yield (Scheme 2.11) to be converted into **BODIPY 5**.



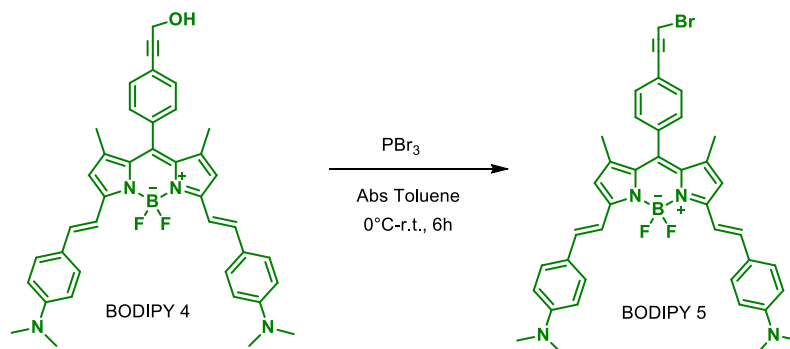
**Scheme 2.11**

The first attempt was made by adding bromine and triphenylphosphine to a solution of **BODIPY 4** in DCM at 0°C.<sup>30</sup> Although TLC after 3h, indicated the formation of a new product, it resulted difficult to purify, because of the contamination of triphenylphosphonium oxide (Scheme 2.12).



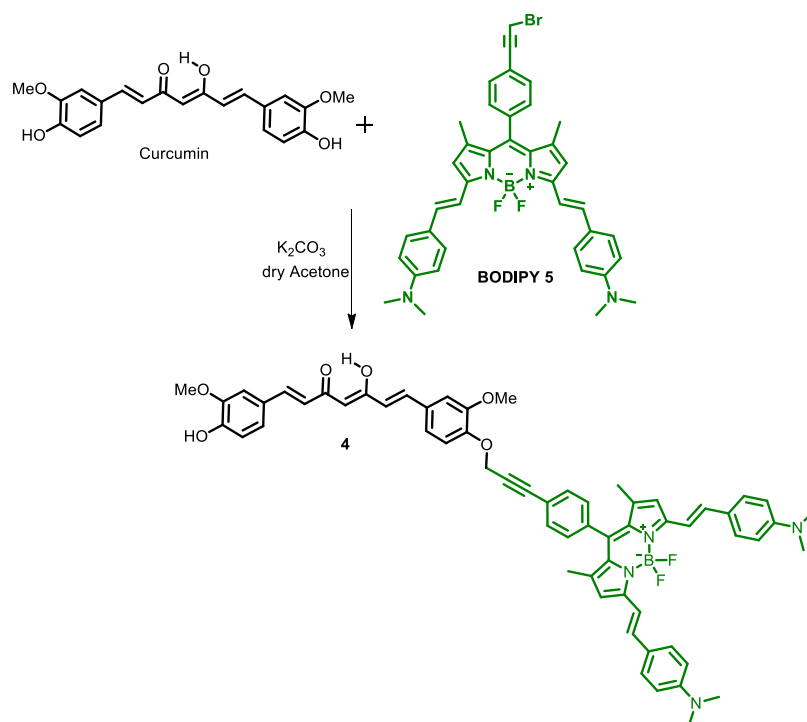
Scheme 2.12

The synthesis of **BODIPY 5** was finally accomplished by adding  $\text{PBr}_3$  to a solution of **BODIPY 4** in absolute toluene at 0°C. Purification of the crude gave **BODIPY 5** in 74% yield (Scheme 2.13).<sup>27</sup>



Scheme 2.13

Compound **4** was obtained as unique product by reaction of pure Curcumin with **BODIPY 5**, using  $\text{K}_2\text{CO}_3$  as base in slightly excess. The yield of the reaction was 34% (Scheme 2.14).



Scheme 2.14

## 2.4 Photophysical properties of the Curcumin-based bichromophoric species

To study and to evaluate the properties of this new Curcumin-based bichromophoric systems, a series of photophysical experiments, including absorption, emission spectroscopy and emission lifetime measurement, were performed in collaboration with the photochemistry group of my department.

The spectroscopic behaviours of compounds **1-4**, compared to that of the subunits, were studied and the results are reported in this chapter.

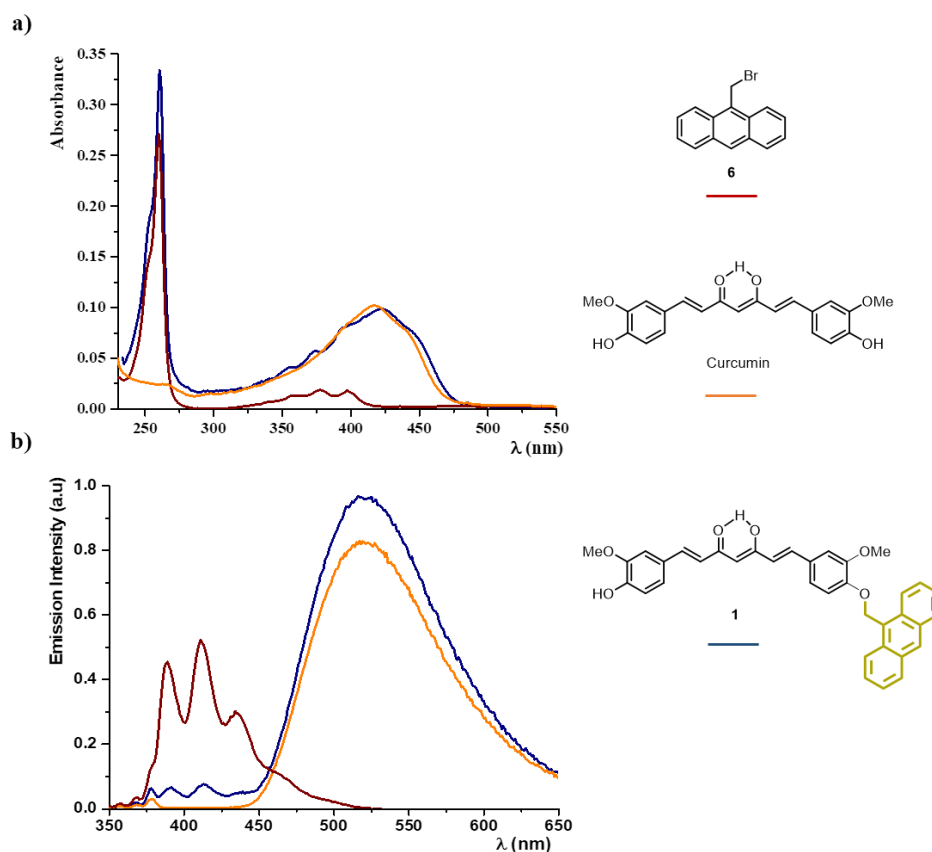


**Figure 2.13:** Absorption (a) and emission (b) spectra of compound **1** (blue line), anthracene derivative **6** (red line) and Curcumin (orange line). Solvent MeCN,  $\lambda_{exc}$  340 nm.

**Table 2.3:** Spectroscopic values characteristic of compound **1** and subunits **6** and Curcumin. Solvent MeCN.

Compound	Absorption	Emission		
	$\lambda_{\text{max}}$ , nm ( $\epsilon$ , M <sup>-1</sup> cm <sup>-1</sup> )	$\lambda_{\text{max}}$ , nm	$\tau$ , ns*	$\Phi$
<b>1</b>	419 (43.800)	520	0.62 (420 nm) 0.55 (550 nm)	0.09
<b>Curcumin</b>	418 (52.900)	518	0.66	0.1
<b>6</b> <sup>31</sup>	374 (10.000)	420	3.3	0.4

The absorption spectrum of compound **1**, recorded in acetonitrile, can be considered as the sum of the absorption spectra of the two chromophoric subunits, the donor anthracene derivative **6** and the acceptor Curcumin. In particular, by comparison of spectrum of compound **1** with the spectra of the two subunits, the band with absorption maximum at about 420 nm is assigned to the Curcumin dye, whereas the bands at 250 nm and 354, 375, 395 nm are characteristics of the anthracene derivative **6** (Figure 2.13, a).

In figure 2.13 (b), the emission spectra of the novel compound **1** and the two precursors are reported. Species **1** exhibits luminescence at room temperature in fluid acetonitrile solution and the spectrum is dominated by a main band centred at 520 nm, attributed – by comparison with the behaviour shown by Curcumin – to the deactivation of excited state localized on Curcumin moiety. By exciting **1** at 340 nm, where both Curcumin and anthracene **6** absorb, it is possible to observe, in the range of 370-440 nm, a low intense structured emission band, finger print of the excited state localized on the anthracene subunit **6** (Figure 2.13, b). This behaviour suggests that in **1** an energy transfer process could be active from the high lying excited state of anthracene **6** to the low-lying excited state of Curcumin moiety. As it is possible to observe in figure 2.14, the excitation spectrum of **1**, registered at 550 nm, is quite similar with the absorption one, demonstrating the contribution of the anthracene (structured absorption band



in the range 370-450 nm) to the population of the excited state of Curcumin in **1**. In table 2.3 both excited state lifetimes and quantum yields for all the investigated species, are reported.

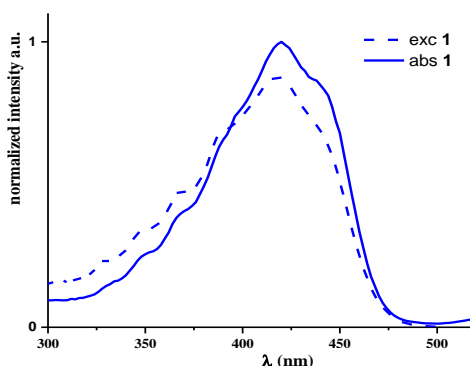


**Figure 2.14:** Comparison between the absorption (straight blue line) and the excitation (dash line) spectra of compound **1**.  $\lambda_{exc}$  550 nm.

The residual emission of anthracene moiety in **1** (Figure 2.13, b) suggests that the energy transfer process is not total. By registering the emission life time of **1** in the residual emission of the anthracene (0.62 ns at 420 nm) and considering the emission lifetimes of the donor anthracene derivative **6**, an efficiency of 82% for the FRET process was estimated using the equation 2.1

$$E = 1 - \tau_{DA} / \tau_D \quad \text{eq. 2.1}$$

where  $\tau_D$  (emission lifetime of the donor subunit **6**) is 3.3 ns and  $\tau_{DA}$  (emission lifetime of the bichromophoric system **1**) is 0.62 ns. Then, the energy transfer rate  $k_{FRET}$   $1.3 \times 10^9 \text{s}^{-1}$  was calculated by using equation 2.2

$$k_{FRET} = 1 / \tau_{DA} - 1 / \tau_D \quad \text{eq. 2.2}$$

The same experiments were performed for the bichromophoric species **2** and **3**, and the results were compared to those of the single subunits, Curcumin derivatives **7** and **8** and **BODIPY 1**.

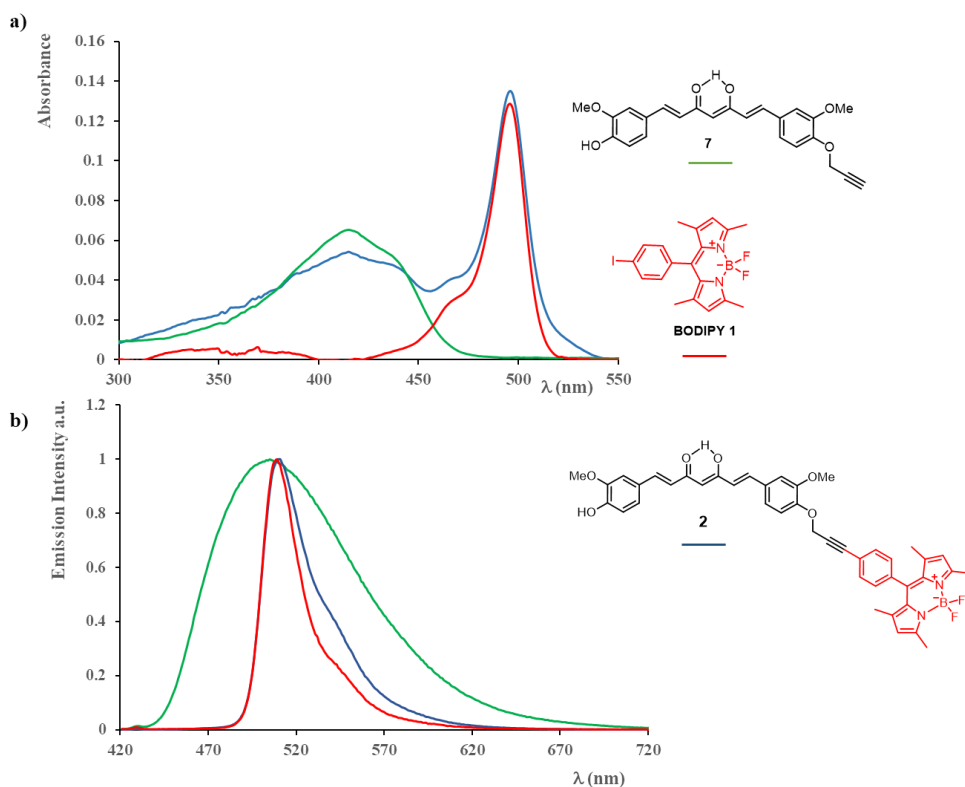


**Figure 2.15:** Absorption (a) and emission (b) spectra of compound **2** (blue line), **BODIPY 1** (red line) and Curcumin derivative **7** (green line). Solvent MeCN.  $\lambda_{exc}$  420 nm.

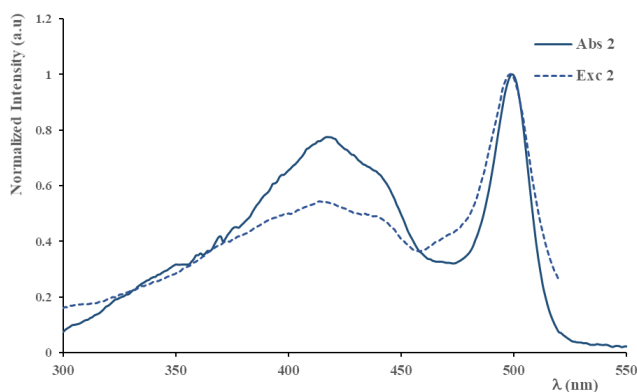
**Table 2.4:** Spectroscopic values characteristic of compound **2**, **3** and the subunits Curcumin derivatives **7** and **8** and **BODIPY 1**.

Compound	absorption	Emission		
	$\lambda_{max}$ , nm ( $\epsilon$ , $M^{-1} cm^{-1}$ )	$\lambda_{max}$ , nm	$\tau$ , ns*	$\Phi$
<b>2</b>	500 (70500)	511	2.9	0.41
<b>3</b>	500 (139950)	510	3.0	0.39
<b>7/8</b>	418 (52900)	506	1.1	0.08
<b>BODIPY 1</b>	500 (69200)	510	3.1	0.4

The absorption spectrum of **2** in acetonitrile solution at room temperature (Figure 2.15) exhibits features that can be assigned to transitions involving the two chromophore frameworks. In particular, the absorption band centred at around 420 nm is typical of the Curcumin subunit (as it is possible to observe by comparison of the absorption spectra of **2** and **7**), whereas the narrow absorption band, with a maximum peak around 500 nm, corresponds to the singlet  $\pi \rightarrow \pi^*$  transition of **BODIPY 1**.<sup>32</sup> By comparison of the absorption spectra of the two subunits, Curcumin **7** and **BODIPY 1** (Figure 2.15, a), it is clearly evident that the absorption contribution of the two moieties are essentially additive in **2**. This indicates that each chromophoric subunit retains its spectroscopic properties in the multicomponent system.

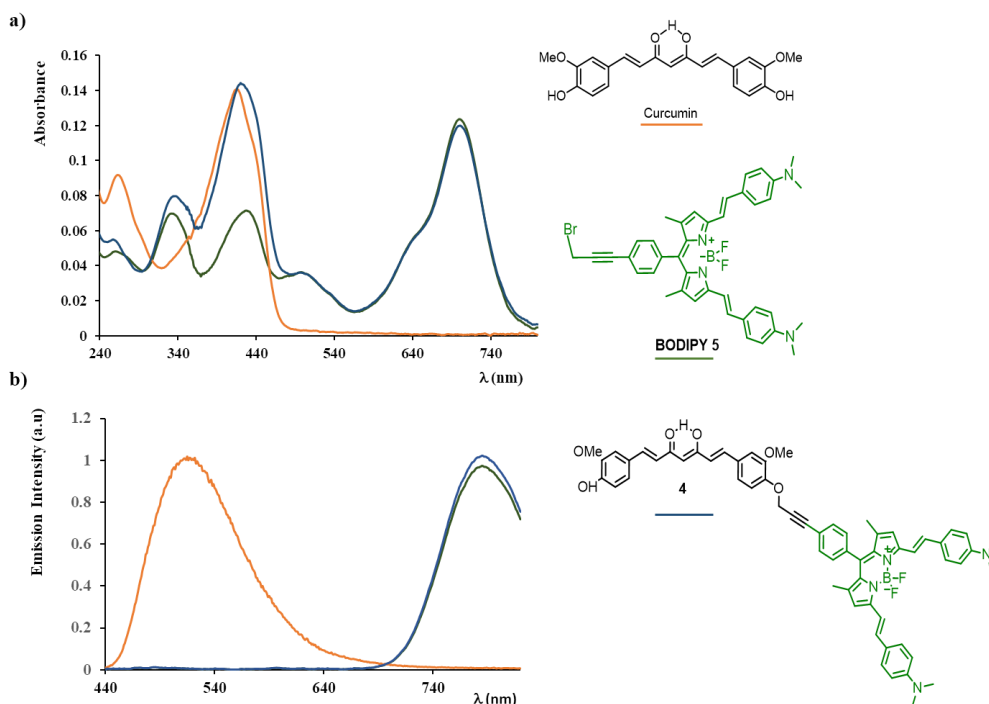
All the species **2**, **7** and **BODIPY 1** are luminescent at room temperature in fluid solution, as shown in figure 2.15 (b) and table 2.4. The emission of **7** in acetonitrile is quite similar to the one exhibited by Curcumin (only 10 nm higher in energy), while, the luminescence spectrum of **2** in MeCN, recorded by exciting on the Curcumin subunit at 420 nm, is characterized by an intense fluorescence band with maximum at about 520 nm that is almost identical to the one exhibited by **BODIPY 1**. This suggests that a photoinduced energy transfer is active in **2** toward the BODIPY fragment, with the Curcumin moiety playing the role of donor, despite the similar energy of the excited states for Curcumin moiety **7** and **BODIPY 1**. This behaviour is confirmed by the excitation spectrum registered for **2** at 530 nm. (Figure 2.16).

Bichromophoric antenna system **3** (photophysical data in table 2.4) shows the same behaviour of compound **2**, hence it was not further discussed.



**Figure 2.16:** Comparison between the absorption (straight blue line) and the excitation (dash line) spectra of **2**.  $\lambda_{\text{exc}}$  530 nm.

The same experiments were performed on the bichromophoric system **4**, in which Curcumin is linked to a low energy red emitter BODIPY (**BODIPY 5**).



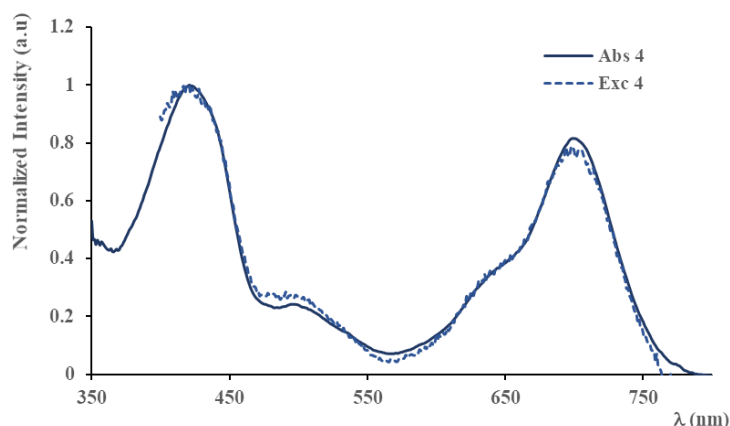
**Figure 2.17:** UV-Vis absorption (a) and emission (b) of **BODIPY 5** (green) and compound **4** (blue), recorded MeCN solutions,  $\lambda_{\text{exc}}$  = 420 nm.

Figure 2.17 reports the absorption and emission spectra recorded in solution of acetonitrile for compound **4** whereas the photophysical data are resumed in table 2.5.

**Table 2.5:** Spectroscopic values characteristic of compound **4** and subunits Curcumin and **BODIPY 5**. Solvent MeCN.

Compound	Absorption	Emission		
	$\lambda_{\text{max}}$ , nm ( $\epsilon$ , $\text{M}^{-1} \text{cm}^{-1}$ )	$\lambda_{\text{max}}$ , nm	$\tau$ , ns	$\Phi$
<b>4</b>	705 (95000)	770	2.2	0.18
<b>Curcumin</b>	418 (52900)	520	0.66	0.1
<b>BODIPY 5</b>	423 (116100)	770	2.2	0.2
	705(94800)			

In this case, as in the precedents, it is possible to clearly distinguish the contributions of the two chromophoric moieties. The absorption band centred at around 420 nm is assigned to the Curcumin moiety, whereas the lowest-energy absorption band around 700 nm is centred on the green **BODIPY 5** subunit and attributed to a  $\pi \rightarrow \pi^*$  with a partial charge transfer character in which the lone pairs of the amine groups are involved (similar to the band reported for **BODIPY 2** in chapter 1) (Figure 2.17, a). The emission spectrum of compound **4** (blue line in Figure 2.17, b) is dominated by a fluorescence band with maximum at about 770 nm that is identical to the one exhibited by **BODIPY 5** (green in in figure 2.17, b). This suggests that, also in this case, an energy transfer takes place from the higher energy absorber moiety Curcumin to the lower energy lying excited state centred on the **BODIPY 5** fragment, as confirmed by the comparison of the excitation spectrum of **4**, registered at 790 nm with the absorption one (Figure 2.18).



**Figure 2.18:** Comparison between the absorption of **4** (straight blue line) and the excitation (dash line) spectra.  $\lambda_{\text{exc}}$  790 nm.

Although more detailed investigation on the kinetics and the efficiency of ET in compounds **2** to **4** are still on running, the absence of residual emission of donor subunits and the superimposition of the emission spectra with those of absorbance for both compounds **2** and **4** (Figures 2.15 and 2.17, respectively) indicate an almost quantitative energy transfer for these two bichromophoric species.

Bichromophoric species **4** in particular attracted my attention because its emission falls in the so-called biological window and it can be regarded as a candidate dye for biological uses.

## 2.5 Biological studies on the bichromophoric antenna systems

In this paragraph preliminary biological results on some of the bichromophoric species described before, are reported. Experiments of cell internalization were performed on erythrocytes, obtained from donor volunteers participating to the study, in collaboration with prof. D. Barreca of my department. First of all, cytotoxicity was evaluated by LDH release analysis.

When the cell membranes are compromised or damaged in any way, lactate dehydrogenase (LDH), a soluble yet stable enzyme found inside every living cell, is released into the surrounding extracellular space. Since this only happens when cell membrane integrity is compromised, the presence of this enzyme in the culture medium can be used as a cell death marker. The relative amounts of live and dead cells within the medium can then be quantitated by measuring the amount of released LDH using a colorimetric or fluorometric LDH cytotoxicity assay.

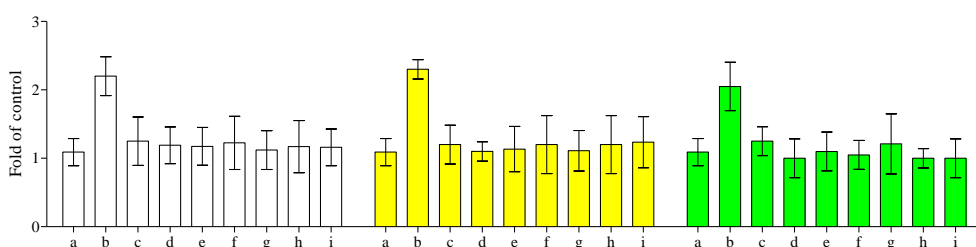


**Figure 2.19:** Spectroscopic determination of LDH release from erythrocytes incubated for 24 h in the absence (a) or in the presence of 20 (b), 10 (c), 5 (d), 1 (e), 0.5 (f), 0.1 (g), 0.05 (h) or 0.025 (i)  $\mu\text{M}$  of compound **4** (white filler), compound **2** (yellow filler) and compound **1** (green filler). Samples were analyzed by one-way ANOVA, followed by Turkey's test. Asterisks (\*\*) indicate a significant difference with respect to controls ( $P < 0.05$ ).

LDH release analysis performed on bichromophoric species **1**, **2** and **4** clearly showed that concentrations superior to 10  $\mu\text{M}$  of each of these compounds induced cell damage, while lower concentrations did not produce any significant change on the cell structure compared to control, as shown in figure 2.19.

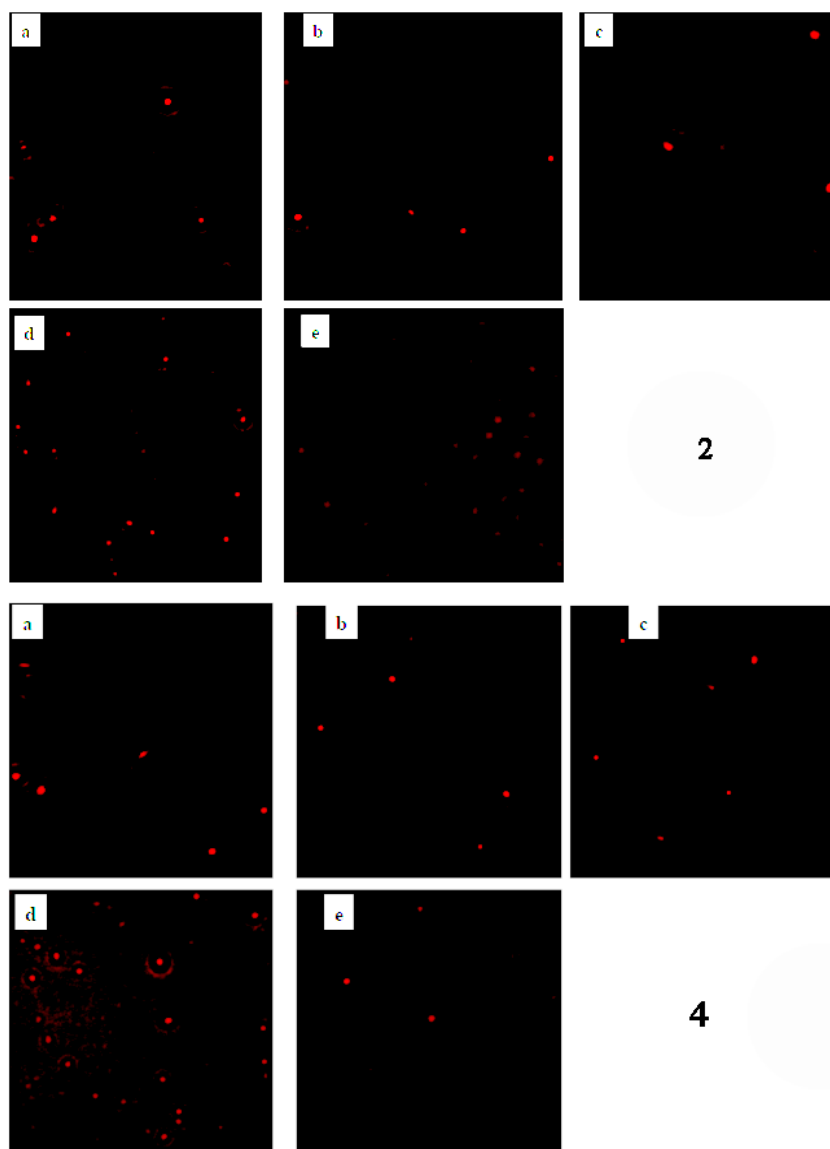


**Figure 2.20:** Fluorescence microscopy images of erythrocytes incubated with 10 (a), 5 (b), 1 (c), 0.5 (d), 0.1 (e)  $\mu\text{M}$  (final concentrations) of compound **2** and compound **4**



Cellular internalization of compounds **1**, **2** and **4** was analyzed by fluorescence microscopy after 24h of erythrocyte incubation in the absence or in the presence of different amounts of the tested compounds.

Detectable amount of the compounds, characterized by red fluorescence inside the cells, has been found in the range of concentration of 0.1-10  $\mu\text{M}$  for bichromophoric specie **2** and **4** (Figure 2.20). Fluorescence microscopy images disclose a clear fluorescence of the cytosol, supporting that compounds **2** and **4** are able to cross the plasmatic membrane.

No fluorescence inside the cells was observed when erythrocytes were exposed to bichromophoric species **1**, in the range of the used concentrations (Figure 2.21).

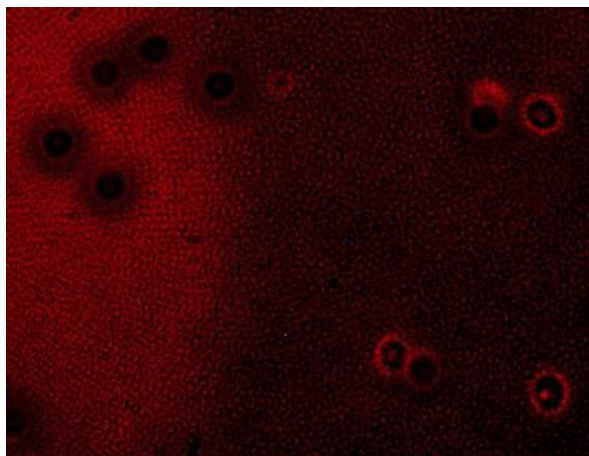


**Figure 2.21:** Fluorescence microscopy images of erythrocytes incubated with 10  $\mu\text{M}$  (final concentrations) of compound **1**.

This last unexpected result cannot be easily understood. However, one hypothesis can be related to the high lipophilic character of anthracene, which belongs to the polycyclic aromatic hydrocarbon (PAH) class. It has been observed that these molecules are strongly embedded in the phospholipidic membrane of cells and their permanence in the membrane is somehow proportional to the size of PAH (bigger sizes longer times of permanence).<sup>33</sup>

Therefore, in case of compound **1**, the curcumin-anthracene species possibly finds difficult to pass through the cellular membrane and internalize.

Finally, the cytoprotective activity of compounds **2** and **4** was exploited in comparison with the effect exerted by Curcumin. The preliminary assays performed for the evaluation of potential cytotoxicity effects of the tested compounds reveal significant changes in the vitality of the cells (monitored by trypan blue coloration) in the range of concentration above 10  $\mu\text{M}$  on isolated lymphocytes vs control sample (data not shown). Based on these results, the cytoprotective potential of the tested compounds has been analyzed on isolated lymphocytes treated with 100  $\mu\text{M}$  of *tert*-butylhydroperoxide in the absence or in the presence (0.1-10  $\mu\text{M}$ ) of compound **2** or **4** and compared with the ones treated with Curcumin at the same concentrations. The obtained results, after 24h of incubation, are depicted in figure 2.22. In the sample treated with *t*-BOOH there is an increase of cells mortality (~43% fall in cell viability vs controls). The presence of 10.0, 5.0 and 1.0  $\mu\text{M}$  of Curcumin resulted in a decrease of cell mortality ranging from ~75 to 5%, respectively, while compounds **2** and **4** showed a potential clearly inferior ranging from ~5.0 to 7.0% only at 10.0  $\mu\text{M}$ . The other tested concentrations showed effects almost completely negligible, with data superimposable with the ones obtained with lymphocytes treated with only *t*-BOOH. The influence of the tested compounds has been further monitored by LDH release. The detection of LDH release in the medium, after oxidative burden due to *t*-BOOH treatment, followed the same behavior as in the case of cell vitality, with some little differences. In the lymphocytes treated for 24h with *t*-BOOH there is a remarkable increase of LDH release, resulting in values about 4.5-fold higher than the control. The release of LDH is decreased of about 6, 32 and 70%, with respect to the sample treated with only *t*-BOOH, by the presence 1.0, 5.0 and 10.0  $\mu\text{M}$  of Curcumin, whereas

compounds **2** and **4** influence is only visible, also in this case, at the highest concentration.

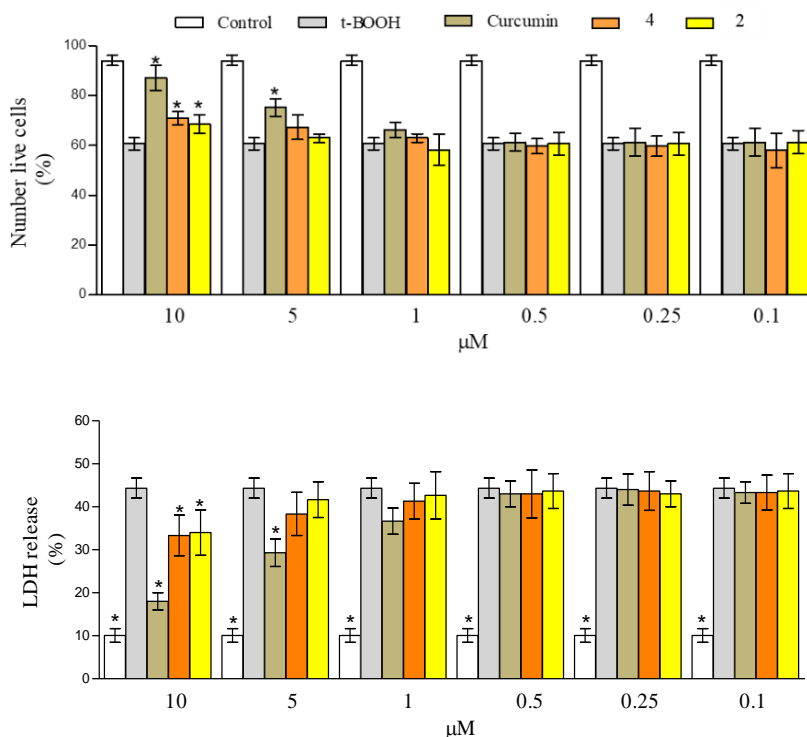


**Figure 2.22:** Cytoprotective effects of the Curcumin, compounds **2** and **4** on *t*-BOOH treated lymphocytes. Lymphocytes plus 100  $\mu\text{M}$  of *t*-BOOH were incubated for 24 h in the absence or in the presence of 10.0, 5.0, 1.0, 0.5, 0.25 and 0.10  $\mu\text{g/mL}$  of the tested compounds. Cell vitality and integrity were analyzed by trypan blue staining (A) and LDH release (B), respectively. The samples were analyzed by one-way ANOVA, followed by Bonferroni's post-hoc comparisons tests. The asterisks (\*) indicate significant differences ( $P < 0.05$ ) of the sample vs treated one. Each value represents mean  $\pm$  SD ( $n = 3$ ).

## 2.6 Luminescent species in mesoporous Silica

---

As part of the PhD program, I spent four months of my third year working in the research group of Dott. Fabio Cucinotta at the Newcastle University. The research in which I have been involved regarded the synthesis of mesoporous silica nanoparticles, the incorporation of the synthesized bichromophoric species and subunits inside the nanoparticles and the study of their photophysical properties.

The incorporation of fluorophores into nanocarriers is a strategy to improve the photostability and to circumvent the sensitivity to air and interactions of most chromophores with their local environment, also allowing to manage high dye concentrations avoiding aggregation, while keeping the characteristic of the chromophores unaltered. With the allocation of organic photoactive guests into nanostructured inorganic frameworks, well-organised multifunctional dye-doped hybrid materials could be obtained.<sup>34</sup> Most of the biological luminescent labels are organic dyes that usually suffer of photo bleaching and quenching, due to interactions with solvent molecules and reactive species such as oxygen dissolved in solution. A promising strategy to overcome the above disadvantages is to form dye-doped silica composites. Shi *et al.*<sup>35</sup> introduced the co-condensation method to covalently graft rhodamine B (RhB) groups within the mesoporous channels of SBA-15 (a class of mesoporous silica nanoparticles) for the synthesis of compounds with red fluorescent emission. This resulted in material that possesses high dye doping amount, high fluorescence quantum yield, excellent photostability and high fluorescence detectivity. Moreover, incorporation in nanoparticles is used as a strategy to enhance the bioavailability and the solubility of lipophilic compounds, such as Curcumin, and as a way to improve the therapeutic effects of the encapsulated compound by protecting it from enzymatic or chemical degradation. By this way a controlled release of the

drug and prolonged blood circulation could be obtained, enhancing the pharmacokinetic properties, decreasing the toxicity, and limiting the nonspecific uptake.<sup>36</sup>

Mesoporous silica nanoparticles (MSNs) are one of the most employed nanosystems.<sup>37</sup> Due to their ordered nanoporous structures, high surface areas, large pore volumes and high surface densities of hydroxyl groups, MSNs can be easily functionalized. Furthermore, silica has good biocompatibility and is accepted as GRAS by the FDA, so MSNs have been intensively suggested for use in biomedical imaging/therapy and biosensors.<sup>38</sup>

Therefore, luminescence functionalized mesoporous silica, that can be easily identified, tracked and monitored to evaluate the efficiency of the drug release and disease therapy, have become a research hot topic. A MCM-41-type mesoporous silica material was first reported as a drug delivery system in 2001.<sup>39</sup> Since then, luminescent materials (such as organic dyes, quantum dots, and rare-earth nanophosphors) or magnetic nanoparticles have been successfully used to functionalize the mesoporous silica.<sup>34</sup>

Nanostructured materials, such as mesoporous silica and zeolites, with their host guest chemistry, represent an appealing class of scaffolds that have opened up new possibilities for the investigations on chromophores confined in constraint space and their use as materials for light harvesting applications. The chance of functionalizing these nanostructures with different luminophores allows the obtainment of materials with tuneable photophysical properties, depending on the doping dye, providing a well organised photoactive material.<sup>40</sup> Dutta *et al.*<sup>41</sup> demonstrated that it is possible to store solar energy by photoelectron transfer in zeolite structure, whereas Tolbert *et al.* and Calzaferri *et al.*<sup>42</sup> have demonstrated that in conjugated polymer immobilized in mesoporous silica, it is possible to control the Forster Resonance Energy Transfer over the molecular scale. For

instance, alumina-silicate zeolite is an ideal solid host, owing to its one-dimensional channel system with a pore opening size and provides an alignment of the guest molecules along the zeolitic channels (Figure 2.23). Thus, the incorporation of luminescent dyes gives rise to a supramolecular organisation in which the energy donors are placed in the centre, while the acceptors are located in the pore entrances. Light can be transferred by a FRET mechanism in a cascade-like unidirectional process, to obtain photoactive materials capable of modulating the colour light output.<sup>43</sup>

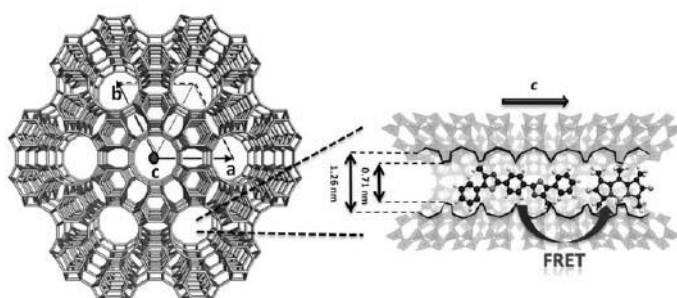


**Figure 2.23:** Zeolite framework and one-dimensional channels suitable for allocating luminescent fluorophores.

Recently Cucinotta *et al.*<sup>44</sup> reported a new class of light-harvesting antenna prepared by exploiting the template-assisted host-guest chemistry of mesoporous organosilica. The employing of green-yellow emitting BODIPY dyes, specifically functionalized to self-assemble into different types of micellar templates, allows the obtainment of different hybrid materials that displayed different energy collection phenomena. The photochemical properties were tuned by varying the dye loading in order to obtain fast energy migration rates (in the ns scale) throughout the whole material. This indicated that the optical bandwidth and the energy collection in artificial antenna systems can be manipulated by employing chromophores able to self-assemble (Figure 2.24).

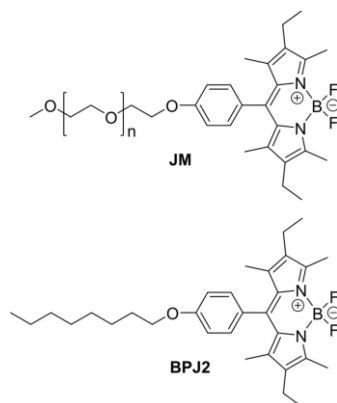
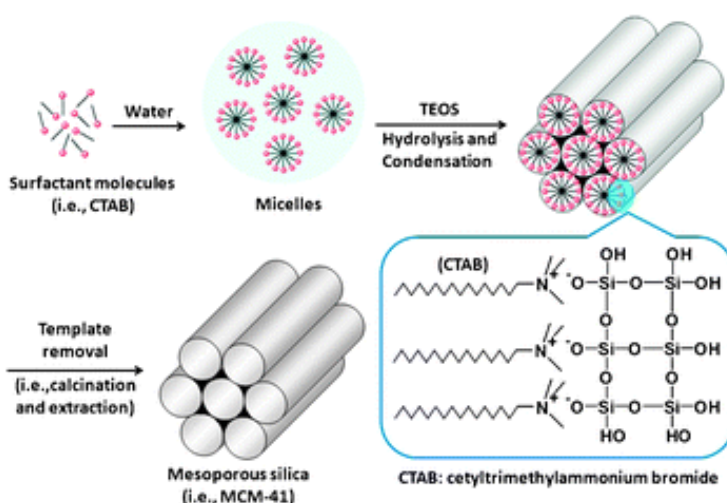


**Figure 2.24:** Modified BODIPY chromophores.

The synthesis of pure inorganic, high ordered porous silica phases was first reported in 1992.<sup>45</sup> These are formed through a sol-gel process in the presence of structure-directing agents (SDAs) like self-assembled aggregates of surfactants. The SDA-mediated synthesis consents the regularity and adjustability of the pores. The most well-known representatives of this class of mesoporous silica nanoparticles (MSNs) are MCM-41 (with a hexagonal arrangement of the mesopores), MCM-48 (with a cubic arrangement of the mesopores) and MCM-50 (with a lamellar structure). The procedure for the synthesis of MSNs nanoparticles is reported in scheme 2.15.



**Scheme 2.15**

The surfactant, usually a long-chain C-16 or C-12 alkyltrimethyl ammonium bromide, is dissolved in water at specific pH and concentration, forming, at the critical micellar concentration (c.m.c), regular mesophases or liquid-crystalline states (hexagonal ordered assemblages of rodlike micelles in the case of MCM-41). The source of silica, an inorganic precursor like tetra-ethylorthosilicate (TEOS) is added. Due to the hydrolysis, this precursor forms siloxane bonds and condensates around the micelles, mirroring the shape of the template. Once the network is built, the surfactants can be removed easily by extraction or calcination. By choosing surfactants that give smaller or larger aggregates in appropriate synthesis conditions, it is possible to adjust the desired pore size in the nm range. Furthermore, it is possible to functionalize the silica structure through a variety of *in situ* or post-synthetically reactions using silane-functionalized organic precursors.<sup>46</sup>

The original synthetic approach has been extended by a number of variations, for example, by the use of a non-ionic triblock copolymer surfactants, Pluronic Triblock (i.e P123) for the synthesis of various large-pore (5 to 30 nm) mesoporous pure silica phases, such as SBA-15 and COK-12, classes of hexagonally large-pore analogue of MCM-41.<sup>47</sup>

Effect of particle size (EPS) is an important factor to determine the biocompatibility of the nanomaterials. Pore structure seems to have an influence on the drug loading and release properties. Depending on the surfactant concentrations or type, MSNs can be synthesized with different mesostructure shapes, such as hexagonal, cubic, etc. The empty mesopore channels are able to absorb or encapsulate relatively large amount of bioactive molecules. The decrease in pore diameter leads to a decrease in drug loading amount and release rate. The specific surface area is an important factor governing the amount of retained drug molecules. A high surface area with more Si-OH groups will provide more active sites, resulting in an increased drug loading amount. A large number of studies have focused



on the relationship between the size of MSNs and their biocompatibility, compared to the conventional drug carriers. The effects of size of MSNs on cellular uptake were investigated in detail by Mou *et al.*<sup>48</sup> Authors synthesized ordered MSNs, with uniform sizes in the range of 30 nm to 280 nm and investigated their internalization into Hela cells. The results show that cellular uptake amount is dependent on the particle size, with particle size of 50 nm being most effective in drug delivery.<sup>49</sup>

As reported in paragraph 2.1, to deliver therapeutic concentrations of Curcumin, and to overcome the main problems of low solubility, instability and poor bioavailability, liposomes, polymeric nanoparticles, micelles, nanogels, cyclodextrins, dendrimers, and solid lipids were employed as useful alternatives.<sup>16,50</sup> Until recently, the word nanocurcumin referred to curcumin-loaded organic formulations only, however in the last few years, researchers have been prepared formulations in which Curcumin is bound to inorganic, such as silica, nanoparticles. Various way to obtain Curcumin-doped silica nanoparticles are reported in literature. Curcumin is either added during the process of synthesis of the nanoparticles,<sup>51</sup> or through a simple physisorption onto the surface of MSNs, in which Curcumin, dissolved in an organic solvent is encapsulated into calcined (hollow) MCM-41 by a simple rotary evaporatory (Rotavap) technique.

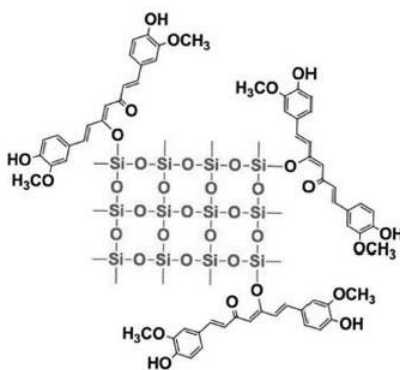



**Figure 2.25:** Immobilization of Curcumin inside silica nanoparticles.

In these systems Curcumin is supposed to bind covalently through a silicon-oxygen bond at the diketone moiety (Figure 2.25).<sup>52</sup>

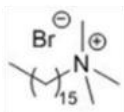
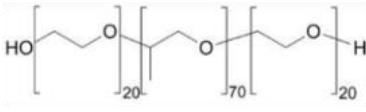
Curcumin release could be controlled for several hours leading to an improvement of the stability and bioavailability. Moreover, the fluorescence of Curcumin is enhanced and therefore these systems have the potential to be employed for imaging biomolecules. Other methods of encapsulation of Curcumin in silica nanoparticles comprehend post-synthetically reactions using silane-functionalized organic precursors, to obtain anchoring groups that can link covalently Curcumin to the surface, i.e. via thiol-ene “click” chemistry, via condensation by nucleophilic substitution or through amine functionalization.<sup>53</sup>

## 2.7 Synthesis of silica nanoparticles with the bichromophoric species and their photophysical characterization

During the time spent at Newcastle University, I focused my attention on two different types of MSNs, the MCM-41 and the COK-12, both of them presenting hexagonal array of ordered rod-like mesopores, with the main differences reported in figure 2.26, and particle size suitable for cell internalization.

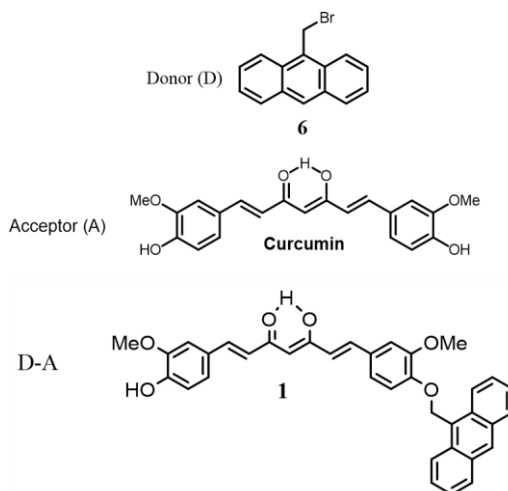
a)	MCM-41	COK-12	b)
pore size	3-4 nm	6-7 nm	
particle size	70-100 nm	500-800 nm	
template	CTAB	P123	
synthesis pH	12	6.5	

c)		
	CTAB	P123

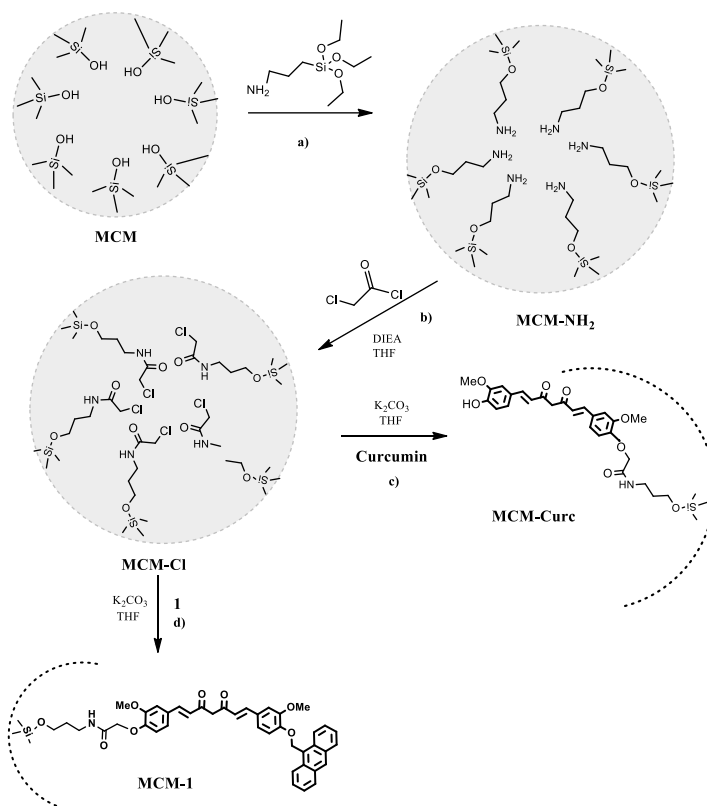
**Figure 2.26:** Comparison of the two materials a); shape and structure b) type of surfactant c).

These nanoparticles were doped with the bichromophoric compound **1** and the subunits, anthracene derivative **6** and Curcumin (Figure 2.27), with the objective of studying the spectroscopic and biologic behaviour of this dyes inside the nanoparticles and to determine possible variations in the energy transfer process.

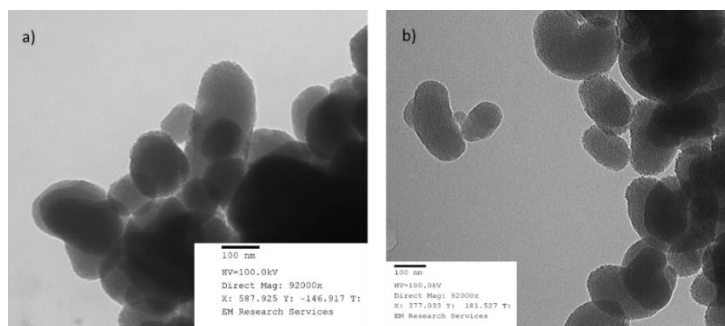


**Figure 2.27:** Dyes used to dope silica.

The first attempt passed through the synthesis of MCM-41 silica nanoparticles. Due to the highly alkaline pH required and its alkaline-lability, it was not possible to insert Curcumin during the synthesis, so I tried a post-synthetic modification of the surface.<sup>53</sup> MCM-41 were synthesized using a literature procedure, then the surfactant tetrabutylammoniumbromide (TBAB) was removed using Soxhlet extraction with EtOH and HCl. The obtained hollow silica nanoparticles were further functionalized with 3-amino-propyl-triethoxysilane (APTES), to give silica with terminal amino groups MCM-NH<sub>2</sub> (Scheme 2.16, a).<sup>54</sup> These were treated with chloroacetyl chloride in presence of ethyldiisopropylamine (DIEA) to obtain MCM-Cl (Scheme 2.16, b).<sup>55</sup> The obtained chloro-functionalized silica nanoparticles, MCM-Cl were reacted, in a ratio 1:1 and in the presence of K<sub>2</sub>CO<sub>3</sub>, with Curcumin (scheme 2.16, c) to obtain MCM-**Curc**, and with compound **1** (Scheme 2.16, d) to obtain MCM-**1**, respectively. The estimated percentage of loading was around 60% in both cases, thus resulting in a distortion of the shape of the nanoparticles, confirmed by TEM microscopy (Figure 2.28). Further efforts to use lower amount of dyes gave no reproducible results, so the procedure was abandoned.



Scheme 2.16

**Figure 2.28:** TEM imaging of MCM-Curc (a) and MCM-1(b).

I moved then toward the synthesis of COK-12 nanoparticles that, as shown in figure 2.26, possess larger pore diameters and their synthesis occurs at quasi-neutral pH. Therefore, a series of COK-12 silica materials were prepared by using a modified templated synthesis,<sup>44</sup> where the dyes previously synthesized and studied (Figure 2.27) were used as dopant into

the Pluronic-123 at different molar ratios of 10% and 20%. This led to the obtainment of COK-10% or COK-20% (meaning COK doped with 10% or 20% of dyes) with Curcumin, anthracene derivative **6** or compound **1**, respectively.

The syntheses were performed using the tri-block copolymer Pluronic-P123 in citrate buffer at pH 6.5, which does not alter the stability of the dyes. The formation of mesoporous silica was achieved upon addition of sodium silicate solution to the micellar phase containing P123 and the chosen dye (Figure 2.29).<sup>46</sup>

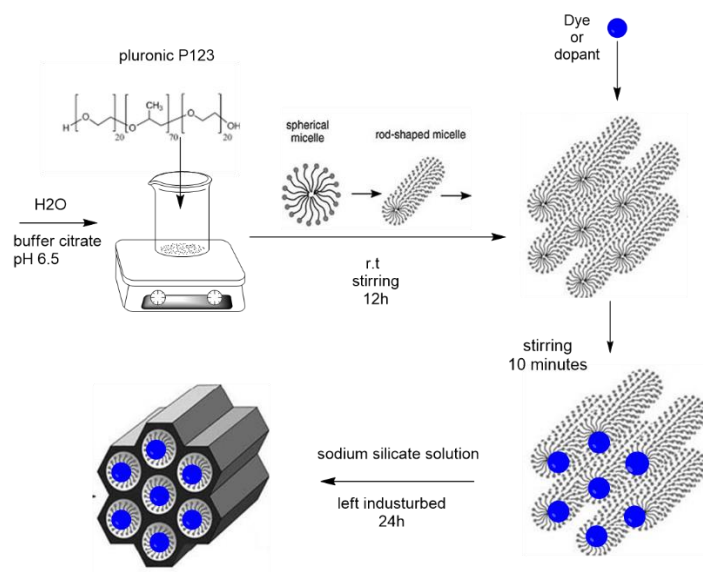


**Figure 2.29:** Schematic representation of the synthesis of COK doped nanoparticles. Notably, the amount of dye is variable, depending on the desired ratio, and the dye could be solubilized before addition to the micelle.

The new hybrid materials were then structurally and spectroscopically characterized. Cucinotta *et al.*<sup>44</sup> reported the structural value for the standard sample of COK-12 obtained with this methodology. TEM images of the newly synthesized COK show that an ordered morphology in the nm range of the micelles is retained independently of the dye concentrations (Figure 2.30).

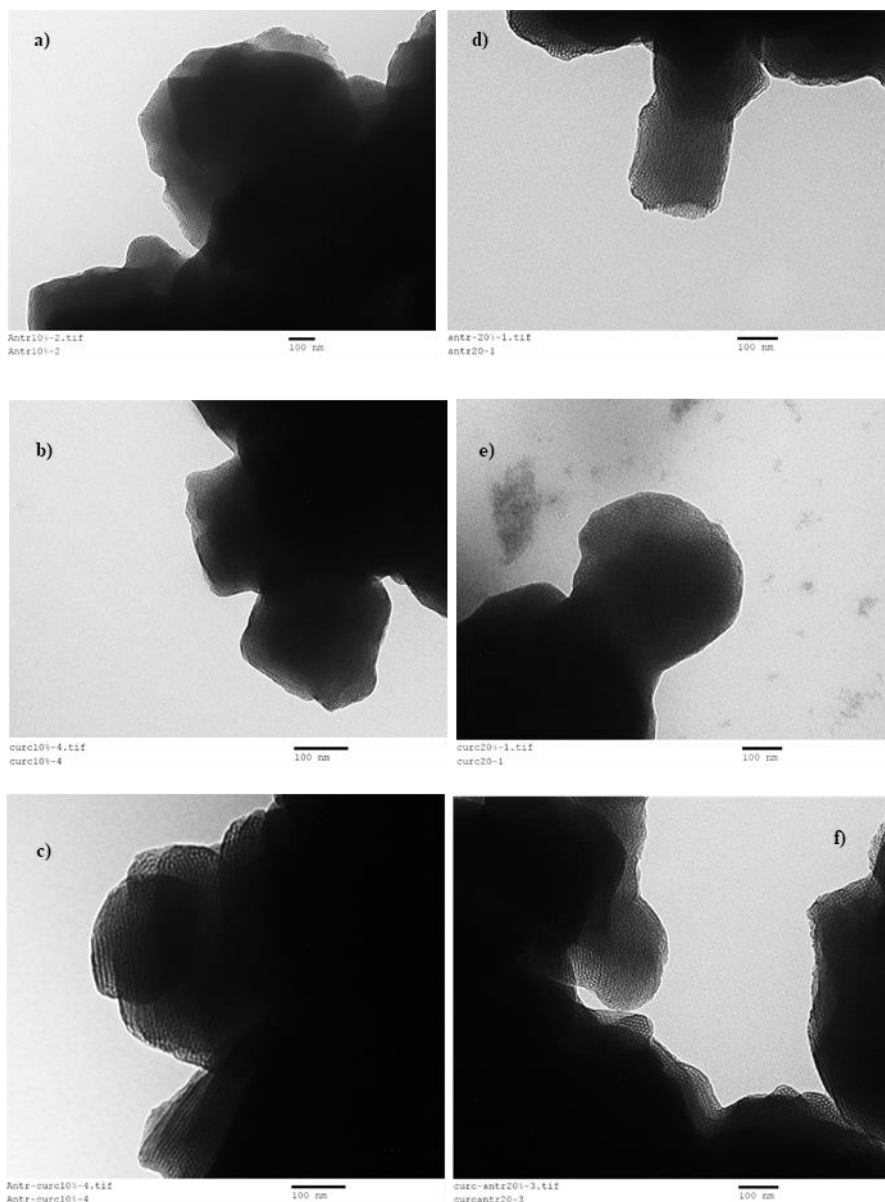


**Figure 2.30:** TEM imaging of COK-10% anthracene derivative **6**, a); Curcumin, b); and compound **1** c); COK-20% anthracene derivative **6**, d); Curcumin, e); and compound **1**, f).

The COK-12 silica materials were characterized by UV/Vis absorption and luminescence spectroscopy, and their properties were compared to those of the free dyes, in order to study the effect on the energy transfer inside the nanoparticles. Optical measurements were performed from suspensions of the

materials in solvent where the particles are finely dispersed, to try to limit the intense scattering that is generated by the suspended particles. The spectra were recorded from stable 0.3 mg/ml suspensions in cyclohexane.<sup>44</sup> However, the absorption spectra were characterized by a high scattering, therefore, only the excitation spectra are reported.

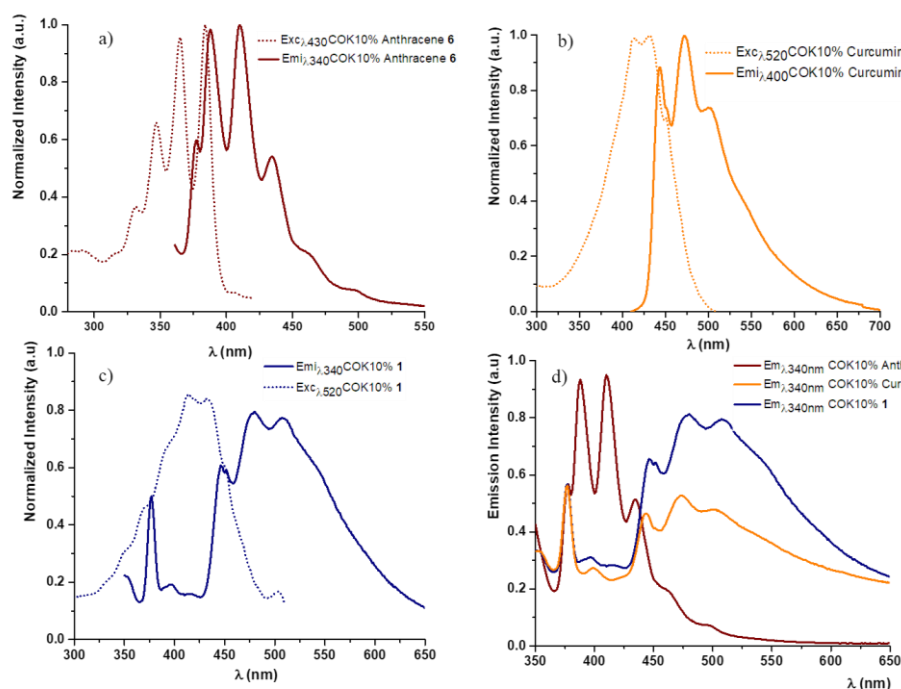


**Figure 2.31:** Excitation and emission spectra of COK-10% doped with anthracene derivative **6**, a); Curcumin, b); and compound **1**, c); Comparison between the emission spectra of the three components upon excitation at 340 nm, d). Spectra recorded in suspension of cyclohexane 0.3 mg/ml.

The excitation and emission spectra of COK-10% anthracene derivative **6**, (Figure 2.31, a) compared with those recorded in solution of acetonitrile (Figure 2.13 and 2.14, paragraph 2.4), show the same behaviour except for a slightly blue shift of 9 nm of the peaks, both in excitation and in emission, probably due to a rigido-chromic effect inside the nanomaterial. The emission decay profiles were obtained using the time correlated single photon counting (TCSPC) technique and the emission lifetime measured at  $\lambda=420$  nm is 2.7



ns, lower compared to those recorded in solution, a possible consequence of non-radiative quenching of the dye that undergoes inside the silica matrix.

The excitation and emission spectra of COK-10% Curcumin, (Figure 2.31, b) are slightly different from those recorded in solution. The excitation spectrum shows a more structured band from 420 to 435 nm. This change could be related to the aggregation of the dye inside the micelles and to the fact that the dye is now constrained in an apolar medium. In the emission spectrum a structured emission from 440 to 550 nm and a blue shift, due to the rigido-chromic effect imposed by the matrix, are observed. The emission lifetime measured at 510 nm is 0.23 ns, lower compared to the emission lifetime of Curcumin in solution, as also observed for anthracene in COK-12 at 10% loading.

The excitation spectrum of COK-10% compound **1** (Figure 2.31, c), shows that the two chromophore subunits contributions, as seen for compound **1** in solution in paragraph 2.4, are essentially additive. In particular, by comparison of the excitation spectrum of COK-10%-**1** with the spectra of the two subunits, the bands from 440-550 nm are assigned to the Curcumin dye, whereas the structured band from 345 to 385 nm are characteristics of the anthracene derivative **6** (Figure 2.31, a). The emission spectrum (blue line in figure 2.31, c) is dominated by a structured emission in the range 440-550 nm, attributed to the deactivation of the excited state localized on the Curcumin moiety. By exciting COK-10%-**1** at 340 nm, where both Curcumin and anthracene **6** absorb, it is possible to observe, in the range of 370-440 nm, a low intense structured emission band, finger print of the excited state localized on the anthracene subunit **6** (Figure 2.31, d). This behaviour suggests that even in COK-10%-**1** an energy transfer process could be active from the excited state of anthracene **6** to the excited state of Curcumin moiety. Due to the high scattering coming from the suspension of nanoparticles, it was not possible to record the absorption spectrum of COK-10%-**1** and to

compare with the excitation one. However, the excitation spectrum of COK-10%-**1** recorded at 510 nm is quite similar (except for the more structured band of Curcumin moiety) to the one recorded in solution, as shown in figure 2.32.

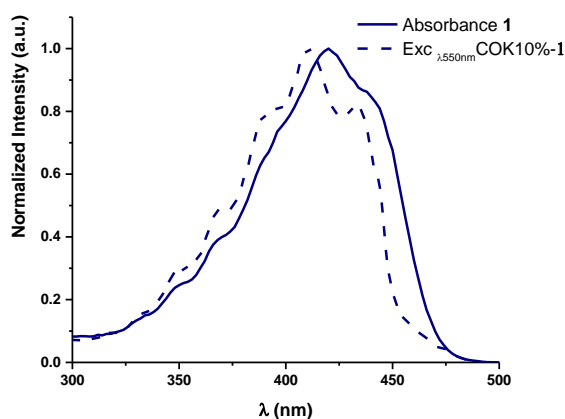


**Figure 2.32:** Comparison between the absorption spectrum of compound **1** (straight blue line) and the excitation of COK-10%-**1** (dash line).  $\lambda_{exc}$  510 nm.

These data demonstrate the contribution of the anthracene to the population of the excited state of Curcumin in COK-10%-**1**, with a residue in the region around 400 nm, due to the anthracene subunit **6** (Figure 2.31, d). Furthermore, they suggest that there is an incomplete energy transfer, from the anthracene subunit **6** to the Curcumin. The emission lifetime of the excited state recorded at  $\lambda=420$  nm is 0.4 ns. From the emission lifetime it is possible to estimate the efficiency of 84% of the ET process and the ET rate of  $2.05 \times 10^{-9} \text{ s}^{-1}$  by using equations **2.1** and **2.2** reported in paragraph 2.4, so confirming what it has been already observed for compound **1** in solution.

In order to study the effects on the energy transfer by varying the concentration, the same experiments were performed on COK-20%.

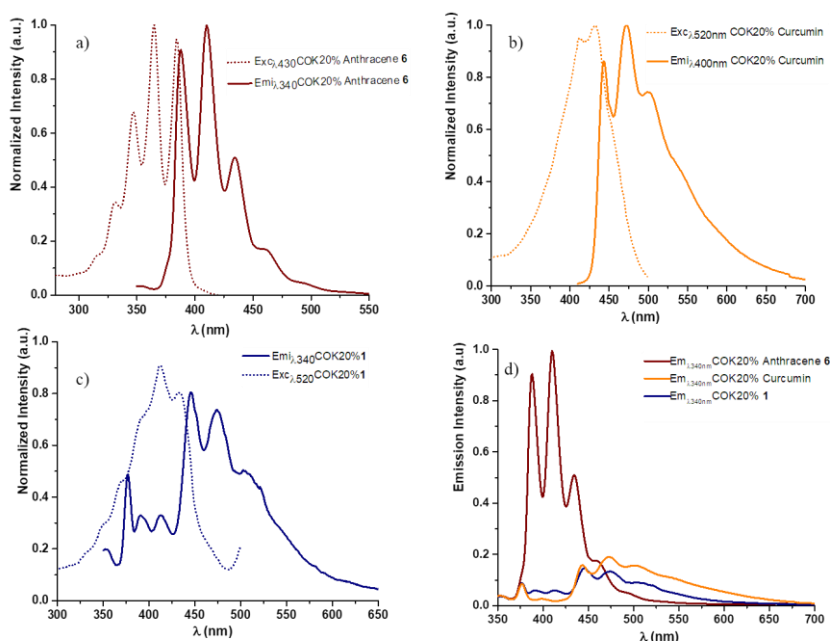


**Figure 2.33:** Excitation and emission spectra of COK-20% doped with anthracene derivative **6**, a); Curcumin, b); and compound **1**, c); Comparison between the emission spectra of the three components upon excitation at  $\lambda$  340 nm, d). Spectra recorded in suspension of cyclohexane 0.3 mg/ml.

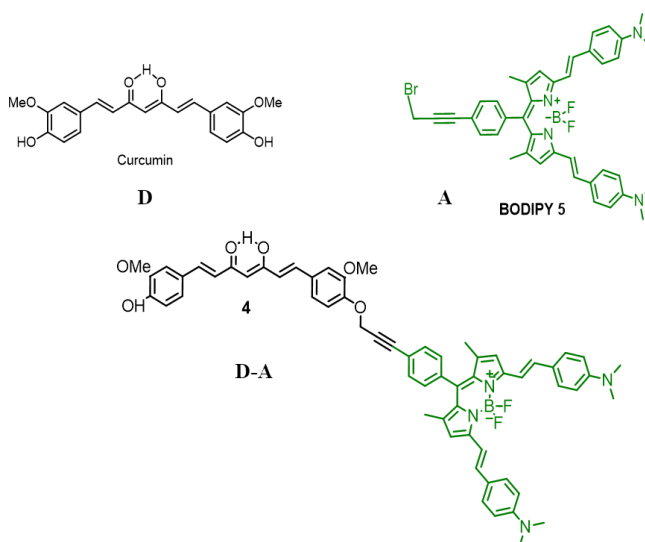
**Table 2.6:** Spectroscopic values characteristic of compound **1** and subunit anthracene derivative **6** and Curcumin in COK silica nanoparticles. Data recorded in suspension of cyclohexane 0.3 mg/ml.

Compound	Absorption		Emission	
	$\lambda_{\text{max}}$ , nm	$\lambda_{\text{max}}$ , nm	$\tau$ , ns*	$\Phi$
<b>COK-10%-1</b>	430	470	0.4 (420 nm) 0.23 (510 nm)	Nd
<b>COK-20%- 1</b>	432	472	0.36 (420 nm) 0.22 (510 nm)	Nd
<b>COK-10%-6</b>	384	411	2.79	Nd
<b>COK-20%-6</b>	384	411	2.72	Nd
<b>COK-10% - Curcumin</b>	430	470	0.60	Nd
<b>COK-20%- Curcumin</b>	432	472	0.66	Nd

\*Notably, all the lifetime measurements were recorded comparing the results to those coming from a suspension of pure silica, namely ludox, to minimize the error from the scattering.

The resulting excitation and emission spectra are reported in figure 2.33 and the photophysical data summarized in table 2.6. The behaviour is the same reported for the COK-10%. The 86% of the efficiency of the energy transfer was calculated with the same equations considering  $\tau_D = 2.72$  ns and  $\tau_{DA} = 0.36$  ns (obtained with emission lifetime measurement performed on the COK-20% samples). The ET rate was  $2.40 \times 10^{-9} \text{ s}^{-1}$ . No considerable effects were found by enhancing the amount of dye from 10 to 20%.

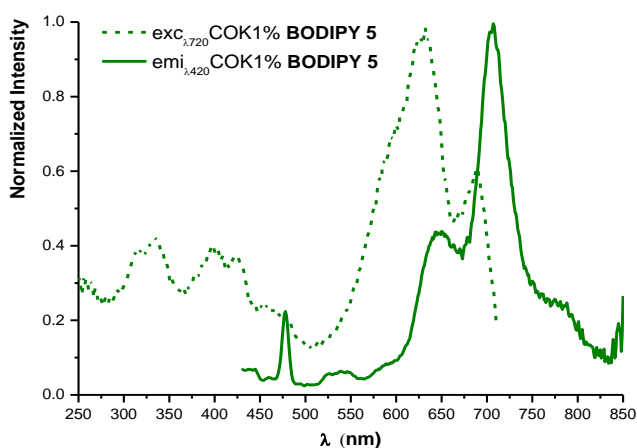
COK mesoporous nanoparticles, hosting the bichromophoric compound **4**, and the relative subunits, Curcumin and **BODIPY 5** (Figure 2.34) were also synthesized and characterized. I will report just the spectroscopy preliminary data and TEM characterization obtained for these systems. The used dye loading amount were 1% and 5%. These dye loadings were chosen on the basis of previous experiment showing that a high loading of BODIPY species inside the nanoparticle results in a fluorescence quenching.<sup>44</sup>



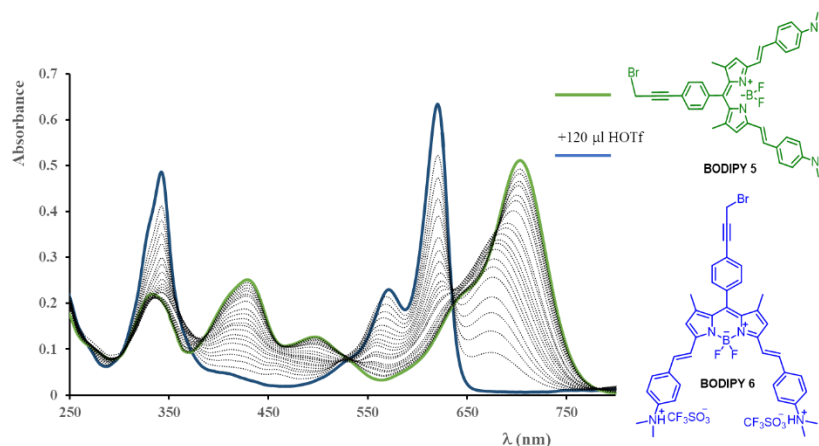
**Figure 2.34:** Dyes used to dope silica.

The synthetic procedure is similar to that adopted for compound **1**, however **BODIPY 5** was first dissolved in solvent before being added to the micelles.<sup>44</sup> Chloroform (2%) was used to solubilize **BODIPY 5**, this led to an

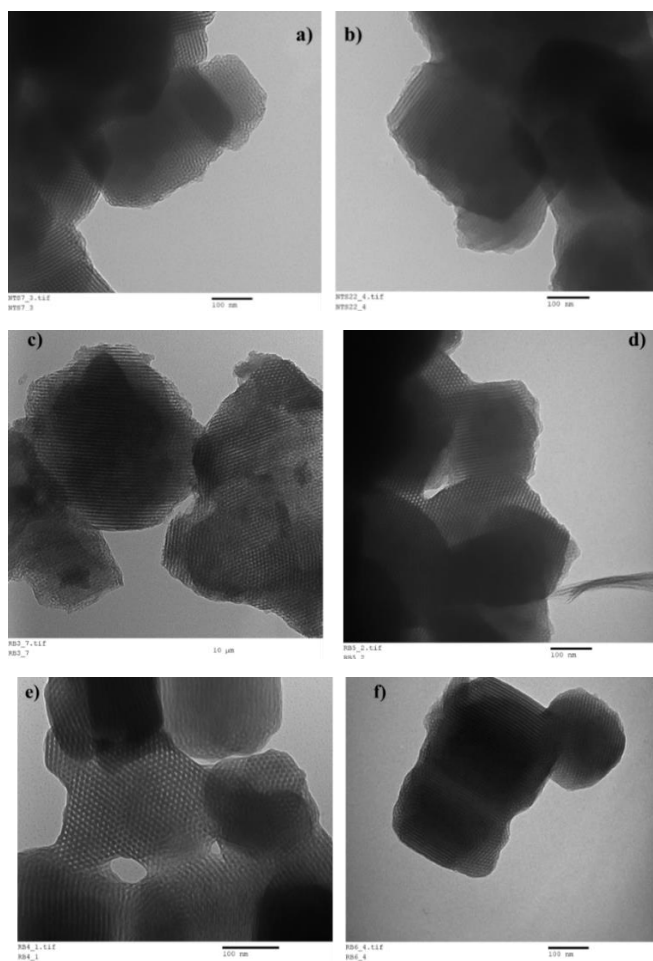
unexpected change in the spectroscopic behaviour of the COK-1% **BODIPY 5**. The excitation spectrum of COK-1% doped with **BODIPY 5** recorded in suspension of cyclohexane shows the presence of two bands, at  $\lambda=620$  nm and at around  $\lambda=700$  nm (Figure 2.35). The first band was absent in the excitation spectrum of **BODIPY 5** recorded in solution of acetonitrile (Figure 2.17, paragraph 2.4). This behaviour could be explained taking into account the sensitivity of **BODIPY 5** to acidic pH.<sup>56</sup> The presence of this band  $\lambda=620$  nm in COK-1% **BODIPY 5** can be attributed to the formation of a species, such as **BODIPY 6** in figure 2.35, with the dimethylamino terminal groups protonated in chloroform, that usually contains traces of HCl ( $2 \text{CHCl}_3 + \text{O}_2 \rightarrow 2 \text{COCl}_2 + 2 \text{HCl}$ ). The formation of the protonated species was confirmed by a titration conducted on **BODIPY 5** with triflic acid. At the end of titration, the absorption spectrum of **BODIPY 5** was transformed into the absorption spectrum of **BODIPY 6** that is identical to the band observed in COK-1% **BODIPY 5** (Compare figure 2.35 with figure 2.36). The blue species **BODIPY 6** absorbs at  $\lambda=620$  nm and emits at  $\lambda=650$  nm.



**Figure 2.35:** Excitation and emission spectra for COK containing 1% of **BODIPY 5**. Suspension of cyclohexane 0.3 mg/ml.  $\lambda_{\text{exc}}$  720 nm.

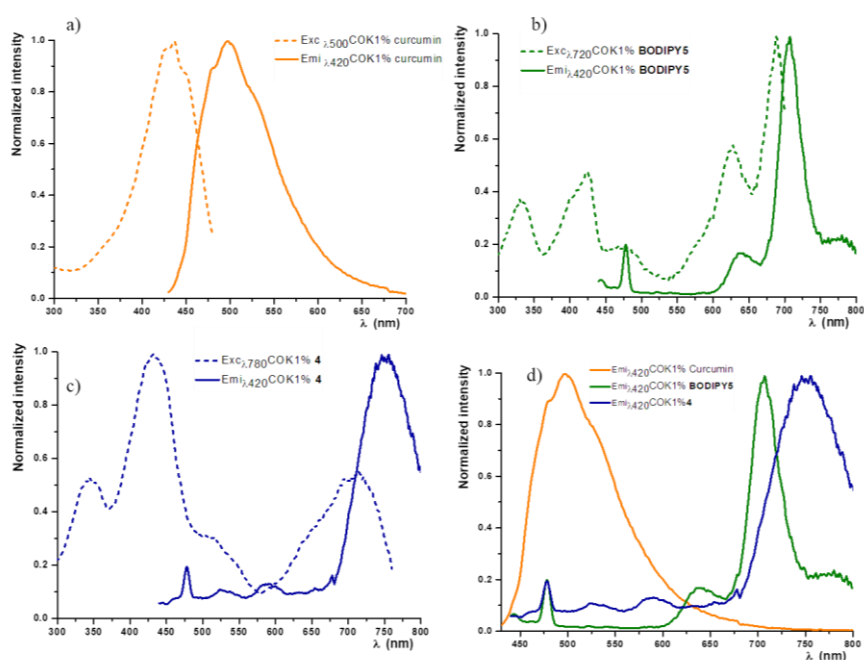


**Figure 2.36:** Spectrophotometric titration of **BODIPY 5** (green line) with triflic acid (1mM); the blue line represents absorption of **BODIPY 6**.



**Figure 2.37:** TEM imaging of COK-1% Curcumin a); **BODIPY 5**, c); compound **4**, e); COK-5% Curcumin b); **BODIPY 5** d); compound **4**, f).

Once I was conscious of these possible protonation in chloroform, I obtained the other samples by dissolving both the **BODIPY 5** and compound **4** in 2% of acetonitrile. The obtained nanoparticles COK-1% and COK-5% were structurally characterized with TEM microscopy (Figure 2.37) and by emission spectroscopy (Figure 2.38). Their properties were compared to those of the free dyes.



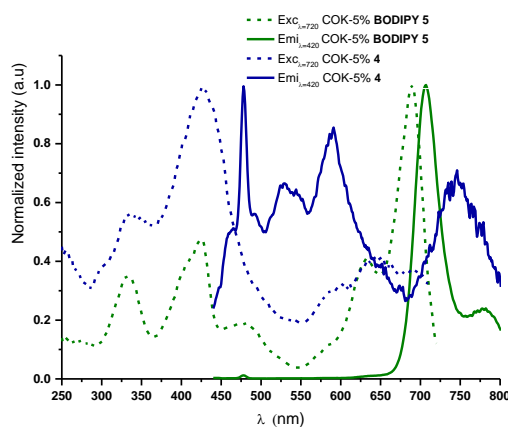
**Figure 2.38:** Excitation and emission spectra of COK-1% Curcumin a); **BODIPY 5**, b); and compound **4**, c); comparison between the emission spectra of the three component upon excitation at 420 nm, d). Spectra are recorded in suspension of cyclohexane 0.3 mg/ml.

Figure 2.38 reports the excitation and emission spectra recorded in a 0.3 mg/ml suspension of cyclohexane for the subunits COK-1% Curcumin (a) COK-1% **BODIPY 5** (b) for the COK-1% compound **4** (c) and the comparison of the emission spectra of the three species (d). The excitation and the emission spectra for COK-1% loaded with Curcumin show the same behaviour exploited for COK-10% and -20% Curcumin. In the first case, the

aggregation is less evident, due to the lower concentration of the dye inside the silica nanoparticles, whereas the blue-shifted emission caused by the rigidity of the system remains unchanged. Both COK-1% **BODIPY 5** and COK-1%-**4** present spectra similar to those recorded in solution of MeCN, (Figure 2.17, paragraph 2.4) with features typical for these species, except for a blue-shift due to the rigido-chromic effect imposed by the matrix.

The excitation and emission spectra of COK-1% loaded with compound **4** (Figure 2.38, c) are consistent with the assumption of an energy transfer from the donor Curcumin to the acceptor **BODIPY 5**. The excitation spectra are essentially additive, whereas the emission spectra show only the component of the acceptor subunit **BODIPY 5**.

Figure 2.39 reports the excitation and the emission spectra recorded in the same conditions for COK-5% loaded with **BODIPY 5** and compound **4**. The spectra for COK-5% Curcumin are not reported because are superimposable with those reported for COK-1% Curcumin sample.



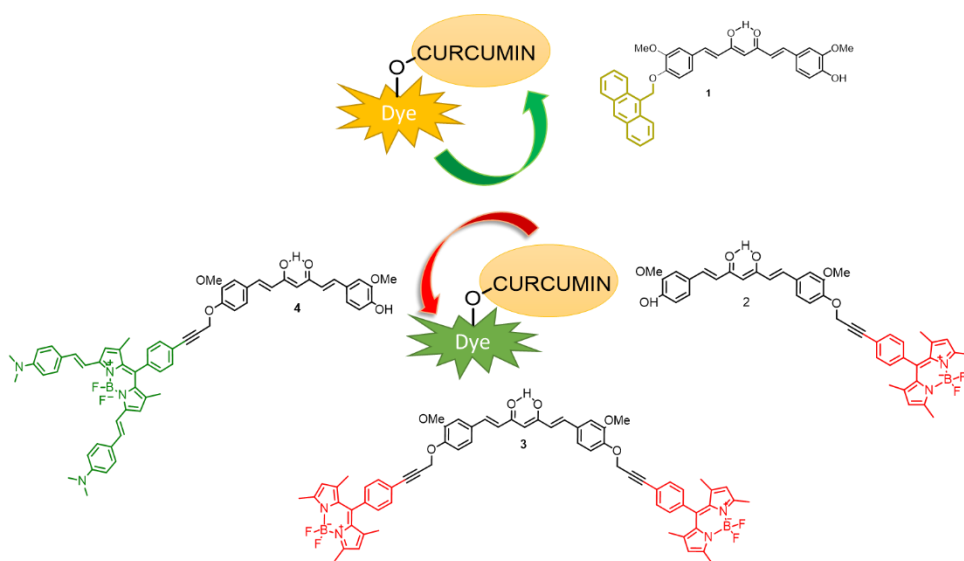
**Figure 2.39:** Excitation and emission spectra of COK-5% doped with **BODIPY 5** (dotted and straight green lines) b); and compound for **4** (dotted and straight blue lines). Spectra are recorded in suspension of cyclohexane 0.3 mg/ml.  $\lambda_{exc}$  420 nm.

Calculation of the emission lifetime and luminescence quantum yield of the hybrid materials are still on going.



## 2.8 Conclusions

A new class of light-harvesting artificial antennas based on Curcumin has been synthesized. In these systems, Curcumin, linked to suitable chromophores, acted as both the acceptor and the donor of the bichromophoric antennas and the photophysical behaviour of this new compounds have been investigated.



In the bichromophoric species **1**, a derivative of anthracene was used as donor and curcumin was the acceptor, whereas for the other systems, two different BODIPY were chosen as acceptor chromophores. The results obtained by absorption and emission spectroscopy and emission lifetime measurement in solution of acetonitrile confirmed that in all the investigated cases an energy transfer can be appreciated. For compound **1** this efficiency was calculated to be 82%. For compound **2** and **4** the ET process is almost quantitative.

A preliminary exploitation of the behaviour of such luminescent species was performed, starting from the cytotoxicity analysis that showed no

significant effect of compounds **1**, **2** and **4**, from 0.025 up to 10  $\mu\text{M}$  of concentration, on the viability of erythrocytes.

Fluorescence microscopy images, in cell internalization experiments, disclose a clear fluorescence of the cytosol of cells, supporting that compounds **2** and **4** are able to cross the plasmatic membrane.

The cytoprotective activity of compounds **2** and **4** on *t*-BOOH treated lymphocytes was also evaluated, in comparison with the effects exerted by Curcumin. Unfortunately, none of the tested compounds showed a cytoprotective power higher or even comparable with that observed for Curcumin.

Finally, compounds **1** and **4** were internalized in mesoporous silica (namely COK-12 nanoparticles) and the behaviour inside this material was studied, by exploiting the template-assisted host-guest chemistry of mesoporous organosilica. The introduction of dyes inside the pluronic micelle does not altered the structure of the mesoporous silica nanoparticle, moreover the COK-12 hybrids behave as monochromatic antenna, in which energy is transferred from the donor anthracene to Curcumin for compound **1** or from Curcumin to the acceptor **BODIPY 5** in compound **4**. The ET efficiency was calculated for compound **1** in the sample COK-10% and COK-20% to be 84% and 86% respectively, a bit higher compared to that recorded in solution.

## 2.9 Experimentals

---

**General Synthetic Methods.** Solvents were purified according to standard procedures. Dry reactions were performed using stove-glass and in inert atmosphere of Argon. All of the reactions were monitored by TLC on commercially available precoated plates (silica gel 60 F254), eluted with Hexane/EtOAc, Toluene/MeCN, Hexane/Chloroform, and the products were visualized with vanillin [1 g dissolved in MeOH (60 mL) and conc. H<sub>2</sub>SO<sub>4</sub> (0.6 mL)] and UV lamp. Silica gel 60 was used for column chromatography. <sup>1</sup>H and <sup>13</sup>C NMR spectra were recorded in CDCl<sub>3</sub> and dimethylsulfoxide-*d*<sub>6</sub> with a Varian 500 spectrometer (at 500 MHz for <sup>1</sup>H; and 125 MHz for <sup>13</sup>C). Chemical shifts are given in parts per million (ppm) (δ relative to residual solvent peak for <sup>1</sup>H and <sup>13</sup>C), coupling constants (J) are given in Hertz, and the attributions are supported by Heteronuclear Single Quantum Coherence (HSQC) experiments, Correlation spectroscopy (COSY), Nuclear Overhauser Effect Spectroscopy (NOESY).

**General Photophysical Methods.** UV/Vis absorption spectra in solution were recorded with a Jasco V-560 spectrophotometer. For steady-state luminescence measurements, a Jobin Yvon-Spex Fluoromax P spectrofluorimeter equipped with a Hamamatsu R3896 photomultiplier was used. For correcting the emission spectra for the photomultiplier response, a program purchased with the fluorimeter was used. Fluorescence spectra and lifetimes were measured using an Edinburgh FLS980 photoluminescence spectrometer, equipped with a 450 W Xenon arc lamp, Czerny Turner excitation and emission monochromators (1.8 nm/mm dispersion; 1800 grooves/mm), time-correlated single photon counting (TCSPC) module and a Hamamatsu R928P photomultiplier tube (in fan assisted TE cooled housing, operating temperature -20 °C). For lifetime measurements, samples were

excited with an EPL-375 (370.8 nm; 61.1 ps pulse width) picosecond pulsed diode lasers and data analysis was performed on the F980 software with numerical data reconvolution based on Marquardt-Levenberg algorithm. Luminescence quantum yields were measured using as reference an aqueous solution of fluorescein (0.1 M NaOH;  $\phi = 0.87$  in MeCN)<sup>57</sup> or dimethylammonium-phenylstyryl BODIPY species ( $\Phi=0.2$  in MeCN)<sup>58</sup> quantum yield was calculated using the equation:  $(\Phi_S/\Phi_R) = (A_S/A_R) \times ((OD)_S/(OD)_R) \times (n_S^2/n_R^2)$ , where  $\Phi_S$  and  $\Phi_R$  are the fluorescence quantum yields of the sample and the reference respectively,  $A_S$  and  $A_R$  are the area under the fluorescence spectra of the sample and the reference respectively,  $(OD)_S$  and  $(OD)_R$  are the respective optical densities of the sample and the reference solution at the wavelength of excitation, and  $n_S$  and  $n_R$  are the refractive indices for the respective solvents used for the sample and the reference.

Transmission electron microscopy images were taken on a 100kV CM100 TEM (FEI).

### **General Biological Methods.**

#### • *Erythrocytes isolation*

Donor volunteers participating in the study were informed of all risks, discomforts and benefits relating to the study, in accordance with the Declaration of Helsinki for research protocols approved by the institutional review boards of the National Institutes of Health (NIH). All subjects provided medical histories, using a standardized questionnaire and declared they had not taken anti-inflammatory medication or nutritional supplements. Blood was obtained by venipuncture from healthy male volunteers and collected in heparinized tubes. Erythrocytes were separated from plasma and buffy coat and washed three times with 10 volume of 0.9 % NaCl and centrifuged at

2,500 rpm for 5 min. During the last washing the packed cells were resuspended in the incubation buffer (phosphate saline buffer), at pH 7.4 and utilized for subsequent experiments.

- *Cellular internalization and cytotoxic effects*

Erythrocytes were incubated for 24 hours at 37°C in the absence or in the presence of 20, 10, 5, 1, 0.5, 0.1, 0.05 and 0.025  $\mu\text{M}$  final concentrations of compounds **1**, **2** and **4**. At the end of incubation time, cells were centrifuged at 2,500 rpm for 5 min. The supernatant was analyzed to detect the release of lactate dehydrogenase, while the pocked cells were resuspended and washed three times in incubation buffer and finally used for fluorescence and visible microscopy. The supernatant was utilized to check cytotoxicity by measuring lactate dehydrogenase (LDH) release from damaged cells into culture medium. LDH activity in the medium was determined using a commercially available kit from BioSystems S.A. The texted compounds, at the concentrations utilized in the experiments, did not interfere with LDH determination. For fluorescence and visible microscopy 10  $\mu\text{L}$  of each samples was placed on a glass slide covered with a coverslip and monitored with a fluorescence microscope.

- *Lymphocyte isolation*

The isolation of lymphocytes was performed from heparinized whole blood collected from healthy volunteers, who have provided written medical histories by a standardized questionnaire and have not taken anti-inflammatory medication or nutritional supplements. Blood samples were diluted with equal volumes of balanced salt solution, layered over Histopaque-1077 (Sigma-Aldrich) in centrifuge tubes and centrifuged at 400g for 30-40 min at 25°C. The peripheral blood

mononuclear cell (PBMCs) layer was removed with a pipette and washed by centrifugation. The PBMCs are passed through a Percoll gradient to enrich the fraction in lymphocytes. The obtained cells (with a viability > 90%) were counted on a haemocytometer and suspended in Roswell Park Memorial Institute (RPMI) 1640 medium supplemented with 10% fetal calf serum, 2 mM glutamine, 100 units/ml penicillin G and streptomycin. Cell concentration was adjusted to  $1 \times 10^5$  cells/ml.

• *Cytotoxicity and Cytoprotective assays*

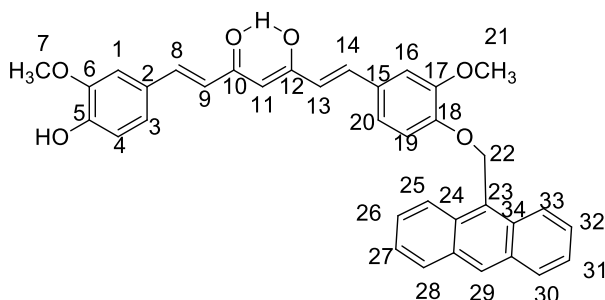
For the cytotoxicity assay, cells ( $1 \times 10^5$ /ml) were incubated in complete medium without or with 10.0, 5.0, 1.0, 0.5, 0.25 and 0.10  $\mu\text{g/mL}$  of Curcumin and compounds **2** and **4** for 24h. For the cytoprotective assay, cells ( $1 \times 10^5$ /ml) were incubated in complete medium without or with 10.0, 5.0, 1.0, 0.5, 0.25 and 0.10  $\mu\text{g/mL}$  of curcumin, compound **2** or **4** for 24h in the presence of 100  $\mu\text{M}$  *tert*-butyl hydroperoxide (*t*-BOOH). After incubation, in both cases, cell viability was assessed by trypan blue staining. Briefly, an aliquot of the cell suspension was diluted 1:1 (v:v) with 0.4% trypan blue and the cells were counted using a haemocytometer. Results are expressed as the percentage of viable or dead cells (ratio of unstained or stained cells to the total number of cells, respectively). Cytotoxicity and cells damages were also analyzed by lactate dehydrogenase (LDH) release. LDH activity in the medium was determined using a commercially available kit from BioSystems S.A and expressed in function of the total amounts of the enzyme present in the cell without *t*-BOOH obtained after total lysis of the cells by sonication.

- *Statistical analysis*

Data are presented as means  $\pm$  standard deviation (S.D.). Data were analyzed by one-way analysis of variance (ANOVA). The significance of the difference from the respective controls for each experimental test condition was assayed by using Tukey's for each paired experiment. A  $P < 0.05$  was regarded as indicating a significant difference.

**Synthesis of bichromophoric species 1-4, Curcumin derivatives 7 and 8, and BODIPY 4 and 5.**

**Bichromophoric species 1.** To a solution Curcumin (200 mg, 0.55 mmol) in dry acetone (10 mL), 9-bromomethylantracene **5** (75mg, 0.27 mmol) and  $K_2CO_3$  (38 mg, 0.27 mmol) were added. The mixture was stirred at reflux temperature for 24h. The reaction was monitored using TLC (toluene/MeCN 80:20), following the disappearance of the starting material. The solvent was removed under reduced pressure. Then, the residue was suspended in water and extracted with ethyl acetate. The combined organic layers were dried over anhydrous  $Na_2SO_4$ , filtered and concentrated under reduced pressure. The crude was purified by column chromatography (eluants: toluene to toluene/MeCN 95:5) on silica gel and afforded compound **1** as a yellow solid 42% yield.  $R_f$ : 0.46 (toluene/MeCN 80:20).



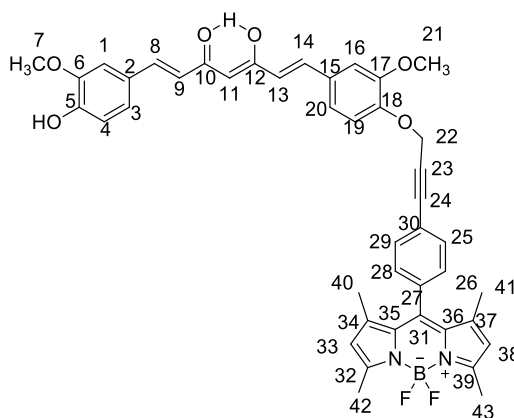
$^1\text{H}$  NMR ( $\text{CDCl}_3$ ):  $\delta$  8.52 (s, 1H, H-29), 8.34 (m, 2H, H-25, H-33), 8.04 (m, 2H, H-28, H-30), 7.63 (1H, d, H-8,  $J=15.7$  Hz), 7.60 (1H, d, H-14,  $J=15.7$  Hz), 7.56-7.52 (2H, m, H-26, H-32), 7.53-7.48 (4H, m, H-28, H-30), 7.26-6.92 (6H, m, H-1, H-3, H-4, H-16, H-19, H-20), 6.52 (1H, d, H-13,  $J=15.7$  Hz), 6.48 (1H, d, H-9,  $J=15.7$  Hz), 6.05 (2H, s, H-22), 5.87 (1H, br s, OH), 5.82 (1H, s, H-11), 5.05 (1H, s, H-22), 3.95 and 3.84 (6H, 2 s,  $\text{OCH}_3$ );  $^{13}\text{C}$  NMR :  $\delta$  183.6 (C-10), 182.9 (C-12), 150.8 (Cq), 150.4 (Cq), 147.9 (Cq), 140.6 (C-8), 140.2 (C-14), 131.5 (Cq), 131.2 (Cq), 129.2 (C-29), 129.1 and 129.0 (C-28, C-30), 126.6 (Cq), 126.5 (C-26, C-32), 125.0 (C-27, C-31), 124.0 (C-25, C-33), 122.9 (C-9), 122.3 (C-13), 122.4, 121.8, 114.9, 114.8, 111.0, 109.6 (C-1, C-3, C-4, C-16, C-19 and C-20), 101.3 (C-11), 64.4 (C-22), 55.9 and 56.0 (C-7, C-21).

**Compound 7.** Curcumin (300 mg, 0.81 mmol) was dissolved in 15 ml of dry acetone, then propargyl bromide (61 mg, 0.40 mmol) and  $\text{K}_2\text{CO}_3$  (56 mg, 0.40 mmol) were added. The mixture was stirred under argon at reflux temperature for 24h. After that, the same amount of propargyl bromide and potassium carbonate were added. The reaction was monitored for other 24h using TLC on silica gel ( $\text{CHCl}_3$ /hexane 90/10). The solvent was removed under reduced pressure. The residue was suspended in water and extracted with ethyl acetate. The combined organic layers were dried over anhydrous  $\text{Na}_2\text{SO}_4$ , filtered and concentrated under reduced pressure. The crude was purified by chromatography (eluants  $\text{CHCl}_3$ /hexane 90/10) on silica gel to obtain compound **7** as a orange solid yield 47%,  $R_f$  0.6 ( $\text{CHCl}_3$ /hexane 90/10). The  $^1\text{H}$  and  $^{13}\text{C}$  NMR data are consistent with the one reported in



literature. The same column provide **8** as a yellow solid, 34% yield, *R*<sub>f</sub> 0.8 (CHCl<sub>3</sub>/Hexane 90/10).

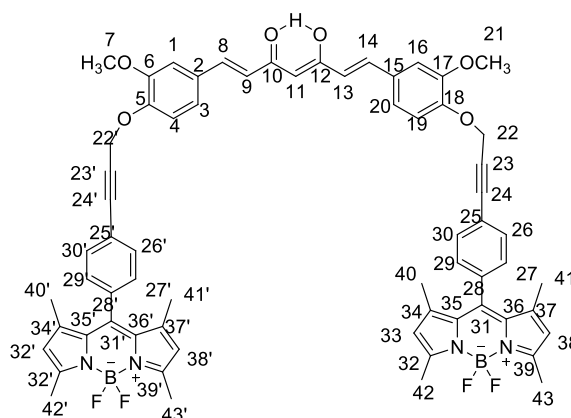
**Bichromophoric species 2.** [Pd(PPh<sub>3</sub>)<sub>4</sub>] (0.0246 mmol) was added to a degassed solution of boron difluoro-2-[(3,5-dimethyl-2*H*-pyrrole-2-ylidene)-(4-iodophenyl) methyl] -3,5-dimethyl-1*H*-pyrrolate (**BODIPY 1**) (111 mg, 0.246 mmol) and curcumine mono-alkyne **7** (100 mg, 0.246 mmol) in DMF/TEA (3 ml, 1:1). The mixture was heated, at 60°C, under argon, for 2h, until the disappearance of compound **7** was observed by TLC (CHCl<sub>3</sub> /MeCN 90:10). Solvents were removed under reduced pressure. The reaction crude was purified by silica gel column chromatography (eluant: CHCl<sub>3</sub>) for obtaining compound **2** as a red solid, yield 65%. *R*<sub>f</sub>: 0.8 (CHCl<sub>3</sub>/MeCN 90:10).



<sup>1</sup>H NMR (CDCl<sub>3</sub>): δ 7.61 (1H, d, H-8, *J*=15.6 Hz), 7.60 (1H, d, H-14, *J*=15.6 Hz), 7.56-7.54 (2H, m, H-25, H-29), 7.26-7.23 (2H, m, H-26, H-28), 7.20-6.92 (6H, m, H-1, H-3, H-4, H-16, H-19, H-20), 6.52 (1H, d, H-13, *J*=15.6 Hz), 6.48 (1H, d, H-9, *J*=15.6 Hz), 5.97 (2H, s, H-33, H-38), 5.88 (1H, br s, OH), 5.81 (1H, s, H-11), 5.05 (1H, s, H-22), 3.95 and 3.94 (6H, 2 s, OCH<sub>3</sub>), 2.54 (6H, s, H-42, H-43), 1.37 (6H, s, H-40, H-41); <sup>13</sup>C NMR: δ 183.6 (C-10), 182.7 (C-12), 155.8 (C-q), 149.7(C-q), 148.8 (Cq), 147.9 (Cq), 146.2 (Cq), 142.9 (Cq), 140.7 (C-8), 140.5 (C-q), 140.0 (C-14), 135.5 (Cq), 132.5

(C-25, C-29), 131.5 (C-q), 131.1 (Cq), 129.2 (Cq), 128.2 (C-26, C-28) 127.6 (Cq), 123 (Cq), 122.1 (C-9), 121.7 (C-13), 121.3 (C-33, C-38), 122.9, 122.5, 114.8, 113.6, 110.3, 109.6 (C-1, C-3, C-4, C-16, C-19, C-20), 101.3 (C-11), 86.9, 84. (C-23, C-24), 57.3 (C-22), 55.9 (C-7, C-21), 14.5 (C-40, C-41, C-42, C-43).

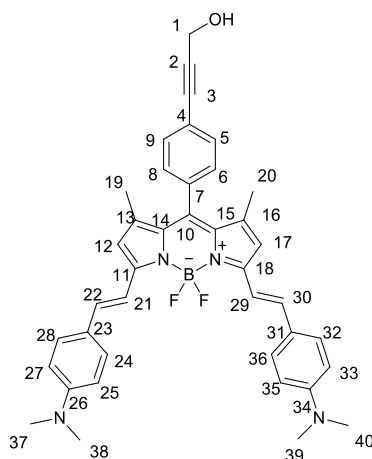
**Bichromophoric species 3.** Pd(PPh<sub>3</sub>)<sub>4</sub>] (0.025 mmol) was added to a degassed solution of boron difluoro-2-[(3,5-dimethyl-2*H*-pyrrole-2-ylidene-)(4-iodophenyl) methyl] -3,5-dimethyl-1*H*-pyrrolate (**BODIPY 1**) (220 mg, 0.50 mmol) and curcumine di-alkyne **8** (100 mg, 0.25 mmol) in DMF/TEA (3 ml, 1:1). The mixture was heated, at 60°C, under argon, for 3h, following the consumption of **BODIPY 1** using NMR spectroscopy. Solvents were removed under reduced pressure. The reaction crude was purified by silica gel column chromatography (eluants: toluene up to toluene/MeCN, 99:1) to obtain compound **3** as a red solid, yield 35%. *R*<sub>f</sub>: 0.75 (toluene/MeCN 70:30)



<sup>1</sup>H NMR (CDCl<sub>3</sub>): δ 7.63 (2H, d, H-8, H-14, *J*=15.6 Hz), 7.57-7.54 (4H, m, H-26, H-26', H-30, H-30'), 7.26-7.23 (4H, m, H-27, H-27', H-29, H-29'), 7.21-7.12 (6H, m, H-1, H-3, H-4, H-16, H-19, H-20), 6.53 (2H, d, H-9, H-13,

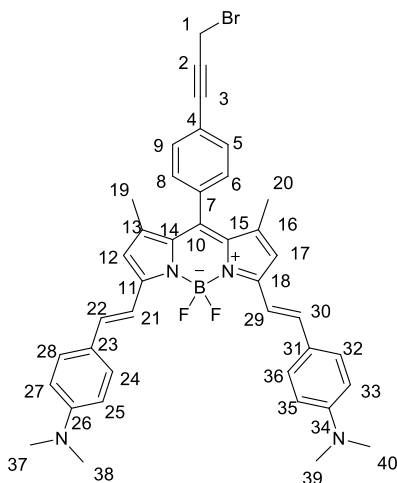
$J=15.6$  Hz), 5.97 (4H, s, H-33, H-33', H-38, H-378'), 5.83 (1H, s, H-11), 5.06 (2H, s, H-22, H-22'), 3.96 (6H, 2 s, OCH<sub>3</sub>), 2.55 (12H, s, H-42, H-42', H-43, H-43'), 1.37 (12H, s, H-40, H-40', H-41, H-41'); <sup>13</sup>C NMR :  $\delta$  183.1 (C-10 and C-12), 155.8 (Cq), 149.7(Cq), 148.8 (Cq), 142.9 (Cq), 140.2 (C-8, C-14), 135.5 (Cq), 132.7 (Cq), 132.5 (C-25, C-25', C-29, C-29'), 131.1 (Cq), 129.0 (Cq), 128.2 (C-26, C-26', C-28, C-28'), 122.9 (Cq), 122.5 (C-9, C-13), 121.3 (C-32, C-32', C-37, C-37'), 122.1, 113.6, 110.3, (C-1, C-3, C-4, C-16, C-19, C-20), 101.4 (C-11), 87.6, 84.7 (C-22, C-22', C-23, C-23'), 57.3 (C-21, C-21'), 55.9 (C- 7, C-21), 14.5 (C-39, C-39', C-40, C-40', C-41, C41', C-42, C-42').

**BODIPY 4.** [Pd(PPh<sub>3</sub>)<sub>2</sub>Cl<sub>2</sub>] (0.0112 mmol) was added to a degassed solution of boron difluoro-4-(1E)-2-[5-[[5-[(1E)-2-[4-(dimethylamino) phenyl] ethenyl] -3-methyl-2H-pyrrol-2-ylidene-](4-iodophenyl methyl]-4-methyl -1H-pyrrol-2-yl]-ethenyl]-N,N-dimethylbenzenamine (**BODIPY 2**) (400 mg, 0.56 mmol) and propargyl alcohol (40  $\mu$ l, 38 mg, 0.67 mmol) in DMF/TEA (12ml, 5:1). In a sealed tube, the mixture was heated, at 80°C, under argon, for 4 h, until the disappearance of **BODIPY 2** was observed by TLC (CHCl<sub>3</sub>/Hexane 90:10). Solvents were removed under reduced pressure. The reaction crude was dissolved in DCM and then filtered over celite/silica 1:2. The solution was evaporated to dryness to obtain **BODIPY 4** as a deep green solid in 90% yield, without needing any purification.  $R_f$ : 0.60 (CHCl<sub>3</sub>/Hexane 90:10).



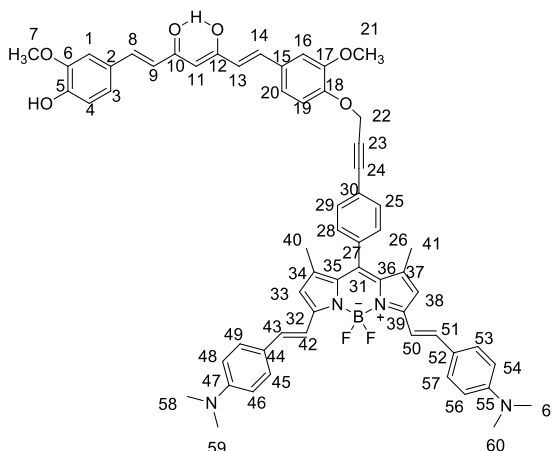
$^1\text{H}$  NMR (DMSO- $d_6$ ):  $\delta$  7.61-7.58 (2H, m, H-5, H-9), 7.48-7.29 (10H, m, H-6, H-8, H-21, H-25, H-27, H-29, H-33, H-35), 6.88 (2H, s, H-12, H-17), 6.80-6.78 (4H, m, H-24, H-28, H-32, H-36), 5.37 (1H, t, -OH,  $J=5.9$  Hz), 4.34 (2H, d,  $J=5.9$  Hz, H-1), 3.00 (12H, H-37, H-38, H-39, H-40), 1.41 (6H, s, H-19, H-20).  $^{13}\text{C}$  NMR:  $\delta$  152.7 (C-q), 151.5 (C-q), 140.7 (Cq), 137.7 and 113.7 (C-21, C-22, C-29, C-30), 135.1 (Cq), 132.4 (Cq), 132.3 (C-5, C-9), 129.6 (Cq), 129.2 (C-6, C-8, C-25, C-27, C-33, C-35), 124.3 (Cq), 123.6 (Cq), 118.2 (C-12, C-17), 112.6 (C-24, C-28, C-32, C-36), 91.6 and 83.6 (C-2, C-3), 49.9 (C-1), 40.2 (C-37, C-38- C-39, C-40), 14.7 (C-12, C-17)

**BODIPY 5.** A solution of **BODIPY 4** (50 mg, 0.08 mmol) in abs. toluene (5 ml) under argon was cooled to  $0^\circ\text{C}$  in an ice-bath.  $\text{PBr}_3$  (31  $\mu\text{l}$ , 70 mg, 0.26 mmol, 3.3 eq) was added dropwise and the reaction mixture was stirred at  $0^\circ\text{C}$  for 10' and then it was allowed to warm to rt. The disappearance of the starting material was followed with TLC ( $\text{CHCl}_3/\text{Hexane}$  90:10). After 6h saturated  $\text{NaCO}_3$  solution was added. The phases were separated and the organic layers were washed with water and brine, dried over  $\text{MgSO}_4$ , filtered and concentrated under reduced pressure. The reaction crude was purified by silica gel column chromatography (eluants:  $\text{CHCl}_3/\text{Hexane}$  90:10) to obtain **BODIPY 5** as a deeply green solid, yield 74%.  $R_f$ : 0.95 ( $\text{CHCl}_3$ ).



$^1\text{H}$  NMR (DMSO- $d_6$ ):  $\delta$  7.64-7.61 (2H, m, H-5, H-9), 7.47-7.26 (10H, m, H-6, H-8, H-21, H-25, H-27, H-29, H-33, H-35), 6.87 (2H, s, H-12, H-17), 6.79-6.76 (4H, m, H-24, H-28, H-32, H-36), 4.54 (1H, s, H-1), 3.00 (12H, H-37, H-38, H-39, H-40), 1.39 (6H, s, H-19, H-20).  $^{13}\text{C}$  NMR:  $\delta$  152.7 (Cq), 151.5 (Cq), 140.7 (Cq), 137.7 and 113.7 (C-21, C-22, C-29, C-30), 135.1 (Cq), 132.4 (Cq), 132.3 (C-5, C-9), 129.8 (Cq), 129.2 (C-6, C-8, C-25, C-27, C-33, C-35), 124.3 (Cq), 123.6 (Cq), 118.2 (C-12, C-17), 112.6 (C-24, C-28, C-32, C-36), 91.4 and 83.5 (C-2, C-3), 60.2 (C-1), 40.2 (C-37, C-38- C-39, C-40), 14.8 (C-12, C-17).

**Bichromophoric species 4.** To a solution of Curcumin (30 mg, 0.08 mmol) in dry acetone (10 mL), **BODIPY 5** (75mg, 0.106 mmol) and  $\text{K}_2\text{CO}_3$  (22 mg, 0.16 mmol) were added. The mixture was stirred at reflux temperature for 48h. The reaction was monitored using TLC ( $\text{CHCl}_3/\text{MeCN}$  99.5:0.5) following the disappearance of the starting material. The solvent was removed under reduced pressure. The crude was purified by column chromatography (eluants:  $\text{CHCl}_3$  up to  $\text{CHCl}_3/\text{MeCN}$  99.5:0.5) on silica gel. The column afforded compound **4** as a green solid, 34% yield.  $R_f$ : 0.50 ( $\text{CHCl}_3/\text{MeCN}$  99.5:0.5).



$^1\text{H}$  NMR ( $\text{DMSO}-d_6$ ):  $\delta$  7.65-7.15 and 6.89-6.75 (28H, 2m, H-1, H-3, H-4, H-8, H-9, H-13-H-14, H-15, H-16, H-19, H-20, H-25, H-26, H-28, H-29, H-33, H-38, H-42, H-43, H-45, H-46, H-48, H-49, H-50, H-51, H-52, H-54, H-56, H-57), 6.1 (1H, s, H-11), 5.15 (1H, s, H-22), 3.87 and 3.83 (6H, s,  $2\times\text{OCH}_3$ ), 3.00 (12H, H-58, H-59, H-60, H-61), 1.4 (6H, s, H-40, H-41).  $^{13}\text{C}$  NMR:  $\delta$  184.3 and 182.9 (C-10, C-12), 152.7 (Cq), 151.4 (Cq), 149.8 (Cq), 149.0 (Cq), 148.4 (C-q), 141.5 (Cq), 140.7 (Cq), 137.7 and 111.8 (C-42, C-43, C-50, C-51), 136.1 (C-q), 135.0 (Cq), 132.6 (C-25, C-29), 132.3 (C-8, C-14), 129.8 (Cq), 129.2 (C-26, C-28, C-46, C-48, C-54, C-56), 129.0 (Cq), 126.7, 124.4, 123.6, 123.0, 122.8 and 122.5 (C1, C-3, C-4, C-16, C-19, C-20), 121.5 (C-q), 118.2 (C-q), 117.5 (Cq), 116.1 (C-33, C-38), 114.1 (Cq), 113.6 (Cq), 112.6 (C-9, C-13, C-45, C-49, C-53, C-57), 111.3 (Cq), 101.4 (C-11), 86.6 and 86.4 (C-23, C-24), 79.6 (C-22), 56.1 (C-7, C-21), 40.4 (C-58, C-59, C-60, C-61), 14.8 (C-40, C-41).

### Synthesis of dye doped silica nanoparticles

**Synthesis of MCM-41, and MCM-NH<sub>2</sub> nanoparticles.** The syntheses were accomplished following literature procedure.<sup>44</sup>

**Synthesis of MCM-Cl nanoparticles.** A solution of chloroacetylchloride (0.45 mL, 0.24 mmol) and N,N-diisopropylethylamine (0.6 mL, 6 mmol) was

added to mesoporous hollow silica particles (300 mg) dispersed in anhydrous THF (15 mL). The reaction mixture was refluxed for 6h. After filtration, the solid product was washed repeatedly with THF to remove the unreacted chloroacetylchloride. The product was dried by vacuum, to obtain a white powder.

**Synthesis of MCM-silica nanoparticles doped with Curcumin.** A solution of Curcumin (20 g, 0.055 mmol) and  $K_2CO_3$  (30 mg, 0.220 mmol) was added to acetyl chloride appended mesoporous hollow silica particles (20 mg) dispersed in anhydrous THF (5 mL). The reaction mixture was refluxed for 48h. After filtration, the solid product was washed, with THF and water, to remove the unreacted Curcumin. To deduce the loading of Curcumin in MCM nanoparticles, the washing water were extracted with  $CHCl_3$  and the combined organic layers were dried over  $MgSO_4$  filtered and reduced under vacuum. The unreacted Curcumin was recovered and weighted. The calculated percentage of loading was 65%.

**Synthesis of MCM-silica nanoparticles doped with compound 1.** A solution of **1** (20 mg, 0.036 mmol) and  $K_2CO_3$  (20 mg, 0.144 mmol) was added to previously synthesized MCM-Cl (20 mg) dispersed in anhydrous THF (5 mL). The reaction mixture was refluxed for 48h. After filtration, the solid product was washed with THF and water to remove the unreacted compound. The product was dried by vacuum, to obtain an orange powder. The percentage of loading was 60%.

### **General procedure for the synthesis of COK-12 silica**

Citric acid monohydrate (954 mg, 4.97 mmol) and trisodium citrate dihydrate (793.5 mg, 3.07 mmol), were dissolved in  $H_2O$ . To this solution, Pluronic-P123 and the subunits or the bichromophoric species were added, separately, to obtain the corresponding intended dye loadings. The solution

was stirred in H<sub>2</sub>O (27 ml for 989 mg of P123) for 12h. Sodium silicate/H<sub>2</sub>O solution (21.36 mmol) was added dropwise to the reaction mixture, which was stirred for 10'. The mixture was left undisturbed for 24h and then was filtered under vacuum. The retentate was washed several time with H<sub>2</sub>O, producing foam. Washing was repeated until the foaming ceased. The retentate was then dried in an oven overnight, producing a powdery solids which fluoresced under UV light.

**Synthesis of COK-12 silica with Curcumin micelles.** **COK-1%-Curcumin** 99:1 (989 mg, 0.169 mmol P123: 0.6 mg, 0.00169 mmol Curcumin), **COK-5%-Curcumin** 95:5 (989 mg, 0.169 mmol P123: 3.16 mg, 0.087 mmol Curcumin) **COK-10%-Curcumin** 90:10 (803.8 mg, 0.068 mmol P123: 5.6 mg, 0.0154 mmol Curcumin), **COK-20%-Curcumin** 80:20 (400.5 mg, 0.068 mmol P123: 5 mg, 0.0137 mmol Curcumin).

**Synthesis of COK-12 silica with Anthracene 6 micelles.** **COK-10%-Anthracene 6** 90:10 (899 mg, 0.154 mmol P123; 4.2 mg, 0.0154 mmol anthracene **6**), **COK-20%-Anthracene 6** 80:20 (400.5 mg, 0.068 mmol P123: 33.71 mg, 0.0137 mmol anthracene **6**).

**Synthesis of COK-12 silica with bichromophoric species 1 micelles.** **COK-10%-1** 90:10 (440 mg, 0.076 mmol P123: 4.5 mg, 0.008 mmol **1**), **COK-20%-1** 80:20 (400 mg, 0.068 mmol P123: 7.65 mg, 0.0137 mmol **1**).

**Synthesis of COK-12 silica with BODIPY 5 micelles.** For **BODIPY 5** the general procedure was modified by first dissolving **BODIPY 5** in acetonitrile and then adding it to the aqueous solution of Pluronic-P123. **COK-1%-BODIPY 5** 99:1 (408 mg, 0.0703 mmol P123: 0.5 mg, 0.00071 mmol **BODIPY 5**), **COK-5%-BODIPY 5** 95:5 (156.6 mg, 0.027 P123: 1mg, 0.0014 mmol **BODIPY 5**).



**Synthesis of COK-12 silica with bichromophoric species 4 micelles.** For compound **4** the general procedure was modified by first dissolving **4** in acetonitrile and then added to the aqueous solution of Pluronic-P123. **COK-1%-4** 99:1 (579.4 mg, 0.09 mmol P123: 1 mg, 0.001 mmol **4**), **COK-5%-4** 95:5 (222 mg, 0.0384 mmol P123: 2 mg, 0.002 **4**).

## 2.10 References

---

1. A. Vogel, J. Pelletier, *J. Pharm Sci. Access*, **1815**, 1, 289-300.
2. J. Milobedzka, Sv. Kostanecki, V. Lampe, *Ber. Deut. Chem. Ges.*, **1910**, 43, 2163-2170.
3. K. R. Srinivas, *J. Pharm. Pharmacol.*, **1953**, 5, 448-457.
4. F. Kiuchi, Y. Goto, N. Sugimoto, N. Akao, K. Kondo, Y. Tsuda, *Chem. Pharm. Bull. (Tokyo)*, **1993**, 41, 1640-643
5. V. S. Govindarajan, *Food Sci. Nutr.*, **1980**, 12, 199–301; S. Shishodia, G. Sethi, B. B. Aggarwal, *Ann. N. Y. Acad. Sci.*, **2005**, 1056, 206-217.
6. A. Oppenheimer, *Lancet*, **1937**, 229, 619-621.
7. T. Esatbeyoglu, P. Huebbe, I. M. A. Ernst, D. Chin, A. E. Wagner, G. Rimbach, *Angew. Chem. Int. Ed.*, **2012**, 51, 5308-5332; Aggarwal B.B., Harikumar K.B.A., *Int. J. Biochem. Cell Biol.*, **2009**, 41, 40-59.
8. S. C. Gupta, S. Patchva, W. Koh, B. B. Aggarwal, *Clin. Exp. Pharmacol. Physiol.*, **2012**, 39, 283-299; S. C. Gupta, S. Patchva, W. Koh, B. B. Aggarwal, *AAPS J.*, **2013**, 15, 195-218.
9. M. Heger, R. F. van Golen, M. Broekgaarden, M. C. Michel. *Pharmacol. Rev.*, **2014**, 66, 222-307.
10. M. Baker, *Nature*, **2017**, 541, 144-145; K. M. Nelson, J. L. Dahlin, J. Bisson, J. Graham, G. F. Pauli, M. A. Walters, *J. Med. Chem.*, **2017**, 60, 1620-1637.
11. G. Xu, D. Wei, J. Wang, B. Jiang, M. Wang, X. Xue, S. Zhou, B. Wu, M. Jiang, *Dyes Pigm.*, **2014**, 101, 312-317; R. D-Vreese, C. Grootaert, S. D'hoore, A. Theppawong, S. V-Damme, M. V-Bogaert, John V-Camp, M. D'hooghe, *E. J. Med. Chem.*, **2016**, 123, 727-736.
12. E. Ferrari, S. Lazzari, G. Marverti, F. Pignedoli, F. Spagnolo, M. Saladini, *Bio. Med. Chem.*, **2009**, 17, 3043-3052; K. Mohri, Y. Watanabe, Y. Yoshida, M. Satoh, K. ISOBE, N. Sugimoto, Y. Tsuda. *Chem. Pharm. Bull.*, **2003**, 51, 1268-1272.

13. F. Kühlwein, K. Polborn, W. Beck, *Z. Anorg. Allg. Chem.*, **1997**, 623, 1211-1219.
14. M. Pröhl, U. S. Schubert, W. Weigand, M. Gottschaldt, *Coord. Chem. Reviews*, **2016**, 307, 32-41; G. Xu, J. Wang, G. Si, M. Wang, X. Xue, B. Wu, S. Zhou, *Sens. Actuator B-Chem.*, **2016**, 230, 684-689.
15. A. Bhattacharyya, A. Dixit, K. Mitra, S. Banerjee, A. A. Karande, A. R. Chakravarty, *Med. Chem. Commun.*, **2015**, 6, 846-851.
16. N. Ghalandarlaki, A. Alizadeh, S. Ashkani-Esfahani, *Int. J. Drug Res. Tech.*, **2016**, 6, 43-57.
17. K. Nagahama, Y. Sano, T. Kumano, *Bio. Med. Chem. Lett.* **2015**, 25, 2519-2522.
18. G. Gilli, V. Bertolasi, V. Ferretti, P. Gilli, *Acta Cryst. B*, **1993**, 49, 564-576; Y. Manolova, V. Deneva, L. Antonov, E. Drakalska, D. Momekova, N. Lambov, *Spectrochim. Acta A Mol. Biomol. Spectrosc.*, **2014**, 132, 815-820.
19. F. Payton, P. Sandusky, W. L. Alworth. *J. Nat. Prod.*, **2007**, 70, 143-146.
20. H.H. Tonnesen, J. Karlsen, A. Mostad, *Acta Chem. Scand. B*, **1982**, 36, 475-480; S.P. Parimita, Y.V. Ramshankar, S. Suresh, T.N. Guru Row, *Acta Crystallogr.*, **2007**, 63, o860-o862.
21. Y. J. Wang, M. H. Pan, A. L. Cheng, L. I. Lin, Y. S. Ho, C. Y. Hsieh, J. K. Lin, J., *Pharm. Biomed. Anal.*, **1997**, 15, 1867-1876.
22. H. H. Tonnesen, J. V. Greenhill, *Int. J. Pharm.*, **1992**, 87, 79-87.
23. D. Patra, C. Barakat, *Spectrochim. Acta A*, **2011**, 79, 1034-1041.
24. K. I. Priyadarsini, *J. Photochem. Photobiol. C*, **2009**, 10, 81-95; M. Khopde, K.I. Priyadarsini, D.K. Palit, T. Mukherjee, *Photochem. Photobiol.*, **2000**, 72, 625-631.
25. C.F. Chignell, P. Bilski, K.J. Reszka, A.N. Motten, R.H. Sik, T.A. Dhal, *Photochem. Photobiol.*, **1994**, 59, 295-302.
26. K.C. Das, C.K. Das, *Biochem. Biophys. Res. Commun.*, **2002**, 295, 62-66.

27. R. C. Wende, A. Seitz, D. Niedek, S. M. Schuler, C. Hofmann, J. Becker, P. R. Schreiner, *Angew. Chem. Int. Ed.*, **2016**, 55, 2719-2723.
28. S. Dolai, W. Shi, C. Corbo, C. Sun, S. Averick, D. Obeysekera, M. Farid, A. Alonso, P. Banerjee, K. Raja, *ACS Chem. Neurosci.*, **2011**, 2, 694-699.
29. R. Roy, S. K. Das, F. Santoyo-Gonzalez, F. Hernandez-Mateo, T. K. Dam, C. F. Brewer, *Chem. Eur. J.*, **2000**, 6, 1757-1762; R. Chinchilla, C. Nàjera, *Chem. Rev.*, **2007**, 107, 874-922.
30. C. Ritter, N. Nett, C. G. Acevedo-Rocha, R. Lonsdale, K. Kr. ling, F. Dempwolff, S. Hoebenreich, P. L. Graumann, M. T. Reetz, E. Meggers, *Angew. Chem. Int. Ed.* **2015**, 54, 13440-13443.
31. I. B. Berlman, *Handbook of Fluorescence Spectra of Aromatic Molecules*, Academic Press, New York and London, **1971**.
32. P. Bonaccorsi, M.C. Aversa, A. Barattucci, T. Papalia, F. Puntoriero, S. Campagna, *Chem. Commun.*, **2012**, 48, 10550-10552.
33. A. L. Plant, R. D. Knapp, L. C. Smith, *J. Biol. Chem.*, **1987**, 262, 2514-2519; A.L. Plant, H. J. Pownall, L. C. Smith, *Chem. Biol. Interactions*, **1983**, 44, 237-246.
34. F. Hoffmann, M. Fròba, *Chem. Soc. Rev.*, 2011, 40, 608-620.
35. Q. He, J. Zhang, F. Chen, L. Guo, Z. Zhu and J. Shi, *Biomaterials*, **2010**, 31, 7785-7796; Q. He, J. Shi, X. Cui, J. Zhao, Y. Chen and J. Zhou, *J. Mater. Chem.*, **2009**, 19, 3395-3403.
36. L. Zhou, X. Duan, S. Zeng, K. Men, X. Zhang, L. Yang, X. Li, *Intern. J. Nanomed.*, **2015**, 10, 5205-5218; C. Barbè, J. Bartlett, L. Kong, K. Finnie, H. Q. Lin, M. Larkin, S. Calleja, A. Bush, G. Calleja, *Adv. Mat.*, **2004**, 16, 1959-1966.
37. P. Yang, S. Gaib, J. Lin, *Chem. Soc. Rev.*, **2012**, 41, 3679-3698; Y. Zhang, J. Yan, S. Liu, *Biointerface Res. App. Chem.*, **2014**, 4, 767-775.
38. J. M. Rosenholm, V. Mamaeva, C. Sahlgren, *Nanomedicine*, **2012**, 7, 111-120; A. E. Garcia-Bennett, *Nanomedicine*, **2011**, 6, 867-877.
39. M. Vallet-Regi, A. Ramila, R. P. Del Real, *Chem. Mat.*, **2001**, 13, 308-311.

40. M. Busby, H. Kerschbaumer, G. Calzaferri, L. De Cola, *Adv. Mater.*, **2008**, 20, 1614-1618; F. Cucinotta, F. Carniato, A. Devaux, L. De Cola, L. Marchese, *Chem. Eur. J.*, **2012**, 18, 15310-15315; B. P. Jarman, F. Cucinotta, *Faraday Discuss.*, **2015**, 185, 471-479;
41. M. Borja, P. K. Dutta, *Nature*, **1993**, 362, 43-45.
42. T. Q. Nguyen, J. Wu, V. Doan, B. J. Schwartz, S. H. Tolbert, *Science*, **2000**, 288, 652-656; D. Bruhwiler, G. Calzaferri, *Microporous Mesoporous Mater.*, **2004**, 72, 1-23; E. Fois, G. Tabacchi, A. Devaux, P. Belser, D. Brühwiler, G. Calzaferri, *Langmuir*, **2013**, 29, 9188-9198.
43. H. Manzano, L. Gartzia-Rivero, J. Bañuelos, and I. López-Arbeloa, *J. Phys. Chem. C.*, **2013**, 117, 13331-13336.
44. F. Cucinotta, B. P. Jarman, C. Caplan, S. J. Cooper, H. J. Riggs, J. Martinelli, K. Djanashvili, E. La Mazza, F. Puntoriero, *ChemPhotoChem*, **2018**, 2, 196-206.
45. C. T. Kresge, M. E. Leonowicz, W. J. Roth, J. C. Vartuli, J. S. Beck, *Nature*, **1992**, 359, 710-712. J. S. Beck, J. C. Vartuli, W. J. Roth, M. E. Leonowicz, C. T. Kresge, K. D. Schmitt, C. T. Chu, D. H. Olson, E. W. Sheppard, *J. Am. Chem. Soc.* **1992**, 114, 10834-10843.
46. D. Bruhwiler, *Nanoscale*, **2010**, 2, 887-892.
47. J. Jammaer, A. Aerts, J. D'Haen, J. W- Seob, J. A. Martens, *J. Mater. Chem.*, **2009**, 19, 8290-8293.
48. F. Lu, S. H. Wu, Y. Hung, *Small*, **2009**, 5, 1408-1413.
49. I. Slowing, B. G. Trewyn, V. S. Y Lin. *J. Am. Chem. Soc.*, **2006**, 128, 14792-14793.
50. B. Jain, *J. Mol. Struct.*, **2017**, 1130, 194-198.
51. W. Stober, A. Fink, E. Bohn, *J. Colloid Interface Sci.*, **1968**, 26, 62-69.
52. K. Gangwar, G. B. Tomar, V. A. Dhumale, S. Zinjarde, R. B. Sharma, S. Datar. *J. Agric. Food Chem.*, **2013**, 61, 9632-9637.

53. D. Jin, K.-W. Park, J. H. Lee, K. Song, J.-G. Kim, M. L. Seo, J. H. Jung, *J. Mater. Chem.*, **2011**, 21, 3641-3645; R; S. Jambhrunkar, S Karmakar, A. Popat, M. Yu, C. Yu, *RSC Adv.*, **2014**, 4, 709-712; R. Kotcherlakota, A.K. Barui, S. Prashar, M. Fajardo, D. Briones, A. Rodríguez-Diéguez, C.R. Patra, S. Gómez-Ruiz, *Biomater Sci.*, **2016**, 4, 448-459.
54. E.Gianotti, B. Martins Estevao, F. Cucinotta, N. Hioka, M. Rizzi, F. Ren, L. Marchese *Chem. Eur. J.* **2014**, 20, 10921-109251; D. R. Radu, C.-Y. Lai, K. Jeftinija, E. W. Rowe, S. Jeftinija, V. S.-Y. Lin, *J. Am. Chem. Soc.* **2004**, 126, 13216-13217.
55. . Xu, S. Lü, C. Gao, C. Feng, C. Wu, X. Bai, N. Gao, Z. Wang, M. Liu, *Chem. Eng. J.*, **2016**, 300, 185-192.
56. R. Ziessel, G. Ulrich, A. Harriman, A. Mohammed, H. Alamiry, B. Stewart, P. Retailleau. *Chem. Eur. J.*, **2009**, 15, 1359-1369.
57. W. R. Dawson, M. W. Windsor, *J. Phys. Chem.*, **1968**, 72, 3251-3260.
58. T. Papalia, G. Siracusano, I. Colao, A. Barattucci, M. C. Aversa, S. Serroni, G. Zappalà, S. Campagna, M. T. Sciortino, F. Puntoriero, P. Bonaccorsi, *Dyes Pig.*, **2014**, 110, 67-71.

## **Chapter Three**

---

**Curcumin-based sulfenic acids for the detection of  
biothiols.**

### 3.1 Detection of biothiols

In recent years, the use of probes for thiol assay has attracted great interest. Biological thiols could be divided into protein thiols (PSH) and non-protein thiols (NPSH). Among NPSH, the thiol-containing amino acids and biomolecules such as cysteine (Cys), homocysteine (Hcy), and glutathione (GSH) are extremely important (Figure 3.1).<sup>1</sup> These, owing to the strong nucleophilicity and redox reactivity of the SH group, play crucial roles in a wide range of physiological processes in living systems, including enzyme activity, signal transduction, cell division.<sup>2</sup> Furthermore, thiols work as mild buffering molecules for maintaining cellular redox states. In response to increases in cellular oxidation, thiols act also as nucleophiles reducing reactive oxygen species (ROS) in order to maintain redox homeostasis, acting as cell protectors against reactive oxygen and nitrogen species.<sup>3</sup>

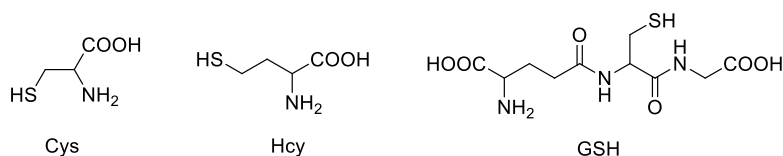


**Figure 3.1:** Chemical structure of Cysteine (Cys), Homocysteine (Hcy) and Glutathione (GSH).

Changes in the levels of biothiols are related to various diseases. For instance, there is a close association of Cys deficiency with neurotoxicity, fat loss, slow growth in children, liver damage and muscle weakness.<sup>4</sup> Abnormal levels of Hcy are proved to be associated with neural tube defects, cardiovascular diseases and osteoporosis.<sup>5</sup> GSH, the most abundant intracellular biothiol, plays a critical role in maintaining the redox cellular state. Imbalance of GSH/GSSG ratios (GSSG=glutathione disulphide) in cells is associated with oxidative stress.<sup>6</sup> Thus, GSH level variation has been directly linked to cancer, leucocyte loss, HIV infection, Parkinson's and



Alzheimer's disease.<sup>7</sup> Therefore, the selective and sensitive detection is highly important to monitor the changes of concentrations of these thiols in living systems, for revealing cellular functions and keeping the balance of biological systems.

Numerous analytical methods have been developed for the detection of thiols, among these the use of fluorescent probes, possessing high sensitivity, fast response times and ability to detect *in vivo* through imaging, are the most exploited. The interaction between analytes and fluorescent probes, can either be based on reversible non-covalent interactions (e.g. hydrogen bond) or on irreversible covalent interactions. Such interaction should change the probe's spectroscopic characteristics, absorbance and/or emission. The reaction must proceed with suitable kinetics in physiological conditions and allow the detection of analytes present even at low concentrations.

Different fluorescence probes are described in literature, appropriately designed to detect the amount of Cys, Hcy or GSH in biological medium.<sup>8</sup>

The rational design of the probe, to exploit the reactivity of the sulfhydryl group of the biological thiols and to obtain a specific response, is crucial. Common groups that react with thiols are shown in figure 3.2. Numerous reaction types have been exploited, including nucleophilic substitution, Michael addition, cyclization, cleavage of disulphide bond, cleavage of sulphonamide and sulfonate esters, metal complexes coordination.

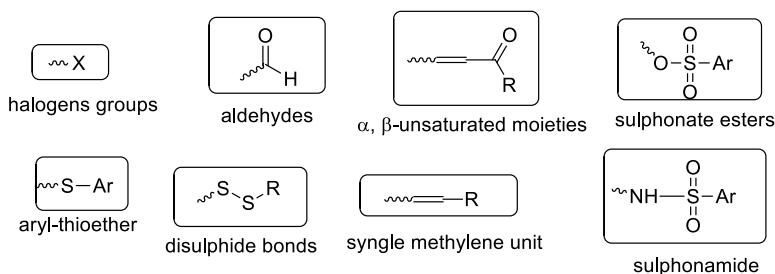
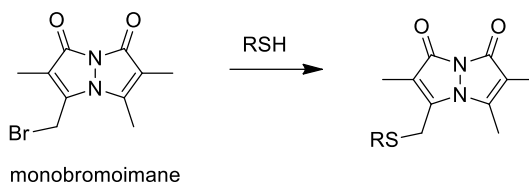


**Figure 3.2:** Common groups reactive with thiols.

Most of the commercially available thiol-detection reagents, like monobromobimane in scheme 3.1,<sup>9</sup> are obtained exploiting the classical reaction with halogen groups, based on the well-known nucleophilicity of the SH functional group.



**Scheme 3.1**

Other probes are designed to exploit the addition of thiol to an  $\alpha,\beta$ -unsaturated carbonyl moiety. This reaction, performed using maleimide and acrylamide derivatives as Michael acceptors, is one of the most reported.<sup>8, 10</sup> Figure 3.3 shows the general reaction mechanism, usually the fluorophores used are BODIPY or xantene derivatives.<sup>11</sup>

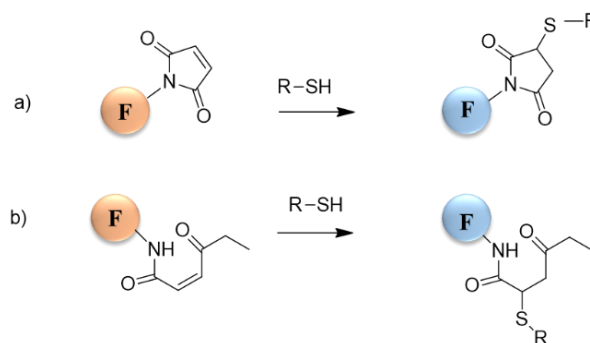


**Figure 3.3:** Schematic reaction of maleimide-bearing fluorophores with thiols a); acrylamide-bearing fluorophores b); F=fluorophores.

However, although these probes can distinguish selectively the biothiols from other amino acids, most of them cannot distinguish Cys/Hcy/GSH from each other, due to the similar structures and reactivity. Yang *et al.*<sup>12</sup> proposed a strategy for the discrimination of GSH over Cys/Hcy, based on an aromatic

substitution-rearrangement cascade reaction (Figure 3.4), in which a fluorophore bearing a labile substituent reacts with thiols, through nucleophilic aromatic substitution ( $S_NAr$ ), to obtain a thioether. The amino groups of Cys/Hcy displace sulfur through a 5- or 6-membered transition state to yield the amino derivatives. The distinct photophysical properties of thioether- and amino-substituted dyes enable the selective detection of GSH, Cys and/or Hcy.

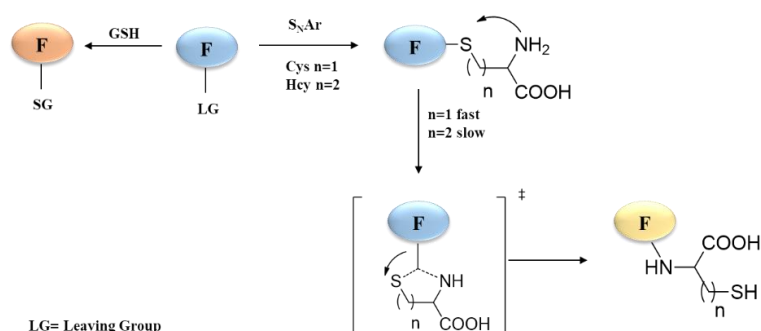


**Figure 3.4:** Selective detection reaction for GSH, Cys and Hcy.

Another convenient way to detect selectively Cys/Hcy from GSH is the conjugate addition–cyclization with acrylates. Acrylic esters of common fluorophores (such as fluorescein, coumarins, naphthalimides and cyanines) are used. In the presence of Cys, Hcy, a thioether is formed by conjugated addition, that can further cyclize to 7-8 membered S-N heterocycles, followed by the release of free fluorophores (Figure 3.5).

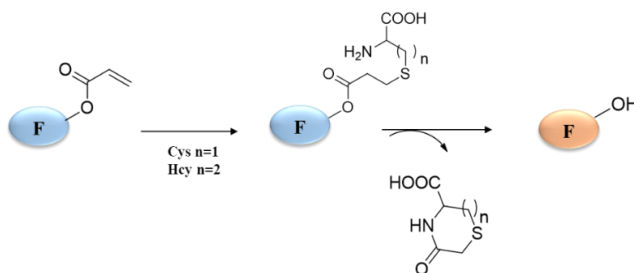


**Figure 3.5:** Reaction of acryl ester fluorophores with Cys and Hcy through conjugated addition.

Differentiation between Cys and Hcy typically results from the much faster intramolecular cyclization of the Cys adducts compared to the Hcy analogues, due to the lower activation energy needed for the formation of a 7- vs. 8-membered ring.

A colorimetric probe for the detection of cysteine in solution, in living cells, and in a living vertebrate organism, exploiting this reaction and using Curcumin as fluorophore, has been recently reported by Zhou *et al.*<sup>13</sup>

The probe CAC, shown in figure 3.6, exhibits itself a strong emission. The conjugate addition-cyclization with Cys, followed by the release of Curcumin, results in a fluorescence quenching. The probe CAC acts as a “naked eye” probe, it is readily synthesized and highly selective for Cys with a lower detection limit of 0.19  $\mu\text{M}$ . In addition, it was successfully applied to detect Cysteine in living cells and zebrafish with good cell and organism permeability, indicating its significant potential in living biological systems.

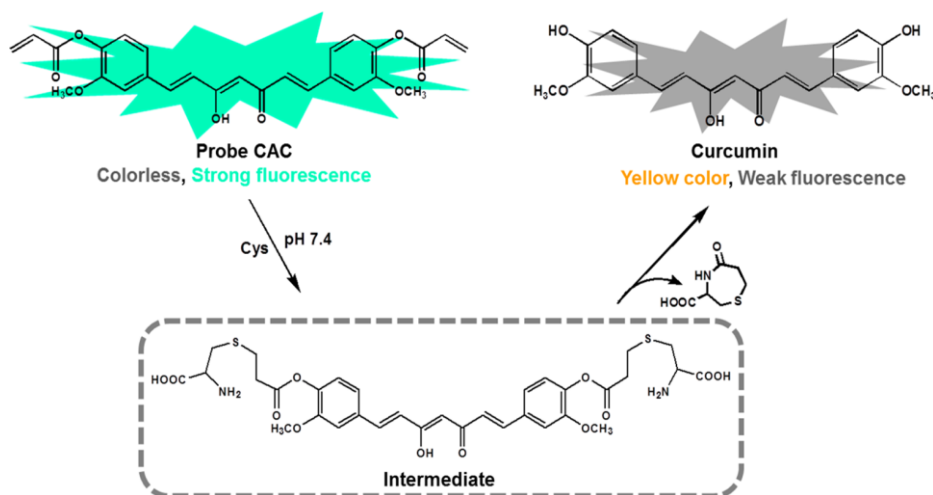


**Figure 3.6:** Reaction of acryl ester fluorophores with Cys and Hcy through conjugated addition.

As discussed in chapter two, Curcumin possesses an  $\alpha,\beta$ -unsaturated carbonyl moiety, which can undergo Michael-type addition reaction with nucleophilic substances.

In 2011, Appendino *et al.*<sup>14</sup> investigated the trapping of thiols by covalent coupling with natural alkenes, dienones,  $\alpha,\beta$ -unsaturated esters, Curcumin included, amides and lactones, and reported an NMR study of the formation of a series of reversible or irreversible product adducts. The test conducted after the addition of Cysteamine ( $\text{SHCH}_2\text{CH}_2\text{NH}_2$ ) to Curcumin showed the formation of a 1:2 reversible adduct of Curcumin-Cysteamine (Figure 3.7).

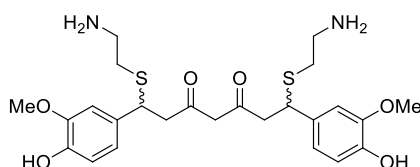


**Figure 3.7:** Adduct of Curcumin with Cysteamine.

This NMR spectroscopic method allows the identification of compounds like Curcumin able to form reversible thiol bonds and predict their potential to modify proteins.

### 3.2 Sulfenic acids generals

Sulfenic acids play important roles as reactive intermediates in organosulfur chemistry and as transient intermediates in biological processes.<sup>15</sup>

In a proteic environment, in response to reactive oxygen species (ROS), thiols oxidize to sulfenic acids. In particular, the nucleophilic attack of a protein thiolate on electrophilic  $\text{H}_2\text{O}_2$  releases water, and results in the formation of cysteine sulfenic acid (Cys-SOH). The reaction is also known as S-sulfenylation. Therefore, biological sulfenic acids are usually considered as the oxidation product of cysteine thiol moiety.<sup>16</sup>

A number of methods have been developed to “trap” proteins in their sulfenylated state and study their role within the cells. Strategies for protein-SOH detection are reported in figure 3.8.<sup>17</sup>

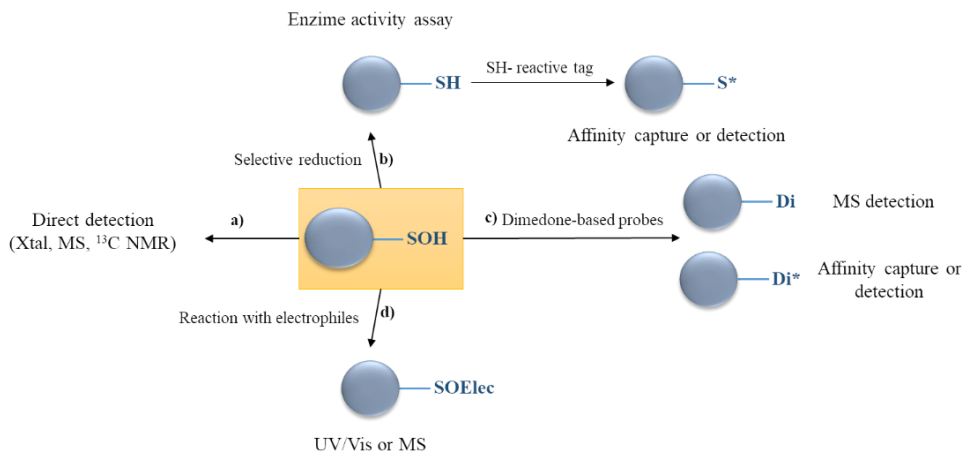


**Figure 3.8:** Methodologies for protein-SOH detection.

Due to the electrophilic as well as nucleophilic character of the sulfur atom in Cys-SOH of proteins, detection methods exploiting both chemical features have been reported (Figure 3.9).<sup>18</sup> The electrophilic attack to C-nucleophiles

leads to thioethers whereas the nucleophilic attack towards electrophiles produces sulfoxides.

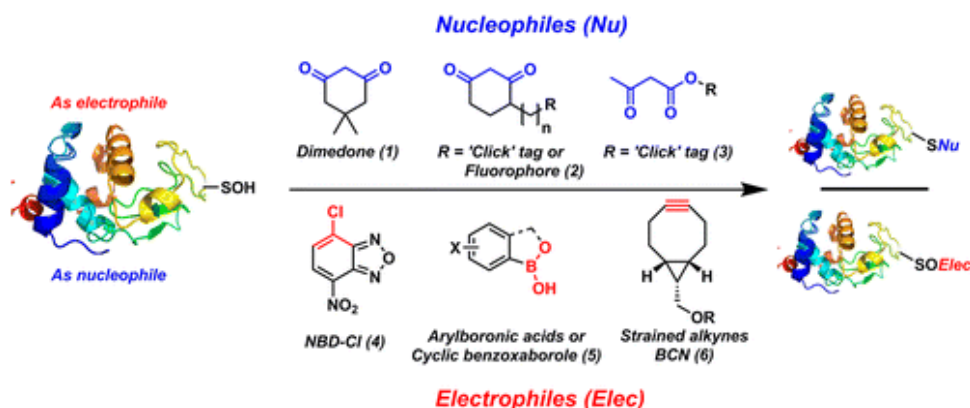


**Figure 3.9:** Reactivity of protein-SOH with both nucleophiles and electrophiles.

However, under physiological conditions, the electrophilic reactivity of Cys-SOH dominates. The vast majority of probes for selective chemical detection protein-SOH, are typically based on cyclic 1,3-carbonyl scaffolds, such as Dimedone (Figure 3.9), that has been employed to label sulfenylated proteins, subsequently characterized by fluorescence or proteomic mass spectrometry. Dimedone and dimedone-like compounds have been widely used for qualitative and quantitative studies, but there are a number of limitations associated with these probes. Dimedone derivatives have slow rates of reaction toward sulfenic acids, compared to competing biological Cys-SOH. To overcome the issue of slow reactivity, Carroll *et al.*<sup>19</sup> recently developed a mass spectrometry-based assay and dipeptide sulfenic acid model (Figure 3.10) that allowed to screen a library of cyclic C-nucleophiles and identify novel compounds with enhanced reactivity, compared to Dimedone. Interesting, among these Curcumin was tested. Curcumin can act as nucleophile toward the sulfenic acid model 2 in figure 3.10, to obtain a thioether. The reactivity was found to be enhanced compared to Dimedone.

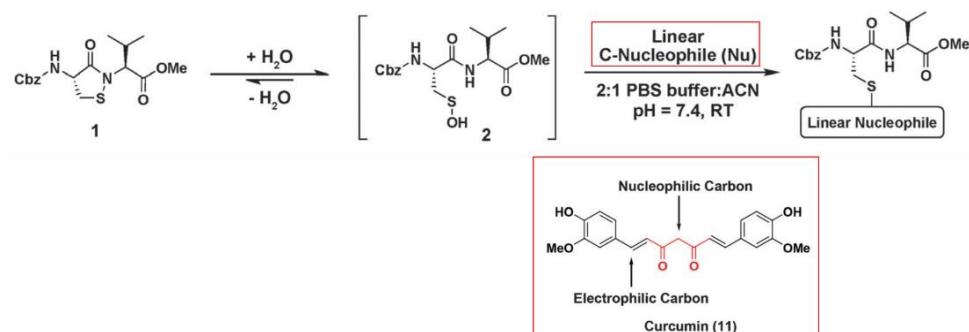
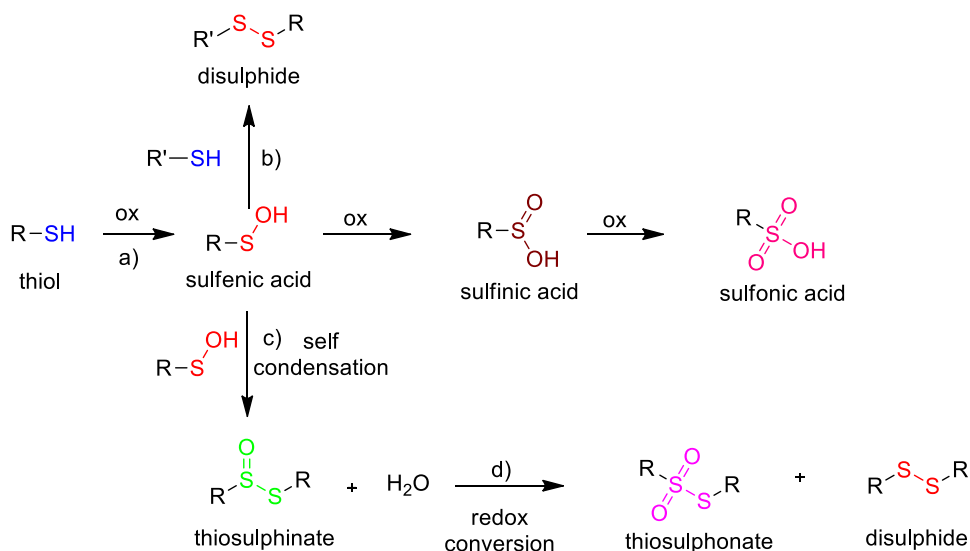


**Figure 3.10:** Structure and reaction of the dipeptide sulfenic acid-model 2 with nucleophilic carbon of Curcumin.

From a synthetic point of view, usually sulfenic acids are unstable moieties that may undergo further oxidation to sulfinic and sulfonic acids. In the absence of a suitable trapper, sulfenic acids either react with other thiols to form disulfides, or self-condense to give thiosulfinates. Thiosulfinates spontaneously undergo redox conversion into thiosulfonates and disulfides, these last being the final isolated products (Scheme 3.2).<sup>20</sup>



**Scheme 3.2**

The majority of known sulfenic acids cannot be isolated, but some stable ones have been obtained.<sup>21</sup> The stability of sulfenic acids isolated has been



explained in terms of steric and electronic effects. A preminent role in the field of stable sulfenic acids is held by Okazaki and Goto.<sup>22</sup> These authors investigated isolation and stabilization of sulfenic acids, by taking advantage of kinetic stabilization afforded by a bulky bowl-type environment (Figure 3.11, a). If a functional group is embedded in a large, shallow molecular bowl with a rigid framework, the cavity inhibits the approach of functional groups on molecules of the same type, while not preventing different molecules from reacting with it. In this case the sulfenic acid function is directly linked to a benzene ring, doubly joined to a calix[6]arene unit, so that the bridged calixarene fixes the sulfur functionality in such a way that it points into the cavity (Figure 3.11, b).<sup>23</sup>

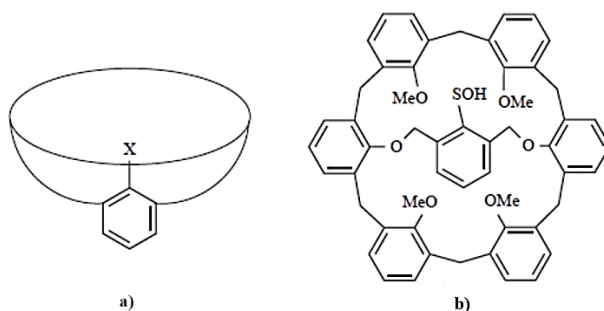
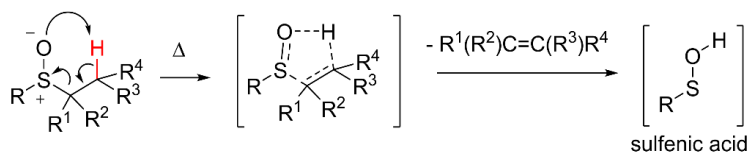


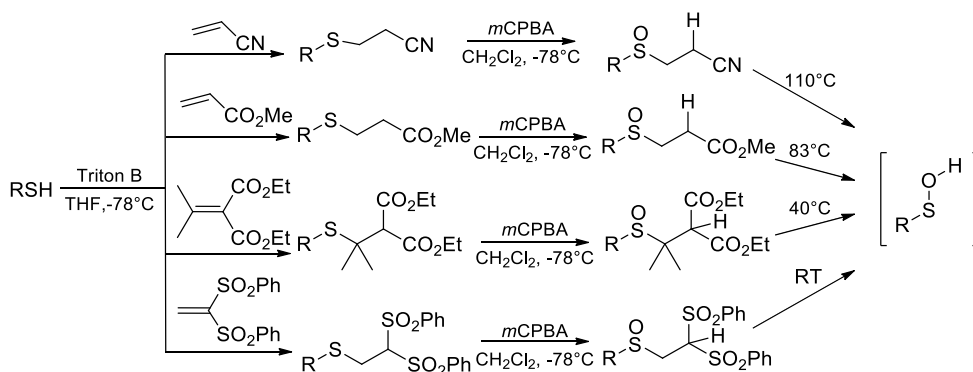
**Figure 3.11:** Reaction bowl (a); stable sulfenic acid (b).

Many papers have been published in the last decade about the sulfenic acid intermediacy in organic chemistry.<sup>24</sup> Among the several ways to obtain them,<sup>25</sup> their *in situ* generation via the thermolysis of suitable sulfoxides bearing a mobile hydrogen in  $\beta$ -position to the sulfur atom (Scheme 3.3), is one of the most exploited methods, first described by Jones *et al.*<sup>26</sup> The reaction is a syn-concerted elimination, and passes through a five membered cyclic transition state.



Scheme 3.3

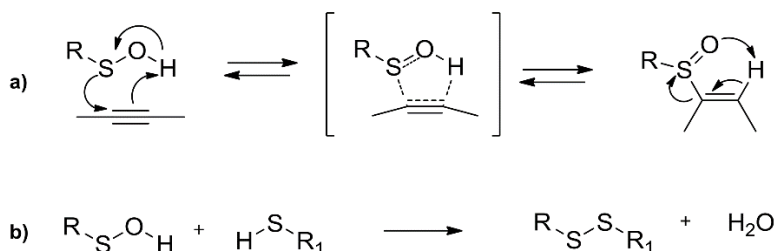
The synthetic route to the sulfinyl precursors of sulfenic acids generally involves two steps: the nucleophilic conjugated addition of a thiolate to an  $\alpha$ - $\beta$  unsaturated compound, and the subsequent oxidation of the obtained thioether to sulfoxide by means of *m*-CPBA. Electron-withdrawing groups linked to the  $\beta$  carbon atom and/or sterically demanding groups on the  $\alpha$  carbon atom are needed to enhance the mobility of the  $\beta$ -H and, hence, to modulate the thermolysis temperature (Scheme 3.4).<sup>27</sup>



Scheme 3.4

Tuning of the thermolysis mildness, and lack of acidic or basic conditions, give the way to the generation of sulfenic acids bearing labile R residue, not obtainable in different processes.

Once generated, many are the applications of sulfenic acids in organic synthesis, even if they are transient species. Among them, intermolecular syn-addition of sulfenic acids to triple bonds gives a wide library of vinyl sulfoxides which include new target compounds containing natural residues (Scheme 3.5, a).<sup>28</sup>

**Scheme 3.5**

Condensation of sulfenic acids with thiols, employed until the last decade only to demonstrate indirectly the in situ generation of these unstable intermediates, has found its application in the formation of unsymmetrical disulfide bonds (Scheme 3.5, b).<sup>29</sup> Exploiting these reactions, a large number of biologically relevant sulfoxides, sulfones and disulfides were reported by Bonaccorsi *et al.*<sup>30</sup> Authors demonstrated that the addition of sulfenic acids to unsaturated molecules can be used as a tool to obtain sulfoxide functions, even in an enantiomerically pure form and biologically relevant sulfinyl compounds, such as *nor*-Alliin. They have also used the condensation of thiols with sulfenic acids to provide an easy access to molecules with a biologically significant disulfide bond linked to two structurally different residues (Chapter 1, paragraph 1.2).

### 3.3 Synthesis and Generation of a Curcumin-based sulfenic acid

During the last part of my PhD, I worked with sulfenic acids, the generation and use of some of which were deeply studied by the research group where I developed my thesis.<sup>30</sup> The aim of this new project was to combine the chemistry of sulfenic acids with the spectroscopic properties of Curcumin in order to synthesize a Curcumin-derived sulfenic acid potentially capable to trap biological thiols, such as Cys or GSH by formation of disulphide bonds (Figure 3.12). In this project I took advantage of the luminescence of Curcumin, to realize a potential probe for the detection of the biothiols.

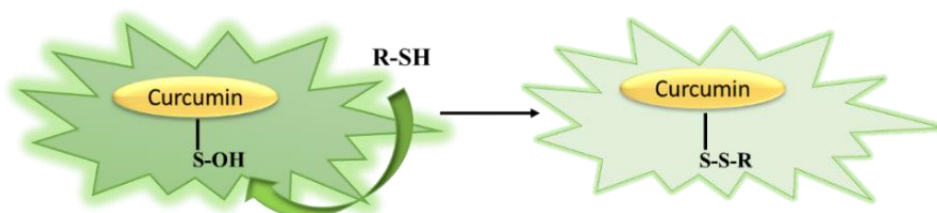
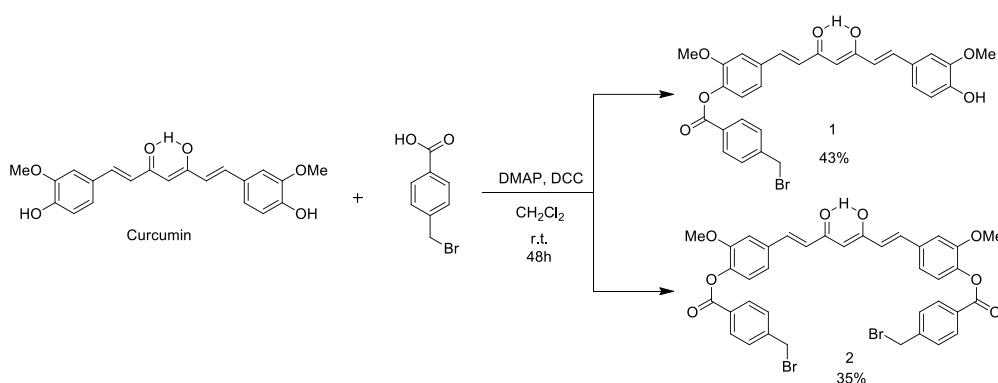


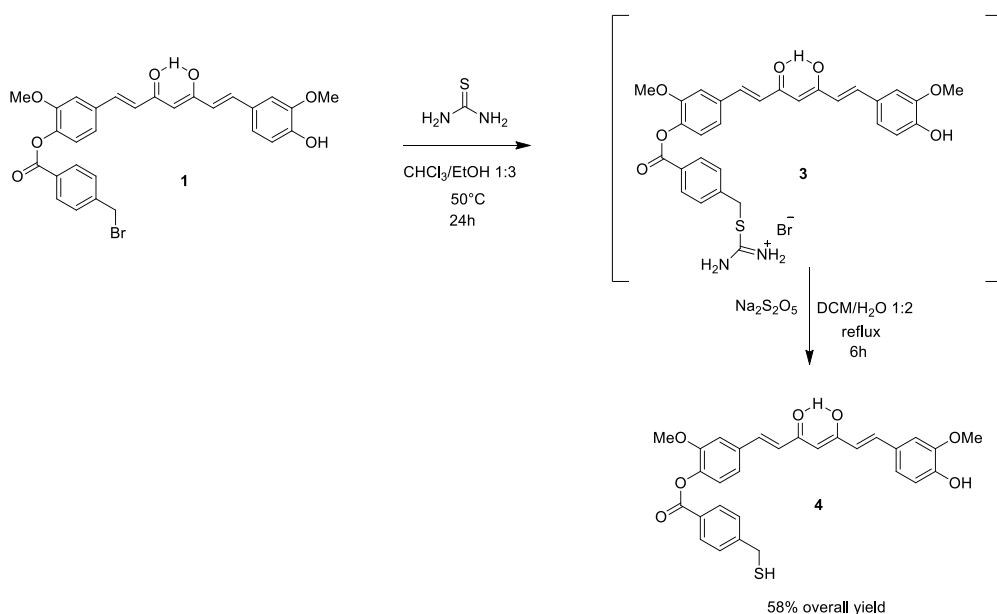
**Figure 3.12:** Schematic representation of the working mechanism of the sulfenic acid-based luminescent probe.

I started with the design and construction of a suitable Curcumin derivative to allow the generation of the sulfenic moiety and opted for a thiol such as **1** in scheme 3.6, from which I could obtain the corresponding Curcumin sulfinyl derivative in two steps. Thermolysis of suitable substituted sulfoxide appeared indeed the most attracting methodology to generate Curcumin-derived sulfenic acid since it doesn't need any acidic or basic conditions, both deleterious for the natural residue. Moreover, this methodology allows sulfenic acid generation in a range of temperatures between 110°C and 25°C, so that even temperature-labile compounds can be involved in reactions with the transient species.

The first reaction, between Curcumin and 4-(bromomethyl)benzoic acid, in the presence of *N,N'*-dicyclohexyl carbodiimide (DCC) and a catalytic amount of 4-dimethylaminopyridine (DMAP), is shown in scheme 3.6.<sup>31</sup> This Steglich-type esterification was conducted at room temperature and under stirring for 48h. Purification of the crude was achieved by two subsequent column chromatography, the first to remove the remaining DCC and unreacted benzoic acid and the second to afford mono-bromo Curcumin derivative **1** and the bis-bromo **2** in 43% and 35% yields, respectively.



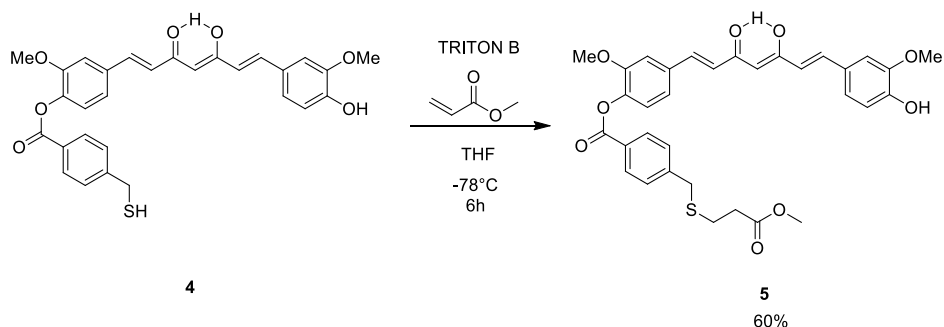
Scheme 3.6



Scheme 3.7

Reaction of compound **1** with thiourea led to the corresponding thiouronium salt that was directly reduced with sodium-meta-bisulphite, to obtain Curcumin mono-thiol **4** in 58% yield over two steps (Scheme 3.7). Curc-mono-SH **4** is luminescent and this suggests that even the corresponding transient Curcumin-derived sulfenic acid is luminescent.

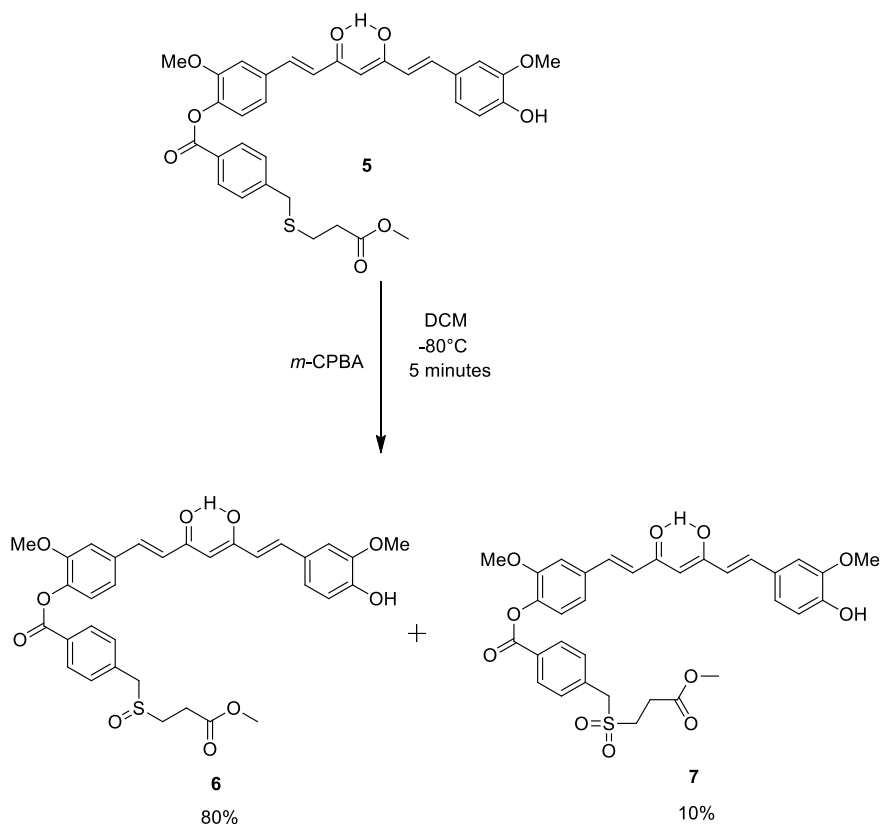
Catalytic basic conditions were tested for the nucleophilic addition of thiol **4** to methyl acrylate (Scheme 3.8). The reaction conducted in the presence of  $K_2CO_3$ , as base, failed, giving poor yield of the product, likely for the presence of the phenolic hydroxyl group, that in similar conditions undergoes nucleophilic substitution reactions. Therefore, I decided to use benzyl (trimethyl) ammonium hydroxide (Triton B) as base in catalytic amount, at a controlled temperature of  $-78^\circ\text{C}$ . Treatment of compound **4** with TRITON B generated the thiolate that reacted with methyl acrylate to afford sulfide **5** in 60% yield.



**Scheme 3.8**

Sodium periodate was first chosen as oxidant of sulfide **5** to sulfoxide **6** (Structures in scheme 3.9) and the reaction was conducted in MeOH at  $0^\circ\text{C}$  to r.t. Unfortunately, the oxidant has not proved effective and sulfide **5** was recovered after 12h of reaction. Thioether **5** was then oxidized using an equivalent amount of *m*-CPBA, at  $-78^\circ\text{C}$ . This reaction needs an accurate control of temperature and time. It's complete after the addition of peroxide,

and goes easily toward the formation of the over oxidation product the sulfone **7** (Scheme 3.9). The corresponding sulfone **7** was eliminated by purification with column chromatography, from which sulfoxide **6** was obtained in 80% yield.

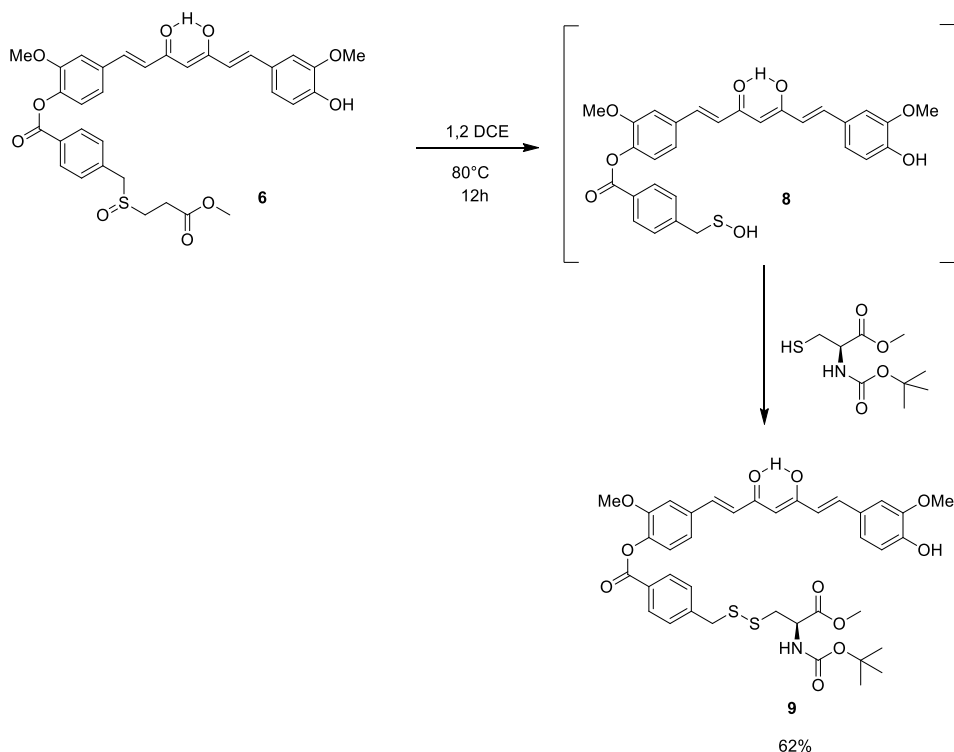


**Scheme 3.9**

With the aims of demonstrating the ability of Curcumin-derived sulfinyl precursor **6** to generate Curc-SOH **8** (structure in scheme 3.10) and a potential use of the latter in the conception of a probe for the detection of biological thiols, I decided to thermolyse sulfoxide **6** in the presence of *N*-(*tert*-butoxycarbonyl)-L-cysteine methyl ester, as trapper of the transient sulfenyl derivative **8** (Scheme 3.10). The reaction, already described in paragraph 3.2, is a condensation between the nearly formed sulfenic acid and the sulphidryl

moiety of the amino acid, leading to a disulphide bond. Disulfides are considered as dynamic-covalent bonds in biology.<sup>32</sup> They are stable to a redox environment present in the extracellular area of a cell and are cleaved intracellularly. The chemo-selective formation of a disulfide bond in a molecule is a demanding task that opens a way to biological uses.

Thermolysis in 1,2-DCE, followed by column chromatography afforded Curcumin-derived disulphide **9** in 62% yield.



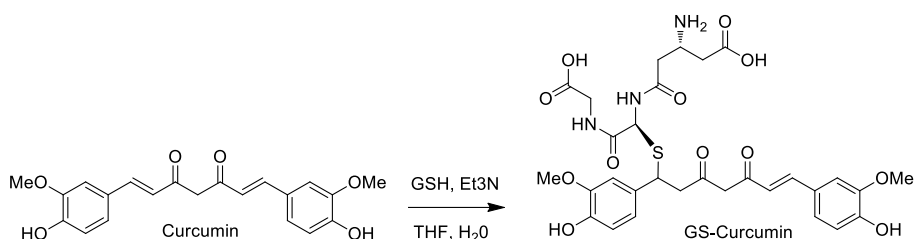
**Scheme 3.10**

To mimic the generation of the Curcumin-derived sulfenic acid **8** in a proteic environment, I decided to exploit the thermolysis of sulfinyl precursor **6** in the presence of the tripeptide GSH.

I found in literature several biological studies about the interaction of Curcumin with Glutathione,<sup>33</sup> such as the one<sup>34</sup> reported in scheme 3.11, in

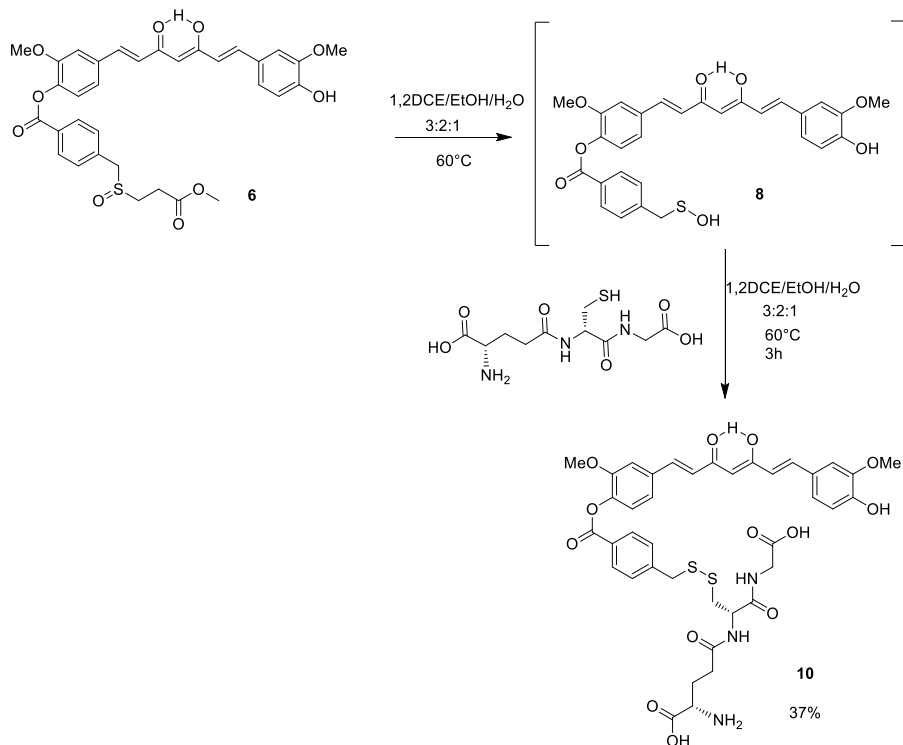


which GSH adds, with a Michael-type 1,4-addition, to one of the two  $\alpha,\beta$ -unsaturated carbonyl groups of Curcumin to lead to adduct GS-Curcumin.



**Scheme 3.11**

The adduct products were characterized by proteomic mass spectrometry and it was studied how the formation of such glutathione conjugates can influence the bioavailability of the yellow natural molecule. However, no example of the use of such reaction to exploit the spectroscopic properties of Curcumin and to develop new fluorescence-based detection methods is reported.



**Scheme 3.12**

GSH is not at all soluble in DCE and is thermolabile, therefore, we decided to use a large excess of GSH and conduct the thermolysis in a DCE/EtOH/H<sub>2</sub>O (3:2:1) mixture, at 60°C, that furnished, in 3h, disulphide **10** (Scheme 3.12). Compound **10** was purified by column chromatography and obtained in 37% yield, together with traces of thiol **4**. I've taken the formation of compound **4** as the proof of the generation of Curc-SOH **8**, some of which was reduced to the corresponding thiol, by the excess of GSH, prior its reaction with the sulfhydryl group of the tripeptide.

### 3.4 Photophysical studies on the detection of biothiols by the Curcumin-based sulfenic acid

Once accomplished the generation of a Curc-SOH and its reaction with GSH, as proteic model, it was necessary to demonstrate that the formation of the disulphide bond between Curcumin and GSH could represent a potential tool to detect the presence of biological thiols. As proof of concept, some preliminary photophysical experiments were carried out in cooperation with the photochemistry group of University of Messina.

UV/Vis and fluorescence spectra were recorded dissolving the Curc-SOH precursor **6** and the final product of thermolysis Curc-Cys **9** or Curc-GSH **10** in a mixture 1:3 of EtOH/PBS (buffer at pH 7.5, ionic strength: 0.55 mM). This solvent mixture, already used in literature for a probe involved in the detection of Cysteine,<sup>13</sup> was found effective also in my case.

As shown in figure 3.13, the absorption spectra of **9** and **10** are very similar to each other and do not show significant differences with respect to the spectrum exhibited by the precursor species **6**.

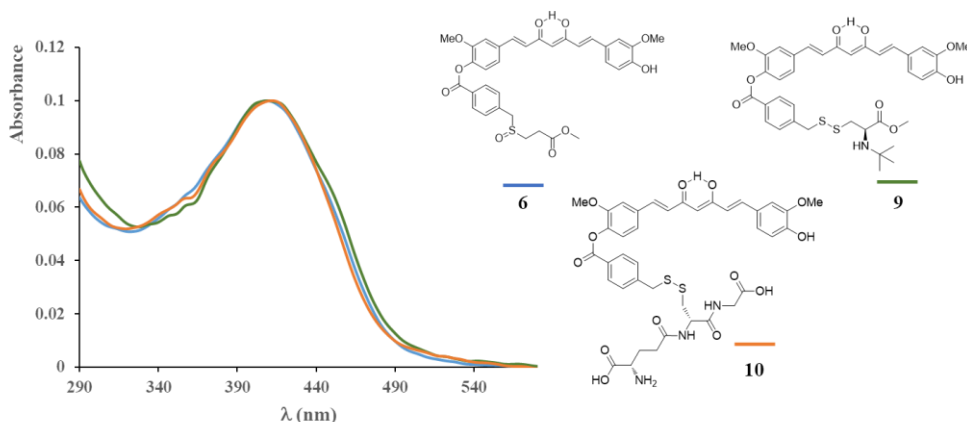


**Figure 3.13:** Absorption spectra of the precursor sulfoxide **6** (blue line), disulphide Curc-cyst **9** (green line) and disulphide Curc-GSH **10** (orange line) in EtOH/PBS (buffer at pH 7.5, ionic strength: 0.55 mM). Conc. =  $2.4 \times 10^{-6}$  M

This behavior clearly indicates that, at least at the ground state, there is no electronic interaction between Curcumin moiety and the Cys or GHS fragments.

For what is concerned with the emission spectra, in the used experimental conditions, sulfoxide **6** exhibits luminescence with a maximum at  $\lambda = 500$  nm and an emission quantum yield of about 25%, independent of the excitation wavelength (Figure 3.14). However, in the case of the novel species **9** and **10** no luminescence was detected, so suggesting that, in these cases, a new deactivation channel is active for the excited state of Curcumin platform. In fact, the presence of lone pair on the amine groups of cysteine and GSH residues allows for a photoinduced electron transfer process that involves the excited state of Curcumin moiety as electron acceptor. Taking as presupposition that the excited state life time of **6** unchanged (0.9 ns), because of the total absence of luminescence in the case of the novel species, the electron transfer process can be assumed to happen in less than 100 ps in both cases.

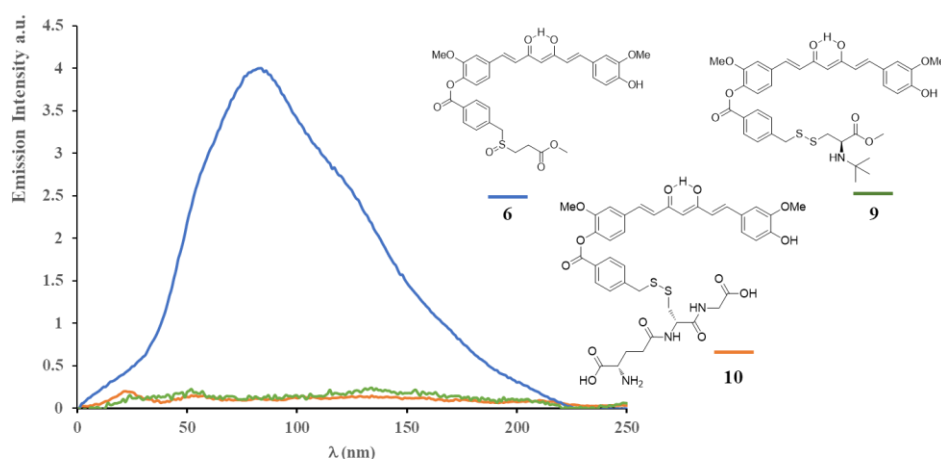


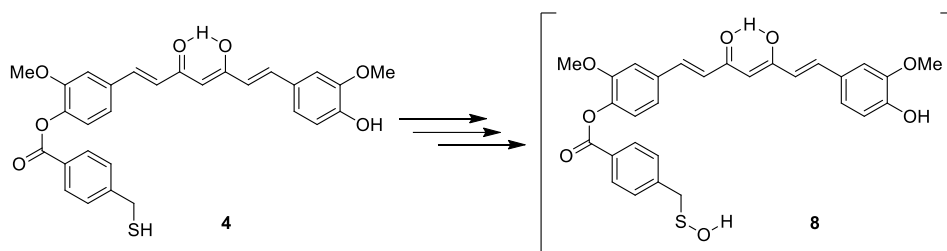
**Figure 3.14:** Emission spectra of the precursor sulfoxide **6** (blue line), disulphide Curc-cyst **9** (green line) and disulphide Curc-GSH **10** (orange line).

Experiments conducted on these substrates suggest that once the luminescent Curcumin derivative **6** generates the luminescent Curc-SOH **8**, it immediately reacts with the sulphydryl functions of a proteic environment causing a shutdown of the emission, as observed for adduct Cur-GSH **10**.

### 3.5 Conclusions

In this chapter I've described the approach to the generation of the new transient sulfenic acid **8**, in which the sulfenic function is linked, through an aryl spacer, to the Curcumin. For the spectroscopic characteristic of the natural residue connected with the SOH moiety, it can be presumed that this is the first example of a luminescent transient sulfenic acid.

Sulfenic acid **8** was generated starting from thiol **4** in three steps (Scheme 3.12), using a well assessed strategy that guaranties very mild conditions in the final reaction of thermolysis. No bases or acids were used to catalyse this reaction that, for this reason, can be spent in a biological environment, if the suitable sulfenic acid precursor is chosen.



Scheme 3.13

To take advantage from the potentialities of Curc-SOH **8**, the trapping reaction was chosen to obtain the formation of a disulphide bond between the Curcumin residue and the sulfhydryl group of biothiols, such as Cys and GSH.

As completion of the study, some photophysical experiments were conducted on sulfoxide **7** and Curc-GSH derivative **10**. I was aimed to demonstrate that a significant difference in the luminescence properties of such species, mimicking a biological environment, could in principle represent a proof of application of the entire system in the detection of protein thiols.

The absorption and emission of compounds **7** and **10** were measured, showing, no differences in the absorption spectra of both the compounds. However, it was observed that while sulfoxide **7** emits at a wavelength of 500 nm, in an EtOH/phosphate buffer mixture, the emission of Curc-GSH derivative **10** was shut down in the same conditions. These results show a scenery in which the suitably generated Curc-SOH can in principle function as a turn-off sensor for biothiols and open the way to future applications.

### 3.6 Experimentals

---

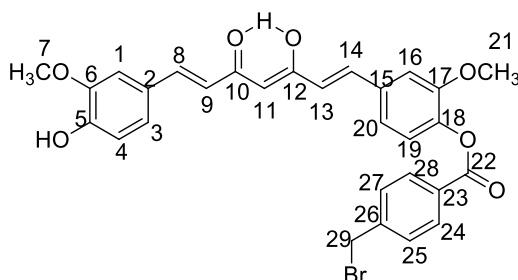
**General Synthetic Methods** Solvents were purified according to standard procedures. Curcumin from *Curcuma L.* (>65%, Sigma-Aldrich) was purified from the mixture of demethoxy curcuminoids, using the procedure described in chapter 2, the other commercial reagents were used without further purification. The syntheses were carried out under atmospheric conditions or under Argon. The reactions were monitored by TLC on commercially available precoated plates (silica gel 60 F254) eluted with Hexane/EtOAc, CHCl<sub>3</sub>/Hexane, CHCl<sub>3</sub>/MeCN, and the products were visualized with vanillin [1 g dissolved in MeOH (60 mL) and conc. H<sub>2</sub>SO<sub>4</sub> (0.6 mL)] and UV lamp. Silica gel 60 was used for column chromatography. <sup>1</sup>H and <sup>13</sup>C NMR spectra were recorded in CDCl<sub>3</sub> or dimethylsulfoxide-d<sub>6</sub> (DMSO-d<sub>6</sub>) with a Varian 500 spectrometer (at 500 MHz for <sup>1</sup>H; and 125 MHz for <sup>13</sup>C). Chemical shifts are given in parts per million (ppm) referenced to the residual solvent CDCl<sub>3</sub> (<sup>1</sup>H NMR 7.27 ppm and <sup>13</sup>C NMR 77.0 ppm) and DMSO-d<sub>6</sub> (<sup>1</sup>H NMR 2.50 ppm and <sup>13</sup>C NMR 39.5 ppm). NMR peak assignments are supported by homonuclear (COSY, COReLationSpectroscopY) and heteronuclear correlation <sup>1</sup>H–<sup>13</sup>C spectroscopy (HSQCAD). Coupling constants (*J*) are given in hertz.

**General Photophysical Methods.** UV/Vis absorption spectra in solution were recorded with a Jasco V-560 spectrophotometer. For steady-state luminescence measurements, a Jobin Yvon-Spex Fluoromax P spectrofluorimeter equipped with a Hamamatsu R3896 photomultiplier was used. For correcting the emission spectra for the photomultiplier response, a program purchased with the fluorimeter was used.



### Synthesis of Compounds 1-7, 9 and 10.

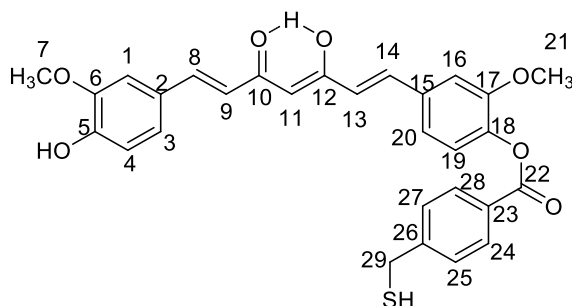
**Compound 1.** Curcumin (500 mg, 1.37 mmol) was dissolved in 15 ml of dry DCM, then, 4-(bromomethyl)benzoic acid (300 mg, 1.37 mmol), 1,3-dicyclohexylcarbodiimide (DCC, 508 mg, 2.26 mmol, 1.8 eq) and 4-dimethylaminopyridine (DMAP, 16.7 mg, 0.137 mmol, 0.1 eq) were added. The reaction mixture was stirred at room temperature for 48h, under argon. The completion of reaction was monitored by TLC ( $\text{CHCl}_3/\text{MeCN}$  95:5). The crude was then filtered to remove the dicyclohexylurea (DCU) formed during the reaction and purified twice with column chromatography on silica gel. The first to remove the remaining DCU and the unreacted 4-(bromomethyl)benzoic acid (Eluants:  $\text{CHCl}_3/\text{Hexane}$  90:10 up to  $\text{CHCl}_3/\text{MeCN}$  95:5) and the second (Eluants: Hexane/EtOAc 80:20 up to 60:40) to obtain compound **1** in 43% yield as an orange solid.  $R_f$  0.6 ( $\text{CHCl}_3/\text{MeCN}$  95:5). From the same final column compound **2** was also obtained in 35% yield as a yellow solid.  $R_f$  0.8 ( $\text{CHCl}_3/\text{MeCN}$  95:5).



$^1\text{H}$  NMR ( $\text{CDCl}_3$ ):  $\delta$  ( 8.2-8.18 (2H, m, H-24, H-28), 7.63 (1H, d, H-8,  $J=16.2$  Hz), 7.61 (1H, d, H-14,  $J=15.6$  Hz), 7.55-7.52 (2H, m, H-25, H-27), 7.20-6.93 (6H, m, H-1, H-3, H-4, H-16, H-19, H-20), 6.58 (1H, d, H-13,  $J=16.2$  Hz), 6.5 (1H, d, H-9,  $J=15.6$  Hz), 5.88 (1H, br s, OH), 5.84 (1H, s, H-11), 4.54 (2H, s, H-29), 3.95 and 3.86 (6H, 2 s,  $\text{OCH}_3$ );  $^{13}\text{C}$  NMR :  $\delta$  184.5 (C-10), 181.8 (C-12), 163.9 (C-22), 151.5 (Cq), 147.9 (Cq), 146.8 (Cq), 141.4

(Cq), 141.3 (Cq), 141.1 (C-8), 139.4 (C-14), 134.2 (Cq), 130.8 (C-24, C-28), 129.2 (C-25,C-27), 127.5 (Cq), 127.1 (Cq), 124.3 (C-9), 121.8 (C-13), 123.3, 123.0, 121.0, 114.8, 111.5 and 109.6 (C-1, C-3, C-4, C-16, C-19, C-20), 101.5 (C-11), 55.9 (C- 7, C-21), 32.0 (C-29).

**Compound 4.** Compound **1** (170 mg, 0.30 mmol) was dissolved in 15 ml of a mixture of EtOH/CHCl<sub>3</sub> (3:1) then thiourea (23 mg, 0.30 mmol) was added. The mixture was warmed up to 50°C and maintained under stirring for 24h, until the TLC Hexane/EtOAc (50:50) showed the formation of the intermediate thiouronium salt **3**. The solvents were removed under reduced pressure and compound **3** was dissolved in a mixture of water/CHCl<sub>3</sub> (1:3), then Na<sub>2</sub>S<sub>2</sub>O<sub>5</sub> (86 mg, 0.45 mmol, 1.5 eq) was added. The mixture was refluxed for 6h. When compound **3** disappeared from TLC (Hexane/EtOAc 60:40), water was added and the two solvent layers were separated. Water was extracted for three times with CHCl<sub>3</sub> and the combined organic layers were dried over MgSO<sub>4</sub> and filtered. After the solvent was removed under reduced pressure, the crude was purified using silica gel column chromatography with Hexane/EtOAc (60:40 up to 50:50) as eluents to obtain **4** as yellow solid in 58% overall yield. Rf: 0.7 Hexane/EtOAc (60:40).



<sup>1</sup>H NMR (CDCl<sub>3</sub>) :  $\delta$  8.19-8.15 (2H, m, H-24, H-28), 7.63 (1H, d, H-8,  $J$ =16.0 Hz), 7.61 (1H, d, H-14,  $J$ =15.7 Hz), 7.49-7.46 (2H, m, H-25, H-27), 7.26-6.92 (6H, m, H-1, H-3, H-4, H-16, H-19, H-20), 6.58 (1H, d, H-13,  $J$ =16.0 Hz), 6.5 (1H, d, H-9,  $J$ =15.7 Hz), 5.89 (1H, br s, OH), 5.84 (1H, s, H-

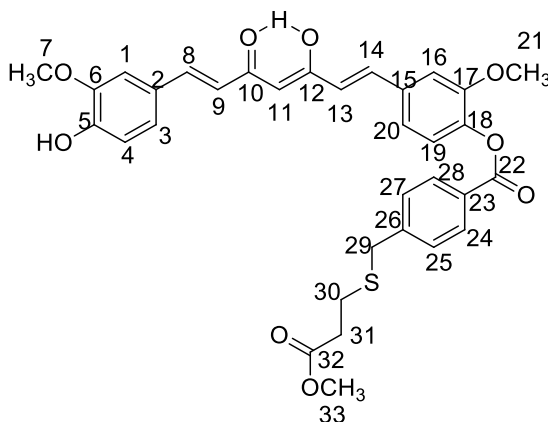
11), 3.95 and 3.86 (6H, 2 s, OCH<sub>3</sub>), 3.82 (2H, d, H-29, *J*=7.3 Hz), 1.82 (1H, t, SH, *J*=7.3 Hz); <sup>13</sup>C NMR : δ 184.5 (C-10), 181.8 (C-12), 164.2 (C-22), 151.6 (Cq), 147.9 (Cq), 147.1 (Cq), 146.8 (Cq), 141.4 (Cq), 141.0 (C-8), 139.4 (C-14), 134.1 (Cq), 130.8 (C-24, C-28), 128.3 (C-25, C-27), 127.9 (Cq), 127.6 (Cq), 124.3 (C-9), 121.8 (C-13), 123.4, 123.0, 121.0, 114.8, 111.5 and 109.6 (C-1, C-3, C-4, C-16, C-19, C-20), 101.5 (C-11), 56.0 (C-7, C-21), 28.7 (C-29).

<sup>1</sup>H and <sup>13</sup>C spectra of thiol **4** were recorded also in DMSO-*d*<sub>6</sub> for comparison with data of compound **10** and are reported as follows:

<sup>1</sup>H NMR (DMSO-*d*<sub>6</sub>): δ 9.69 (1H, s, OH), 8.08-8.05 (2H, m, H-24, H-28), 7.64 (1H, d, *J*=16.1 Hz, H-8), 7.60 (1H, d, *J*=16.1 Hz, H-14), 7.62-6.81 (9H, m, H-25, H-27, H-1, H-3, H-4, H-9, H-16, H-19, H-20), 6.80 (1H, d, *J* = 15.6 Hz, H-13), 6.14 (1H, s, H-11), 3.85-3.82 (8H, m, 2xOCH<sub>3</sub>, H-29), 3.04 (1H, t, *J*=8.1 Hz, SH); <sup>13</sup>C NMR (125 MHz, DMSO-*d*<sub>6</sub>) δ (ppm): 185.3 and 181.8 (C-10, C-12), 164.1 (C-22), 151.7 (Cq), 150.0 (Cq), 148.8 (Cq), 148.4 (Cq), 142.0 and 139.4 (C-8, C-14), 141.3 (Cq), 134.4 (Cq), 130.5 and 129.2 (C-24, C-25, C-27, C-28), 127.2 (Cq), 126.6 (Cq), 125.1 and 121.8 (C-9, C-13), 124.9 (Cq), 123.0 (Cq), 123.9, 123.8, 121.5, 116.1, 112.4 and 111.9 (C-1, C-3, C-4, C-16, C-19, C-20), 101.8 (C-11), 56.5 and 56.1 (C-7, C-21), 27.8 (C-29).

**Compound 5.** To a stirred solution of the Curcumin-mono-thiol **4** (100 mg, 0.19 mmol) in anhydrous THF (5 mL) at -78 °C, in an inert atmosphere of Argon, Triton B (40 wt. % solution in MeOH, 25 µL, 0.06 mmol, 0.3 eq) and, after 10', methyl acrylate (34 µL, 0.38 mmol, 2eq) were added. The mixture was allowed to reach rt spontaneously, and after 6h, when the reaction appeared complete by TLC (Hexane/ EtOAc 50:50), the solvents was removed under reduced pressure and the crude purified on silica gel using

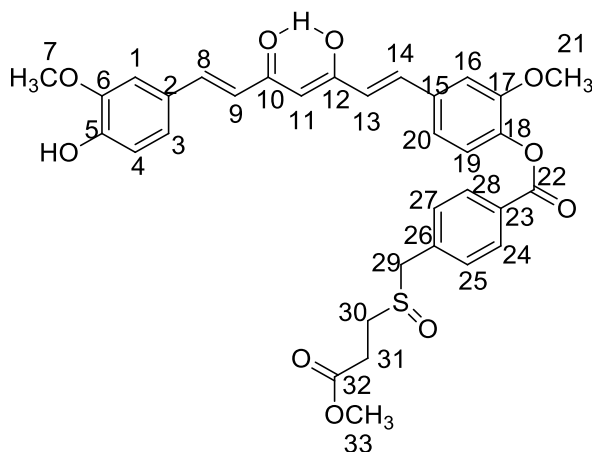
Hexane/EtOAc (60:40) as eluants. Compound **5** was obtained as a yellow solid in 60% yield. Rf: 0.6 (Hexane/EtOAc 60:40).



$^1\text{H}$  NMR ( $\text{CDCl}_3$ ) :  $\delta$  8.18-8.14 (2H, m, H-24, H-28), 7.63 (1H, d, H-8,  $J=15.6$  Hz), 7.61 (1H, d, H-14,  $J=15.6$  Hz), 7.48-7.45 (2H, m, H-25, H-27), 7.21-6.92 (6H, m, H-1, H-3, H-4, H-16, H-19, H-20), 6.58 (1H, d, H-13,  $J=15.6$  Hz), 6.5 (1H, d, H-9,  $J=15.6$  Hz), 5.84 (1H, s, H-11), 3.95 and 3.87 (6H, 2 s,  $\text{OCH}_3$ ), 3.80 (2H, s, H-29), 3.70 (3H, s,  $\text{CO}_2\text{CH}_3$ ) 2.72 and 2.58 (4H, 2t, H-30 and H-31,  $J=7.3$  Hz);  $^{13}\text{C}$  NMR :  $\delta$  184.5 (C-10), 181.8 (C-12), 172.2 (C-32), 164.2 (C-22), 151.6 (C-q), 147.9 (Cq), 146.8 (Cq), 144.4 (Cq), 141.4 (Cq), 141.1 (C-8), 139.4 (C-14), 134.1 (Cq), 130.6 (C-24 and C-28), 129.0 (C-25 and C-27), 127.9 (Cq), 127.6 (Cq), 124.2 (C-9), 121.8 (C-13), 123.4, 123.0, 121.0, 114.8, 111.5, and 109.6 (C-1, C-3, C-4, C-16, C-19, C-20), 101.5 (C-11), 55.9 (C-7, C-21), 51.8 (C-33), 36.2 (C-29), 34.2 (C-31), 26.3 (C-30).

**Compound 6.** *m*-CPBA (80%, 5.8 mg, 0.032 mmol) was dissolved in DCM (1 ml) and added dropwise to a solution of the thioether **5** (20 mg, 0.034 mmol) in DCM (1 ml), maintained under vigorous stirring at  $-78^\circ\text{C}$ . The reaction appeared complete by TLC (EtOAc) just after finishing the addition of the oxidant, and then a 10% water solution of  $\text{Na}_2\text{S}_2\text{O}_3$  (2 ml) was added. The separated organic layers were washed twice with a saturated solution of

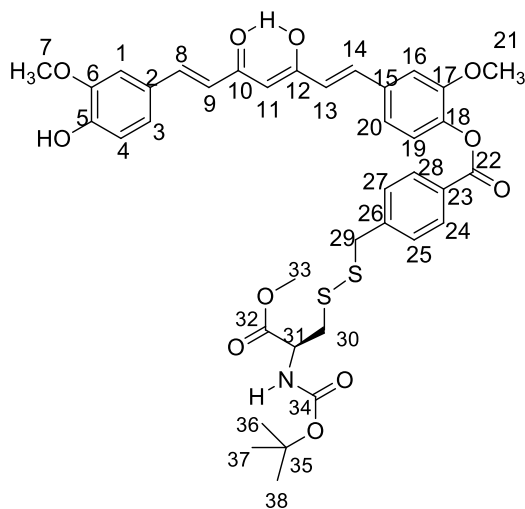
NaHCO<sub>3</sub> and twice with brine. Evaporation of the solvent gave the expected sulfoxide **6** in 80% yield. R<sub>f</sub> 0.1 (100% EtOAc) and the sulfone **7** in 10% yield. R<sub>f</sub> 0.4 (100% EtOAc)



<sup>1</sup>H NMR (CDCl<sub>3</sub>) :  $\delta$  8.24-8.21 (2H, m, H-24, H-28), 7.63 (1H, d, H-8,  $J=15.7$  Hz), 7.61 (1H, d, H-14,  $J=15.6$  Hz), 7.50-7.43 (2H, m, H-25, H-27), 7.22-6.90 (6H, m, H-1, H-3, H-4, H-16, H-19, H-20), 6.58 (1H, d, H-13,  $J=15.7$  Hz), 6.50 (1H, d, H-9,  $J=15.6$  Hz), 5.92 (1H, br s, OH) 5.84 (1H, s, H-11), 4.12-4.05 (2H, m, H-29) 3.95 and 3.86 (6H, 2 s, OCH<sub>3</sub>), 3.73 (3H, s, CO<sub>2</sub>CH<sub>3</sub>), 3.73-2.80 (4H, m, H-30, H-31); <sup>13</sup>C NMR :  $\delta$  184.5 (C-10), 181.8 (C-12), 172.0 (C-32), 164.0 (C-22), 151.5 (Cq), 148.0 (Cq), 146.8 (Cq), 141.3 (Cq), 141.1 (C-8), 139.4 (C-14), 135.4 (Cq), 134.2 (Cq), 130.9 (C-24, C-28), 130.3 (C-25, C-27), 129.3 (Cq), 127.5 (Cq), 124.3 (C-9), 121.8 (C-13), 123.3, 123.0, 120.9, 114.8, 111.5, and 109.6 (C-1, C-3, C-4, C-16, C-19, C-20), 101.5 (C-11), 58.2 (C-29), 55.9 (C-7 and C-21), 52.2 (C-33), 45.9 (C-30), 26.7 (C-31).

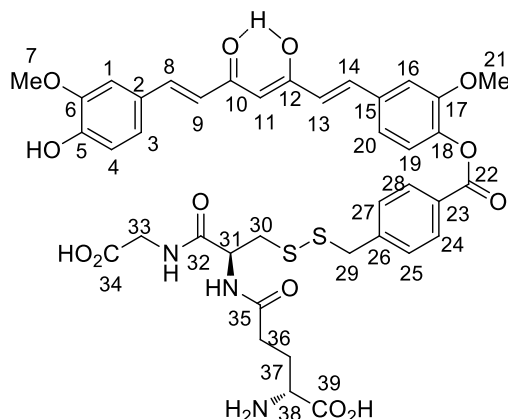
**Compound 9.** Curcumin sulfoxide **7** (10 mg, 0.016 mmol) and N-(*tert*-butoxycarbonyl)-L-cysteine methyl ester (97%, 11.6 mg, 0.048 mmol, 3 eq) were dissolved in 1 mL of 1,2-dichloroethane (DCE). The mixture was

maintained under stirring, at reflux temperature (83°C) and monitored via TLC (Hexane/EtOAc 50:50) for 12h until disappearance of sulfoxide **7**. The solvent was removed under reduced pressure and the crude was purified on silica gel (Hexane/EtOAc 70:30 up to 50:50). Compound **9** was obtained as a yellow solid in 62 % yield. R<sub>f</sub> 0.6 (Hexane/EtOAc 50:50).



$^1\text{H}$  NMR ( $\text{CDCl}_3$ ) :  $\delta$  8.19-8.15 (2H, m, H-24, H-28), 7.63 (1H, d, H-8,  $J=15.6$  Hz), 7.61 (1H, d, H-14,  $J=15.6$  Hz), 7.49-7.45 (2H, m, H-25, H-27), 7.21-6.92 (6H, m, H-1, H-3, H-4, H-16, H-19, H-20), 6.58 (1H, d, H-13,  $J=15.6$  Hz), 6.49 (1H, d, H-9,  $J=15.6$  Hz), 5.88 (1H, br s, OH), 5.84 (1H, s, H-11), 5.30-5.24 (1H, m, NH), 4.56-4.10 (1H, m, H-31), 3.97 (2H, s, H-29), 3.95 and 3.86 (6H, 2 s,  $\text{OCH}_3$ ), 3.75 (3H, s,  $\text{CO}_2\text{CH}_3$ ), 2.93-2.80 (2H, m, H-30), 1.45 (9H, s, H-36, H-37, H-38);  $^{13}\text{C}$  NMR :  $\delta$  184.5 (C-10), 181.8 (C-12), 170.0 (C-32), 164.2 (C-22), 151.6 (C-34), 148.0 (Cq), 146.8 (Cq), 146.0 (Cq), 143.2 (Cq), 141.4 (Cq), 141.1 (C-8), 139.4 (C-14), 134.2 (Cq), 130.6 (C-24, C-28), 129.5 (C-25, C-27), 128.3 (Cq), 127.5 (Cq), 124.3 (C-9), 121.8 (C-13), 123.4, 123.0, 121.0, 114.8, 111.5 and 109.6 (C-1, C-3, C-4, C-16, C-19, C-20), 101.5 (C-11), 76.1 (C-35), 55.9 (C-7, C-21), 52.7 (C-31), 52.6 (C-33), 43.0 (C-29), 40.7 (C-30), 28.3 (C-36, C-37, C-38).

**Compound 10.** To a solution of Curcumin sulfoxide **7** (16 mg, 0.025 mmol) in about 1 ml of 1,2-DCE, a solution of Glutathione (23.6 mg, 0.075, 3 eq) in EtOH/ water (0.6 ml/0.3 ml) was added. The mixture (DCE/EtOH /water 4:2:1) was maintained at 60°C for 3h in the dark, during which it was followed using TLC (EtOAc/ iso-Propanol 95:5) until the disappearance of sulfoxide **7**. The solvents were then removed under reduced pressure and the reaction crude was purified by column chromatography on silica gel (up to EtOAc 100% up to EtOAc/iso-propanol 95:5). Compound **10** was obtained as a pale yellow solid in 37% yield. Rf: 0.1 (EtOAc/ iso-propOH 95:5), together with traces of thiol **4**.



$^1\text{H}$  NMR (DMSO- $d_6$ ) :  $\delta$  9.68 (1H, s, OH), 8.27-8.19 (3H, m,  $\text{NH}_2$  and 2xNH), 8.09-8.06 (2H, m, H-24, H-28), 7.63 (1H, d,  $J=15.6$  Hz, H-8), 7.58 (1H, d,  $J=15.7$  Hz, H-14), 7.57-7.54 (2H, m, H-25, H-27), 7.38-6.81 (6H, m, H-1, H-3, H-4, H-16, H-19, H-20), 6.98 (1H, d,  $J=15.7$  Hz, H-9), 6.79 (1H, d,  $J=15.6$  Hz, H-13), 6.14 (1H, s, H-11), 4.15-4.04 (3H, m, H-31 and H-33), 3.83 (8H, s, 2xOCH $_3$  and H-29), 3.82-3.65 (3H, m, H-36, H-38), 3.19-2.99 (2H, m, H-30), 2.49-2.47 (2H, m, H-37);  $^{13}\text{C}$  NMR :  $\delta$  185.4 and 181.8 (C-10, C-12), 166.6 (CO), 166.3 (CO), 163.9 (C-22), 151.7 (Cq), 150.0 (Cq), 148.4 (Cq), 144.7 (Cq), 141.2 (Cq), 142.0 and 139.4 (C-8 and C-14), 139.4 (Cq), 134.5 (Cq), 130.4 and 129.8 (C-24, C-25, C-27, C-28), 128.6 (Cq),

126v.7 (Cq), 125.2 and 121.8 (C-9, C-13), 123.8, 121.6, 116.2, 112. 5 and 111.9 (C-1, C-3, C-4, C-16, C-19, C-20), 101.8 (C-11), 56.5 (C-7, C-21), 56.2 (C-31), 54.3 (C-38), 44.8 (C-33), 43.4 (C-30 and C-36), 42.0 (C-29), 29.4 (C-37).



### 3.7 References

---

1. N. Haugaard, *Ann. N Y. Acad. Sci.* **2000**, 899, 148-58.
2. Y. M. Go, D. P. Jones, *Crit. Rev. Biochem. Mol. Biol.*, **2013**, 48, 173-181; A. Fava, A. Iliceto, E. Camera, *J. Am. Chem. Soc.* **1956**, 70, 833-838.
3. K. Wang, H. Peng, B. Wang, *J. Cell. Biochem.*, **2014**, 115,1007-1022.
4. A.K. Elshorbagy, A. D. Smith, V. Kozich, H. Refsum, *Obesity*, **2012**, 20, 473-481; S. Shahrokhian, *Anal. Chem.*, **2001**, 73, 5972-5978.
5. S. Seshadri, A. Beiser, J. Selhub, P. F. Jacques, I. H. Rosenberg, R. B. D'Agostino, P. W. F. Wilson, P. A. Wolf, *New Engl. J. Med.*, **2002**, 346, 476-483; H. Refsum, P. M. Ueland, O. Nygard, S. E. Vollset, *Annu. Rev. Med.*, **1998**, 49, 31-62.
6. C. Hwang, A. J. Sinskey, H. F. Lodish, *Science*, **1992**, 257, 1496-1502; F. Q. Schafer, G. R. Buettner, *Free Radic. Biol. Med.* **2001**, 30, 1191-1212.
7. J. M. Estrela, A. Ortega, E. Obrador, *Crit. Rev. Clin. Lab. Sci.*, **2006**, 43, 143-181; R. Franco, O. J. Schoneveld, A. Pappa, M. I. Panayiotidis, *Arch. Physio. Biochem.*, **2007**, 113, 234-258.
8. L.-Y. Niu, Y.-Z. Chen, H.-R. Zheng, L.-Z. Wu, C.-H. Tungbc, Q.-Z. Yang, *Chem. Soc. Rev.*, **2015**, 44, 6143-6160; H. Chen, Y. Tang, W. Lin, *Trends Anal. Chem.*, **2016**, 76, 166-181.
9. H. Kamencic, A. Lyon, P. Paterson, B. Juurlink, *Anal Biochem.*, **2000**, 286, 35-37.
10. S. Ding, G. Feng, *Sensor. Actuat. B Chem.*, **2016**, 235,691-697.
11. L.-Y. Niu, Y.-S. Guan, Y.-Z. Chen, L.-Z. Wu, C.-H. Tung, Q.-Z. Yang, *J. Am. Chem. Soc.*, **2012**, 134, 18928-18931.
12. X. Yang, Y. Guo, R. Strongin, *Angew. Chem. Int Ed.*, **2011**, 50, 10690-10693.

13. L. Pang, Y. Zhou, W. Gao, J. Zhang, H. Song, X. Wang, Y. Wang, X. Peng, *Ind. Eng. Chem. Res.*, **2017**, 56, 7650-7655.
14. C. Avonto, O. Taglialatela-Scafati, F. Pollastro, A. Minassi, V. Di Marzo, L. De Petrocellis, G. Appendino, *Angew. Chem.*, **2011**, 123, 487-491.
15. E. Block, *Angew. Chem. Int. Ed. Engl.*, **1992**, 3, 1135-1178; S. Patai, John Wiley & Sons: Chichester, **1990**, 361-402; M. Feng, B. Tang, S.H. Liang, X. Jiang, *Curr. Top. Med. Chem.*, **2016**, 16, 1200-1216.
16. V. Gupta, K. S. Carroll, *Biochim. Biophys. Acta*, **2014**, 1840, 847-875.
17. N. J. Kettenhofen, M. Wood, *Chem. Res. Toxicol.*, **2010**, 23, 1633-1646.
18. V. Gupta, H. Paritala, K. S. Carroll, *Bioconjugate Chem.*, **2016**, 1411-1418.
19. V. Gupta, K. S. Carroll, *Chem. Commun.*, **2016**, 52, 3414-3417; V. Gupta, K. S. Carroll, *Chem. Sci.*, **2016**, 7, 400-415.
20. Jean-Philippe R. Chauvin and Derek A. Pratt, *Angew. Chem. Int. Ed.*, **2017**, 56, 6255-6259.
21. K. Fries, *Chem. Ber.*, **1912**, 45, 2965-2973.
22. K. Goto, K. Shimada, S. Furukawa, S. Miyasaka, Y. Takahashi, T. Kawashima, *Chemistry Letters*, **2006**, 35,
23. K. Goto, M. Holler, R. Okazaki, *J. Am. Chem. Soc.*, **1997**, 119, 1460-1461; R. Okazaki, K. Goto, *Heteroatom. Chem.*, **2002**, 13, 414. (d) Saiki, T.; Goto, K.; Tokitoh, N.; Goto, M.; Okazaki, R. *J. Organomet. Chem.*, 2000, 611, 146. (e) Okazaki, R. *Phosphorus Sulfur Silicon Relat. Elem.*, 1999, 153-154, 155.
24. S. Wu, X. Lei, E. Fan, Z. Sun, *Org. Lett.* **2018**, 20, 522-525; A. Barattucci, M. C. Aversa, A. Mancuso, T. M. G. Salerno, P. Bonaccorsi *Molecules* **2018**, 23(5), 1030-1042.

25. M. C. Aversa, A. Barattucci, P. Bonaccorsi, P. Giannetto, *Curr. Org. Chem.* **2007**, 11, 1034-1052; J. Pan, K. S. Carroll, *Org. Lett.* **2015**, 17, 6014-6017.
26. D. N. Jones, D. R. Hill, D. A. Lewton, C. Sheppard, *J. Chem. Soc., Perkin Trans. 1*, **1977**, 0, 1574-1587.
27. H. Adams, J. C. Anderson, R. Bell, D. N. Jones, M. R. Peel, N. C. O. Tomkinson, *J. Chem. Soc. Perkin Trans.*, **1998**, 1, 3967-3974; M. C. Aversa, A. Barattucci, P. Bonaccorsi, P. Rollin, A. Tatibouët, *Arkivoc*, **2009**, 8, 187-198.
28. M. C. Aversa, A. Barattucci, M. C. Bilardo, P. Bonaccorsi, P. Giannetto, P. Rollin, A. Tatibouët, *J. Org. Chem.*, **2005**, 70, 7389-7396; M. C. Aversa, A. Barattucci, P. Bonaccorsi, P. Giannetto, *J. Org. Chem.*, **2005**, 70, 1986-1992.
29. M. C. Aversa, A. Barattucci, P. Bonaccorsi, *Synlett* 2011, 254-258.
30. A. Barattucci, M. C. Aversa, A. Mancuso, T. M. G. Salerno, P. Bonaccorsi, *Molecules*, **2018**, 23, 1030-1042.
31. S. Srivastava, P. Gupta, Amandeep, R. P. Singh, *J of Mol. Struct.*, **2016**, 1109, 58-66.
32. G. Zhang, V. Nitteranon, L. Y. Chan, K. L. Parkin, *Food Chem.* **2013**, 140, 1-8; J. Fernandes, C. R. Gattass, *J. Med. Chem.* **2009**, 52, 1214-1218; M. Usta, H. M. Wortelboer, J. Vervoort, M. G. Boersma, I. M. C. Rietjens, P. J. van Bladeren, N. H. P. Cnubben, *Chem. Res. Toxicol.* **2007**, 20, 1895-1902.
33. M. Usta, H. M. Wortelboer, J. Vervoort, M. G. Boersma, I. M. C. M. Rietjens, P. J. van Bladeren, N. H. P. Cnubben, *Chem. Res. Toxicol.*, **2007**, 20, 1895-1902; G. Zhang, V. Nitteranon, L. Yan Chan, K. L. Parkin, *Food Chem.*, **2013**, 140, 1-8.
34. J. Fang, J. Lu, A. Holmgren, *J. Biol. Chem.*, **2005**, 280, 25284-25290.

## Final remarks

The research reported in this thesis has investigated:

- a) The synthesis of new bichromophoric systems. In one case, they were designed as artificial antenna systems in which two differently absorbing and emitting chromophores, such as two BODIPY, were connected by a carbohydrate-based spacer. In the second case, the yellow pigment Curcumin was connected to different chromophores, and, taking advantage from its luminescent properties, worked as one of the two dyes of the bichromophoric systems.
- b) The synthesis of a suitable Curcumin derivative to generate in situ a Curcumin-derived sulfenic function (Curc-SOH) that can react with biological thiols such as Cysteine or Glutathione. This was realized with idea of create a potential probe for the detection of sulfhydryl groups in a biological environment.

Carbohydrate-based bichromophoric species have been characterized photophysically to confirm their nature of light-harvesting systems and biological studies have shown that some of these systems can give useful information on cell composition, paving the way to their use for cell information based on luminescence imaging.

Curcumin-based bichromophoric species have shown appreciable photophysical properties of artificial antenna systems and preliminary biological studies demonstrated their internalization into cells. These results highlight a new use of Curcumin, and might account for many other intriguing biological activities of this natural product.

Finally, the generation of a Curc-SOH and the formation of a disulphide bond with thiol groups such as GSH showed the capability of the former species to trap biological thiols. A preliminary photophysical experiment demonstrated

the possibility of using the properties of the system based on the formation/reaction of Curc-SOH to act as a turn-off sensor for protein thiols.

In order to go beyond these ‘demonstrations’, however, and produce models capable of biological applications requires rather more than a simulation. Future insights on the molecules shown in this thesis, their possible structural modifications and their behaviour, are envisaged.

Products of my three-year work are as follows:

### **Publications**

1. T. Papalia, A. Barattucci, S. Campagna, F. Puntoriero, T.M.G. Salerno, P. Bonaccorsi, *Org Biomol Chem.*, **2017**, 15, 8211-8217. **DOI:** 10.1039/c7ob01764b.  
*Synthesis and Photophysical Properties of a Bichromophoric System Hosting a Disaccharide Spacer*
2. S. Campagna, F. Puntoriero, P. Bonaccorsi, A. Barattucci, T. M. G. Salerno, T. Papalia, C. Rosano, P. Castagnola, M. Viale and M. Monticone, *Dalton Trans.*, **2018**, 47, 4733-4738. **DOI:** 10.1039/C7DT04850E.  
*Localization-controlled two-color luminescence imaging via environmental modulation of energy transfer in a multichromophoric species*
3. A. Barattucci, M. C. Aversa, A. Mancuso, T. M. G. Salerno, P. Bonaccorsi, *Molecules*, **2018**, 23, 1030. **DOI:** 10.3390/molecules23051030.  
*Transient Sulfenic Acids in the Synthesis of Biologically Relevant Products*
4. A. Mancuso, A. Barattucci, P. Bonaccorsi, A. Giannetto, G. La Ganga, M. Musarra-Pizzo, T. M. G. Salerno, A. Santoro, M. T. Sciortino, F. Puntoriero, M. L. Di Pietro, *Chem. Eur. J.* **DOI:** 10.1002/chem.201803804.  
*Carbohydrates and charges on OPEs: towards the design of cancer bullets*

## Member of the organizing committee

1. **Workshop in the S.C.I. (Italian Chemical Society) convegno delle sezioni Sicilia e Calabria**, Messina, 9-10 February 2017.
2. **I° DOCTOCHEM-UNIME**, Messina, incubatore di impresa, 22 June 2018.

## Communications

1. **15<sup>th</sup> RSC-SCI Joint meeting on Heterocyclic Chemistry**, Taormina, 12-15, May 2016. **Oral communication**  
*New Bodipy Derivatives as Selective Luminescent Sensors*  
T.M.G. Salerno, T. Papalia, A. Barattucci, F. Puntoriero, S. Campagna, P. Bonaccorsi.
2. **Joint Congress of the French and Italian Photochemists and Photobiologists**, Bari, 19-22 September 2016. **Oral Communication**  
*Localization-controlled two-color luminescence imaging via environmental modulation of energy transfer in a BODIPY dyad*  
P. Bonaccorsi, T. Papalia, A. Barattucci, T. M.G. Salerno, C. Rosano, P. Castagnola, M. Viale, S. Campagna, F. Puntoriero  
Prize: **BEST ORAL COMMUNICATION**
3. **4<sup>th</sup> International Workshop on Pericyclic Reactions and Synthesis of Hetero-and Carbocyclic Systems**, Milan, 28-30 June 2017. **Oral communication**  
*Curcumin: how much more is there to explore?*  
T.M.G. Salerno, A. Barattucci, A. Mancuso, P. Bonaccorsi
4. **XLIII "A. Corbella" International Summer School on Organic Synthesis - ISOS 2018**, Gargnano, Palazzo Feltrinelli, 10-14 June 2018. **Oral communication**  
*The use of Curcumin in the synthesis of luminescent probes*  
T. M.G. Salerno, A. Barattucci, A. Mancuso, Paola Bonaccorsi

5. **IDOCTOCHEM-UNIME**, Messina, incubatore di impresa, 22 June 2018.

**Oral communication**

*Curcumin: a natural dye. Synthesis of new derivatives and their applications*

T. M.G. Salerno, A. Barattucci, A. Mancuso, P. Bonaccorsi

6. **XXVIII Convegno Nazionale della Divisione di Chimica Organica della Società Chimica Italiana- CDCO 2018**, Milan, 9-13 September 2018.

**Oral communication**

*Curcumin from nature to laboratory: new ways to improve its properties*

T.M.G. Salerno, A. Barattucci, A. Mancuso, F. Puntoriero, S. Campagna, P. Bonaccorsi